LOREN CHISTÉ

AGRONOMIC EFFICIENCY OF BIOCHAR-BASED MICRONUTRIENT FERTILIZERS

LAVRAS – MG
2024

LOREN CHISTÉ

AGRONOMIC EFFICIENCY OF BIOCHAR-BASED MICRONUTRIENT FERTILIZERS

Thesis presented to the Federal University of Lavras, as part of the requirements of the Graduate Program in Soil Science, concentration area Soil Fertility and Plant Nutrition, to obtain the title of Doctor.

Advisor
Prof. Leônidas Carrijo Azevedo Melo

LAVRAS - MG
2024

Ficha catalográfica elaborada pelo Sistema de Geração de Ficha Catalográfica da Biblioteca Universitária da UFLA, com dados informados pelo(a) próprio(a) autor(a).

CHISTÉ, LOREN.
Agronomic Efficiency of Biochar-Based Micronutrient Fertilizers / LOREN CHISTÉ. - 2024.
224 p. : il.

Orientador(a): Leônidas Carrijo Azevedo Melo.

Tese (doutorado) - Universidade Federal de Lavras, 2024.
Bibliografia.

1. organometallic complexes. 2. fertilizer composites. 3. biochar-micronutrient composites. I. Melo, Leônidas Carrijo Azevedo. II. Título.

LOREN CHISTÉ

AGRONOMIC EFFICIENCY OF BIOCHAR-BASED MICRONUTRIENT FERTILIZERS
EFICIÊNCIA AGRONÔMICA DE FERTILIZANTES A BASE DE MICRONUTRIENTES COM BIOCARVÃO

Thesis presented to the Federal University of Lavras, as part of the requirements of the Graduate Program in Soil Science, concentration area Soil Fertility and Plant Nutrition, to obtain the title of Doctor.

APPROVED on August 22, 2024.
Dr. Edson Marcio Mattiello, UFV
Dr. Renato Ribeiro Passos, UFES
Dr. Clistenes Williams Araujo Do Nascimento, UFRPE
Dr. Flavio Henrique Silveira Rabelo, ESALQ

Advisor
Prof. Dr. Leônidas Carrijo Azevedo Melo

LAVRAS - MG
2024

To God, to my parents, Zilma F. Chisté and Alceu P. Chisté, and to my sister Hérica Chisté, to my husband Daniel L. de Oliveira Ferreira, for their immense love and understanding, which have strengthened me in the pursuit of this great dream. 'The Lord has done great things for us, and we are filled with joy.' Psalm 126:3.

I DEDICATE.

ACKNOWLEDGMENTS

I extend my sincere gratitude for the invaluable support received during my doctoral studies:

To the Federal University of Lavras (UFLA), the School of Agricultural Sciences, and particularly the Department of Soil Science.

To the Coordination for the Improvement of Higher Education Personnel (CAPES) for providing the student scholarship.

To the National Council for Scientific and Technological Development (CNPq) and the Minas Gerais Research Support Foundation (FAPEMIG) for their financial support.

To my advisors at UFLA, Prof. Dr. Leônidas Carrijo Azevedo Melo and Carlos Alberto Silva.

To all the professors in the Department of Soil Science at the Federal University of Lavras.

To all the laboratory technicians, especially Lívia Botelho, Mariene Duarte, Aline Mesquita, Geila Carvalho, and José Roberto Fernandes.

To my research group, colleagues, and friends: Everton Geraldo de Morais, Raul Oliveira, and Gabrielly Nayara Tavares da Silva.

To everyone, thank you very much!

"But in all these things we are more than conquerors through Him who loved us." Romans 8:37

SUMÁRIO

RESUMO

O biochar, um subproduto da pirólise, pode ser combinado com micronutrientes para criar compostos que melhoram a entrega de nutrientes às culturas. Este estudo foca no desenvolvimento de compósitos à base de biochar enriquecidos com boro (B), cobre (Cu) e zinco (Zn), visando melhorar o suprimento de nutrientes para mudas de eucalipto, trigo e milho. Devido ao alto custo e à escassez de micronutrientes, a utilização de biomassa enriquecida em B, Cu e Zn integrada à matriz orgânica do biochar oferece uma abordagem promissora para atender às demandas nutricionais das culturas. Os objetivos do estudo foram: i) produzir e caracterizar biochars a partir de diversas biomassas combinadas com fontes solúveis e insolúveis de B, Cu e Zn em diferentes temperaturas de pirólise; ii) investigar a cinética de liberação de B, Cu e Zn e seus efeitos sobre a disponibilidade e residualidade desses micronutrientes em solos contrastantes; e iii) avaliar o valor agronômico e a eficiência dos compósitos à base de biochar no cultivo de eucalipto, trigo e milho. Os compósitos de biochar foram preparados a partir de esterco de galinha, carapaça de camarão e lodo de esgoto, dopados separadamente com ácido bórico, borax, sulfato de cobre, óxido de cobre, sulfato de zinco e óxido de zinco, e as misturas foram pirolisadas a temperaturas de 300 °C e 550 °C. Os compósitos foram analisados por espectroscopia de infravermelho por transformada de Fourier (FTIR) e microscopia eletrônica de varredura (MEV), e testados quanto à cinética de liberação de Cu em ácido cítrico a 2%. A eficiência agronômica dos compósitos foi avaliada em três experimentos com plantas de eucalipto, trigo e milho, cultivadas em dois diferentes Latossolos. O estudo utilizou um delineamento inteiramente casualizado com três repetições, e o impacto na nutrição e crescimento das culturas foi avaliado. O FTIR confirmou a integração bem-sucedida de B na matriz do biochar, com o CSC-BA: resíduo de camarão + ácido bórico a 300 °C; compósito a 300 °C demonstrando notável estabilidade térmica, retenção de B e disponibilidade, melhorando a cinética de liberação de B. No Experimento 2, a análise FTIR confirmou a incorporação de Cu, com o compósito CSS/CS-5: lodo de esgoto + sulfato de cobre a 550°C apresentando desempenho agrícola superior, reduzindo a liberação de Cu na água e aumentando a acumulação de Cu nas partes aéreas do trigo. O CSS/CS-5 manteve baixas concentrações de Cu, indicando liberação controlada que atende às altas demandas nutricionais de Cu do trigo. No Experimento 3, os compósitos dopados com Zn, particularmente a 300 °C, exibiram maior liberação de Zn e melhor disponibilidade de Zn para o crescimento do milho. Os compósitos atenderam efetivamente às demandas nutricionais das mudas de milho e mostraram potencial em melhorar o desempenho das culturas. No geral, o estudo demonstrou que compósitos à base de biochar enriquecidos com B, Cu e Zn fornecem de forma eficaz micronutrientes para eucalipto, trigo e milho, atendendo suas demandas nutricionais em comparação com fontes minerais comerciais.

Palavras-chave: complexos organometálicos, compósitos de fertilizantes, compósitos de biochar-micronutriente, cinética de liberação de micronutrientes.

ABSTRACT

Biochar, a byproduct of pyrolysis, can be combined with micronutrients to create composites that enhance nutrient delivery to crops. This study focuses on the development of biochar-based composites enriched with boron (B), copper (Cu), and zinc (Zn), aiming to enhance the nutrient supply for eucalyptus, wheat, and maize seedlings. Due to the high cost and scarcity of micronutrients, utilizing biomass enriched in B, Cu, and Zn integrated into the organic biochar matrix offers a promising approach to meet crop's nutritional demands. The objectives of the study were: i) to produce and characterize biochars from various biomasses combined with both soluble and insoluble sources of B, Cu, and Zn under different pyrolysis temperatures; ii) to investigate the release kinetics of B, Cu, and Zn and their effects on the availability and residuality of these micronutrients in contrasting soils; and iii) to evaluate the agronomic value and efficiency of biochar-based composites in the cultivation of eucalyptus, wheat, and maize. The biochar composites were prepared from chicken manure, shrimp carcass and sewage sludge, doped separately with boric acid, borax, copper sulfate, copper oxide, zinc sulfate and zinc oxide, and the mixtures were pyrolyzed at temperatures of 300 °C and 550 °C. The composites were analyzed using Fourier transform infrared spectroscopy (FTIR) and scanning electron microscopy (SEM) and tested for Cu release kinetics in 2% citric acid. The agronomic efficiency of the composites was evaluated in three experiments with eucalyptus, wheat and maize plants, grown in two different Oxisols. The study used a completely randomized design with three replicates, and the impact on crop nutrition and growth was evaluated. FTIR confirmed successful B integration into the biochar matrix, with the CSC-BA: shrimp waste + boric acid at 300 °C; composite at 300 °C demonstrating notable thermal stability, B retention, and availability, enhancing B release kinetics. In Experiment 2, FTIR analysis confirmed the incorporation of Cu, with the CSS/CS-5: sewage sludge + copper sulfate at 550°C composite showing superior agricultural performance, reducing Cu release into water and enhancing Cu accumulation in wheat shoots. CSS/CS-5 maintained low Cu concentrations, indicating controlled release that meets wheat's high Cu nutritional demands. In Experiment 3, Zn-doped composites, particularly at 300 °C, exhibited higher Zn release and improved Zn availability for maize growth. The composites effectively met the nutritional demands of maize seedlings and showed promise in enhancing crop performance. Overall, the study demonstrated that biochar-based composites enriched with B, Cu, and Zn effectively supply micronutrients to eucalyptus, wheat, and maize, meeting their nutritional demands compared to commercial mineral sources.

Keywords: organometallic complexes, fertilizer composites, biochar-micronutrient composites, micronutrient release kinetics.

Impactos sociais, tecnológicos, econômicos e culturais

O trabalho de pesquisa realizado sobre a "Eficiência Agronômica de Fertilizantes à Base de Micronutrientes com Biochar", apresenta impactos tecnológicos, sociais e ambientais significativos, com potencial para transformar práticas agrícolas em regiões tropicais, especialmente no Brasil. A combinação de biochar com micronutrientes como boro, cobre e zinco oferece uma solução sustentável e eficiente para enfrentar a escassez e o alto custo desses elementos essenciais para o crescimento saudável das plantas. Ao aprimorar a disponibilidade de nutrientes e promover uma liberação controlada no solo, os compostos desenvolvidos têm o potencial de aumentar a eficiência no uso de fertilizantes, reduzindo a necessidade de aplicação de produtos químicos convencionais, o que pode impactar diretamente a sustentabilidade ambiental e a conservação dos solos. Além disso, os resultados indicam uma melhoria no desempenho de culturas como eucalipto, trigo e milho, com implicações econômicas positivas para pequenos e grandes produtores que dependem dessas culturas. O estudo, alinhado aos Objetivos de Desenvolvimento Sustentável (ODS) da ONU, especialmente aos ODS 2 (Fome Zero e Agricultura Sustentável), 12 (Consumo e Produção Responsáveis) e 15 (Vida Terrestre), contribui para o avanço das práticas agrícolas sustentáveis e para a mitigação de impactos ambientais, ao mesmo tempo em que promove a produtividade agrícola. O público diretamente beneficiado inclui agricultores, consultores agronômicos e indústrias de fertilizantes, com potencial de escalonamento para outras regiões tropicais. Embora o impacto concreto deste trabalho esteja nas fases iniciais de validação, a aplicação extensiva dos compostos desenvolvidos pode gerar benefícios de longo prazo, como a redução da dependência de fertilizantes minerais importados e a melhoria da saúde dos solos, atendendo assim a um público amplo e diversificado, incluindo pesquisadores, estudantes e profissionais do agronegócio. Dessa forma, o projeto tem um caráter extensivo, envolvendo atores externos à UFLA e fortalecendo parcerias em territórios agrícolas, especialmente em áreas onde a degradação do solo é um problema crescente.

Social, technological, economic and cultural impacts

The research on "Agronomic Efficiency of Biochar-Based Micronutrient Fertilizers" presents significant technological, social, and environmental impacts, with the potential to transform agricultural practices in tropical regions, particularly in Brazil. The combination of biochar with micronutrients such as boron, copper, and zinc offers a sustainable and efficient solution to address the scarcity and high cost of these essential elements for healthy plant growth. By improving nutrient availability and promoting controlled release in the soil, the developed composites have the potential to increase fertilizer use efficiency, reducing the need for conventional chemical applications, which can directly impact environmental sustainability and soil conservation. Additionally, the results indicate improved performance of crops such as eucalyptus, wheat, and maize, with positive economic implications for both small and large-scale farmers who depend on these crops. The study, aligned with the United Nations' Sustainable Development Goals (SDGs), particularly SDG 2 (Zero Hunger and Sustainable Agriculture), SDG 12 (Responsible Consumption and Production), and SDG 15 (Life on Land), contributes to advancing sustainable agricultural practices and mitigating environmental impacts while promoting agricultural productivity. The directly benefited audience includes farmers, agronomic consultants, and the fertilizer industry, with potential scalability to other tropical regions. Although the concrete impact of this work is in its early stages of validation, the extensive application of the developed composites can generate long-term benefits, such as reducing dependence on imported mineral fertilizers and improving soil health, thereby reaching a broad and diverse audience, including researchers, students, and agribusiness professionals. Thus, the project has an extensionist character, involving actors outside UFLA and strengthening partnerships in agricultural territories, especially in areas where soil degradation is an increasing problem.

General introduction

New routes in the synthesis of fertilizers, both from mineral and organic sources, have led to rapid scientific and technological advancements. These advancements aim to improve crop performance, increase productivity, and enhance the quality of harvested products, addressing the global demand for food and generating revenue and wealth in developing countries (UN, 2019). However, it is essential to employ and value sustainable inputs that meet the needs of the soil-plant system to maximize crop performance (Maciel, 2021).

Micronutrients, such as copper (Cu), zinc (Zn), and boron (B), are often neglected in fertilization schedules due to high costs and logistical challenges (Pivoto et al., 2018). Tropical soils are characterized by high concentrations of iron and aluminum oxides, low pH, low organic matter, and reduced cation exchange capacity (CEC), which limit micronutrients' availability. These micronutrients are vital for plant growth and development, influencing processes such as protein synthesis, energy production, and nucleic acids and chlorophyll formation.

A promising approach to overcome these limitations is the use of metal-doped biochar. Biochar is produced by the pyrolysis of organic residues under low or no oxygen conditions, resulting in a material that can improve soil properties, increase nutrient availability, and promote soil health and crop yield (Liu et al., 2015; Song et al., 2019; Radenahmad et al., 2020). Pyrolysis produces biochars with varying levels of carbon (C) and nutrients, whose chemical composition and recalcitrance are influenced mainly by the pyrolysis temperature.

Using biochar as a matrix combined with mineral products can result in efficient fertilizers with a gradual nutrient release kinetics, leveraging insoluble sources that cannot be directly added to the soil. This is especially relevant for micronutrients such as Cu, Zn, and B, whose availability can be improved by complexation and chelation in forms available to plants (Chen et al., 2007).

Brazil has an abundance of biomass and organic residues (Ferreira-Leitao, 2010), and recycling these residues with high levels of Cu, Zn, and B can be an effective process for utilizing these nutrients in crops. The research will focus on the effects of different pyrolysis temperatures on the solubilization, complexation, and prevention of micronutrient losses, allowing regulated biochars to synchronize nutrient supply with the stages of highest nutrient demand of the crops.

Thesis Objectives and Research Questions

The overall objective of this research was to develop and evaluate biochar composites enriched with boron, copper, and zinc, aimed at enhancing the agronomic efficiency of seedlings of eucalyptus, wheat, and maize. This study seeks to address the following research questions:

1. Do biochar composites made from chicken manure, shrimp shell, and sewage sludge, and doped with boric acid, sodium borate, copper oxide, copper sulfate, zinc oxide, and zinc sulfate, show a higher release of boron, copper, and zinc compared to pure biochars. Under which pyrolysis conditions does this occur.

2. How do biochar composites enriched with boron, copper, and zinc influence the release of these micronutrients, and how do they impact the growth and nutrient uptake of eucalyptus, wheat, and maize seedlings. What are the optimal doping conditions and pyrolysis temperatures for these effects.

Dissertation outline

The above research questions were addressed and answered in three chapters:

Chapter 1: Biochar-boron composites: synthesis, properties, and agronomic effectiveness for eucalyptus seedlings

In this chapter, we explore the availability of boron in biochar composites made from chicken manure, shrimp shells, and sewage sludge, doped with boric acid and borax, at two pyrolysis temperatures (300 °C and 550 °C). The study involves:

1. Characterization of Composites:
   - Techniques: Fourier transform infrared spectroscopy (FTIR), scanning electron microscopy with energy-dispersive X-ray spectroscopy (SEM-EDS).
   - Chemical Extractants: Analysis using 2% citric acid, neutral ammonium citrate, and water.
   - Boron Release Kinetics: Evaluating boron release over time under different conditions.
2. Impact on Eucalyptus Seedlings:
   - Growth and Nutrient Uptake: Assessing the effects of boron-enriched biochars on eucalyptus seedlings.
   - Pyrolysis Conditions: Investigating the influence of different doping conditions and pyrolysis temperatures on micronutrient availability and plant growth.
3. Effectiveness as Fertilizer:

- Soil Types: Testing the composites in two contrasting Oxisols.
- Fertilizer Efficiency: Evaluating the performance of biochars as fertilizers for eucalyptus seedling growth.

Chapter 2: Assessing the effect of copper-biochar composites on nutrition and growth of wheat cultivated in Oxisols

This chapter focuses on the availability of copper in biochar composites derived from chicken manure, shrimp shells, and sewage sludge, doped with copper sulfate (CuS) and copper oxide (CuO) at two pyrolysis temperatures (300 °C and 550 °C). The study includes:

1. Characterization of Composites:
   - Techniques: Fourier transform infrared spectroscopy (FTIR), scanning electron microscopy with energy-dispersive X-ray spectroscopy (SEM-EDS).
   - Chemical Extractants: Utilizing 2% citric acid, neutral ammonium citrate, and water.
   - Copper Release Kinetics: Analyzing copper release rates under various conditions.
2. Impact on Wheat Seedlings:
   - Growth and Nutrient Uptake: Studying the effects of copper-enriched biochars on wheat seedlings.
   - Pyrolysis Conditions: Examining the impact of different doping conditions and pyrolysis temperatures on micronutrient availability and plant growth.
3. Effectiveness as Fertilizer:
   - Soil Types: Application in two contrasting Oxisols.
   - Fertilizer Efficiency: Testing the effectiveness of biochars as fertilizers for wheat growth.

Chapter 3: Impact of zinc-biochar composites on enhancing Zn availability, uptake, and maize yield in contrasting Oxisols

In this chapter, we investigate the availability of zinc in biochar composites made from chicken manure, shrimp shells, and sewage sludge, doped with zinc sulfate and zinc oxide, at two pyrolysis temperatures (300 °C and 550 °C). The study covers:

1. Characterization of Composites:
   - Techniques: Fourier transform infrared spectroscopy (FTIR), scanning electron microscopy (SEM).
   - Chemical Extractants: Assessing zinc release using 2% citric acid.
   - Zinc Release Kinetics: Measuring the release kinetics of zinc under various conditions.
2. Impact on Maize Seedlings:

- Growth and Nutrient Uptake: Evaluating the effects of zinc-enriched biochars on maize seedlings.
- Pyrolysis Conditions: Investigating the effects of different doping conditions and pyrolysis temperatures on micronutrient availability and plant growth.

3. Effectiveness as Fertilizer:
   - Soil Types: Testing in two distinct Oxisol soils.
   - Fertilizer Efficiency: Assessing the potential of biochars in enhancing zinc availability and improving crop performance.

REFERENCES

Anstey, T. J., Le, D. M., Li, J., Rumpel, C., & Pan, G. (2016). Synergistic interactions between biochar and fertilizer alter the nutrient dynamics and increase biomass production in a pot experiment. Soil and Tillage Research, 160, 56-63.

Ayeni, L. S., Omole, T. A., & Ojeniyi, S. O. (2012). Comparative effectiveness of different levels of poultry manure with NPK fertilizer on soil fertility improvement, growth and yield of maize. African Journal of Biotechnology, 11(50), 11024-11030.

Chen, B., Chen, Z., & Lv, S. (2007). A novel magnetic biochar efficiently sorbs organic pollutants and phosphate. Bioresource Technology, 102(2), 716-723.

Ding, Y., Liu, Y. X., Wu, W. X., Shi, D. Z., Yang, M., & Zhong, Z. K. (2017). Evaluation of biochar effects on nitrogen retention and leaching in multi-layered soil columns. Water, Air, & Soil Pollution, 231(11), 503.

Ferreira-Leitão, V. S. (2010). Avaliação do potencial de biomassas residuais para produção de etanol. Química Nova, 33(6), 1422-1427.

IBI (2015). International Biochar Initiative. Retrieved from https://www.biochar-international.org.

Jeffery, S., Abalos, D., Prodana, M., Bastos, A. C., Van Groenigen, J. W., Hungate, B. A., & Verheijen, F. G. (2017). Biochar boosts tropical but not temperate crop yields. Environmental Research Letters, 12(5), 053001.

Liu, X., Zhang, A., Ji, C., Joseph, S., Bian, R., Li, L., Pan, G., & Paz-Ferreiro, J. (2016). Biochar's effect on crop productivity and the dependence on experimental conditions—a meta-analysis of literature data. Plant and Soil, 373(1-2), 583-594.

Liu, Z., & Han, G. (2015). Production and characterization of biochar from agricultural residues. Biomass and Bioenergy, 45, 88-96.

Liu, Z., Quek, A., Kent Hoekman, S., & Balasubramanian, R. (2015). Production of solid biochar fuel from waste biomass by hydrothermal carbonization. Fuel, 103, 943-949.

Maciel, V. G. (2021). Adubação sustentável e eficiência no uso de nutrientes. Revista Brasileira de Agroecologia, 12(3), 123-134.

ONU (2019). Relatório de Desenvolvimento Humano. Organização das Nações Unidas. Retrieved from https://www.un.org.

Palansooriya, K. N., Wong, J. T. F., Hashimoto, Y., Huang, L., Rinklebe, J., Chang, S. X., Bolan, N., Wang, H., & Ok, Y. S. (2020). Response of microbial communities to biochar-amended soils: A critical review. Biochar, 2, 1-24.

Pivoto, D., Dias, T. M., Vieira, P. R., & Carvalho, P. C. F. (2018). Desafios logísticos e custos na adubação com micronutrientes. Agropecuária Catarinense, 31(2), 74-78.

Radenahmad, N., Afif, A., Petra, P. I., Rahman, S. M., Eriksson, S. G., & Azad, A. K. (2020). Proton conducting electrolytes for direct methanol and direct ethanol fuel cells–a state-of-the-art review. Renewable and Sustainable Energy Reviews, 117, 109434.

Song, X. D., Xue, X. Y., Chen, D. Z., He, P. J., & Dai, X. H. (2019). Application of biochar from sewage sludge to plant cultivation: Influence of pyrolysis temperature and biochar-to-soil ratio on yield and heavy metal accumulation. Chemosphere, 239, 124753.

CHAPTER I

BIOCHAR-BORON COMPOSITES: SYNTHESIS, PROPERTIES, AND AGRONOMIC EFFECTIVENESS FOR EUCALYPTUS SEEDLINGS

Published at Chemical and Biological Technologies in Agriculture
DOI: 10.1186/s40538-024-00645-2

Loren Chisté[1], Leônidas Carrijo Azevedo Melo[1*], Keiji Jindo[2], Carlos Alberto Silva[1]

[1]Department of Soil Science, School of Agricultural Sciences, Federal University of Lavras, Lavras, Minas Gerais 37200-900, Brazil;

[2]Agrosystems Research, Wageningen University & Research, PO Box 16, 6700 AA Wageningen, Holanda.

[*]Corresponding author: leonidas.melo@ufla.br

Abstract

Boron (B) is critical for plant growth, yet its movement in soil is often hindered by leaching and adsorption, leading to deficiencies. Tackling these issues is essential for boosting agricultural productivity, especially in plants like Eucalyptus with high B needs. This paper aims to address these challenges by evaluating B-doped biochar composites (biochar-B) that enhance B distribution and stability in the soil, focusing on Eucalyptus grandis cultivation in two distinct Oxisol types. Biochar-B composites were created using shrimp carcass (FSC), chicken manure (FCM) and sewage sludge (FSS), combined with boric acid (BA) and borax (BX), and pyrolyzed at 300 °C and 550 °C. The experimental design was a completely randomized design (CRD) with three replicates. Fourier Transform Infrared Spectroscopy (FTIR) analysis confirmed successful B integration and interaction with organic matrices, highlighting functional groups responsible for composite properties. This facilitated the development of highly predictive Partial Least Squares (PLS) regression models (R^2pred ~ 0.8). The FSC-BA composite at 300 °C showed notable thermal stability, B retention and availability, enhancing B release kinetics. These findings emphasize the importance of considering the soluble B rate in composite applications for Eucalyptus cultivation. The use of these composites provides a sustainable method for gradual B release, potentially outperforming conventional fertilization techniques. This approach may lead to improved plant growth and productivity. Further field investigations are recommended in order to validate these findings and refine sustainable fertilization strategies; thus, benefiting a range of crops.

Keywords: B-carbon complexes, pyrolysis conditions, kinetics of B release, FTIR, B availability in soil.

1. Introduction

Boron (B) is a vital trace element for numerous biochemical and physiological processes in plants. It plays a pivotal role in nucleic acid synthesis, chlorophyll formation, protein synthesis, carbohydrate transport, pollen tube growth and root development (de Mello Prado, 2021). Boron deficiency can hinder water uptake, resulting in the desiccation of growth tissues. This scenario is especially evident in eucalyptus during drought (Jha et al., 2022). Such deficiency not only obstructs reforestation efforts but also diminishes the commercial value of eucalyptus timber, which requires a substantial amount of B to thrive (Damasceno et al., 2023). However, ensuring adequate B levels in the soil is a significant challenge due to the swift depletion of traditional B supplements, highlighting the need for more reliable and effective B supplementation methods.

Boron availability in soil is influenced by pH, B source solubility, adsorption, complexation and transportation involving organic matter, metal hydroxides and clay minerals (Chen et al., 2024). The precise evaluation of B fractions faces challenges due to the intricate characteristics of soils and constraints in extraction techniques. These challenges often result in inconsistent B-release kinetics, having an impact on the nutritional management of eucalyptus plantations (Zhang et al., 2020b). B-doped biochar has shown promise in enhancing electron transfer rates, acting as an efficient carbon (C) catalyst without metal components (Liu et al., 2020). However, research on the influence of composites on the solubility and stability of B-C complexes within carbonized matrices, as well as the dynamics of B release from these materials for fertilization purposes in different soil types, remains limited. The production of B-doped biochar focuses on stable B-C interactions through complexation (Huang et al., 2019) and chelation (Ding et al., 2017), affecting structural properties and functional group density (Hao et al., 2021), offering a novel approach to B fertilization efficiency via the B adsorption mechanism when associated with biochar (Luo et al., 2023).

The selection of feedstocks and pyrolysis temperatures is crucial, influencing B and C interactions and, thus, nutrient bioavailability in soil and plants (Hao et al., 2021). Selecting ash-rich sources such as shrimp shells, chicken manure and sewage sludge is strategic, leveraging their capacity to produce biochars with fertilizing benefits (de Oliveira Paiva et al., 2024; do Amaral Leite et al., 2024; Faria et al., 2018). Generally, these wastes are discarded in landfills or used for composting, animal feed and soil amendments. Nevertheless, converting them into biochar mitigates waste disposal issues and fully harnesses their high-value properties. This process enhances nutrient cycling efficiency, improves soil health and reduces potential environmental impacts. High-temperature processes enable B to form stable covalent bonds with C, enhancing biochar structural and functional qualities (Pan et al., 2023a). The incorporation of boric acid (BA) and sodium borate (borax) (BX) not only bolsters biochar's thermal and physicochemical properties (Xin Zhang et al., 2022a) but also holds an agricultural purpose as a nutrient. This research explores the B-C interaction within biochar, which is essential for controlled releases and soil fertility improvement. By investigating these composites, our goal is to enhance sustainable agriculture by optimizing the properties of biochar, demonstrating its innovative applications in agriculture, and paving the way for more sustainable farming practices. Oxisol was selected for this study because it is the most common soil order in tropical regions and is widely affected by B deficiency, posing significant challenges for B management in plant nutrition.

This study examines the production of composites from chicken manure (FCM), shrimp carcass (FSC) and sewage sludge (FSS) doped with BA and BX, pyrolyzed at temperatures from 300 °C to 550 °C. The main intent is to assess the kinetics of B release to optimize its utilization by eucalyptus seedlings while minimizing leaching, thereby enhancing the efficiency of B fertilizers. Additionally, FTIR-based prediction models are utilized to understand chemical interactions between B and C atoms during pyrolysis, with focus on elucidating environmental processes, remediation strategies, organic waste utilization and nutrient cycling management in Oxisols.

2. Material and Methods

2.1. Preparation and Characterization of the Feedstocks

We selected three feedstocks for the synthesis of biochars and their composites: chicken manure (FCM), shrimp shell (FSC) and municipal sewage sludge (FSS). The FCM was sourced from an agricultural facility in Nepomuceno, Minas Gerais, Brazil, (Latitude: -21.236110° S; Longitude: -45.234970° W). The FSC was procured from a marine processing enterprise in Linhares, Espírito Santo, Brazil (Latitude: -19.373030° S; Longitude: -40.054680° W The FSS was obtained from a treatment facility at the Universidade Federal de Lavras, located in Lavras, Minas Gerais, Brazil (Latitude: -21.23008° S; Longitude: -44.98981° W).). Comprehensive specifications for each material are delineated in Table 1.

Table 1- Identification of feedstocks, B sources and abbreviated temperatures of synthesized biochar composites.

Acronym	Feedstock	B source
	Temperature 60 °C	
FCM	Chicken Manure	
FSC	Shrimp Carcass	no
FSS	Sewage Sludge	
	Pyrolysis temperature – 300 °C	
BCM	Chicken Manure	
BSC	Shrimp Carcass	no
BSS	Sewage Sludge	
CCM-BA	Chicken Manure	Boric Acid
CCM-BX		Borax
CSC-BA	Shrimp Carcass	Boric Acid
CSC-BX		Borax
CSS-BA	Sewage Sludge	Boric Acid
CSS-BX		Borax
	Pyrolysis temperature – 550 °C	
BCM’	Chicken Manure	
BSC’	Shrimp Carcass	no
BSS’	Sewage Sludge	

CCM-BA'	Chicken Manure	Boric Acid
CCM-BX'		Borax
CSC-BA'	Shrimp Carcass	Boric Acid
CSC-BX'		Borax
CSS-BA'	Sewage Sludge	Boric Acid
CSS-BX'		Borax

Initially, the feedstocks were subjected to air drying at room temperature in order to eliminate surface moisture. This was followed by subsequent dehydration in a forced air oven at 65 °C until a constant mass was reached. After drying, the samples were ground and passed through a sieve to obtain a uniform particle diameter of less than 0.25 mm. To inhibit rehumidification, the processed materials were subsequently stored in hermetically sealed plastic containers.

2.2. *Preparation of biochar and B-doped biochar*

Six distinct biochar specimens were produced utilizing the aforementioned feedstocks and two pyrolysis temperatures (300 °C and 550 °C). Additionally, twelve composites doped with B were created by incorporating boric acid (H_3BO_3) and borax ($Na_2B_4O_7$) obtained from ISOFAR and Exodus Scientific, aiming to reach a final B concentration of 7%. The pyrolysis process involved a controlled temperature increase at 10 °C per minute up to the target temperatures (300 or 550 °C), using a muffle furnace equipped with an airtight chamber to block oxygen infiltration. This temperature was maintained for 60 minutes, then gradually cooled to room temperature before opening the furnace. Subsequently, the biochar and composite samples were pulverized and sifted to obtain a particle size below 0.25 mm, which were then meticulously preserved for subsequent analysis.

2.3. *Characterization of Biochars and Composites*

Equations 1, 2 and 3 were employed to calculate volatile matter (VM), moisture (M) and ash concentration (As) of biochar using a modified ASTM D1762-84 method designed specifically for biochar analysis. This adaptation included pre-firing crucibles, heating them to 750 °C for six hours and cooling them to 105 °C to fully volatilize any remaining binders before the analysis took place (Johnston, 2017). The residue left after burning indicated the ash concentration (Ash) as described in Equation 3. Fixed carbon (FC) was calculated based on Equation 4 and the biochar yield (Y) was assessed using Equation 5 (ASTM International, 1984).

$$VM(\%) = \frac{DW\ at\ 105°C - DW\ at\ 950°C}{DW\ at\ 105°C}\ x100 \quad \text{(Eq. 1)}$$

$$M(\%) = \frac{RW - DW\ at\ 105°C}{RW}\ x\ 100 \quad \text{(Eq. 2)}$$

$$Ash(\%) = \frac{RW - DW\ at\ 750ºC}{DW\ AT\ 105ºC}\ x\ 100 \quad \text{(Eq. 3)}$$

$$FC(\%) = \frac{DW\ at\ 105ºC - DW\ at\ 950ºC - DW\ at\ 750ºC}{DW\ at\ 105ºC}\ x\ 100 \quad \text{(Eq. 4)}$$

$$Y(\%) = 100\ x\ \frac{biochar\ mass}{105ºC\ dried\ biomass} \quad \text{(Eq. 5)}$$

The pH and electrical conductivity (EC) of the pyrolyzed matrices and feedstocks were measured using a digital pH meter (Toledo CE, Mettler-Toledo AG) pre-calibrated with pH 4 and 7 buffer solutions (Balwant Singh , Marta Camps Arbestain, 2017). C concentration was determined using a Vario TOC cube analyzer via the dry combustion method. The Kjeldahl method quantified total nitrogen (N) concentration following digestion with concentrated sulfuric acid (Mašek et al., 2018). Nutrient concentration was analyzed using inductively coupled plasma optical emission spectroscopy (ICP-OES) after digestion with a mixture containing sulfuric acid, potassium sulfate, copper sulfate and selenium (Table S1). Quality control was maintained using certified reference materials (NIST-SRM-1573a, 2018)(Mašek et al., 2018) and blank samples in order to monitor for cross-contamination.

The levels of water-soluble B (W), 2% citric acid-soluble B (CA%) and neutral ammonium citrate (NAC) soluble B were determined via clear filtrate, following established protocols (Brasil, 2014). B concentration in the samples was obtained using ICP-OES analysis. To compare the B solubility of the samples, a B index was calculated, considering the ratio of the soluble fractions of B (B-W, B-NAC and B-CA%) and the total B concentration of each matrix, according to (Eq. 6).

$$B\ (\%) = \frac{Soluble\ B\ (g.kg-1)}{Total\ B\ (g.kg-1)} x\ 100 \qquad \text{(Eq. 6)}$$

2.4. *Fourier Transform Infrared Spectroscopy (FTIR)*

Spectral signature characterization was performed in the mid-infrared region using an Agilent® Cary 630 FTIR spectrometer with a ZnSe-ATR crystal (Agilent Technologies, U.S.), with a scanning resolution of 4 cm^{-1}, in the wavelength range of 4000 to 650 cm^{-1}. Each FTIR spectrum was normalized (Liberda et al., 2021). The interpretation of the spectra and the identification of their respective spectral bands detected by the FTIR apparatus employed specific libraries and bands of biochars treated with B, described in (Khan et al., 2017).

2.5. *Scanning Electron Microscope (SEM)*

The scanning electron microscope (SEM) analysis was conducted using a JSM-7610F Schottky Field Emission Scanning Electron Microscope (JEOL, Tokyo, Japan) at the Electron Microscopy and Ultrastructural Analysis Laboratory, within the Universidade Federal de Lavras Department of Phytopathology. Samples were prepared by oven drying 0.5 × 0.5 × 0.5 cm non-conductive pieces, mounting them on stubs with double-sided C tape and applying a C bath.

2.6. *Boron Release Kinetics*

A controlled incubation experiment was conducted to evaluate the kinetics of B release from pyrolyzed matrices. A composite sample weighing 1.0 g was transferred to a 50 mL container for incubation. Falcon tubes, combined with 20 mL of 0.1 mol L^{-1} citric acid (2% concentration) were horizontally stirred at 90 rpm and leachate was collected at predetermined intervals: 15 minutes, 30 minutes, 1 hour, 2, 4, 12, 24, 48, 72, 120 and 250 hours. After each extraction, the tubes were centrifuged for 5 minutes at 3500 rpm and the supernatant was collected for determination using ICP-OES.

2.7. *Agronomic Efficiency of the Composites*

The study was conducted at the Universidade Federal de Lavras, specifically in the Laboratory for the Study of Soil Organic Matter (LEMOS) at the Department of Soil Science, in Brazil. Eucalyptus seedlings were cultivated under greenhouse conditions using surface soil samples (0 - 20 cm) of representative Oxisols obtained within the university's campus and named dystrophic red-yellow Oxisol (RYL) and typical dystrophic red Oxisol (DRL). A detailed characterization is shown in Table 2.

Table 2. The main chemical and physical characteristics of Oxisols used in eucalyptus cultivation.

Oxisol	pH	C	Clay	Silt	Sand	N	P	K	Ca^{2+}	Mg^{2+}	B
		---------- g kg^{-1} ----------				--- mg dm^{-3} ---			cmol dm^{-3}		mg dm^{-3}
RYL	4.7	4.5	460	85	455	329	6.1	218	0.8	0.4	0.1
DRL	4.5	19.8	770	100	130	2580	8.3	30.1	0.3	0.2	0.06

* RYL- Red Yellow Oxisol (medium texture); DRL- Dystroferric Red Oxisol; pH in a soil-water-Ratio of 1:2.5; C: C determined (dry combustion) in an automatic TOC analyzer; clay, silt and sand analyzed by the Boyoucos method. All methods are described in detail (Teixeira et al., 2017a); N: total nitrogen – Kjeldahl; P: available phosphorus determined by the resin soil test; K, Fe^{2+}, Mn^{2+}, Cu^{2+} and Zn^{2+}: available determined by the Mehlich^{-1} soil test; B: Hot water extractor; exchangeable calcium (Ca^{2+}), exchangeable magnesium (Mg^{2+}) extracted by a 1 mol L^{-1} KCl solution soil test.

The soil samples were air-dried, sieved (2 mm) and treated with calcium (Ca) and magnesium (Mg) carbonates ($CaCO_3$ and $MgCO_3$) to attain a pH of 5.5 ± 0.2 (Teixeira et al., 2017a), so as to optimize conditions for eucalyptus growth and ensure Ca and Mg availability in the soils. The study employed a completely randomized design, with three feedstocks pyrolyzed at two temperatures and enriched with two B sources, totaling 12 B composites. Boron was applied to 1.8 mg kg^{-1} of soil using three replicates. Seedlings were planted in pots containing 3 kg of soil, which had additional fertilization with macro and micronutrients and irrigation was maintained at ~70% of the maximum water-holding capacity.

Soil solution samples from each pot were collected using Suolo Acqua® (do Carmo et al., 2016) at 1, 13, 28 and 70 days, filtered (<0.45 µm) and measured for pH (Mettler Toledo benchtop pH meter) and B concentration via ICP-OES. Also, available B in soil (extracted in hot water) was determined using a spectrophotometer at the beginning (day 3) and at the end (day 100) of the experiment (Teixeira et al., 2017a). Subsequently, the plants were harvested, oven-dried at 65 °C for 72 h, their shoot dry matter (SDM) and root dry matter (RDM) were recorded, then they were ground in a mill (<1 mm) and digested in a mixture of nitric and perchloric concentrated acids (Silva, 2009) whilst B was measured in ICP-OES. B uptake in the shoot dry matter of Eucalyptus (g) was calculated by multiplying the total nutrient concentration in the plant tissue (mg g^{-1}).

2.8. Statistical analysis

Data was submitted through a Two-Way ANOVA and when there was a significant difference ($p<0.05$), the means of the treatments were compared with each other using Tukey's test ($p<0.05$) (after meeting the ANOVA's analysis assumptions). Multivariate analyses were used to measure, explain and predict the relationship between B properties and pools in the composites. All statistical analyses were performed in R software using the agricolae, factoextra, FactoMineR, pvclust, corrplot, tideverse and nlstools packages (R-Core-Team, 2020).

The ATR-FTIR spectral signatures of the samples were used to generate and validate the PLS regression models and a total of 54 observations were used for the calibration and generation of the PLS mathematical models. In contrast, 13 samples (20 %) were used for independent random external validation. The models were evaluated by analyzing the square root of the mean calibration error ($RMSE_{cal}$), coefficient of determination (R^2) and coefficient of calibration (R^2_{cal}). The model was cross-validated, using cross-validation RMSE ($RMSE_{cv}$), y-randomization RMSE ($RMSE_{y-rand}$), cross-validation R^2 (R^2_{cv}) and y-randomization R^2 (R^2_{y-}

rand). The number of latent variables was determined by the lowest $RMSE_{cv}$ value of the 54 observations used for validation and used to calculate RMSE ($RMSE_{pred}$) (Eq. 8) and R^2 (Eq. 9) prediction (R^2_{pred}) (Kiralj and Ferreira, 2009). Other validation parameters, such as R^2 between experimental and predicted values for the test dataset ($r^2{}_m$) and R^2 of randomization prediction y (r^2_p) were calculated based on the equations (Eq. 10 and 11) (Roy et al., 2009). The graphic images of the FTIR were obtained using the Origin Pro 8.5 software (OriginLab Co., Northampton, USA).

$$RMSE = \sqrt{\frac{\sum_{i=1}^{n}\left(yi - \hat{Y}i\right)^2}{n}} \qquad \text{(Eq. 7)}$$

$$R^2 = 1 - \frac{\sum_{i=1}^{n}\left(yi - \hat{Y}i\right)^2}{\sum_{i=1}^{n}(yi - \bar{Y}i)^2} \qquad \text{(Eq. 8)}$$

$$r_m^2 = R^2 \left[1 - (R^2 - R_0^2)^{\frac{1}{2}}\right] \qquad \text{(Eq. 9)}$$

$$r_p^2 = R_{cal}^2\left(R_{cal}^2 - R_{y-rand}^2\right)^{\frac{1}{2}} \qquad \text{(Eq. 10)}$$

The dataset of B release kinetics in 2% citric acid - CA% was adjusted for different nonlinear mathematical models as an output of the relationship between the incubation time *versus* the amount of B released from each nutrient source. The following mathematical models were fitted to the kinetics B dataset: Elovich model (Eq. 12), simple exponential model (Eq. 13), power function (Eq. 14) and hyperbolic model (Eq. 15).

$$Nt = a + blnt \qquad \text{(Eq. 11)}$$

$$Nt = N0\left(1 - e^{-kt}\right) \qquad \text{(Eq. 12)}$$

$$Nt = a\,x\,b^t \qquad \text{(Eq. 13)}$$

$$Nt = \frac{N0\,x\,t}{(N0\,x\,b + t)} \qquad \text{(Eq. 14)}$$

Where: Nt= fraction of B released at the evaluated time; a= initial concentration of B released; b = B released at a constant rate; t= release time (hour); N0= maximum amount of B released during the kinetic study. The best model was selected based on the highest coefficient of determination (R^2), the lowest value of the root mean square of error (RMSE) and the lowest value of the Akaike information criterion (AIC) (Akaike, 1979). Principal component analysis (PCA) was performed to evaluate the relationship between the properties of the composites produced in this study.

3. Results and Discussion

3.1 Chemical properties of Biochar and Composites

Research demonstrated that there were distinct variations in biochar characteristics influenced by feedstock type and pyrolysis temperature (Table 3). Elevated temperatures generally increased biochar pH, ash concentration and fixed carbon (FC), enhancing the potential for soil amendment and C sequestration. Notably, the electrical conductivity (EC) of biochar decreased in BSC' feedstock due to the formation of stable inorganic compounds at higher temperatures. Additionally, while higher temperatures reduced biochar yield and volatile matter across all feedstocks, the loss of C and N was particularly pronounced in FSC due to its higher susceptibility to thermal degradation. This phenomenon can be attributed to the composition of FSC, which is mainly amino acids and proteins and is prone to degradation at higher temperatures due to the higher N concentration (Leng et al., 2020). The temperature rise led to a decrease in VM, implying an increase in the concentration of inorganic elements in the pyrolyzed materials (Piash et al., 2022), due to the progressive loss of acidic surface functional groups, primarily aliphatic carboxylic acids (Almutairi et al., 2023). This caused an increase in pH and aromatic character of the carbonized matrices at 550 °C (Rimena R Domingues et al., 2017). However, the extent of this pH increase was found to be dependent on the pyrolyzed feedstock, as reported in other studies for FCM (Carneiro et al., 2021), FSC (Salawu et al., 2022) and FSS (Xin Zhang et al., 2022a).

Table 3. Biochar properties as influenced by feedstock.

Biochar	pH	EC	Yield	VM	Ash	FC	Elemental Composition	C: N Ratio
		(dS m^{-1})	---------------------------------(%)---------------------------------					

							C	N	C: N
BCM	9.1	6.4	69	57	52	9.3	35	2.1	16.6
BCM’	10.7	8.2	53	56	60	11.1	26	1.9	13.1
BSC	9.2	7.3	81	72	32	3.9	41	6.5	6.4
BSC’	10.4	2.9	60	53	60	12.5	25	2.4	10.7
BSS	6.2	1.3	88	34	71	4.8	16	2.1	7.6
BSS’	7.1	1.5	69	28	78	5.4	12	1.2	10.3

Values are mean ± standard deviation (n = 3), except yield (%) (n = 1); EC: electrical conductivity; VM: volatile matter; Ashes; FC: fixed carbon; C: Carbon; N: nitrogen; C/N: carbon/nitrogen ratio. BCM: chicken manure biochar at 300 °C; BCM’: chicken manure biochar at 550 °C; BSC: shrimp shell biochar at 300 °C; BSC’: shrimp shell biochar at 550 °C; BSS: sewage sludge biochar at 300 °C; BSS’: sewage sludge biochar at 550 °C.

There was an increase in EC with the rise of pyrolysis temperatures owing to the optimization of conductive properties possibly due to the greater presence of more soluble salts (Almutairi et al., 2023), except for BSC’, which reduced EC with the intensification of the carbonization process. Additionally, an increase in pyrolysis temperature led to a reduction in biochar yield, VM and C and N concentrations across all biochars. These changes are attributed to enhanced thermal degradation, chemical transformations and volatilization of organic compounds from the feedstocks at higher temperatures (Ippolito et al., 2020). The ash and FC concentration relatively increased with pyrolysis temperatures, possibly due to the accumulation and formation of compounds such as hydroxide and carbonate, which elevate the FC (Rafique et al., 2020) and the pH values for most biochars (Ippolito et al., 2020).

Our study investigated the impact of B sources, feedstock types and pyrolysis temperatures on biochar properties, as detailed in Table 4. The incorporation of B into biochars, specifically in the form of BA, led to a reduction in acidification across several samples (CCM-BA, CCM-BA', CSC-BA, CSC-BA', CSS-BA, CSS-BA'), with decrease values ranging from 6.4% to 28.0% compared to controls. This reduction is linked to the swift removal of organic compounds and the introduction of basic cations. Elevated pyrolysis temperatures increased the pH in certain BA-doped samples (CCM-BA', CSC-BA', CSS-BA'), with increase values between 7.0% and 16.7%.

Table 4. Basic characterization of the composites.

Composite	pH	EC	Yield	VM	Ashes	FC	Elemental Composition		C:N Ratio
		(dS m^{-1})	--- (%)--						
							C	N	C:N
CCM-BA	6.6±0.1	9.0±0.0	70	45±0.0	47±0.0	6.0±0.0	19.9±0.1	3.6±0.0	5.6
CCM-BA'	7.7±0.0	9.6±0.0	55	37±0.0	35±0.0	24.0±0.0	20.2±0.1	1.9±0.0	10.7
CCM-BX	9.3±0.0	16.3±0.0	72	54±0.0	43±0.0	1.4±0.0	21.6±0.1	3.4±0.0	6.3
CCM-BX'	9.3±0.1	16.0±0.0	53	38±0.0	28±0.0	33.0±0.0	19.5±0.1	1.5±0.0	13.4
CSC-BA	7.1±0.0	9.0±0.0	72	52±0.0	40±0.0	5.8±0.0	21.1±0.1	5.3±0.0	3.9
CSC-BA'	7.6±0.1	5.6±0.0	48	60±0.0	22±0.0	18.0±0.0	16.5±0.1	2.6±0.0	6.4
CSC-BX	9.2±0.0	14.9±0.0	70	52±0.0	41±0.0	3.7±0.0	18.2±0.1	2.6±0.0	6.9
CSC-BX'	9.7±0.0	11.0±0.0	47	30±0.0	26±0.0	42.0±0.0	16.7±0.0	2.2±0.0	7.5
CSS-BA	5.8±0.0	3.2±0.0	75	39±0.0	38±0.0	20.0±0.0	9.7±0.1	3.4±0.0	2.8
CSS-BA'	6.3±0.1	1.30±0.0	62	36±0.0	15±0.0	49.0±0.0	8.7±0.0	1.0±0.0	8.3
CSS-BX	9.2±0.0	14.0±0.0	77	13±0.0	37±0.0	53.0±0.0	12.1±0.1	1.7±0.0	6.9
CSS-BX'	9.1±0.0	8.5±0.0	63	21±0.0	12±0.0	66.0±0.0	9.7±0.0	1.0±0.0	9.9

Values are mean ± standard deviation (n = 3), except yield (%) (n = 1); VM: volatile matter; Ashes; FC: fixed carbon; C: Carbon; N: nitrogen; C/N: carbon/nitrogen ratio. Composites: CCM-BA: chicken manure + boric acid at 300 °C; CCM-BX: chicken manure + borax at 300 °C; CCM-BA': chicken manure + boric acid at 550 °C; CCM-BX': chicken manure + borax at 550 °C; CSC-BA: shrimp waste + boric acid at 300 °C; CSC-BX: shrimp carcass + borax at 300 °C; CSC-BA': shrimp carcass + boric acid at 550 °C; CSC-BX': shrimp carcass + borax at 300 °C; CSS-BA: sewage sludge + boric acid at 300 °C; CSS-BX: sewage sludge + borax at 300 °C; CSS-BA': sewage sludge + boric acid at 550 °C; CS-BX': sewage sludge + borax at 550 °C.

Conversely, BX-doped biochars (CCM-BX’, CSC-BX’) exhibited pH reductions of 13.1% and 6.7%, respectively. In contrast, CCM-BX, CSS-BX and CSS-BX' samples showed pH increase, indicating a shift towards alkaline conditions. The increased values were 2.2%, 48.4% and 28.2%, respectively, with CSC-BX remaining stable. High pyrolysis temperatures slightly increased CSC-BX' pH by 5.4%, while CSS-BX' had a 1.1% decrease. The introduction of B significantly influences the thermal decomposition of biochars, affecting the functional group composition from feedstocks and the acid-base equilibrium of the end product. These alterations impact the characteristics and stability of the biochar composites.

Investigating the catalytic effects of B-doped biochar during pyrolysis uncovers significant pH alterations and the creation of active chemical sites within the carbonized structures, as demonstrated by Chen et al. (C. Chen et al., 2022). The atomic radius similarity between B and C leads to unique structural interactions that are pivotal for enhancing the biochar composites' physicochemical attributes, a concept further detailed by Kim et al. (Kim et al., 2023). BA application typically maintains the composite pH near neutrality due to its weak acid nature and is prone to donating H^+ ions. In contrast, BX shifts the environment towards alkalinity by releasing borate ions and elevating the OH^- ion concentration in the synthesis medium, corroborating other findings (Yang et al., 2011). Such variations in pH modulation are crucial, given the influence of active sites on the composites' physicochemical transformations (H. Zhang et al., 2023). Other researchers (Bo and Guo, 2013) point out that the distinct pH modulation effects of BA and BX underscore the nuanced impact of biochar-B properties. This emphasizes the criticality of choosing appropriate B sources for targeted environmental applications, offering a comprehensive perspective on their role in enhancing soil health and environmental sustainability.

While conducting this research, we observed a general trend where higher pyrolysis temperatures increased the EC in all biochar composites except for the CSS-BA composite. This particular composite showed a 13.3% reduction in ash concentration compared to its non-B-doped counterpart. Conversely, the CCM-BA composite experienced a 6.7% increase in ash concentration relative to its biochar-B variant, indicating that pyrolysis temperatures generally boosts EC.

Contrastingly, BA composite EC diminished with rising pyrolysis temperatures, an effect that was not observed when BX was used for doping, potentially due to increased deprotonation of groups. This process likely facilitates a new electronic structural modulation of the C matrix, as suggested by Chen et al. (C. Chen et al., 2022). Supporting literature indicates that pH elevation leads to deprotonation, altering EC by enhancing the medium's conductivity through the introduction of charged ions (Schmidt et al., 2021). This is significant because EC is directly influenced by charged ions, suggesting a more efficient electron conduction pathway.

Our analysis demonstrated a notable improvement in composite yields when B was incorporated into FCM C matrix composites. Specifically, B-doping at a pyrolysis temperature of 300 °C resulted in a 5.1% increase in yield with the BX-doping method, while at 550 °C, BA-doping led to a 4.4% increase. Conversely, the beneficial effects of B-doping were not evident in biochars from alternative feedstocks, where yields declined regardless of the doping method. Minimal impact on yields was observed from B-doping in feedstock-B mixtures. What is noteworthy is that the composites CCM-BX, CSC-BA and CSS-BX recorded the highest average yields of 72.5%, 71.8% and 77.3%, respectively. This suggests that B acts as a potent chemical activator in the carbonization process, promoting the development of a more favorable pore structure within the biochar, thereby enhancing yield. Our findings align with those of Zhang et al. (Zhang et al., 2020b), who also identified B sources as advantageous activators for biochar yield enhancement.

The VM concentration in CSC-BA', CSS-BA and CSS-BA' composites was increased by 13.7%, 14.7% and 28.8%, respectively, compared to their unmodified biochar counterparts, reaching levels of 60%, 39% and 36%. Typically, the VM concentration decreases as the pyrolysis temperature increases. However, an unexpected rise in VM by 15% and 68.5% for CSC-BA' and CSS-BX', respectively, from 300 °C to 550 °C, indicates more intense pyrolysis conditions. This suggests that B-doped biochars might follow unique thermal decomposition pathways, increasing VM production at higher temperatures.

Furthermore, while VM preservation usually increases with pyrolysis temperatures, reducing the emissions of volatile gases and liquids, CSC-BA' and CSS-BA' showed an increase in VM. This increase could be due to the preferential loss of less stable molecular oxygen (O), while more stable B structures remain (Huang et al., 2023). Additionally, an increase in aromaticity, associated with higher losses, reduces substance volatility. This process results in a more stable and less volatile composition, potentially offering benefits for using B to improve catalytic activity (Huang et al., 2023) and proposing a non-radical degradation pathway based on direct electron transfer, especially for FSC and FSS matrices.

Composites CCM-BA, CSC-BA and CSS-BA, produced at 300 °C, exhibited the highest ash concentrations, with 47%, 40.1% and 38.5%, respectively. These concentrations decreased as the temperature increased, showing an inverse relationship between temperature and ash concentration. This phenomenon contrasts with the increases in ash concentration observed in another feedstock-derived biochar (CSC-BA and CSC-BX), which were 26.5% and 30.3%, respectively. This underscores the significant impact of the property of sugarcane FSC feedstock, enriched with minerals such as Ca, P and Mg, which show greater resistance to volatilization during pyrolysis (Yang et al., 2021).

The unique mineral composition of FSC feedstock is crucial for the varied ash concentration outcomes following pyrolysis. Due to their thermal stability, these minerals tend to accumulate in higher concentrations after pyrolysis at elevated temperatures (Saha et al., 2023). Specifically, calcium carbonate ($CaCO_3$) present in FSC decomposes into calcium oxide (CaO) and carbon dioxide (CO_2) during the process, with CaO contributing significantly to the high ash concentration of the biochar. In contrast, CO_2 is volatilized (Rødde et al., 2008). Additionally, the thermal degradation of chitin found in FSC results in an ash-rich residue due to its N and mineral concentration (Rødde et al., 2008). These variations in ash concentration, especially the notable increases in CSC-BA and CSC-BX, highlight the influence of feedstock composition on pyrolysis and the resulting characteristics.

The incorporation of BX into the FSS matrix significantly catalyzed an increase in FC concentration, achieving a rise of over 1000% when compared to traditional biochars. This notable enhancement was especially evident in the CCM-BX' and CSC-BX' composites at higher temperatures. The relationship between pyrolysis temperatures and the FC concentration is strongly positive, highlighting the effectiveness of C preservation within the matrix. This relationship indicates that at higher temperatures, C forms more robust bonds with the matrix, which enhances stability. This effect is crucial for the functionality of BA-based composites for thermal stability (Zhang et al., 2020a), where B atoms substitute C atoms. This substitution is facilitated by the similarity in their atomic radii and the integration of B into the C sp^2 network (Gao et al., 2021), thereby enhancing structural integrity and C preservation during pyrolysis, boosting the FC concentration. Additionally, this finding paves the way for optimizing C structuring at various scales, including morphology, crystalline parameters and the B-doping environment (Wu et al., 2022), underlining the materials' versatility and efficacy in C preservation.

At the pyrolysis temperature of 550 °C there was a decrease in the total N concentration in the biochar (Table 3). However, BA-containing composites, specifically CCM-BA, CSC-BA and CSS-BA, exhibited N preservation, with increases of 71%, 8.3% and 62%, respectively, compared to pristine biochars. This preservation can be attributed to the ability of B to act as a stabilizing agent for N. B forms complexes with nitrogen molecules, reducing volatilization during pyrolysis due to the interaction between the empty p orbital of B and the partially filled p of elements such as N and O (Wang et al., 2021).

On the other hand, adding BX reduced N concentration, except for CCM-BX, which recorded an increase of 62%. High-temperature treatment at 550 °C with BX-doping resulted in composites with a high C/N ratio, notably in CCM-BX (13.4), CSC-BX (7.5) and CSS-BX (9.9), when compared to pristine biochars. BA-doping led to lower C/N ratios, suggesting that the association of N concentration with the porous structure of the biochar helps preserve N during pyrolysis or minimizes the loss of nutrients to the gas phase during carbonization. Conversely, compositions that exhibited decreased ash, C and N concentration indicated that the residues were more readily volatilized or converted into gases, thereby diminishing B levels in alkaline composites due to reduced polymerization. Consequently, this leads to a less condensed C structure that is more vulnerable to thermal degradation (Yang et al., 2021).

The FSC feedstock is rich in proteins, chitin and N, which decompose during pyrolysis, potentially releasing N as ammonia (NH_3) or incorporating it into the biochar structure, enhancing the adsorption and retention of nitrogenous functional groups. The presence of BA-doping revealed a chemical bonding between B and N, forming amino-borane complexes and the interaction of nucleophilic sites in amides with boranes, creating thermally stable bonds (Haque et al., 2020). This stability is influenced by the electronic value (Haque et al., 2020) of B-substituted groups, reducing the likelihood of decomposition and preserving the concentration within the matrix.

This research demonstrated that the behavior of B in doped materials significantly varies based on the feedstock type and the doping agent used, as well as the pyrolysis temperatures employed. It was noted that CCM-BA showed a 16.8% reduction in B concentration. The FCM, being rich in volatile organic compounds, suggests that chemical reactions or thermal decomposition of certain manure components may affect B retention, attributing to the higher volatility of BA at elevated temperatures which facilitates B loss during pyrolysis. Conversely, CSC-BA (138 g kg^{-1}) and CSS-BA (146 g kg^{-1}) exhibited increases in B concentration of 3.4% and 14.4%, respectively (Table 5). This phenomenon could be explained by the formation of more stable structures that incorporate B, possibly due to the interaction of BA with specific components such as chitin and various organic and inorganic compounds, which may form structures that encapsulate B, preventing its volatilization and potentially forming stable B-organic compounds at high temperatures.

Both CCM-BX and CCM-BX’ maintained stable B levels when doped with BX. BX, being a thermally more stable B compound than BA, tends to integrate into the matrix more efficiently, preventing loss during pyrolysis. In contrast, CSC-BX and CSS-BX showed decreases of 19.4% and 4.4%, respectively, while CCM-BX' displayed thermal stability differing from the other composites. These results suggest that although BX forms stable structures with some organic components, it may not interact as effectively with substances in these other feedstocks; otherwise, these substances may facilitate the degradation of BX at higher temperatures.

Furthermore, the increase in total B concentration with rising pyrolysis temperatures in BA-doped composites, which enhances the microstructure and improves oxidation resistance, aligns with the observations of Smith et al. (Sui et al., 2021), who noted improved nutrient stabilization in biochar under high thermal conditions. However, the reduction in total B concentration in BX-doped composites at higher temperatures highlights the complex interactions during pyrolysis that may involve decomposition and chemical transformations (Waclawska, 1995), potentially affecting how B is incorporated into biochar (Labanya et al., 2022). The observed volatilization of B at elevated temperatures reflects the findings of Jones et al. (Waclawska, 1995), who documented the susceptibility of certain B compounds to thermal degradation, thereby reducing the amount of B retained in biochar and impacting its stability.

Table 5. Boron pools in biochar-based composites

	Boron (B)						
Composite	W	T	NAC	CA%	W Index	NAC Index	CA% Index
	------------------------(g kg^{-1}) ------------------------				-----------------(%)----------------		
CCM-BA	1.6±0.1	166.7±0.1	101.5±4.9	80.9±0.2	0.9±0.1	60.9±2.9	48.5±0.1
CCM-BX	0.9±0.1	75.6±0.1	53.2±1.9	70.7±0.3	1.2±0.1	70.5±2.6	93.6±0.4
CCM-BA'	2.1±0.1	138.7±0.1	100.0±3.1	86.6±6.3	1.5±0.1	72.1±2.2	62.4±4.6
CCM-BX'	1.0±0.1	75.5±0.1	55.5±0.8	56.3±4.0	1.4±0.1	73.5±1.0	74.5±5.4
CSC-BA	2.4±0.1	133.2±0.1	125.9±4.8	90.0±1.1	1.8±0.1	94.5±3.6	68.2±0.8
CSC-BX	1.6±0.1	91.3±0.1	88.3±0.8	89.8±1.0	1.8±0.1	96.8±0.9	98.4±1.2
CSC-BA'	2.6±0.1	137.7±0.1	132.5±1.9	83.5±3.1	1.9±0.1	96.2±1.3	60.7±2.3
CSC-BX'	1.6±0.1	73.6±0.1	70.8±0.7	56.3±0.1	2.2±0.1	96.2±0.7	61.7±0.2
CSS-BA	2.2±0.1	127.5±0.1	114.9±3.1	83.2±6.4	1.7±0.1	90.1±2.5	65.2±5.0
CSS-BX	1.1±0.1	66.2±0.1	57.0±0.9	50.0±1.0	1.7±0.1	86.0±1.3	75.5±1.5
CSS-BA'	2.0±0.1	145.8±0.1	113.6±2.6	64.1±5.8	1.3±0.1	77.9±1.8	44.0±3.9
CSS-BX'	1.1±0.1	63.3±0.1	61.2±1.0	35.8±0.3	1.8±0.1	96.8±1.6	56.6±0.4

Values are mean (n = 3); B in H_2O was determined ± 0.01 in a solution of H_2O at a ratio of 1:10 (w/v); concentration of soluble B in total (T) was determined by total digestion of the composites; B in neutral ammonium citrate water (NAC); B in concentration of B soluble in citric acid at 2% (CA%); H_2O Index, NAC Index and CA% Index represent the B concentration in relation to the extractors and the total B concentration. Composites: CCM-BA: chicken manure + boric acid at 300 °C; CCM-BX: chicken manure + borax at 300 °C; CCM-BA': chicken manure + boric acid at 550 °C; CCM-BX': chicken manure + borax at 550 °C; CSC-BA: shrimp waste + boric acid at 300 °C; CSC-BX: shrimp carcass + borax at 300 °C; CSC-BA': shrimp carcass + boric acid at 550 °C; CSC-BX': shrimp carcass + borax at 300 °C; CSS-BA: sewage sludge + boric acid at 300 °C; CSS-BX: sewage sludge + borax at 300 °C; CSS-BA': sewage sludge + boric acid at 550 °C; CS-BX': sewage sludge + borax at 550 °C.

Water solubility assessments showed that CSC-BA and CSC-BA' composites have higher immediate B availability, making them particularly effective for soil applications. The enhanced total B concentration due to BA-doping suggests that these composites could offer prolonged B supplementation. The solubility and availability metrics, specifically NAC and CA%, indicate that CSC-BA and CSC-BA' are well-suited for agricultural applications, with CSC-BX demonstrating an impressive CA% of 98.4%, showcasing its effectiveness in B solubility and its potential to facilitate B distribution in acidic soils.

The water solubility of B in the CSC-BA and CSC-BA' composites suggests they can provide immediate B availability to plants, which aligns with the findings of Shireen et al. (Shireen et al., 2018), who emphasized the importance of micronutrient accessibility for plant health. The rapid solubility of B in these composites indicates their utility in quickly addressing B deficiencies in agricultural settings, potentially enhancing soil fertility and crop yield.

The significant CA% index observed in the BX composites suggests their capacity to interact with metal ions, enhancing the solubility of these metals through the formation of chelated complexes. This is in line with another paper (Omiri et al., 2022), which emphasized the role of biochar composition and modification in effective dye degradation. Meanwhile, the NAC index observed in the BA composites indicates that these composites can form soluble complexes under neutral pH conditions without necessarily undergoing an acidification reaction (Morais et al., 2023).

3.2 Infrared Spectroscopy

The detection of hydroxyl groups (-OH) with peaks spanning 3.100 to 3.500 cm^{-1} indicates the presence of carboxyl, phenols, alcohols and water (Figure 1). This range suggests possible changes in amide compounds, such as dehydration or decomposition, illustrated in Figures 1(a) and 1(c). The retention of hydroxyl groups and the distinct peak linked to the B-O/B-C bond, as shown in Figures 1(a) and 1(b), indicate the effective integration of B atoms into the pyrolyzed matrix. This integration not only enhances the composite's physicochemical properties but also contributes to increased B solubility in water, as observed by Zhang et al. (Xin Zhang et al., 2022a).

The observation of CH aliphatic stretching vibrations between 2.920 and 2.885 cm^{-1}, alongside a specific vibration at 2.351 cm^{-1} indicating C-CO_2 stretching, validates the presence of porous structures with significant graphitization. This observation, indicating disordered defects, is further confirmed by characteristic CH stretching peaks at 3220 cm^{-1} in CSC-BA' and CSS-BA', and by our SEM findings (Figure 5) (Du et al., 2021).

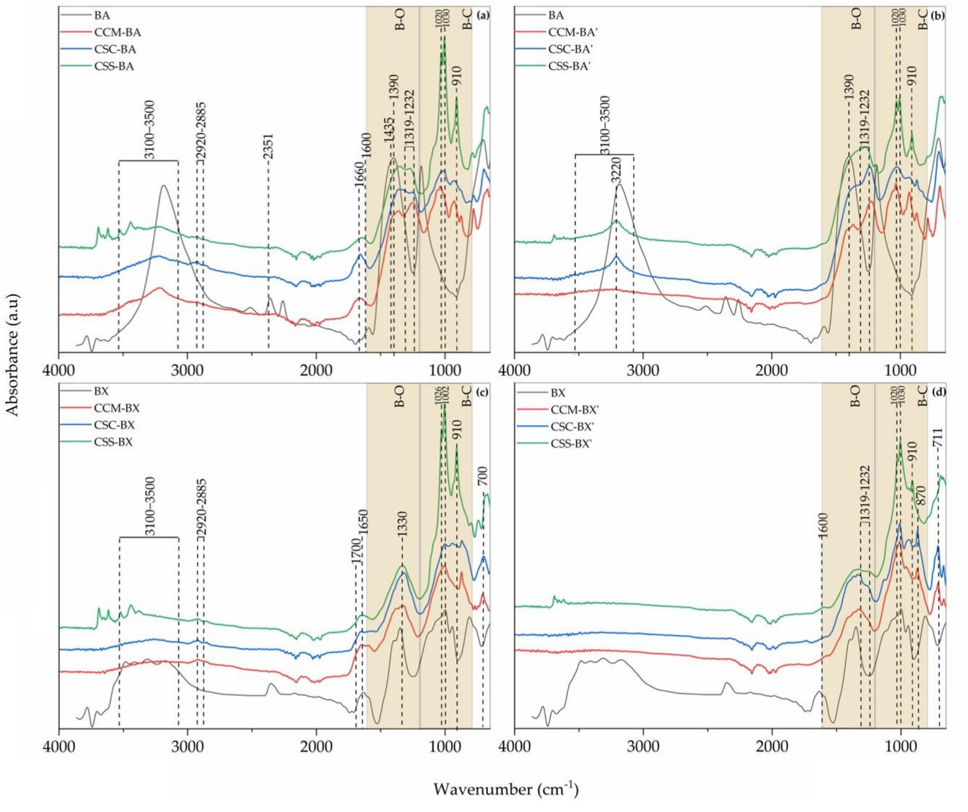

Figure 1. Fourier transform infrared spectroscopy (FTIR) and the main peaks and characteristics of the chemical groups found in composites produced from biochar doped or not with boric acid or borax. (a) composites doped with boric acid at 300 °C; (b) composites doped with boric acid at 550 °C; (c) composites doped with borax at 300 °C and (d) composites doped with borax at 550 °C.

An intensified band near 1600 cm^{-1} points to the presence of aromatic (C=C, C=N), ketonic/aldehydic (C=O) and steric (−COO) vibrations, according to Ateş et al. (Ateş et al., 2023b), crucial for the composite's chemical characterization, as depicted in Figures 1(b) and 1(d). The B-C bond vibration observed at 1020 cm^{-1} aligns with previous research (Jia et al., 2013), highlighting the significance of infrared vibrations associated with B-C bonds. This suggests that a meaningful interaction occurs in these groups within the composites' structures and confirms the origin of the aromatic C=C bond at 1430 cm^{-1}, essential for understanding the physicochemical transformations triggered by functional group modifications at the lower pyrolysis temperature of 300 °C.

Notably, amide groups are distinguishable in the 1650 to 1700 cm^{-1} range, as detailed in Figure 1(c). Moreover, Zhou et al. (Zhou et al., 2020) emphasized the enhancement in performance and stabilization of B when associated with N-containing borate ester groups, facilitated by the lone electron pairs on N that complex B empty 2*p* orbit. This interaction, revealing a substantial presence of B and N elements (Table 3), demonstrates the functional groups' superior activity in BA-doped composites at both 300 °C and 550 °C.

Signals around 1435 cm^{-1} might indicate carbonyls or carbonates, with stretching in carboxylic acids between 1319 and 1232 cm^{-1}, especially notable in composites produced at 300 °C. The B-doped C-rich materials exhibit configurations in both the graphitized and surface edge regions, more so with BA-doping at 550 °C. This outcome, likely due to carbonyl-like groups (C=O) that form C-O-B type bonds and groups, alongside carboxylic acids (-COO), suggests enhanced oxygen activation compared to BX-doping, which displays less interaction with C under pyrolysis (Sun et al., 2018b).

The role of B in O activation, improving surface charge distribution and inducing polarization, is well documented (Friedrich et al., 2020; Quílez-Bermejo et al., 2020) and leads to the formation of acidic functional groups. Conversely, BX-doping tends to make the composites more alkaline by introducing unpolarized basic groups. The presence of B-O and B-O-B bonds around 1390 cm^{-1}, indicative of B incorporation via borates or esters, is particularly prominent in composites processed at 300 °C. This enhances interactions with certain feedstocks, improving the composite's chemical properties like acidity and polarity, as elaborated in Figure 1(b) (Xu Zhang et al., 2022) and highlighted by recent findings that highlight the importance of these bonds in biochar activation with BA.

Spectral analysis within 800-1200 cm^{-1} and 1200-1600 cm^{-1} showcases interactions of B-C and B-O groups, respectively, without evidence of B-B bonds. Changes in the 1180-950 and 950-750 cm^{-1} regions hint at P-O-B bonding in BX-doped samples, with significant shifts observed for pyrolysis temperature changes, as shown by the absorption peaks at 3419 cm^{-1} for (-OH) in BX-doped composites produced at 300 °C and water stretching vibration deformation around 1330 cm^{-1} with temperature increase, as illustrated in Figures 1(c) and 1(d). Considering this relationship, using BA with its B–Asymmetric stretch should yield an active peak at around 1200-1600 cm^{-1}, while BX has a broad band of asymmetric stretching with a peak around 800-1000 cm^{-1} (Nakamoto, 2009).

Principal Component Analysis (PCA) and cluster analysis revealed significant effects on the composites, indicating that B is incorporated into the matrix via borate ester bonds (Figure 2). Variations in the water solubility of B across different composites displayed unique patterns influenced by the doping material used. In composites extracted by neutral ammonium citrate (B-NAC), an increase in B solubility was noted, whereas those doped with BX showed reduced solubility. This variation is further highlighted by an observed inverse relationship between solubility and other composite properties, such as pH, VM, ash concentration and C concentration.

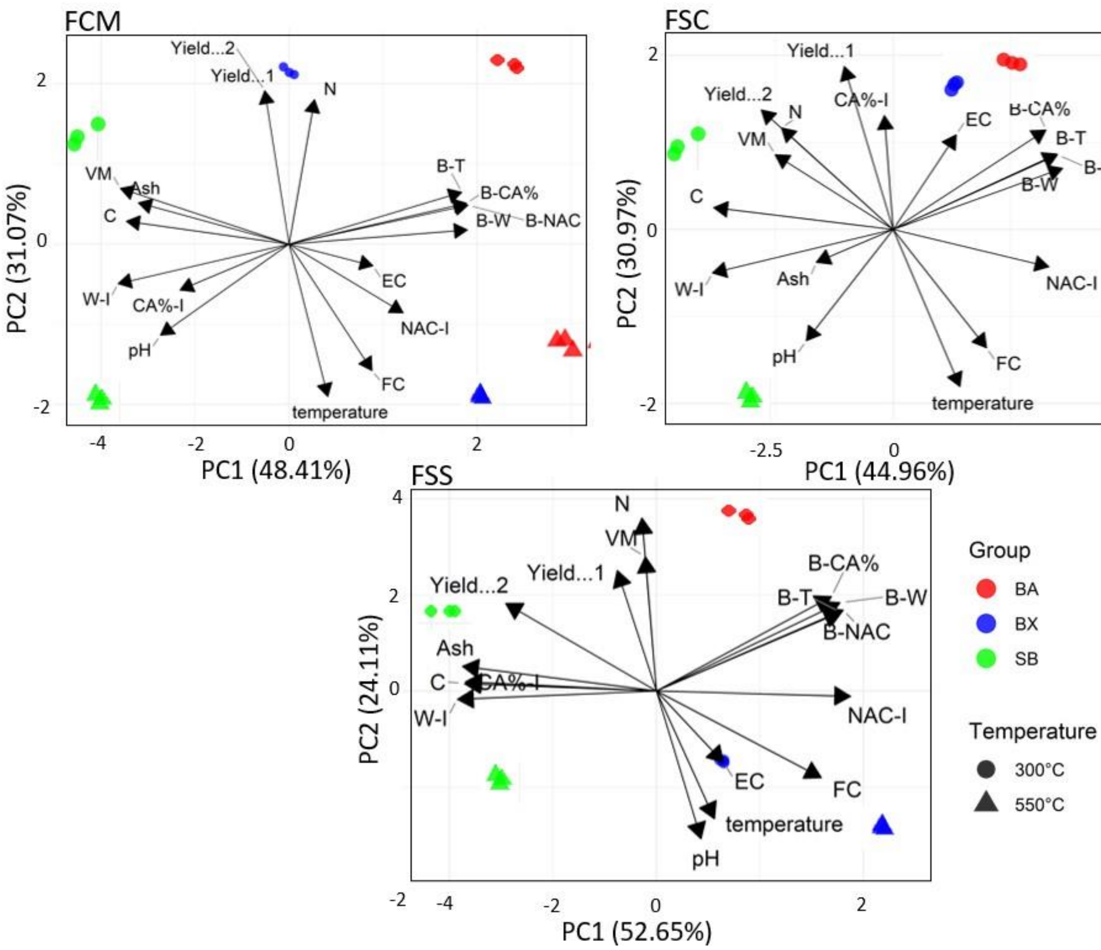

Figure 2. Principal Component Analysis (PCA) of compounds produced in relation to the absence or source of B.

For the CSC-BA there was an increased availability and solubility of B, especially when in the NAC form. This interaction aligns well with the composites' properties such as N, VM, FC and EC (Tables 3 and 4). Additionally, doping with BX modified the solubility of B-CA% at 300 °C and enhanced the solubility of B-NAC at 550 °C. These changes in solubility were associated with shifts in electrical conductivity and ash concentration, ultimately leading to a decrease in the total B concentration within the composite.

CA%, acting as a mimic of natural root exudates, proved effective in enhancing B release, especially in the CCM-BX, CCM-BX' and CSC-BX composites under alkaline pH conditions that favor the solubilization of borate ions. The presence of CA% facilitated the formation of soluble B complexes with metal ions, thereby enhancing B bioavailability. These alkaline conditions also led to an increase in ash concentration and the C/N ratio, which helped stabilize

B within the composite. This stabilization was further supported by the promotion of BO functional group formation, alongside an increase in the concentration of B and N (Zhou et al., 2020).

The CSS-BA doping was found to promote clustering of B solubility in NAC, linked to VM. there was an increase in the VM concentration and N preservation in CSC-BA', consequently increasing the VM and B levels. The spectral feature retention at 3220 cm^{-1}, associated with a bend around 1630 cm^{-1} as observed in CSS-BA' samples, might be due to the preservation of hydroxyl groups even at raised pyrolysis temperatures. These findings suggest that specific functional groups such as C-OH and B-OH found at 3446 cm^{-1} and 3220 cm^{-1} are conserved while reducing the B-C bonding at 1020 cm^{-1}. This change corresponds to the presence of monocrystalline B carbide in covalent organic structures and amorphous B carbide, crucial for composites' structural integrity (Wang et al., 2013). In conclusion, the PCA provided valuable insight regarding the physicochemical dynamics of B incorporation into different matrices. These findings showcase the interaction between doping agents, pyrolysis temperature and matrix composition, collectively influencing the solubility and bioavailability of B in the resulting composites.

3.3 Prediction capacity of PLS models

Modeling through FTIR-PLS proved to be far superior when forecasting specific properties, highlighting the efficacy of the suggested approach for accurately determining key characteristics. Traditionally, this process has involved significant manual effort and substantial consumption of laboratory resources (Table S2). In particular, the introduction of B into biochar derived from chicken manure, shrimp carcass and sewage sludge matrices led to composites exhibiting diverse nutrient profiles and a broad spectrum of chemical and physical-chemical traits. The models we developed, based on ATR-FTIR, were notably successful in predicting the B concentration within these composites, furnishing dependable estimates of their properties (Figure 3).

The calibration phase for our PLS models revealed exceptionally high correlation coefficients (R^2), all surpassing 0.93, while in some instances, reaching an R^2 of 0.60, which is considered satisfactory according to Kiralj et al. (Kiralj and Ferreira, 2009). This strength was also apparent in cross-validation phases, where R^2 values exceeded 0.81 alongside minimal RMSE, as supported by others (Wang et al., 2014). Notably, y-randomization test results for R^2 values exceeded the 0.5 thresholds, except for B-NAC, which neared 0.49, still within the acceptable range as defined by Roy et al. (Roy et al., 2009). The discrepancy between R^2 values for calibration and prediction in each PLS model was consistently less than 0.2, showing no overfitting, in line with the criteria set by Kiralj et al. (Kiralj and Ferreira, 2009). Furthermore, employing FTIR-ATR spectrum database-based PLS models for pH prediction showcased R^2 calibration values of 0.73 and prediction values between 0.71 to 0.73, with calibration RMSE of 0.11 and prediction RMSE of 0.27, indicating an accuracy comparable to existing literature (Ruangratanakorn et al., 2020).

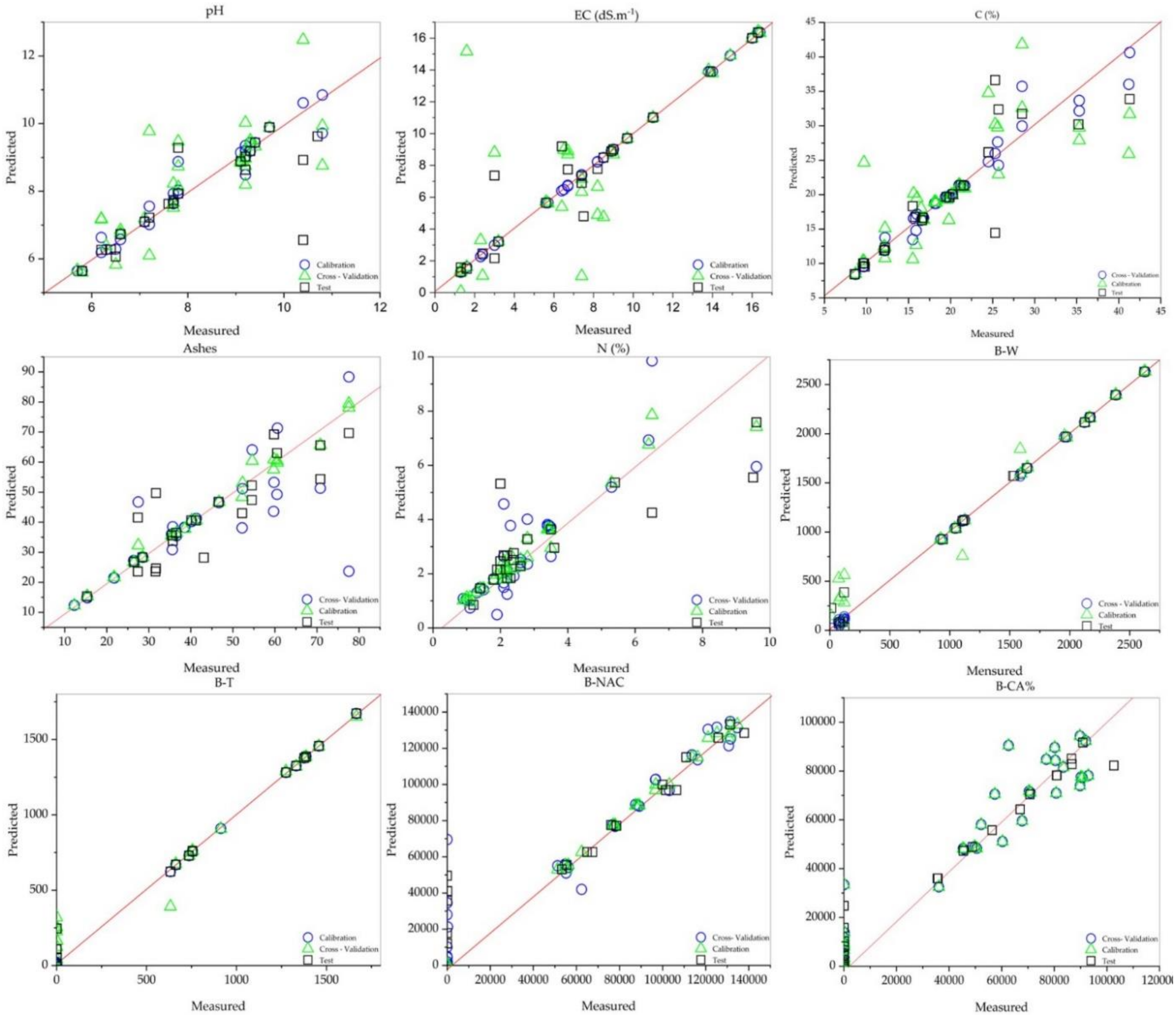

Figure 4. PLS regression based on ATR-FTIR in order to predict the properties and nutrient pools found within the composites.

The application of near-infrared reflectance spectroscopy for quick analysis of manure composites yielded calibration and validation determination coefficients of 0.788 and 0.615, respectively, with associated standard errors (SEE for pH being 0.48 and SEP 0.60), demonstrating the potential of this approach (Huang et al., 2019). For EC specifically, calibration R^2 stood at 0.8704, with validation R^2 at 0.8953, complemented by SEE of 1.74 and SEP of 1.87, underlining the method's effectiveness (Huang et al., 2019).

The robustness of the technique in predicting C concentration was confirmed with a calibration R^2 of 0.9610 and validation R^2 of 0.9128, highlighting the model's accuracy (SEE of 16.46 and SEP of 26.34) (Huang et al., 2019). The NIR spectrum model for predicting biochar ash concentration was reported to have a prediction of R^2 of 0.92 and a cross-validation RMSE of 0.26 (Yue et al., 2018), while another study using NIR spectroscopy for biochars processed at various temperatures obtained a calibration R^2 of 0.99, RMSEC of 0.3, cross-validation R^2 of 0.94 and cross-validation RMSE of 0.8 (Yang and Sheng, 2012).

Lastly, infrared spectroscopy provided substantial predictive accuracy for N concentration in NPK minerals and organic mineral fertilizers (OMFs), with calibration and cross-validation of R^2 values of 0.98 and 0.97 and corresponding RMSEs of 1.91 g kg^{-1} and 2.00 g kg^{-1}, respectively (Ruangratanakorn et al., 2020). Near-infrared reflectance spectroscopy for manure composites showcased calibration and cross-validation coefficients of 0.9874 and 0.9735, with an SEE of 1.61 and SEP of 3.96 (Huang et al., 2019).

3.4 Kinetics of B Release

The B release kinetics from biochar composites synthesized at 300 °C and 550 °C were detailed and assessed through an FTIR spectroscopic approach (Figure 4). The application of an Exponential model described the release over time, with the Elovich model better characterizing the release for specific composites, offering insight into the nutrient release patterns essential for optimizing fertilization processes.

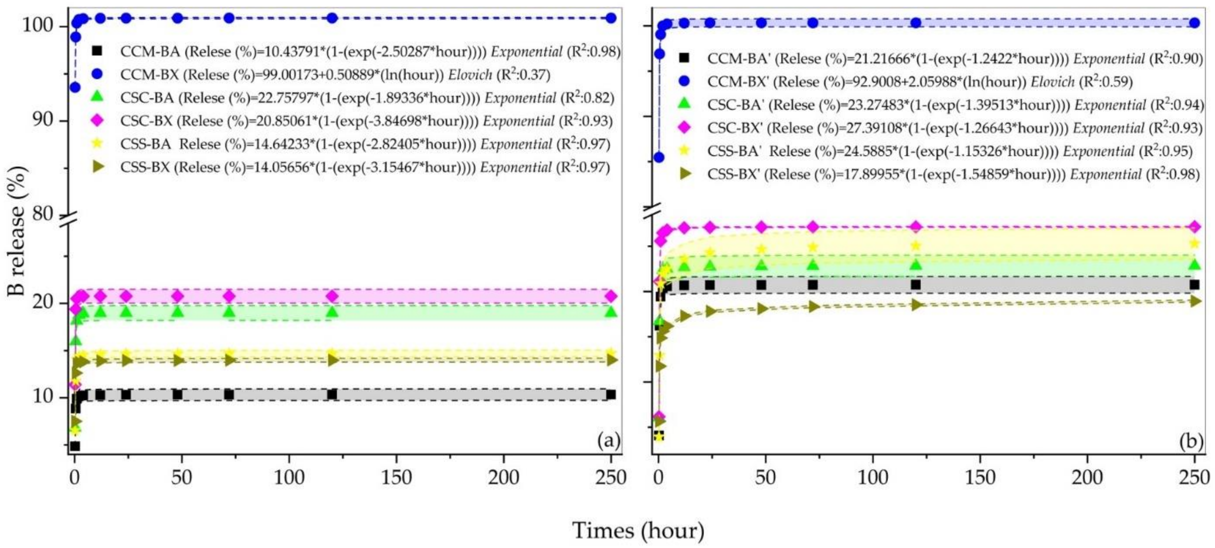

Figure 5. Kinetics of B Release (B) as related to composites produced at 300 °C (a) and 550 °C (b) with the mixture of chicken manure, shrimp carcass and sewage sludge plus boric acid and borax prior to pyrolysis.

At 300 °C, biochars exhibited distinct release behaviors, with CCM-BX showing a striking 100% B release between 2 to 4 hours, suggesting high solubility and minimal organic matrix binding. The order of B release was recorded as CCM-BX > CSC-BA > CSC-BX > CSS-BA > CSS-BX > CCM-BA. This is indicative of the influence a B source holds on nutrient release in chicken manure-based composites. For CCM-BA, an initial rapid release was observed, reaching a 10% release within the first hour and stabilizing thereafter.

With an increase in pyrolysis temperature to 550 °C, the B release was generally rapid, potentially due to modifications in surface adsorption characteristics. For composites doped with BX, the CCM-BX' showed an impressive 100% B release within the 24 to 48-h range. The B release trend for 550 °C biochars was: CCM-BX' > CSC-BX' > CSS-BA' > CSC-BA' > CCM-BA'. The elevation of pyrolysis temperature contributed to an 11% increase in the release rate for CCM-BA, while CSC-BA showed no significant difference, and CSS-BA presented a 10% increase.

With an increase in pyrolysis temperature to 550 °C, B release was generally rapid, potentially due to modifications in surface adsorption characteristics. These results suggest that doping with B significantly influences the nutrient release in chicken manure-based composites.

The presence of B-O bonds, evidenced by the spectra at 550 °C, indicates a greater interaction at this temperature (Kim et al., 2023; Sun et al., 2018a). This interaction of B with organic compounds, whether through complexation or adsorption into the composites (Xu et al., 2025), contributes to the gradual release of B (Lustosa Filho et al., 2017), which aligns with the patterns observed throughout our research (Figure 6).

The doping also provides acidic Lewis sites and alters the electronic structure of the C matrix, enhancing the electron transfer rate and catalytic capacity, albeit influenced by thermal degradation (Liu et al., 2020). This underscores the importance of carefully selecting the pyrolysis temperature to ensure the stability and functional efficacy of the biochar composites, as it modulates B release over time, which is crucial for sustainable agricultural practices.

3.5 Fourier transform infrared spectroscopy (FTIR)

SEM images depict variations in particle size and surface morphology among feedstocks, biochars, BA-based and BX-based (Figure 5). BCM exhibits a heterogeneous, amorphous structure with a rough and porous surface, indicating diverse pore sizes and shapes. BCM’ demonstrates structural loss and thermoplastic properties at 550 °C, leading to complete destruction during pyrolysis.

For CCM-BA, the SEM revealed elongated pores akin to channels, indicating a structure conducive to the release of gases and volatiles, aligning with the observed preferential release patterns. In contrast, the CCM-BA' sample, when subjected to higher temperatures, showed rounded pores, indicative of structural compromises such as pore collapse and overall matrix deterioration. CCM-BX biochars possessed shallow pores, consistent with a rapid 100% B release profile, whereas CCM-BX' displayed elongated but obstructed pores, potentially hindering the exchange of substances and ionic interactions, as confirmed by kinetic analyses.

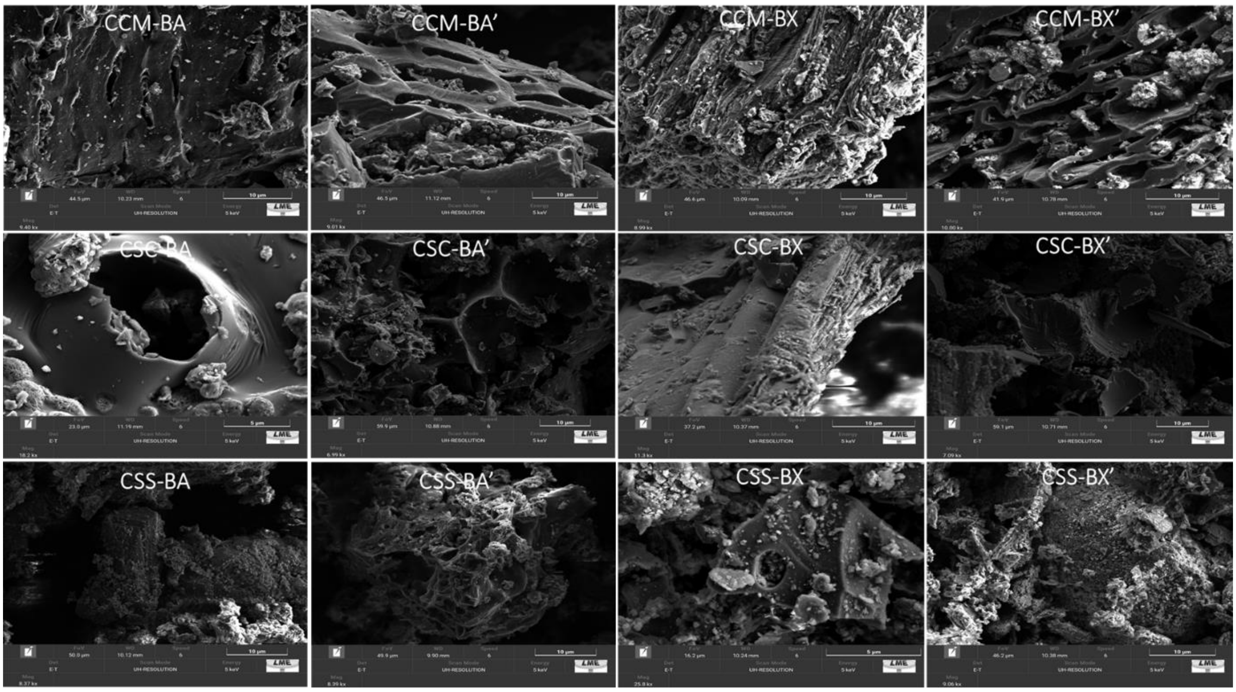

Figure 6. Scanning microscopy obtained by FCM, FSC and FSS both under the influence of temperature 300 and 550 °C, as well as enriched with BA and BX. Magnified images at 10 µm.

CSC-BA biochar showed surface pores reminiscent of volcanic textures, augmenting pore orientation and connectivity, which likely contributed to a reduction in VM. Conversely, CSC-BA' was characterized by a highly porous structure with a hexagonal motif, while CSC-BX' retained a porous surface integrated with lamellar zones. The CSC-BX' variant, however, appeared massive and monolithic with a notable absence of discernible pores and cavities. The surface morphologies of both CSS-BA and CSS-BA' were rugged and porous, with high-temperature pyrolysis fostering the formation of surface precipitates. Similarly, CSS-BX and CSS-BX' biochars exhibited homogeneous surfaces as temperature escalated, lacking conspicuous porosity, and were peppered with opaque impurities owing to the synthesis of B compounds during pyrolysis (Werheit et al., 2000).

Selected for greenhouse trials with Eucalyptus due to their substantial total B concentration, C, ash and VM, CSS-BA', CSC-BA and CSS-BX composites also demonstrated the retention of functional groups associated with B complexation. The slow B release, as indicated in the kinetic study, places these composites as promising candidates for meeting the nutritional requirements of eucalyptus seedlings over different growth stages.

The SEM images captured in Figure 5 illustrate the biochars and their composites, highlighting the morphological variances instrumental in B species implantation, as evidenced by the distinctive textural and structural characterizations when doped with BA and BX. The prominent peak attributed to C–B/B–O/C–O compounds (Thirumal et al., 2016) underscores the unique porosity and structural arrangement of CSC-BA (Figure 1(a)), CSS-BA' (Figure 1(b)) and CSS-BX (Figure 1(c)). CSC-BA exhibits profound porosity akin to volcanic formations (Ateş et al., 2023a) and clearly defines the borate ester structure (H. Zhang et al., 2023). Simultaneously, CSS-BA' emphasizes surface precipitates with elevated pyrolysis temperatures and CSS-BX accentuates the valorization of compounds, maintaining structural integrity without noticeable porosity or cavities (Ateş et al., 2023a).

3.6 Agronomic Efficiency of Composites: Nutrition and Growth of Eucalyptus

The results obtained in the cultivation of Eucalyptus in Oxisols showed an increase in the production of shoot dry matter (SDM) when compared to the control without B addition (NB) (Figure 6). The addition of composites not only increases the total dry matter (TDM) in comparison to plants treated only with B (BA p.a.), but also promotes a significant increase in root dry matter (RDM), which ensures an increase in vigor and establishment capacity of the seedlings, which is an important contribution to agricultural practices and eucalyptus cultivation management as described elsewhere (Hodecker et al., 2014).

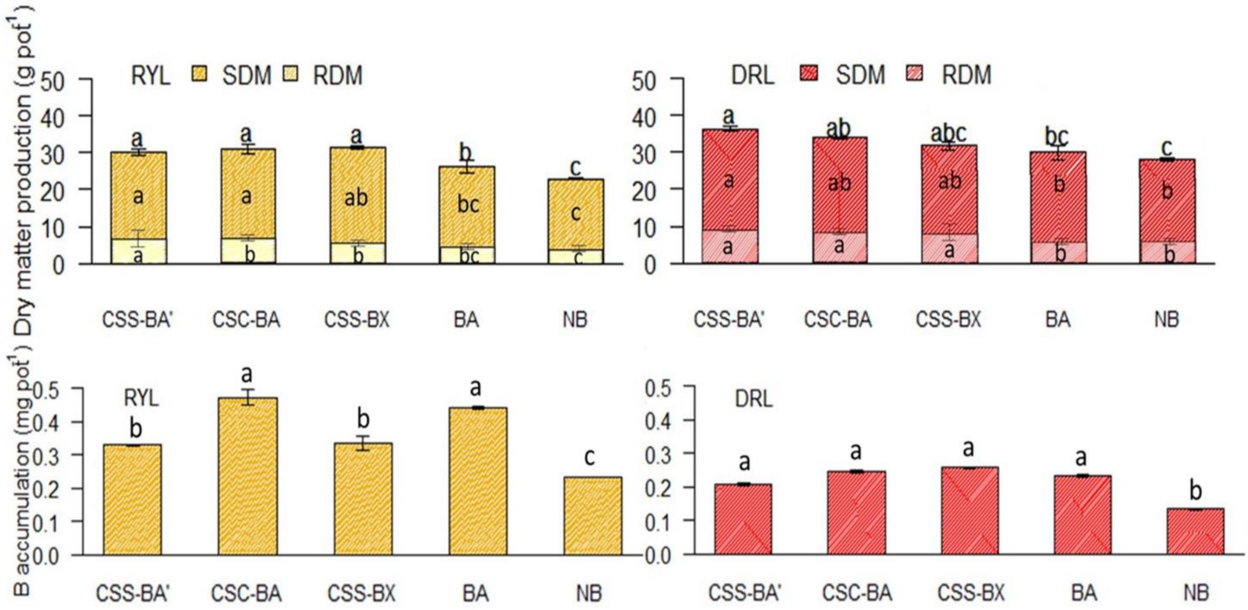

Figure 7. Impact of fertilization with composites on eucalyptus growth characteristics and B nutrition in contrasting oxisols: a study of aerial (SDM) and root dry matter production (RDM), B-accumulation in Eucalyptus and total production. In the graph, the solid bar represents total dry matter production (TDM). Dystrophic red-yellow Oxisol (RYL) and Dystrophic red Oxisol (DRL). Lowercase letters were used to compare the means of each parameter evaluated between treatments using the Tukey test ($p < 0.05$).

The CSC-BA composite demonstrated a marked improvement over the BA treatment in enhancing dry matter production in Eucalyptus grown in Oxisols. Specifically, in the RYL soil, there was an increase of 71.9% in Root Dry Mass (RDM), 106% in Stem Dry Mass (SDM), and 96.9% in Total Dry Mass (TDM). Similarly, in the DRL soil, the CSC-BA composite facilitated increases of 139% in RDM, 99.2% in SDM and 107% in TDM. Moreover, the treatment also led to a significant enhancement in B accumulation in eucalyptus leaves, with increase values of 69.7% in RYL Oxisol and 84.5% in DRL Oxisol. These results clearly exceed the performances of treatments using BA alone, showing remarkable productivity with dry matter yields reaching 31 (g pot^{-1}) in RYL Oxisol and 36 (g pot^{-1}) in DRL Oxisol. This highlights the composites' efficacy in improving nutrition and growth in eucalyptus plants. It is important to note, however, that while the composites contribute significantly to growth, the total N concentration delivered via the composites is relatively low. Furthermore, the N available from these composites is either unavailable or only minimally available to Eucalyptus.

The dynamics of B availability in soil, a critical factor for root absorption, varied significantly in the first 30 days, underlining the importance of composite choice for sustained B release, illustrating the importance of precipitation-dissolution and adsorption-desorption processes (Bhupenchandra et al., 2020) and/or organic complex formation and soil organic matter (Hansson et al., 2020). RYL showed higher B availability compared to DRL soil, affecting the extraction sequence by the composites (Figure 7).

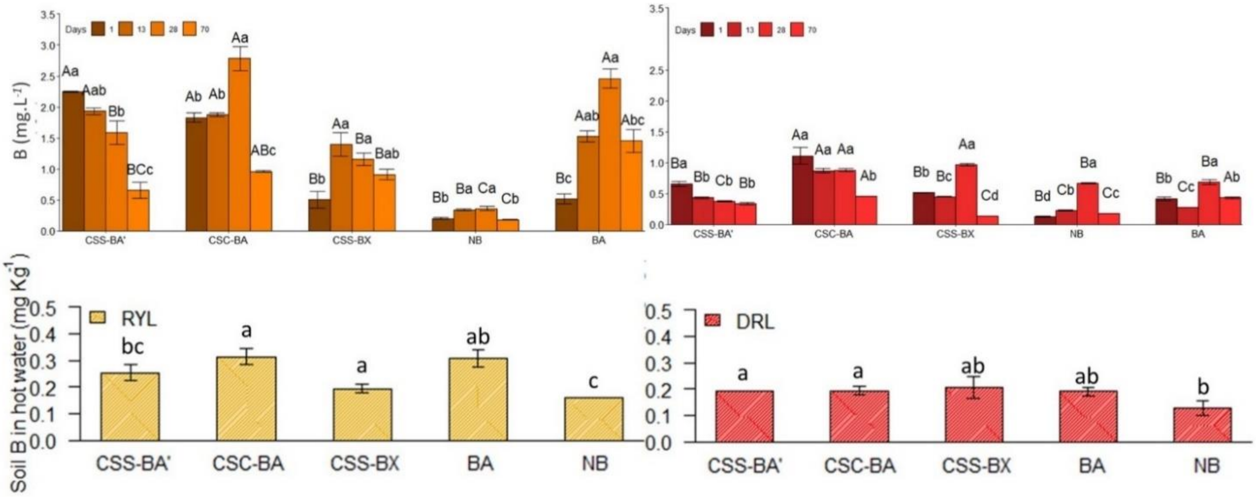

Figure 8. Impact of fertilization with composites and boric acids on the availability of B (mg L^{-1}) and B in contrasting Oxisols cultivated with Eucalyptus (mg Kg^{-1}). CSS-BA': sewage sludge + boric acid at 550 °C; CSC-BA: shrimp waste + boric acid at 300 °C; CSS-BX: sewage sludge + borax at 300 °C; BA: Boric Acid; NB: No B. Dystrophic red-yellow Oxisol (RYL) and Dystrophic red Oxisol (DRL). Lowercase letters were used to compare the means of each parameter evaluated between treatments using the Tukey test ($p < 0.05$).

Doping the FSC biochar matrix with B benefited the eucalyptus plants. B ensures greater preservation of N in the biochar and possibly increases chemical stability of C functional groups in the carbonized matrices, as shown in previous studies (Pan et al., 2023b). Moreover, groups ensuring higher CEC and adsorption capacity of composites are preserved when B is adsorbed through complexation due to the high ionization and selectivity of adsorbents (Pan et al., 2023b). Thus, synergy can accelerate eucalyptus development, ensuring a greater offer of B in controlled optimization of crop nutrition. Moreover, the composite can directly impact nutrient absorption and physiological processes, possibly improving drought tolerance through modulation of H^+ and ATP activity. This function of B contributes to B accumulation by the crop, with treatments surpassing NB (Ferreira et al., 2021). The capacity of B-doped biochar composites to promote chemical stability and increase CEC reinforces the viability these materials possess in improving the nutrition and growth of Eucalyptus (Pan et al., 2023b).

The availability of B in the soil was significantly impacted in the NB treatment, but the application of composites enhanced B availability. This contributed to the soil's ability to maintain optimal B levels for successive harvests (Schmidt et al., 2021), particularly those enriched with B sources (Bhupenchandra et al., 2024). Nevertheless, the significance of B extends beyond its role as a plant nutrient; it also contributes to the formation of organic composites that exhibit prolonged stability in the soil.

In this study, applications of CSC-BA were observed to enhance TDM and RDM significantly (Figure 6). Additionally, this treatment markedly improves the solubility and accumulation of B in plants (Figure 7). These findings indicate a high adaptability of CSC-BA to various soil conditions, which is crucial for effective nutrient management. The noted improvements in plant growth and photosynthetic efficiency can largely be attributed to the increased mobility of B - a critical element in soils susceptible to nutrient leaching. Customizing these treatments enhances soil quality significantly, promotes C sequestration and reduces dependence on chemical fertilizers, thereby bolstering sustainable agricultural practices (Khan et al., 2024). Adapting agricultural management strategies to integrate precise B treatments according to local soil characteristics is vital for promoting the sustainable growth of eucalyptus plantations. Future research should focus on corroborating these findings in diverse environmental conditions and extending observational periods to fully ascertain the long-term impacts and efficacy of such tailored treatments.

4. Conclusions

This study demonstrates that the efficiency of boron (B) solubilization and release is significantly influenced by feedstock type, pyrolysis conditions and the form of B utilized.

Nitrogen-rich feedstocks, particularly at 300 °C, were found to enhance B stabilization and performance in composites, effectively reducing volatilization losses. FTIR spectroscopy confirmed successful B integration into the carbon matrix via B-O and B-C bonds. Composites derived from boric acid (BA) exhibited superior molecular configurations, enhancing B release dynamics compared to those derived from borax (BX). Predictive PLS-FTIR models provided rapid and non-destructive characterizations of B within composites.

Incorporating B via BA before pyrolysis significantly improved composite properties, moderating B leachate in water and enhancing solution release dynamics. This showcases the potential these composites have of enhancing eucalyptus nutrition and growth in Oxisols. CSC-BA composites, in particular, maintained B availability in Oxisols with low organic matter, supporting extended cultivation periods and successive plantings.

Future investigations should validate these findings through field applications under practical agricultural conditions. Research should also focus on formulating application methods for composites in different cropping systems. Additionally, long-term studies are needed to assess the environmental impacts and economic viability of B-biochar composites in sustainable agriculture.

Funding

This research was funded by the Coordination for the Improvement of Higher Education Personnel (CAPES), CAPES-PROEX/AUXPE 593/2018 Scholarship, the National Council for Scientific and Technological Development (CNPq) and the Minas Gerais State Research Support Foundation (FAPEMIG).

Acknowledgments

This work was financially supported by the CAPES agencies (CAPES-PROEX/AUXPE 593/2018), CNPq and FAPEMIG, for the funding and research grants granted. The Universidade Federal de Lavras (UFLA) is a provider of opportunities. L.C.A. Melo and C.A. Silva are research fellows of the National Council for Scientific and Technological Development (CNPq—Processes N° 311634/2021-4, 311212/2023-9, and 307447/2019-7). Keiji Jindo thanks the Agrosystems Research Group of Wageningen University and Research for the financial support (3710473400). L. Chisté acknowledges Dr. Everton Morais for the data analyses and support, Dr. Lívia Botelho and Dr. Mariene Duarte for the help with laboratory analyses and also thanks José Roberto Fernandes for the help with conducting experiments.

Declarations

Ethics approval and consent to participate

Not applicable.

Consent for publication

Not applicable.

Competing interests

The authors declare that they have no known competing financial interests or personal relationships that could have influenced the work reported in this paper.

5. References

Abbasi, M., Rizvi, O.S., Hussain, S.Z., Jilani, A., Osra, F. a, Kajjumba, G.W., Bhatnagar, A., Khan, E., Abbas, T., 2024. Nano-zerovalent copper biochar composite for treating selenium oxyanions in water: synthesis, evaluation, removal mechanism, density functional theory, and molecular dynamics simulations. Chemical Engineering Journal 485, 149954. https://doi.org/https://doi.org/10.1016/j.cej.2024.149954

Abdullah, R., Ishak, C.F., Osman, N., Halim, N.S.A., Panhwar, Q.A., 2021. Determining the characteristics and potential of plantbased biochars to reduce copper uptake in maize. Bragantia.

Agricolae, 2022. Pacote Agricolae- CRAN - Embalagem Agrícola [WWW Document]. 2022. URL https://cran.r-project.org/web/packages/agricolae/index.html (accessed 8.14.23).

Akaike, H., 1979. A Bayesian extension of the minimum AIC procedure of autoregressive model fitting. Biometrika 66, 237–242. https://doi.org/10.1093/BIOMET/66.2.237

Akhil, D., Lakshmi, D., Kartik, A., Vo, D.-V.N., Arun, J., Gopinath, K.P., 2021. Production, characterization, activation and environmental applications of engineered biochar: a review. Environmental Chemistry Letters 19, 2261–2297. https://doi.org/10.1007/s10311-020-01167-7

Aleosfoor, A., Rahimpour, M.R., 2024. Highly dispersed copper on biochar carbon as a promising catalyst for reverse water gas shift reaction. Journal of the Energy Institute 115, 101680. https://doi.org/https://doi.org/10.1016/j.joei.2024.101680

Almutairi, A.A., Ahmad, M., Rafique, M.I., Al-Wabel, M.I., 2023. Variations in composition and stability of biochars derived from different feedstock types at varying pyrolysis temperature. Journal of the Saudi Society of Agricultural Sciences 22, 25–34. https://doi.org/10.1016/J.JSSAS.2022.05.005

Altıkat, Alperay, Alma, M.H., Altıkat, Aysun, Bilgili, M.E., Altıkat, S., 2024. A Comprehensive Study of Biochar Yield and Quality Concerning Pyrolysis Conditions: A Multifaceted Approach. Sustainability. https://doi.org/10.3390/su16020937

Alva, A.K., Graham, J.H., Anderson, C.A., 1995. Soil pH and copper effects on young ‘Hamlin’orange trees. Soil Science Society of America Journal 59, 481–487.

ASTM International, 1984. Standard Test Method for Chemical Analysis of Wood Charcoal - Designation: D 1762 – 84 (Reapproved 2001). Annual Book of ASTM Standards 84, 292–293. https://doi.org/10.1520/D1762-84R07.2

Atchaya, S., Meena Devi, J., 2024. Experimental Investigation on Structural, Optical, Electrical and Magnetic Properties of Copper Oxide Nanoparticles. Proceedings of the National Academy of Sciences, India Section A: Physical Sciences 94, 153–160. https://doi.org/10.1007/s40010-023-00855-7

Ateş, A., Aydemir, B., Emre, K., 2023a. Investigation of physicochemical and biological properties of boron - doped biochar. Biomass Conversion and Biorefinery. https://doi.org/10.1007/s13399-023-04567-1

Ateş, A., Aydemir, B., Öksüz, K.E., 2023b. Investigation of physicochemical and biological properties of boron-doped biochar. Biomass Conversion and Biorefinery. https://doi.org/10.1007/s13399-023-04567-1

Balwant Singh , Marta Camps Arbestain, J.L., 2017. Biochar: A Guide to Analytical Methods.

Barrow, N.J., Hartemink, A.E., 2023. The effects of pH on nutrient availability depend on both soils and plants. Plant and Soil 487, 21–37. https://doi.org/10.1007/s11104-023-05960-5

Baty, F., Charles, S., Flandrois, J., Delignette-Muller, M.-L., 2015a. The R package nlstools: a toolbox for nonlinear regression. Journal of Statistical Software 66, 1–21.

Baty, F., Ritz, C., Charles, S., Brutsche, M., Flandrois, J.P., Delignette-Muller, M.L., 2015b. A Toolbox for Nonlinear Regression in R: The Package nlstools. Journal of Statistical Software 66, 1–21. https://doi.org/10.18637/JSS.V066.I05

Bhatnagar, A., Sillanpää, M., 2009. Applications of chitin-and chitosan-derivatives for the detoxification of water and wastewater—a short review. Advances in colloid and Interface science 152, 26–38.

Bhupenchandra, I., Basumatary, A., Dutta, S., Das, A., Choudhary, A.K., Lal, R., Dhanachandra Sharma, A., Sen, A., Prabhabati, Y., Ranjan Sahoo, M., 2024.

Repercussions of fertilization with boron and enriched organic manure on soil chemical characteristics, boron and phosphorus fractions, and French bean productivity in an acidic Inceptisol of eastern Himalaya. Scientia Horticulturae 324, 304–4238. https://doi.org/10.1016/j.scienta.2023.112589

Bhupenchandra, I., Basumatary, A., Dutta, S., Singh, L.K., Datta, N., 2020. Impact of boron fertilization on boron fractions at different crop growth stages in cauliflower_cowpea_okra sequence in an inceptisols of North East India. Journal of Plant Nutrition 43, 1175–1188. https://doi.org/10.1080/01904167.2020.1724300

Bo, X., Guo, L., 2013. Carbonos mesoporosos dopados com boro ordenados como eletrocatalisadores isentos de metal para a reação de redução de oxigênio em solução alcalina. Physical Chemistry Chemical Physics 15, 2459–2465. https://doi.org/10.1039/c2cp43541a

Brasil, 2016. Instrução Normativa MAPA Nº 46 DE 22/11/2016 - Federal - LegisWeb [WWW Document]. URL https://www.legisweb.com.br/legislacao/?id=332894 (accessed 6.27.24).

Brasil, M. da A.P. e A., 2014. Manual De Métodos Analíticos oficiais para fertilizantes e corretivos.

Capo, L., Battisti, M., Blandino, M., 2024. The role of zinc fertilization and its interaction with nitrogen and phosphorus starter fertilization on early maize development and grain yield. Field Crops Research 307, 109245. https://doi.org/https://doi.org/10.1016/j.fcr.2023.109245

Carmo, D.L. do, Silva, C.A., Lima, J.M. de, Pinheiro, G.L., 2016. Electrical conductivity and chemical composition of soil solution: comparison of solution samplers in tropical soils. Revista brasileira de Ciência do Solo 40.

Carneiro, J.S. da S., Leite, D.A. da C., Castro, G.M. de, Franca, J.R., Botelho, L., Soares, J.R., Oliveira, J.E. de, Melo, L.C.A., 2022. Biochar-graphene oxide composite is efficient to adsorb and deliver copper and zinc in tropical soil. Journal of Cleaner Production 360, 132170. https://doi.org/https://doi.org/10.1016/j.jclepro.2022.132170

Carneiro, J.S. da S., Ribeiro, I.C.A., Nardis, B.O., Barbosa, C.F., Lustosa Filho, J.F., Melo, L.C.A., 2021. Long-term effect of biochar-based fertilizers application in tropical soil: Agronomic efficiency and phosphorus availability. Science of the Total Environment 760, 143955. https://doi.org/10.1016/j.scitotenv.2020.143955

Chaves Fernandes, B.C., Ferreira Mendes, K., Dias Júnior, A.F., da Silva Caldeira, V.P., da Silva Teófilo, T.M., Severo Silva, T., Mendonça, V., de Freitas Souza, M., Valadão Silva, D., 2020. Impact of Pyrolysis Temperature on the Properties of Eucalyptus Wood-Derived Biochar. Materials. https://doi.org/10.3390/ma13245841

Chen, C., Zhou, L.L., Huang, Y.N., Wang, W.K., Xu, J., 2022. Boron regulates catalytic sites of biochar to enhance the formation of surface-confined complex for improved peroxydisulfate activation. Chemosphere 301, 134690. https://doi.org/10.1016/J.CHEMOSPHERE.2022.134690

Chen, H., Gao, Y., El-Naggar, A., Niazi, N.K., Sun, C., Shaheen, S.M., Hou, D., Yang, X., Tang, Z., Liu, Z., Hou, H., Chen, W., Rinklebe, J., Pohořelý, M., Wang, H., 2022. Enhanced sorption of trivalent antimony by chitosan-loaded biochar in aqueous solutions: Characterization, performance and mechanisms. Journal of Hazardous Materials 425, 127971. https://doi.org/https://doi.org/10.1016/j.jhazmat.2021.127971

Chen, J., Zhu, J., Wang, N., Feng, J., Yan, W., 2019. Hydrophilic polythiophene/SiO2 composite for adsorption engineering: Green synthesis in aqueous medium and its synergistic and specific adsorption for heavy metals from wastewater. Chemical Engineering Journal 360, 1486–1497. https://doi.org/https://doi.org/10.1016/j.cej.2018.10.228

Chen, Z., Xu, Q., Yan, L., Wang, Y., Sun, A., Liu, Q., 2024. Fractionation of stable boron isotopes in alfisols: Application of a novel tool for tracing boron behavior in two soil profiles. Geoderma 441, 116766. https://doi.org/10.1016/J.GEODERMA.2023.116766

Cho, D.-W., Kim, S., Tsang, Y.F., Song, H., 2019. Preparation of nitrogen-doped Cu-biochar and its application into catalytic reduction of p-nitrophenol. Environmental Geochemistry and Health 41, 1729–1737. https://doi.org/10.1007/s10653-017-9966-x

Clough, T.J., Condron, L.M., Kammann, C., Müller, C., 2013. A Review of Biochar and Soil Nitrogen Dynamics. Agronomy. https://doi.org/10.3390/agronomy3020275

Conte, P., Bertani, R., Sgarbossa, P., Bambina, P., Schmidt, H.-P., Raga, R., Lo Papa, G., Chillura Martino, D.F., Lo Meo, P., 2021. Recent Developments in Understanding Biochar's Physical–Chemistry. Agronomy. https://doi.org/10.3390/agronomy11040615

D1762-84, A., 2013. Standard test method for chemical analysis of wood charcoal.

Dai, L., Zhu, W., He, L., Tan, F., Zhu, N., Zhou, Q., He, M., Hu, G., 2018. Calcium-rich biochar from crab shell: an unexpected super adsorbent for dye removal. Bioresource technology 267, 510–516.

Damasceno, A.S. da S., Boechat, C.L., Souza, H.A. de, Capristo-Silva, G.F., Mendes, W. de S., Teodoro, P.E., Morais, P.G.C., Oliveira, R.I. de, Della-Silva, J.L., Souza, I.A.M. de, Silva Junior, C.A. da, 2023. Nutritional monitoring of boron in Eucalyptus spp. in the Brazilian cerrado by multispectral bands of the MSI sensor (Sentinel-2). Remote Sensing Applications: Society and Environment 29, 100913. https://doi.org/10.1016/J.RSASE.2022.100913

Das, S.K., Ghosh, G.K., Avasthe, R.K., Sinha, K., 2021. Compositional heterogeneity of different biochar: Effect of pyrolysis temperature and feedstocks. Journal of Environmental Management 278. https://doi.org/10.1016/j.jenvman.2020.111501

de Mello Prado, R., 2021. Boron BT - Mineral nutrition of tropical plants, in: de Mello

Prado, R. (Ed.), . Springer International Publishing, Cham, pp. 175–190. https://doi.org/10.1007/978-3-030-71262-4_10

de Mendiburu, F., de Mendiburu, M.F., 2019. Package ‘agricolae.’ R Package, version 1, 1143–1149.

de Oliveira Paiva, I., de Morais, E.G., Jindo, K., Silva, C.A., 2024. Biochar N Content, Pools and Aromaticity as Affected by Feedstock and Pyrolysis Temperature. Waste and Biomass Valorization. https://doi.org/10.1007/s12649-023-02415-x

Deng, J., Liu, Y., Liu, S., Zeng, G., Tan, X., Huang, B., Tang, X., Wang, S., Hua, Q., Yan, Z., 2017. Competitive adsorption of Pb(II), Cd(II) and Cu(II) onto chitosan-pyromellitic dianhydride modified biochar. Journal of Colloid and Interface Science 506, 355–364. https://doi.org/https://doi.org/10.1016/j.jcis.2017.07.069

Di Palma, L., Mecozzi, R., 2007. Heavy metals mobilization from harbour sediments using EDTA and citric acid as chelating agents. Journal of Hazardous Materials 147, 768–775. https://doi.org/https://doi.org/10.1016/j.jhazmat.2007.01.072

Ding, Y., Liu, Y., Liu, S., Huang, X., Li, Z., Tan, X., Zeng, G., Zhou, L., 2017. Potential Benefits of Biochar in Agricultural Soils: A Review. Pedosphere 27, 645–661. https://doi.org/10.1016/S1002-0160(17)60375-8

do Amaral Leite, A., de Souza Cardoso, A.A., de Almeida Leite, R., Barrera, A.M.V., Queiroz, D.D.L., Viana, T.C., de Oliveira-Longatti, S.M., Silva, C.A., de Souza Moreira, F.M., Lehmann, J., Melo, L.C.A., 2024. Phosphate-solubilizing bacteria increase maize phosphorus uptake from magnesium-enriched poultry manure biochar. Biology and Fertility of Soils 60, 421–436. https://doi.org/10.1007/s00374-024-01808-x

do Carmo, D.L., Silva, C.A., de Lima, J.M., Pinheiro, G.L., 2016. Electrical Conductivity and Chemical Composition of Soil Solution: Comparison of Solution Samplers in Tropical Soils. Revista Brasileira de Ciência do Solo 40.

https://doi.org/10.1590/18069657RBCS20140795

Domingues, Rimena R., Trugilho, P.F., Silva, C.A., De Melo, I.C.N.A., Melo, L.C.A., Magriotis, Z.M., Sánchez-Monedero, M.A., 2017. Properties of biochar derived from wood and high-nutrient biomasses with the aim of agronomic and environmental benefits. PLoS ONE 12, 1–19. https://doi.org/10.1371/journal.pone.0176884

Domingues, Rimena R, Trugilho, P.F., Silva, C.A., Melo, I.C.N.A. de, Melo, L.C.A., Magriotis, Z.M., Sánchez-Monedero, M.A., 2017. Properties of biochar derived from wood and high-nutrient biomasses with the aim of agronomic and environmental benefits. PLOS ONE 12, e0176884.

Dong, X., Wang, C., Li, H., Wu, M., Liao, S., Zhang, D., Pan, B., 2014. The sorption of heavy metals on thermally treated sediments with high organic matter content. Bioresource technology 160, 123–128.

Du, Y., Dai, M., Naz, I., Hao, X., Wei, X., Rong, R., Peng, C., Ali, I., 2021. Carbothermal reduction synthesis of zero-valent iron and its application as a persulfate activator for ciprofloxacin degradation. Separation and Purification Technology 275, 119201. https://doi.org/10.1016/j.seppur.2021.119201

Elsherpiny, mohamed atef, 2023. Effect of Organic Amendments and Synthetic Substances on Copper Availability, Absorption, and Wheat Productivity. Egyptian Journal of Soil Science 63, 429–442. https://doi.org/10.21608/ejss.2023.220516.1614

Erenstein, O., Jaleta, M., Sonder, K., Mottaleb, K., Prasanna, B.M., 2022. Global maize production, consumption and trade: trends and R&D implications. Food Security 14, 1295–1319. https://doi.org/10.1007/s12571-022-01288-7

Extract, 2020. Extract and Visualize the Results of Multivariate Data Analyses [R package factoextra version 1.0.7].

Factoextra, 2022. R: The R Project for Statistical Computing [WWW Document]. URL https://www.r-project.org/ (accessed 8.14.23).

Fan, J., Li, Yan, Yu, H., Li, Yuxuan, Yuan, Q., Xiao, H., Li, F., Pan, B., 2020. Using sewage sludge with high ash content for biochar production and Cu(II) sorption. Science of The Total Environment 713, 136663. https://doi.org/https://doi.org/10.1016/j.scitotenv.2020.136663

Faria, W.M., Figueiredo, C.C. de, Coser, T.R., Vale, A.T., Schneider, B.G., 2018. Is sewage sludge biochar capable of replacing inorganic fertilizers for corn production? Evidence from a two-year field experiment. Archives of Agronomy and Soil Science 64, 505–519. https://doi.org/10.1080/03650340.2017.1360488

Ferreira, G.A., Hippler, F.W.R., Prado, L.A. do. S., Rima, J.A.H., Boaretto, R.M., Quaggio, J.A., Façanha, A.R., Mattos-Jr, D., 2021. Boron modulates the plasma membrane H+-ATPase activity affecting nutrient uptake of Citrus trees. Annals of Applied Biology 178, 293–303. https://doi.org/10.1111/AAB.12630

Friedrich, N., Brandimarte, P., Li, J., Saito, S., Yamaguchi, S., Pozo, I., Peña, D., Frederiksen, T., Garcia-Lekue, A., Sánchez-Portal, D., Pascual, J.I., 2020. Magnetism of Topological Boundary States Induced by Boron Substitution in Graphene Nanoribbons. PHYSICAL REVIEW LETTERS 125, 146801. https://doi.org/10.1103/PhysRevLett.125.146801

Fuentez-Torres, M.O., Ortiz-Chi, F., Espinosa-González, C.G., Aleman, M., Cervantes-Uribe, A., Torres-Torres, J.G., Kesarla, M.K., Collins-Martínez, V., Godavarthi, S., Martínez-Gómez, L., 2021. Facile Synthesis of Zn Doped g-C3N4 for Enhanced Visible Light Driven Photocatalytic Hydrogen Production. Topics in Catalysis 64, 65–72. https://doi.org/10.1007/s11244-020-01298-9

Gao, Y., Wang, Q., Ji, G., Li, A., Niu, J., 2021. Doping strategy, properties and application of heteroatom-doped ordered mesoporous carbon. RSC Advances 11, 5361–5383. https://doi.org/10.1039/D0RA08993A

Ghorbani, M., Amirahmadi, E., Neugschwandtner, R.W., Konvalina, P., Kopecký, M., Moudrý, J., Perná, K., Murindangabo, Y.T., 2022a. The Impact of Pyrolysis Temperature on Biochar Properties and Its Effects on Soil Hydrological Properties. Sustainability. https://doi.org/10.3390/su142214722

Ghorbani, M., Konvalina, P., Walkiewicz, A., Neugschwandtner, R.W., Kopecký, M., Zamanian, K., Chen, W.-H., Bucur, D., 2022b. Feasibility of Biochar Derived from Sewage Sludge to Promote Sustainable Agriculture and Mitigate GHG Emissions—A Review. International Journal of Environmental Research and Public Health. https://doi.org/10.3390/ijerph191912983

GRANULOMÉTRICA, B.A., 2014. Manual de métodos analíticos oficiais para fertilizantes minerais, orgânicos, organominerais e corretivos.

Hailegnaw, N.S., Mercl, F., Pračke, K., Praus, L., Száková, J., Tlustoš, P., 2020. The Role of Biochar and Soil Properties in Determining the Available Content of Al, Cu, Zn, Mn, and Cd in Soil. Agronomy. https://doi.org/10.3390/agronomy10060885

Hansson, K., Laclau, J.P., Saint-André, L., Mareschal, L., van der Heijden, G., Nys, C., Nicolas, M., Ranger, J., Legout, A., 2020. Fertilidade química dos ecossistemas florestais. Parte 1: Análises químicas comuns do solo foram preditores fracos da produtividade do povoamento em uma ampla gama de solos florestais ácidos. Ecologia e manejo florestal 461, 117843. https://doi.org/10.1016/j.foreco.2019.117843

Hao, W., Luo, P., Wu, Z., Mi, Y., Gao, Z., 2021. The effect of biomass pyrolysis temperature on the performance of biochar-fed molten hydroxide direct carbon fuel cells. Biomass and Bioenergy 150, 106122. https://doi.org/10.1016/j.biombioe.2021.106122

Haque, A., Al-Balushi, R.A., Raithby, P.R., Khan, M.S., 2020. Recent Advances in π-Conjugated N^C-Chelate Organoboron Materials. Molecules. https://doi.org/10.3390/molecules25112645

Heckler, G.S., da Costa, R.C., Fransozo, A., Rosso, S., Munehisa Shimizu, R., 2014. Long-term Patterns of Spatial and Temporal Distribution in the Seabob Shrimp Xiphopenaeus kroyeri (Decapoda: Penaeidae) Population in Southeastern Brazil. Journal of Crustacean Biology 34, 326–333. https://doi.org/10.1163/1937240X-00002231

Hodecker, B.E.R., De Barros, N.F., Da Silva, I.R., Diola, V., Sarkis, J.E.S., Loureiro, M.E., 2014. Boron delays dehydration and stimulates root growth in Eucalyptus urophylla (Blake, S.T.) under osmotic stress. Plant and Soil 384, 185–199. https://doi.org/10.1007/S11104-014-2196-4/FIGURES/7

Hortin, J.M., Anderson, A.J., Britt, D.W., Jacobson, A.R., McLean, J.E., 2020. Copper oxide nanoparticle dissolution at alkaline pH is controlled by dissolved organic matter: influence of soil-derived organic matter, wheat, bacteria, and nanoparticle coating. Environmental Science: Nano 7, 2618–2631.

Houben, D., Evrard, L., Sonnet, P., 2013. Mobility, bioavailability and pH-dependent leaching of cadmium, zinc and lead in a contaminated soil amended with biochar. Chemosphere 92, 1450–1457. https://doi.org/https://doi.org/10.1016/j.chemosphere.2013.03.055

Hu, Z., Wei, L., 2023. Review on Characterization of Biochar Derived from Biomass Pyrolysis via Reactive Molecular Dynamics Simulations. Journal of Composites Science. https://doi.org/10.3390/jcs7090354

Huang, J., Zhu, Y., Bian, H., Song, L., Liu, Y., Lv, Y., Ye, X., Lin, C., Li, X., 2023. Insights into Enhanced Peroxydisulfate Activation with B and Fe Co-Doped Biochar from Bark for the Rapid Degradation of Guaiacol. Molecules. https://doi.org/10.3390/molecules28227591

Huang, Q., Song, S., Chen, Z., Hu, B., Chen, J., Wang, X., 2019. Biochar-based materials and their applications in removal of organic contaminants from wastewater: state-of-the-art review. Biochar 2019 1:1 1, 45–73. https://doi.org/10.1007/S42773-019-00006-5

Husson, F., Josse, J., Le, S., Mazet, J., Husson, M.F., 2016. Package 'factominer.' An R package 96, 698.

Ippolito, J.A., Liqiang Cui, ·, Kammann, C., Wrage-Mönnig, N., Estavillo, J.M., Fuertes-Mendizabal, T., Cayuela, M.L., Gilbert Sigua, ·, Novak, J., Spokas, K., Borchard, N., 2020. Feedstock choice, pyrolysis temperature and type influence biochar characteristics: a comprehensive meta-data analysis review 1, 421–438. https://doi.org/10.1007/s42773-020-00067-x

Jalali, Mohsen, Imanifard, A., Jalali, Mahdi, 2023. Heavy metals accumulation in wheat (Triticum aestivum L.) roots and shoots grown in calcareous soils treated with non-spiked and spiked sewage sludge. Environmental Science and Pollution Research 30, 20862–20873.

Jez, E., Pellegrini, E., Contin, M., 2023. Copper bioavailability and leaching in conventional and organic viticulture under environmental stress. Applied Sciences 13, 2595.

Jha, S.K., Mishra, V.K., Damodaran, T., Singh, A.K., Singh, Y.P., Sharma, D.K., 2022. Does conservation tillage on partially reclaimed sodic soil restore land degradation by influencing boron dynamics, bioavailability for plant's uptake and nutritional security? Land Degradation & Development 33, 1260–1268. https://doi.org/10.1002/LDR.4206

Jia, M., Wang, F., Bian, Y., Jin, X., Song, Y., Kengara, F.O., Xu, R., Jiang, X., 2013. Effects of pH and metal ions on oxytetracycline sorption to maize-straw-derived biochar. Bioresource Technology 136, 87–93. https://doi.org/10.1016/j.biortech.2013.02.098

Jin, H., Zhang, D., Yan, Y., Yang, C., Fang, B., Li, X., Shao, Y., Wang, H., Yue, J., Wang, Y., Cheng, H., Shi, Y., Qin, F., 2022. Short-term application of chicken manure under different nitrogen rates alters structure and co-occurrence pattern but not diversity of soil microbial community in wheat field. Frontiers in Microbiology 13.

Jin, J., Li, Y., Zhang, Jianyun, Wu, S., Cao, Y., Liang, P., Zhang, Jin, Wong, M.H., Wang, M., Shan, S., 2016. Influence of pyrolysis temperature on properties and environmental safety of heavy metals in biochars derived from municipal sewage sludge. Journal of hazardous materials 320, 417–426.

Johnston, C.T., 2017. Biochar analysis by Fourier-transform infra-red spectroscopy, in: Singh, B., Camps-Arbestain, M., Lehmann, J. (Eds.), Biochar: A Guide to Analytical Methods. CRC Press/Taylor and Francis Group, LLC, Boca Raton, pp. 199–213.

Jones, J.B., 2001. Laboratory guide for conducting soil tests and plant analysis. CRC press.

Joseph, S., Cowie, A.L., Van Zwieten, L., Bolan, N., Budai, A., Buss, W., Cayuela, M.L., Graber, E.R., Ippolito, J.A., Kuzyakov, Y., Luo, Y., Ok, Y.S., Palansooriya, K.N., Shepherd, J., Stephens, S., Weng, Z., Lehmann, J., 2021. How biochar works, and when it doesn't: A review of mechanisms controlling soil and plant responses to biochar. GCB Bioenergy 13, 1731–1764. https://doi.org/10.1111/gcbb.12885

Joseph, S., Graber, E.R., Chia, C., Munroe, P., Donne, S., Thomas, T., Nielsen, S., Marjo, C., Rutlidge, H., Pan, G.X., Li, L., Taylor, P., Rawal, A., Hook, J., 2013. Shifting paradigms: development of high-efficiency biochar fertilizers based on nano-structures and soluble components. Carbon Management 4, 323–343. https://doi.org/10.4155/cmt.13.23

Kabiri, P., Motaghian, H., Hosseinpur, A., 2021. Impact of Biochar on Release Kinetics of Pb (II) and Zn (II) in a Calcareous Soil Polluted with Mining Activities. Journal of Soil Science and Plant Nutrition 21, 22–34. https://doi.org/10.1007/s42729-020-00336-5

Kalbarczyk, M., Szcześ, A., Belcarz, A., Kazimierczak, P., May, Z., 2023. Zn-doped Mono- and Biphasic Calcium Phosphate Materials Derived from Agriculture Waste and Their Potential Biomedical Applications: Part I. Materials. https://doi.org/10.3390/ma16051971

Karimi, B., Masson, V., Guilland, C., Leroy, E., Pellegrinelli, S., Giboulot, E., Maron, P.-A., Ranjard, L., 2021. Ecotoxicity of copper input and accumulation for soil biodiversity in vineyards. Environmental Chemistry Letters 19, 2013–2030. https://doi.org/10.1007/s10311-020-01155-x

Kassambara, A., Mundt, F., 2017. Package 'factoextra.' Extract and visualize the results of multivariate data analyses 76.

Kayani, Z.N., Umer, M., Riaz, S., Naseem, S., 2015. Characterization of copper oxide nanoparticles fabricated by the sol–gel method. Journal of Electronic Materials 44, 3704–3709.

Khan, A., Harfield, D., Hillen, B., Stenzel, F., Homung, A., 2017. Long-termaging of biochar. https://doi.org/10.13140/RG.2.2.21385.75366

Khan, S., Irshad, S., Mehmood, K., Hasnain, Z., Nawaz, M., Rais, A., Gul, S., Wahid, M.A., Hashem, A., Abd_Allah, E.F., Ibrar, D., 2024. Biochar Production and Characteristics, Its Impacts on Soil Health, Crop Production, and Yield Enhancement: A Review. Plants. https://doi.org/10.3390/plants13020166

Khaokaew, S., Landrot, G., Chaney, R.L., Pandya, K., Sparks, D.L., 2012. Speciation and Release Kinetics of Zinc in Contaminated Paddy Soils. Environmental Science & Technology 46, 3957–3963. https://doi.org/10.1021/es204007t

Kim, S., Kim, U. gi, Ryu, J., Kim, D., Kim, M., Joo, Y.C., Lee, S.Y., 2023. Boron-doped amorphous carbon deposited by DC sputtering for a hardmask: Microstructure and dry etching properties. Applied Surface Science 637, 157895. https://doi.org/10.1016/J.APSUSC.2023.157895

Kiralj, R., Ferreira, M.M.C., 2009. Basic validation procedures for regression models in QSAR and QSPR studies: theory and application. Journal of the Brazilian Chemical Society 20, 770–787. https://doi.org/10.1590/S0103-50532009000400021

Kleber, M., Bourg, I.C., Coward, E.K., Hansel, C.M., Myneni, S.C.B., Nunan, N., 2021. Dynamic interactions at the mineral–organic matter interface. Nature Reviews Earth & Environment 2, 402–421.

Labanya, R., Srivastava, P.C., Pachauri, S.P., Shukla, A.K., Shrivastava, M., Mukherjee, P., Srivastava, P., 2022. Sorption–desorption of some transition metals, boron and sulphur in a multi-ionic system onto phyto-biochars prepared at two pyrolysis temperatures. Environmental Science: Processes & Impacts 24, 2378–2397. https://doi.org/10.1039/D2EM00212D

Lamichhane, J.R., Osdaghi, E., Behlau, F., Köhl, J., Jones, J.B., Aubertot, J.-N., 2018. Thirteen decades of antimicrobial copper compounds applied in agriculture. A review. Agronomy for Sustainable Development 38, 28. https://doi.org/10.1007/s13593-018-0503-9

Lê, S., Josse, J., Husson, F., 2008a. FactoMineR: An R Package for Multivariate Analysis. Journal of Statistical Software 25, 1–18. https://doi.org/10.18637/JSS.V025.I01

Lê, S., Josse, J., Husson, F., 2008b. FactoMineR: an R package for multivariate analysis. Journal of statistical software 25, 1–18.

Lehmann, J., Joseph, S., 2024. Biochar for environmental management: science, technology and implementation. Taylor & Francis.

Leitner, J., Sedmidubský, D., Jankovský, O., 2018. Effect of ZnO nanosizing on its solubility in aqueous media. Micro & Nano Letters 13, 1585–1589.

Leng, L., Xu, S., Liu, R., Yu, T., Zhuo, X., Leng, S., Xiong, Q., Huang, H., 2020. Nitrogen containing functional groups of biochar: An overview. Bioresource Technology 298, 122286. https://doi.org/https://doi.org/10.1016/j.biortech.2019.122286

Li, L., Niu, W., Cong, H., Meng, H., Niu, Z., Shen, X., Cao, L., Kong, X., 2023. Effects of Pyrolysis Temperature on the Release Characteristics of Polycyclic Aromatic

Hydrocarbons during Pyrolysis of Corn Stover Pellet. BioResources 18, 2112–2136. https://doi.org/10.15376/biores.18.1.2112-2136

Liang, H., Zhao, Y., Liu, T., Li, Ruijuan, Li, Rumei, Zhu, Y., Fang, F., 2024. Zn-Doped MnCO3/CS Composite Photocatalyst for Visible-Light-Driven Decomposition of Organic Pollutants. Molecules. https://doi.org/10.3390/molecules29051094

Liberda, D., Pięta, E., Pogoda, K., Piergies, N., Roman, M., Koziol, P., Wrobel, T.P., Paluszkiewicz, C., Kwiatek, W.M., 2021. The impact of preprocessing methods for a successful prostate cell lines discrimination using partial least squares regression and discriminant analysis based on Fourier transform infrared imaging. Cells 10, 953.

Lin, C.-W., Chen, F.-Y., Liu, S.-H., Ma, C.-Y., 2024. Optimized combination of zero-valent iron and oxygen-releasing biochar as cathodes of microbial fuel cells to enhance copper migration in sediment. Bioelectrochemistry 158, 108699. https://doi.org/https://doi.org/10.1016/j.bioelechem.2024.108699

Ling, C., Wu, S., Han, J., Dong, T., Zhu, C., Li, X., Xu, L., Zhang, Y., Zhou, M., Pan, Y., 2022. Sulfide-modified zero-valent iron activated periodate for sulfadiazine removal: Performance and dominant routine of reactive species production. Water Research 220, 118676.

Liu, B., Guo, W., Wang, H., Si, Q., Zhao, Q., Luo, H., Ren, N., 2020. B-doped graphitic porous biochar with enhanced surface affinity and electron transfer for efficient peroxydisulfate activation. Chemical Engineering Journal 396, 125119. https://doi.org/10.1016/J.CEJ.2020.125119

Liu, C., Lin, J., Chen, H., Wang, W., Yang, Y., 2021. Comparative Study of Biochar Modified with Different Functional Groups for Efficient Removal of Pb(II) and Ni(II). https://doi.org/10.21203/rs.3.rs-487894/v1

Liu, J., Wang, F., Xu, W., 2023. Characteristics of zinc adsorption onto biochars derived from different feedstocks. Water 15, 3789.

Liu, Q., Zang, G.-L., Zhao, Q., 2021. Removal of copper ions by functionalized biochar based on a multicomponent Ugi reaction. RSC Advances 11, 25880–25891. https://doi.org/10.1039/D1RA04156H

Lou, T., Yin, Y., Wang, J., 2024. Mechanisms of biochar promoting medium chain fatty acids production from sewage sludge: Effect of biochar type. Journal of Cleaner Production 451, 141995. https://doi.org/https://doi.org/10.1016/j.jclepro.2024.141995

Luo, M., Zhu, C., Chen, Q., Song, F., Hao, W., Shen, Z., Konhauser, K.O., Alessi, D.S., Zhong, C., 2023. In-situ growth of ZIF-8 nanocrystals on biochar for boron adsorption. Colloids and Surfaces A: Physicochemical and Engineering Aspects 657, 130504. https://doi.org/https://doi.org/10.1016/j.colsurfa.2022.130504

Lustosa Filho, J.F., Penido, E.S., Castro, P.P., Silva, C.A., Melo, L.C.A., 2017. Co-Pyrolysis of Poultry Litter and Phosphate and Magnesium Generates Alternative Slow-Release Fertilizer Suitable for Tropical Soils. ACS Sustainable Chemistry and Engineering 5, 9043–9052. https://doi.org/10.1021/ACSSUSCHEMENG.7B01935/ASSET/IMAGES/LARGE/SC-2017-01935U_0005.JPEG

Manogaran, M.D., Shamsuddin, R., Mohd Yusoff, M.H., Lay, M., Siyal, A.A., 2022. A review on treatment processes of chicken manure. Cleaner and Circular Bioeconomy 2, 100013. https://doi.org/https://doi.org/10.1016/j.clcb.2022.100013

Maqbool, M.A., Beshir, A., 2019. Zinc biofortification of maize (Zea mays L.): Status and challenges. Plant breeding 138, 1–28.

Masek, O., Buss, W., Sohi, S., 2018. Standard biochar materials. Environmental science & technology 52, 9543–9544.

Mašek, O., Buss, W., Sohi, S., 2018. Standard Biochar Materials. Environmental Science and

Technology 52, 9543–9544. https://doi.org/10.1021/acs.est.8b04053

McAfee, L., 2000. Infrared and Raman spectra of inorganic and coordination compounds. Part A: theory and applications in inorganic chemistry; Part B: application in coordination, organometallic, and bioinorganic chemistry, (Nakamoto, Kazuo).

Meenu, Rani, M., Shanker, U., 2024. Efficient photodegradation of hexabromocyclododecane leached from polystyrene by biochar and sulfur doped CuO nanocomposite: Optimization factors, kinetics, and photoactivity. Environmental Pollution 340, 122818. https://doi.org/https://doi.org/10.1016/j.envpol.2023.122818

Morais, E.G., Jindo, K., Silva, C.A., 2023. Biochar-Based Phosphate Fertilizers: Synthesis, Properties, Kinetics of P Release and Recommendation for Crops Grown in Oxisols. Agronomy. https://doi.org/10.3390/agronomy13020326

Morais, E.G., Silva, C.A., Jindo, K., 2021. Humic Acid Improves Zn Fertilization in Oxisols Successively Cultivated with Maize–Brachiaria. Molecules. https://doi.org/10.3390/molecules26154588

Morais, E.G., Silva, C.A., Maluf, H.J.G.M., Guilherme, L.R.G., 2022. Slow-Release Humic Acid-Based Zinc Fertilizers Improve Growth and Nutrition of Maize and Brachiaria Grass Successively Grown in Oxisols. ACS Agricultural Science & Technology 3, 17–32.

Mortvedt, J.J., Gilkes, R.J., 1993. Zinc fertilizers, in: Zinc in Soils and Plants: Proceedings of the International Symposium on 'Zinc in Soils and Plants' Held at The University of Western Australia, 27–28 September, 1993. Springer, pp. 33–44.

Muzyka, R., Misztal, E., Hrabak, J., Banks, S.W., Sajdak, M., 2023. Various biomass pyrolysis conditions influence the porosity and pore size distribution of biochar. Energy 263, 126128. https://doi.org/https://doi.org/10.1016/j.energy.2022.126128

Nakamoto, K., 2009. Infrared and Raman spectra of inorganic and coordination compounds, part B: applications in coordination, organometallic, and bioinorganic chemistry. John Wiley & Sons.

Nan, H., Yin, J., Yang, F., Luo, Y., Zhao, L., Cao, X., 2021. Pyrolysis temperature-dependent carbon retention and stability of biochar with participation of calcium: Implications to carbon sequestration. Environmental Pollution 287, 117566. https://doi.org/https://doi.org/10.1016/j.envpol.2021.117566

Nepal, J., Ahmad, W., Munsif, F., Khan, A., Zou, Z., 2023. Advances and prospects of biochar in improving soil fertility, biochemical quality, and environmental applications . Frontiers in Environmental Science .

Nguyen, N.-T., Lee, S.-Y., Chen, S.-S., Nguyen, N.-C., Chang, C.-T., Hsiao, S.-S., Trang, L.T., Kao, C.-Y., Lin, M.-F., Wang, L., 2018. Preparation of Zn-Doped Biochar from Sewage Sludge for Chromium Ion Removal. Journal of nanoscience and nanotechnology 18, 5520–5527. https://doi.org/10.1166/jnn.2018.15392

NIST-SRM-1573a, 2018. Standard Reference Material 1573 - Tomato Leaves.

Novais, R.F. de, Neves, J.C.L., Barros, N.F. de, 1991. Ensaio em ambiente controlado. Métodos de pesquisa em fertilidade do solo. Brasília: Embrapa-SEA 392.

Omiri, J., Snoussi, Y., Bhakta, A.K., Truong, S., Ammar, S., Khalil, A.M., Jouini, M., Chehimi, M.M., 2022. Citric-Acid-Assisted Preparation of Biochar Loaded with Copper/Nickel Bimetallic Nanoparticles for Dye Degradation. Colloids and Interfaces. https://doi.org/10.3390/colloids6020018

ON THE OCCURRENCE OF COPPER IN TROPICAL SOILS Author (s): J . G . VERMAAT and G . J . VAN DER BIE Published by : Springer Stable URL : https://www.jstor.org/stable/42931553, 1950. 2, 257–282.

Otoni, J.P., Matoso, S.C.G., Pérez, X.L.O., da Silva, V.B., 2024. Potential for agronomic and environmental use of biochars derived from different organic waste. Journal of Cleaner

Production 449, 141826. https://doi.org/https://doi.org/10.1016/j.jclepro.2024.141826

Pan, G., Wei, J., Xu, M., Li, Jiamei, Wang, L., Li, Y., Cui, N., Li, Jun, Wang, Z., 2023a. Insight into boron-doped biochar as efficient metal-free catalyst for peroxymonosulfate activation: Important role of -O-B-O- moieties. Journal of Hazardous Materials 445, 130479. https://doi.org/https://doi.org/10.1016/j.jhazmat.2022.130479

Pan, G., Wei, J., Xu, M., Li, Jiamei, Wang, L., Li, Y., Cui, N., Li, Jun, Wang, Z., 2023b. Insight into boron-doped biochar as efficient metal-free catalyst for peroxymonosulfate activation: Important role of -O-B-O- moieties. Journal of Hazardous Materials 445, 130479. https://doi.org/10.1016/j.jhazmat.2022.130479

Penido, E.S., Martins, G.C., Mendes, T.B.M., Melo, L.C.A., do Rosário Guimarães, I., Guilherme, L.R.G., 2019. Combining biochar and sewage sludge for immobilization of heavy metals in mining soils. Ecotoxicology and Environmental Safety 172, 326–333. https://doi.org/https://doi.org/10.1016/j.ecoenv.2019.01.110

Piash, M.I., Iwabuchi, K., Itoh, T., 2022. Synthesizing biochar-based fertilizer with sustained phosphorus and potassium release: Co-pyrolysis of nutrient-rich chicken manure and Ca-bentonite. Science of The Total Environment 822, 153509. https://doi.org/10.1016/J.SCITOTENV.2022.153509

Quílez-Bermejo, J., Morallón, E., Cazorla-Amorós, D., 2020. Metal-free heteroatom-doped carbon-based catalysts for ORR: A critical assessment about the role of heteroatoms. Carbon 165, 434–454. https://doi.org/10.1016/J.CARBON.2020.04.068

R-Core-Team, 2020. R: A language and environment for statistical computing.

Rafique, M.I., Usman, A.R.A., Ahmad, M., Sallam, A., Al-Wabel, M.I., 2020. In situ immobilization of Cr and its availability to maize plants in tannery waste–contaminated soil: effects of biochar feedstock and pyrolysis temperature. Journal of Soils and Sediments 20, 330–339. https://doi.org/10.1007/S11368-019-02399-Z/TABLES/5

Rødde, R.H., Einbu, A., Vårum, K.M., 2008. A seasonal study of the chemical composition and chitin quality of shrimp shells obtained from northern shrimp (Pandalus borealis). Carbohydrate Polymers 71, 388–393. https://doi.org/https://doi.org/10.1016/j.carbpol.2007.06.006

Roy, P.P., Paul, S., Mitra, I., Roy, K., 2009. On Two Novel Parameters for Validation of Predictive QSAR Models. Molecules 2009, Vol. 14, Pages 1660-1701 14, 1660–1701. https://doi.org/10.3390/MOLECULES14051660

Rúa-Díaz, S., Forjan, R., Lago-Vila, M., Cerqueira, B., Arco-Lázaro, E., Marcet, P., Baragaño, D., Gallego, J.L.R., Covelo, E.F., 2023. Pyrolysis temperature influences the capacity of biochar to immobilize copper and arsenic in mining soil remediation. Environmental Science and Pollution Research 30, 32882–32893. https://doi.org/10.1007/s11356-022-24492-6

Ruangratanakorn, J., Suwonsichon, T., Kasemsumran, S., Thanapase, W., 2020. Installation design of on-line near infrared spectroscopy for the production of compound fertilizer. Vibrational Spectroscopy 106, 103008. https://doi.org/10.1016/J.VIBSPEC.2019.103008

Ryota Suzuki, A., 2022. Package "pvclust" Title Hierarchical Clustering with P-Values via Multiscale Bootstrap Resampling.

Sadeek, S.A., Mohammed, E.A., Shaban, M., Abou Kana, M.T.H., Negm, N.A., 2020. Synthesis, characterization and catalytic performances of activated carbon-doped transition metals during biofuel production from waste cooking oils. Journal of Molecular Liquids 306, 112749. https://doi.org/https://doi.org/10.1016/j.molliq.2020.112749

Saha, S., Islam, M.T., Calhoun, J., Reza, T., 2023. Effect of Hydrothermal Carbonization on Fuel and Combustion Properties of Shrimp Shell Waste. Energies. https://doi.org/10.3390/en16145534

Salawu, O.A., Han, Z., Adeleye, A.S., 2022. Shrimp waste-derived porous carbon adsorbent: Performance, mechanism, and application of machine learning. Journal of Hazardous Materials 437, 129266. https://doi.org/10.1016/J.JHAZMAT.2022.129266

Sánchez-Rodríguez, A.R., Rey, M.-D., Nechate-Drif, H., Castillejo, M.Á., Jorrín-Novo, J. V, Torrent, J., del Campillo, M.C., Sacristán, D., 2021. Combining P and Zn fertilization to enhance yield and grain quality in maize grown on Mediterranean soils. Scientific Reports 11, 7427. https://doi.org/10.1038/s41598-021-86766-2

Schellekens, J., Silva, C.A., Buurman, P., Rittl, T.F., Domingues, R.R., Justi, M., Vidal-Torrado, P., Trugilho, P.F., 2018. Molecular characterization of biochar from five Brazilian agricultural residues obtained at different charring temperatures. Journal of Analytical and Applied Pyrolysis 130, 106–117.

Schmidt, M.P., Siciliano, S.D., Peak, D., 2021. The role of monodentate tetrahedral borate complexes in boric acid binding to a soil organic matter analogue. Chemosphere 276, 130150. https://doi.org/10.1016/j.chemosphere.2021.130150

Shaban, M., Zayed, M., Hamdy, H., 2017. Nanostructured ZnO thin films for self-cleaning applications. RSC Advances 7, 617–631. https://doi.org/10.1039/C6RA24788A

Shabbir, Z., Sardar, A., Shabbir, A., Abbas, G., Shamshad, S., Khalid, S., Natasha, Murtaza, G., Dumat, C., Shahid, M., 2020. Copper uptake, essentiality, toxicity, detoxification and risk assessment in soil-plant environment. Chemosphere 259, 127436. https://doi.org/https://doi.org/10.1016/j.chemosphere.2020.127436

Shireen, F., Nawaz, M.A., Chen, C., Zhang, Q., Zheng, Z., Sohail, H., Sun, J., Cao, H., Huang, Y., Bie, Z., 2018. Boron: Functions and Approaches to Enhance Its Availability in Plants for Sustainable Agriculture. International Journal of Molecular Sciences. https://doi.org/10.3390/ijms19071856

Shuailong, C., Qintie, L.I.N., Rongbo, X., Haoyu, L.U.O., Hengyi, F.U., 2020. Removal of

EDTA-Cu in wastewater by copper-based biochar activated sodium persulfate. Chinese Journal of Environmental Engineering 14, 3298–3307.

Sieber, V., Hofer, M., Brück, W.M., Garbe, D., Brück, T., Lynch, C.A., 2018. ChiBio: An Integrated Bio-refinery for Processing Chitin-Rich Bio-waste to Specialty Chemicals BT - Grand Challenges in Marine Biotechnology, in: Rampelotto, P.H., Trincone, A. (Eds.), . Springer International Publishing, Cham, pp. 555–578. https://doi.org/10.1007/978-3-319-69075-9_14

Silva, F.C. da, 2009. Manual de análises químicas de solos, plantas e fertilizantes, Empresa Brasileira de Pesquisa Agropecuária Embrapa Solos Embrapa Informática Agropecuária Ministério da Agricultura, Pecuária e Abastecimento.

Silverstein, R.M., Bassler, G.C., 1962. Spectrometric identification of organic compounds. Journal of Chemical Education 39, 546.

Singh, A., Yadav, K., Thakur, P., Wan, F., Ravelo, B., Thakur, A., 2024. Review on the amelioration of ZnO and its composites: synthesis and applications. Indian Journal of Physics. https://doi.org/10.1007/s12648-024-03181-9

Singh, B., Dolk, M.M., Shen, Q., Camps-Arbestain, M., 2017. Biochar: A Guide to Analytical Methods, in: Singh, B., Camps-Arbestain, M., Lehmann, J. (Eds.), Biochar: A Guide to Analytical Methods. CRC Press/Taylor and Francis Group, LLC, Boca Raton, pp. 23–38.

Socrates, G., 2004. Infrared and Raman characteristic group frequencies: tables and charts. John Wiley & Sons.

Stuart, B.H., 2004. Infrared Spectroscopy: Fundamentals and Applications, Analytical Techniques in the Sciences. John Wiley & Sons, Ltd, Chichester, UK. https://doi.org/10.1002/0470011149

Sui, L., Tang, C., Du, Q., Zhao, Y., Cheng, K., Yang, F., 2021. Preparation and characterization of boron-doped corn straw biochar: Fe (II) removal equilibrium and kinetics. Journal of Environmental Sciences 106, 116–123. https://doi.org/https://doi.org/10.1016/j.jes.2021.01.001

Sukumar, S., Rudrasenan, A., Padmanabhan Nambiar, D., 2020. Green-synthesized rice-shaped copper oxide nanoparticles using Caesalpinia bonducella seed extract and their applications. ACS omega 5, 1040–1051.

Sun, F., Bin Wu, H., Liu, X., Liu, F., Han, R., Qu, Z., Pi, X., Wang, L., Gao, J., Lu, Y., 2018a. A high-rate and ultrastable anode enabled by boron-doped nanoporous carbon spheres for high-power and long life lithium ion capacitors. https://doi.org/10.1016/j.mtener.2018.07.009

Sun, F., Qu, Z., Gao, J., Wu, H. Bin, Liu, F., Han, R., Wang, L., Pei, T., Zhao, G., Lu, Y., 2018b. In Situ Doping Boron Atoms into Porous Carbon Nanoparticles with Increased Oxygen Graft Enhances both Affinity and Durability toward Electrolyte for Greatly Improved Supercapacitive Performance. Advanced Functional Materials 28. https://doi.org/10.1002/ADFM.201804190

Suzuki, R., Terada, Y., Shimodaira, H., Suzuki, M.R., 2019. Package 'pvclust.' R Package. Hierarchical Clustering with P-Values via Multiscale Bootstrap Resampling. Version 2.

Taiyun Wei, M., Taiyun Wei cre, A., Simko aut, V., Levy ctb, M., Xie ctb, Y., Jin ctb, Y., Zemla ctb, J., Freidank ctb, M., Cai ctb, J., Protivinsky ctb, T., 2022. Package "corrplot" Title Visualization of a Correlation Matrix NeedsCompilation no.

Teixeira, P.C., Donagemma, G.K., Fontana, A., Teixeira, W.G., 2017a. Manual de Métodos de Análise de Solo 3ª edição revista e ampliada. Manual de métodos de análise de solo - Capítulo 8 - Densidade de partículas 574.

Teixeira, P.C., Donagemma, G.K., Fontana, A., Teixeira, W.G., 2017b. Manual de métodos de análise de solo.

Thapa, S., Bhandari, A., Ghimire, R., Xue, Q., Kidwaro, F., Ghatrehsamani, S., Maharjan, B., Goodwin, M., 2021. Managing Micronutrients for Improving Soil Fertility, Health, and Soybean Yield. Sustainability. https://doi.org/10.3390/su132111766

Thirumal, V., Pandurangan, A., Jayavel, R., Ilangovan, R., 2016. Synthesis and characterization of boron doped graphene nanosheets for supercapacitor applications. https://doi.org/10.1016/j.synthmet.2016.07.011

Tu, P., Zhang, G., Wei, G., Li, J., Li, Y., Deng, L., Yuan, H., 2022. Influence of pyrolysis temperature on the physicochemical properties of biochars obtained from herbaceous and woody plants. Bioresources and Bioprocessing 9, 131. https://doi.org/10.1186/s40643-022-00618-z

Vale, F., Alcarde, J.C., 2002. Extratores para avaliar a disponibilidade do zinco em fertilizantes. Revista Brasileira de Ciência do Solo.

Vinodkumar, R., Navas, I., Porsezian, K., Ganesan, V., Unnikrishnan, N. V, Pillai, V.P.M., 2014. Structural, spectroscopic and electrical studies of nanostructured porous ZnO thin films prepared by pulsed laser deposition. Spectrochimica Acta Part A: Molecular and Biomolecular Spectroscopy 118, 724–732.

Waclawska, I., 1995. Thermal decomposition of borax. Journal of thermal analysis 43, 261–269. https://doi.org/10.1007/BF02635993

Wang, C., Dai, H., Liang, L., Li, N., Cui, X., Yan, B., Chen, G., 2023. Enhanced mechanism of copper doping in magnetic biochar for peroxymonosulfate activation and sulfamethoxazole degradation. Journal of Hazardous Materials 458, 132002. https://doi.org/https://doi.org/10.1016/j.jhazmat.2023.132002

Wang, C., Huang, C., Qian, J., Xiao, J., Li, H., Wen, Y., He, X., Ran, W., Shen, Q., Yu, G., 2014. Rapid and Accurate Evaluation of the Quality of Commercial Organic Fertilizers Using Near Infrared Spectroscopy. PLOS ONE 9, e88279. https://doi.org/10.1371/JOURNAL.PONE.0088279

Wang, H., Chen, D., Wen, Y., Cui, T., Liu, Y., Zhang, Y., Xu, R., 2023. Insights into influence of aging processes on zero-valent iron modified biochar in copper(II) immobilization: from batch solution to pilot-scale investigation. Frontiers of Chemical Science and Engineering 17, 880–892. https://doi.org/10.1007/s11705-022-2282-8

Wang, H., Dong, Y., Yang, Y., Toor, G.S., Zhang, X., 2013. Changes in heavy metal contents in animal feeds and manures in an intensive animal production region of China. Journal of Environmental Sciences 25, 2435–2442. https://doi.org/10.1016/S1001-0742(13)60473-8

Wang, P., Tang, L., Wei, X., Zeng, G., Zhou, Y., Deng, Y., Wang, J., Xie, Z., Fang, W., 2017. Synthesis and application of iron and zinc doped biochar for removal of p-nitrophenol in wastewater and assessment of the influence of co-existed Pb(II). Applied Surface Science 392, 391–401. https://doi.org/10.1016/j.apsusc.2016.09.052

Wang, Z., Xu, X., Ma, S., Wang, H., Zhao, H., Wang, Y., Tong, S., Su, Z., Wang, W., Bai, J., 2021. The superior adsorption capacity of boron-nitrogen co-doping walnut shell biochar powder for Au(III), Pt(IV), and Pd(II). Journal of Environmental Chemical Engineering 9, 106288. https://doi.org/https://doi.org/10.1016/j.jece.2021.106288

Wei, T., Simko, V., Levy, M., Xie, Y., Jin, Y., Zemla, J., 2017. Package 'corrplot.' Statistician 56, e24.

Werheit, H., Au, T., Schmechel, R., Shalamberidze, S.O., Kalandadze, G.I., Eristavi, A.M., 2000. IR-Active Phonons and Structure Elements of Isotope-Enriched Boron Carbide. Journal of Solid State Chemistry 154, 79–86. https://doi.org/10.1006/JSSC.2000.8815

Wickham, H., Averick, M., Bryan, J., Chang, W., D', L., Mcgowan, A., François, R., Grolemund, G., Hayes, A., Henry, L., Hester, J., Kuhn, M., Lin Pedersen, T., Miller, E., Bache, S.M., Müller, K., Ooms, J., Robinson, D., Seidel, D.P., Spinu, V., Takahashi, K., Vaughan, D., Wilke, C., Woo, K., Yutani, H., 2019. Welcome to the Tidyverse. Journal of Open Source Software 4, 1686. https://doi.org/10.21105/JOSS.01686

Wickham, H., Wickham, M.H., 2019. Package ‘tidyverse.’ See http://tidyverse. tidyverse. org 1–5.

Wijitkosum, S., Jiwnok, P., 2019. Elemental Composition of Biochar Obtained from Agricultural Waste for Soil Amendment and Carbon Sequestration. Applied Sciences. https://doi.org/10.3390/app9193980

Wu, D., Sun, F., Qu, Z., Wang, H., Lou, Z., Wu, B., Zhao, G., 2022. Multi-scale structure optimization of boron-doped hard carbon nanospheres boosting the plateau capacity for high performance sodium ion batteries. Journal of Materials Chemistry A 10, 17225–17236. https://doi.org/10.1039/D2TA04194D

Wu, P., Cui, P., Fang, G., Gao, J., Zhou, D., Wang, Y., 2018. Sorption mechanism of zinc on reed, lignin, and reed- and lignin-derived biochars: kinetics, equilibrium, and spectroscopic studies. Journal of Soils and Sediments 18, 2535–2543. https://doi.org/10.1007/s11368-018-1928-0

Wu, P., Guo, Z., Hua, K., Wang, D., 2023. Long-term application of organic amendments changes heavy metals accumulation in wheat grains by affecting soil chemical properties and wheat yields. Journal of Soils and Sediments 23, 2136–2147. https://doi.org/10.1007/s11368-023-03473-3

Wydro, U., Jankowska, M., Wołejko, E., Kondzior, P., Łozowicka, B., Kaczyński, P., Rodziewicz, J., Janczukowicz, W., Pietryczuk, A., Cudowski, A., Jabłońska-Trypuć, A., 2022. Changes in Soil Biological Properties after Sewage Sludge and Pesticide Application in Wheat Cultivation. Applied Sciences. https://doi.org/10.3390/app122211452

Xiao, Y., Xue, Y., Gao, F., Mosa, A., 2017. Sorption of heavy metal ions onto crayfish shell biochar: effect of pyrolysis temperature, pH and ionic strength. Journal of the Taiwan

Institute of Chemical Engineers 80, 114–121.

Xinxin, M.O., Siebecker, M.G., Wenxian, G.O.U., Ling, L.I., Wei, L.I., 2021. A review of cadmium sorption mechanisms on soil mineral surfaces revealed from synchrotron-based X-ray absorption fine structure spectroscopy: Implications for soil remediation. Pedosphere 31, 11–27.

Xu, L., Qi, Y., He, S., Wang, C., Jin, X., Wang, Q., Wang, K., Jin, P., 2025. Facile synthesis of boron-doped porous biochar as a metal-free adsorbent for efficient removal of aqueous tetracycline antibiotics. Journal of Environmental Sciences 152, 235–247. https://doi.org/https://doi.org/10.1016/j.jes.2024.04.044

Xu, L., Xing, X., Peng, J., Ji, M., 2022. Effects of In Situ Remediation on Copper Distribution and Soil Aggregate Adsorption–Desorption Characteristics in Smelter-Impacted Soil . Frontiers in Environmental Science .

Xu, P., Gao, Y., Cui, Z., Wu, B., Yan, B., Wang, Yifan, Zaitongguli, K., Wen, M., Wang, H., Jing, N., Wang, Yingze, Chao, C., Xue, W., 2023. Research Progress on Effects of Biochar on Soil Environment and Crop Nutrient Absorption and Utilization. Sustainability. https://doi.org/10.3390/su15064861

Yang, F., Wang, C., Sun, H., 2021. A comprehensive review of biochar-derived dissolved matters in biochar application: Production, characteristics, and potential environmental effects and mechanisms. Journal of Environmental Chemical Engineering 9, 105258. https://doi.org/10.1016/J.JECE.2021.105258

Yang, H., Sheng, K., 2012. Characterization of Biochar Properties Affected by Different Pyrolysis Temperatures Using Visible-Near-Infrared Spectroscopy. International Scholarly Research Network ISRN Spectroscopy 2012. https://doi.org/10.5402/2012/712837

Yang, Z., Yao, Z., Li, G., Fang, G., Nie, H., Liu, Z., Zhou, X., Chen, an, Huang, S., 2011.

Sulfur-Doped Graphene as an Efficient Metal-free Cathode Catalyst for Oxygen Reduction. https://doi.org/10.1021/nn203393d

Younis, U., Rahi, A.A., Danish, S., Ali, M.A., Ahmed, N., Datta, R., Fahad, S., Holatko, J., Hammerschmiedt, T., Brtnicky, M., Zarei, T., Baazeem, A., Sabagh, A. El, Glick, B.R., 2021. Fourier Transform Infrared Spectroscopy vibrational bands study of Spinacia oleracea and Trigonella corniculata under biochar amendment in naturally contaminated soil. PloS one 16, e0253390. https://doi.org/10.1371/journal.pone.0253390

Yue, X., Fei-Yue, L., Xing-Jun, F., Shui-Jin, H., Xin, X., Jian-Fei, W., 2018. Cite this article as: Chinese. CHINESE JOURNAL OF ANALYTICAL CHEMISTRY 46, 609–615. https://doi.org/10.1016/S1872-2040(17)61081-8

Zhang, D., Sun, J., Li, Q., Song, H., Xia, D., 2022. Cu-Doped magnetic loofah biochar for tetracycline degradation via peroxymonosulfate activation. New Journal of Chemistry 46, 17223–17234. https://doi.org/10.1039/D2NJ02885A

Zhang, H., Cao, Q., Zhang, K., Xie, L., Xu, K., Qin, Y., Zhang, L., Chai, X., 2023. Boron-doped biochar-nano loaded zero-valent iron to activate persulfate for the degradation of oxytetracycline. Journal of Environmental Chemical Engineering 11, 111502. https://doi.org/10.1016/J.JECE.2023.111502

Zhang, J., Koubaa, A., Xing, D., Liu, W., Wang, Q., Wang, X., Wang, H., 2020a. Improving lignocellulose thermal stability by chemical modification with boric acid for incorporating into polyamide. Materials & Design 191, 108589. https://doi.org/https://doi.org/10.1016/j.matdes.2020.108589

Zhang, J., Koubaa, A., Xing, D., Liu, W., Wang, Q., Wang, X.M., Wang, H., 2020b. Improving lignocellulose thermal stability by chemical modification with boric acid for incorporating into polyamide. Materials & Design 191, 108589. https://doi.org/10.1016/J.MATDES.2020.108589

Zhang, Xu, Gang, D.D., Zhang, J., Lei, X., Lian, Q., Holmes, W.E., Zappi, M.E., Yao, H., 2022. Insight into the activation mechanisms of biochar by boric acid and its application for the removal of sulfamethoxazole. Journal of Hazardous Materials 424, 127333. https://doi.org/https://doi.org/10.1016/j.jhazmat.2021.127333

Zhang, Xin, Zhao, B., Liu, H., Zhao, Y., Li, L., 2022a. Effects of pyrolysis temperature on biochar's characteristics and speciation and environmental risks of heavy metals in sewage sludge biochars. Environmental Technology & Innovation 26, 102288. https://doi.org/10.1016/j.eti.2022.102288

Zhang, Xin, Zhao, B., Liu, H., Zhao, Y., Li, L., 2022b. Effects of pyrolysis temperature on biochar's characteristics and speciation and environmental risks of heavy metals in sewage sludge biochars. Environmental Technology & Innovation 26, 102288. https://doi.org/https://doi.org/10.1016/j.eti.2022.102288

Zhang, Y., Zhang, W., Zhang, H., He, D., 2023. Nano-Zero-Valent Zinc-Modified Municipal Sludge Biochar for Phosphorus Removal. Molecules 28, 3231.

Zhao, J., Li, H., Wang, Y., Yu, J., Li, N., Wang, S., 2023. Cu/CuO-Decorated Peanut-Shell-Derived Biochar for the Efficient Degradation of Tetracycline via Peroxymonosulfate Activation. Catalysts. https://doi.org/10.3390/catal13091246

Zhou, Y., Yan, W., Yu, X., Chen, T., Wang, S., Zhao, W., 2020. Boron and nitrogen co-doped porous carbon for supercapacitors: A comparison between a microwave-assisted and a conventional hydrothermal process. Journal of Energy Storage 32, 101706. https://doi.org/10.1016/j.est.2020.101706

Zhu, X., Chen, B., Zhu, L., Xing, B., 2017. Effects and mechanisms of biochar-microbe interactions in soil improvement and pollution remediation: A review. Environmental Pollution 227, 98–115. https://doi.org/https://doi.org/10.1016/j.envpol.2017.04.032

Supplementary Material

Table S 1. Chemical characterization of the raw material, biochar and composites produced.

ID	Al	B	Ca	Cu	Fe	Mg	Mn	Na	P	Zn
	--- ($mg\ kg^{-1}$) ---									
FCM	2669	299	102606	178	2533	6466	462	2929	21060	551
FSC	1844	222	96764	98	1137	8433	92	1774	18473	109
FSS	6867	47	9471	348	11106	2489	200	922	3843	623
BCM	2780	243	108732	166	2170	9516	597		30035	787
BSC	2268	162	86603	147	3437	8513	114	IN	23074	1683
BSS	7399	94	10293	423	5565	2347	230	IN	4745	812
BCM'	4719	196	105307	169	3657	13158	882	IN	46275	968
BSW'	3648	164	125101	188	4749	17627	156	IN	44359	2238
BSS'	10537	95	12647	481	11439	2738	301	IN	6129	922
CCM-BA	6334	166651	101517	14657	3271	<LQ	1857	7527	27145	567
CCM-BX	4879	75525	108679	<LQ	2712	<LQ	1843	84240	29341	233
CCM-BA'	7342	138655	157750	<LQ	4312	<LQ	2143	11461	32208	412
CCM-BX'	7169	62159	142800	<LQ	4366	<LQ	2185	77565	33387	338
CSC-BA	2275	133155	112591	1396	1601	12482	52	20552	44250	4105
CSC-BX	2567	91268	83212	2364	1547	9455	62	145502	36883	1238
CSC-BA'	3356	137659	237362	326	1839	19350	127	24298	68037	3865
CSC-BX'	3446	73609	292200	256	1629	22464	154	129040	66508	1640
CSS-BA	77711	127459	2465	1788	41466	3622	126	10527	11182	1366
CSS-BX	260387	66247	2411	546	135316	4983	210	96636	12786	1151
CSS-BA'	35608	145763	<LQ	719	28450	<LQ	1240	677	<LQ	111
CSS-BX'	35104	63252	<LQ	<LQ	10251	<LQ	1137	77757	<LQ	163

Table S 2. Parameters for PLS regression models to predict the chemical properties of composites produced under different pyrolysis temperatures.

	pH	EC	C	ASHES	N	Boron			
		$ds\ m^{-1}$	----------- (%)-----------			W	T	NAC	CA%
Latent variables	9	19	14	15	12	19	18	18	14
RMSE of calibration	0.3102	0.0313	1.7013	1.7183	0.4699	9.67	6.7153	1.6737e+03	4.7407e+03
R^2 of calibration	0.9523	1.0	0.9563	0.9901	0.9274	0.99	0.999	0.9989	0.9836
RMSE of y-randomization	0.8608	2.4726	5.1602	10.5778	1.1497	483.93	321.9165	2.4757e+04	2.0032e+04
R^2 of y-randomization	0.6291	0.7313	0.5918	0.6219	0.5520	0.713	0.6894	0.7586	0.7024
r^2 of y-randomization prediction	0.5548	0.5183	0.5904	0.6039	0.5900	0.535	0.5572	0.4899	0.5259
RMSE of cross-validation	0.8158	2.8066	5.2704	11.0505	1.0307	203.7268	117.0171	1.4720e+04	1.0447e+04
R^2 of cross-validation	0.7148	0.7088	0.6085	0.6253	0.7096	0.9516	0.96	0.9199	0.9212
RMSE of prediction	0.9375	1.2319	4.0673	8.7589	1.2423	136.388	71.4326	0.9199	8.3545e+03
R^2 of prediction	0.6203	0.9158	0.7611	0.7258	0.7192	0.9789	0.9870	0.8820	0.9563
r^2 of test set	0.4299	0.8584	0.6780	0.6503	0.4219	0.9428	0.9844	0.7988	0.8511

pH: hydrogen potential; EC: electrical conductivity; C: Total organic carbon concentration; ASHES: glad ashes; N: nitrogen concentration; W: H2O and T: concentration of boron total; NAC and CA%: neutral ammonium citrate plus water and concentration of B soluble in water, citric acid at 2%; LV: latent variable; RMSE: root mean square error; R2 or r2: squared correlation coefficient; RMSEcal: RMSE of calibration; R2cal: R2calibration; RMSEcv: RMSEcross-validation; R2cv: R2cross-validation; RMSEy-rand: RMSE of y-randomization; R2y-rand: R2y-randomization; r2p: r2 of y-randomization prediction; RMSEpred: RMSE of prediction; R2 pred: R2 of prediction; r2m: r2 between the experimental and predicted values for the test set.

CHAPTER II

ASSESSING THE EFFECT OF COPPER-BIOCHAR COMPOSITES ON NUTRITION AND GROWTH OF WHEAT CULTIVATED IN OXISOLS

To be submitted to ACS Agricultural Science & Technology

Loren Chisté[1], Carlos Alberto Silva[1]; Flávio Henrique Silveira Rabêlo[1]; Keiji Jindo[2];

Leônidas Carrijo Azevedo Melo[1*].

[1]Department of Soil Science, School of Agricultural Sciences, Federal University of Lavras, Lavras, Minas Gerais 37203-202, Brazil;

[2]Agrosystems Research, Wageningen University & Research, PO Box 16, 6700 AA Wageningen, Holanda.

*Corresponding author: leonidas.melo@ufla.br

Abstract

Copper (Cu) is essential for the growth and development of wheat, significantly enhancing grain quality. Proper Cu management is crucial to avoid deficiency and toxicity, with Cu-organic matter interactions effectively regulating soil Cu levels for crops. This study investigates the effects of Cu-doped biochar composites on the nutrition and growth of wheat (*Triticum aestivum*) in different Oxisols. Biochar-Cu composites were synthesized using chicken manure (FCM), shrimp shells (FSC), and municipal sewage sludge (FSS), combined with either copper sulfate (CuS) or copper oxide (CuO), and then pyrolyzed at 300 °C or 550 °C. The experimental design was a completely randomized design (CRD) with three replicates. Fourier Transform Infrared Spectroscopy (FTIR) analysis confirmed Cu incorporation into the biochar, highlighting significant adsorption patterns and functional groups such as OH, C=O, C-O-C, and SO_4^{-2}, particularly in the sewage sludge composite doped and pyrolyzed with CuS at 550 °C (CSS/CS-5). The CSS/CS-5 composite outperformed pure CuS, enhancing Cu accumulation in wheat shoots in DRL soil. In RYL soil, CSC/CS-3 promoted higher dry matter production and Cu accumulation in the shoots. The CSS/CO-3 treatment showed a peak of Cu availability on the 7th day in the RYL soil, although this did not correlate with increased wheat dry matter production. In DRL soil, CSC/CS-3, followed by CuS (control), showed peak Cu availability on the 1st day. Residual effects were more significant in soils treated with CuS across both soil types. These findings suggest that Cu application rates for wheat should consider the soluble Cu concentration in neutral ammonium citrate plus water in the composites, with CSS/CS-5 emerging as a promising alternative to enhance Cu use efficiency in DRL and CSC/CS-3 in RYL.

Keywords: Cu-doping, chemometrics, Cu release kinetics, ATR-FTIR, soil Cu availability.

1. Introduction

Copper (Cu) is an essential element for plant growth, yet its availability is often limited in tropical soils, such as those found in the Brazilian cerrado. These soils usually have high concentrations of iron and aluminum oxides, low-activity colloids, acidic pH, low to medium organic matter concentration and low CTC (Vermaat et al., 1950). These properties enhance the adsorption of Cu within soil colloids, significantly reducing its bioavailability to plants (Hortin et al., 2020). As a result, conventional Cu fertilizers, such as copper sulfate (CuS) and copper oxide (CuO), have limited effectiveness in these soils and are rarely used, particularly for crops like wheat. Winter wheat, which has a high demand for Cu, often receives insufficient fertilization, leading to reduced yields (Jez et al., 2023).

Cu-doped biochar composites offer a novel solution to this problem (D. Zhang et al., 2022). These composites, enriched with Cu in the form of oxides or sulfates, can potentially serve as high-value micronutrient sources able to reduce Cu fixation in tropical soils and increase its availability to plants (Carneiro et al., 2022; Cho et al., 2019). The conditions under which biochar is produced, including the temperature and type of feedstock used, significantly influence its composition and properties, subsequently affecting Cu availability in the soil (Altıkat et al., 2024). The feedstock selection influences the elemental composition, pH, and potential contaminants, as well as the effectiveness of biochar as a nutrient source or soil conditioner (Otoni et al., 2024). Consequently, Cu-biochar composites can address Cu deficiency in soil and support sustainable, efficient Cu fertilization strategies, thereby improving crop growth and yields in tropical soils (Hu and Wei, 2023), such as winter wheat (Wijitkosum and Jiwnok, 2019).

This study focuses on converting abundant organic wastes in Brazil, specifically chicken manure (FCM), shrimp shells (FSC) and sewage sludge (FSS), into biochar composites. When pyrolyzed with Cu sources, these materials exhibit increased pH, structural changes, and the presence of alkaline functional groups in the biochar matrix, which enhance Cu surface complexation through deprotonation (Q. Liu et al., 2021). The selection of these feedstock is based on their availability and their demonstrated potential for biochar production in previous studies (Jin et al., 2022), (Heckler et al., 2014) and (Wydro et al., 2022). Applying Cu-biochar composites can increase cation exchange capacity, catalyze various reactions, and improve Cu availability to plants in pH-dependent environments (Xu et al., 2022). Analytical techniques, such as infrared spectroscopy, are used to identify chemical bonds and compounds within the composites. Comprehensive chemical analyses for Cu speciation, pools, and availability aim to meet plant nutritional requirements and enhance the agronomic effectiveness of Cu fertilizers in tropical, highly weathered soils (Xu et al., 2022). Higher pyrolysis temperatures typically produce biochar with enhanced Cu sorption capacity but may also destroy organic functional groups essential for Cu complexation (Zhu et al., 2017).

The hypothesis of this study is that Cu-biochar composites are more efficient than traditional Cu fertilizers in promoting wheat growth in Oxisols. The study aims to (i) identify synthesis routes and evaluate properties of Cu composites (CuS and CuO) based on biochars derived from FCM, FSC, and FSS pyrolyzed at 300 °C or 550 °C; (ii) assess the efficiency of Cu-biochar composites in supplying Cu to wheat plants, and examine Cu release in Oxisols; (iii) determine the agronomic effectiveness of Cu-biochar composites in ensuring robust wheat growth compared to plants fertilized with CuS.

2. Material and Methods

2.1. Feedstock Preparation and Characterization

Three types of feedstocks for the synthesis of biochars and composites were selected: chicken manure (FCM), shrimp shell (FSC), and sewage sludge (FSS). FCM was acquired from a farm located in Nepomuceno, Minas Gerais, Brazil (Latitude: -21.236110° S; Longitude: -45.234970° W); FSS was collected from a sewage treatment station at the Federal University of Lavras (UFLA) in Lavras, Minas Gerais, Brazil (Latitude: -21.23008° S; Longitude: -44.98981° W); and FSC was obtained from a seafood processing corporation located in Linhares, Espírito Santo, Brazil (Latitude: -19.373030° S; Longitude: -40.054680° W), (Figure S 1).

The feedstocks were initially air-dried at room temperature to remove constitutional moisture. Subsequently, they were dried in a forced-air oven at 65 °C until reaching constant weight. After drying, the samples were ground and sieved to ensure a uniform particle diameter of less than 0.25 mm. The processed feedstocks were stored in desiccators and airtight plastic bags to prevent re-moisturization.

2.2. *Synthesis of Biochar and Copper-Doped Biochar*

Six biochar samples were produced by pyrolyzing each feedstock and two Cu sources in a JUNG muffle furnace at either 300 °C or 550 °C, with a heating rate of 10 °C per minute and a holding time of 60 minutes followed by slow cool-down to room temperature. Twelve Cu-doped composites were synthesized by mixing feedstocks with either copper sulfate ($CuSO_4 \cdot 5H_2O$) or copper oxide (CuO), sourced from ISOFAR and Exodus Scientific, to achieve a target Cu concentration of 20 % (w/w) in the final composite. The selection of a 20% Cu concentration was defined based on preliminary studies demonstrating that this concentration optimizes the catalytic catalytic activity and structural stability of the composites, preventing excessive agglomeration of Cu particles and ensuring uniform metal distribution (Aleosfoor and Rahimpour, 2024). Additionally, this concentration was deemed appropriate to ensure efficient synthesis without compromising the integrity of the biochar. The pre-treated mixture, weighing 100 g, was subjected to pyrolysis under the same conditions as the untreated biochars. After pyrolysis, all samples were ground and sieved through a 60-mesh screen for consistency, and the ground, dried and prepared samples were stored in desiccators until further analysis. Refer to Table 1 for the nomenclature of feedstocks and Cu sources, biochar, and Cu-biochar composites.

Table 6- Identification of feedstocks, biochar sources, and synthesis temperatures for the biochar composites

Acronym	Feedstock	Temperature (°C)	Cu Source
FCM	Chicken Manure	60	no
FSC	Shrimp Carcass		
FSS	Sewage Sludge		
BCM-3	Chicken Manure	300	No
BSC-3	Shrimp Carcass		
BSS-3	Sewage Sludge		
CCM/CS-3	Chicken Manure	300	Copper Sulfate
CCM/CO-3	Chicken Manure		Copper Oxide
CSC/CS-3	Shrimp Carcass		Copper Sulfate
CSC/CO-3	Shrimp Carcass		Copper Oxide
CSS/CS-3	Sewage Sludge		Copper Sulfate
CSS/CO-3	Sewage Sludge		Copper Oxide
BCM-5	Chicken Manure	550	No
BSC-5	Shrimp Carcass		
BSS-5	Sewage Sludge		
CCM/CS-5	Chicken Manure	550	Copper Sulfate
CCM/CO-5	Chicken Manure		Copper Oxide
CSC/CS-5	Shrimp Carcass		Copper Sulfate
CSC/CO-5	Shrimp Carcass		Copper Oxide
CSS/CS-5	Sewage Sludge		Copper Sulfate
CSS/CO-5	Sewage Sludge		Copper Oxide

2.3. *Characterization of Biochar and Composite Properties*

The concentrations of volatile matter (VM), moisture (M), and ash (As) were determined following ASTM D1762-84, with modifications for biochar (Eqs. 1-3) (Balwant Singh , Marta Camps Arbestain, 2017) (ASTM International, 1984), (D1762-84, 2013). Biochar yield (Y) was calculated according to the Eq. 5. Post-VM determination, ash concentration was quantified by incinerating the sample at 750 °C for six hours. Fixed carbon concentration (FC) was computed as outlined in Eq. 4.

$$VM(\%) = \frac{DW\ at\ 105°C - DW\ at\ 950°C}{DW\ at\ 105°C}\ x100 \quad \text{(Eq. 1)}$$

$$M(\%) = \frac{RW - DW\ at\ 105°C}{RW}\ x\ 100 \quad \text{(Eq. 2)}$$

$$\mathrm{As}(\%) = \frac{\mathrm{RW - DW\ at\ 750ºC}}{\mathrm{DW\ AT\ 105ºC}}\ \mathrm{x}\ 100 \quad \text{(Eq. 3)}$$

$$\mathrm{FC}(\%) = \frac{\mathrm{DW\ at\ 105ºC - DW\ at\ 950ºC - DW\ at\ 750ºC}}{\mathrm{DW\ at\ 105ºC}}\ \mathrm{x}\ 100 \quad \text{(Eq. 4)}$$

$$\mathrm{Y}(\%) = 100\ \mathrm{x}\ \frac{\mathrm{biochar\ mass}}{\mathrm{105\ ºC\ dried\ feedstock}} \quad \text{(Eq. 5)}$$

The pH and electrical conductivity (EC) of the studied samples were assessed using a 1:10 ratio of biochar to water, measured with a digital meter from (Toledo CE, Mettler-Toledo AG) (Singh et al., 2017). Carbon (C) concentration was determined through a dry combustion technique using a Vario TOC cube analyzer from Elementar, Germany. Total nitrogen (N) concentration was measured following sulfuric acid digestion employing the Kjeldahl method (Singh et al., 2017). The carbonized samples underwent a digestion process involving sulfuric acid mixed with selenium and potassium sulfate in digestion tubes. The process began with a 12-hour pre-digestion phase, followed by a gradual increase in temperature up to 250 °C until the samples were completely solubilized. After digestion, the nutrient concentrations were quantified using the inductively coupled plasma optical emission spectroscopy (ICP-OES) technique, with certified reference materials used to ensure quality control of the results during the digestion phase, Table S 1.

All digestion procedures utilized certified tomato leaf samples from the National Institute of Standards and Technology (NIST) SRM 1573a; as well as biochar samples derived from sewage sludge and wheat straw in the UK, supplied by the Biochar Research Centre, School of Geosciences - University of Edinburgh (SS550, SS700, WSP550, and WSP700) (Masek et al., 2018). These standard samples were utilized to ensure quality control, along with blank samples whose concentrations were factored into the calculations to determine the final elemental composition of feedstocks, biochars, and composites.

Water-soluble (W), 2% citric acid-soluble (CA%), and neutral ammonium citrate-soluble (NAC) Cu levels were assessed in filtrate using standard methods (GRANULOMÉTRICA, 2014). The indices of Cu in the sources used in this study were quantified through chemical analysis and subsequently determined using the ICP-OES method. To compare the Cu solubility of the samples, a Cu index was calculated, taking into account the ratio of the soluble fractions of Cu (Cu-W, Cu-CA% and Cu-NAC) and the total Cu concentration of each matrix, according to (Eq. 6).

$$\text{Cu (\%)} = \frac{\text{Soluble Cu (g kg}^{-1}\text{)}}{\text{Total Cu (g kg}^{-1}\text{)}} \text{ x } 100 \qquad \text{(Eq. 6)}$$

2.4. *Fourier Transform Infrared Spectroscopy (FTIR)*

A spectral signature characterization was conducted using Fourier-transform infrared spectroscopy (FTIR) with attenuated total reflectance (ATR) on an Agilent® Cary 630 FTIR spectrometer with a ZnSe-ATR crystal (Agilent Technologies, U.S.), Infrared spectroscopy analysis was performed at a 4 cm^{-1} scan resolution, covering a wavelength range of 4000 to 650 cm^{-1}. The normalization procedure was applied to each FTIR spectrum (Liberda et al., 2021). Spectrum interpretation and identification of specific spectral bands for Cu-treated biochars were performed using libraries and bands and organic groups assignments described in (Balwant Singh , Marta Camps Arbestain, 2017; Khan et al., 2017).

2.5. *Scanning Electron Microscopy (SEM)*

The scanning electron microscope (SEM) was used to analyze the elemental composition of the samples, utilizing the Schottky Field Emission Scanning Electron Microscope JEOL JSM-7610F, located at the Electron Microscopy and Ultrastructural Analysis Laboratory of the Federal University of Lavras (LME/UFLA) in Brazil- Department of Phytopathology. Non-conductive, dried samples measuring 0.5 × 0.5 × 0.5 cm were oven-dried, mounted on stubs using double-sided carbon tape, and then carbon-coated.

2.6. *Copper Release Kinetics*

The kinetics of Cu release from various matrices was assessed through sequential extractions over time. The experimental procedure involved weighing 1.0 g of the sample, which was then transferred to a 50 mL falcon tube, combined with 20 mL of 2% citric acid solution. The mixture was horizontally shaken at 90 rotations per minute (rpm), and extracts were collected at predetermined intervals at 0.25, 0.5, 1, 2, 4, 12, 24, 48, 72, 120 and 250 hours of sequential analysis to evaluate the Cu quantities released by the biochars and their composites. After each extraction time, tubes containing samples were centrifuged for 5 minutes at 3500 rpm. The resultant supernatant was carefully collected and transferred to another falcon tube, reserved for further analysis of the extracted analytes, focusing on Cu measurement in leachate extracts using an inductively coupled plasma optical emission spectrometer (ICP-OES).

2.7. *Agronomic Impact of Cu Composites*

The agronomic study was conducted in a greenhouse experiment involving wheat Triticum aestivum cultivation in surface samples (0-20 cm) of typical Dystrophic Red-Yellow Oxisol (RYL) and Dystroferric Red Oxisol (DRL) whose main attributes are shown Table 2.

Table 7. Physicochemical characterization of Oxisols (under natural conditions) utilized in wheat cultivation

Oxisol	pH	C	Clay	Silt	Sand	N	P	K	Ca	Mg	Fe	Mn	B	Cu	Zn
		---------- $g\ kg^{-1}$ ----------				--- $mg\ dm^{-3}$ ---			$cmol_c\ dm^{-3}$		------------ $mg\ dm^{-3}$ -------------				
RYL	4.7	4.5	460	85	455	329	6.1	217.5	0.8	0.4	35.7	3.0	0.1	0.0	0.2
DRL	4.5	19.8	770	100	130	2580	8.3	30.1	0.3	0.2	50.6	3.4	0.06	1.1	0.3

RYL- Red Yellow Oxisol (medium texture); DRL-Dystroferric Red Oxisol; pH in a soil-water-Ratio of 1:2.5; C: carbon determined (dry combustion) in an automatic TOC analyzer; clay, silt and sand analyzed by the Boyoucos method. All methods are described in detail (Teixeira et al., 2017a); N: total nitrogen – *Kjeldahl* method; P: available phosphorus determined by the resin soil test; K, Fe^{2+}, Mn^{2+}, Cu^{2+} and Zn^{2+}: available determined by the Mehlich^{-1} soil test; B: EDTA extractor; exchangeable calcium (Ca^{2+}), exchangeable magnesium ($Mg^{2+)}$ extracted by a 1 mol L^{-1} KCl solution soil test.

Soil samples underwent air-drying, grounding, and sieving (2 mm) to obtain air-dried fine earth. Soil acidity was corrected using calcium carbonate ($CaCO_3$) and magnesium carbonate

($MgCO_3$) at a 4:1 molar ratio to achieve a target pH of 5.5 ± 0.2, aiming to maximize the availability of essential macro and micronutrients and optimize growth conditions for the plants, avoiding aluminum toxicity that is common in these soils. This approach ensures that the soil conditions are optimized for the specific crop, providing a balanced environment for healthy plant development (Barrow and Hartemink, 2023). The lime application aimed to provide optimal growth conditions for wheat and to ensure the availability of calcium (Ca) and magnesium (Mg) in the soil (Teixeira et al., 2017a). A randomized complete block design with a 5x3 factorial arrangement was employed, combining five biochar-Cu composites: CCM/CS-3, CSC/CS-5, and CSS/CS-5 with and without Cu addition. Regardless of the source, Cu was added to both Oxisols at the concentration of 4.0 mg kg^{-1} (Shabbir et al., 2020). The choice of the composites CCM/CS-3, CSC/CS-5, and CSS/CS-5, over others presented in Table 1 was based on their specific properties and demonstrated efficacy in this study. These composites were selected to deliver an ideal combination of physical and chemical characteristics that maximize nutrient availability in the soil, in addition to showing uniform Cu distribution and thermal stability, making them more effective for the experimental conditions of this study.

After liming, each pot containing 3 kg of soil was fertilized, and wheat was sown with four seeds per pot, incorporating a nutrient regimen that includes 300; (600 DRL and 300 RYL), 300; 40; 1.80; 5, 20 and 0.15 mg kg^{-1}, of N, P, K, S, B, Mn, Mo, Zn and Fe, respectively, and using the following sources: $NH_4H_2PO_4$, K_2SO_4, H_3BO_3, $MnCl_2.4H_2O$, $(NH_4)_6Mo_7O_2.4H_2O$ (p.a), except for N and K, which were split into three applications at 7, 15 and 30 days after wheat seed germination (Novais et al., 1991). Irrigation was maintained at approximately ~70% of the soils maximum water-holding capacity. The trial lasted 90 days, with daily soil water level adjustments.

At the beginning of the experiment, a *Suolo Acqua*® sampler (Carmo et al., 2016) was installed in the lower third of the pots, centrally, where the soil was carefully packed and slightly compressed around the soil solution sampler to avoid the entry of air in the soil-water-sampler system. After 12 hours of the wheat sowing, the first aliquot of the soil solution (20 mL) was collected throughout the experimental period at 1, 7 and 15 days. The collected solution was filtered through a membrane with a pore size of 0.45 µm, and soil Cu concentration was determined by ICP-OES. After 190 days of wheat sowing, 50 g of soil was collected from each experimental unit. The soil samples were then dried and sieved (2 mm). The Cu concentration in the soil was determined at the end of the experiment to evaluate the residual Cu available in the soil after wheat cultivation (Teixeira et al., 2017a).

Upon harvest, 190 days after sowing, wheat plants were separated into shoots, roots, and grains. The dry matter weight for each part was obtained after drying at 60 °C. Shoot dry matter (SDM), root dry matter (SDR) and grain yield (GP) were ground in a mill of Willey knives, sieved (1 mm) and digested in a nitric-perchloric mixture (Silva, 2009), and the Cu concentration in the plant tissue was determined using an ICP-OES, while Cu accumulation in the SDM was calculated by multiplying the dry matter by the Cu concentration in shoot (Eq. 7).

$$Shoot\ Cu\ content\ =\ shoot\ dry\ matter\ (g)\ \times\ Cu\ concentration\ in\ the\ shoot\ tissue\ (mg\ g^{-1}) \qquad \text{(Eq. 7)}$$

2.8. *Statistical analysis*

Data were processed to yield mean values, which were then subjected to a Two-Way ANOVA to discern any statistically significant differences (p<0.05) among treatments, followed by means comparison using Tukey's test (p<0.05). All assumptions for ANOVA were verified, and significance was assessed at p<0.05 using R software (Factoextra, 2022). Multivariate analyses were conducted using R to elucidate the relationships between the properties and Cu pools within the composites. The packages employed in these analyses included agricolae, factoextra, FactoMineR, pvclust, corrplot, tidyverse, and nlstools

(Agricolae, 2022; Baty et al., 2015b; Extract, 2020; Lê et al., 2008a; Ryota Suzuki, 2022; Taiyun Wei et al., 2022; Wickham et al., 2019).

The dataset of Cu release kinetics in 2% citric acid - (CA%), was fitted to different non-linear mathematical models, as an output of the relationship between incubation time versus the amount of Cu released from each source. of the nutrient. The following mathematical models were fitted to the Cu kinetics data set: Elovich model (Eq. 12), simple exponential model (Eq. 13), power function (Eq. 14), hyperbolic model (Eq. 15).

$$Nt = a + blnt \quad \text{(Eq. 8)}$$
$$Nt = N0\left(1 - e^{-kt}\right) \quad \text{(Eq. 15)}$$
$$Nt = a\,x\,b^{t} \quad \text{(Eq. 10)}$$
$$Nt = \frac{N0\,x\,t}{(N0\,x\,b + t)} \quad \text{(Eq. 11)}$$

Model selection for Cu release kinetics was informed by the highest determination coefficient (R^2), the lowest root mean square error (RMSE), and the smallest Akaike information criterion (AIC) values (Akaike, 1979). Notation: *Nt* is the fraction of Cu released at time *t*; *a* represents the initial Cu release rate; *b* is the constant rate of Cu release; and *N*0 is the maximum amount of Cu released during the kinetics study.

3. Results and Discussion

3.1 Chemical properties of the Composites

The pH of the biochars varied significantly, ranging from 6.2 to 10.7 (Table 3). Biochars derived from FCM and FSC exhibited higher pH values, indicating a more alkaline nature. In contrast, those derived from FSS showed lower pH values, which could influence their application in acidic soils (Penido et al., 2019). The high alkalinity of the FCM and FSC biochars may be beneficial for neutralizing acidic soils. Although the FSS biochars have a lower pH of 6.2, this does not necessarily limit their effectiveness in such conditions. Overall, the pH of the biochars increases with the pyrolysis temperature for all feedstocks due to the increased generation of ash, which contains basic cations that can be associated with alkaline species such as carbonates, oxides, and hydroxides (Das et al., 2021), especially in nutrient-rich raw materials (Rimena R. Domingues et al., 2017), such as FCM and FCS.

Electrical conductivity (EC) ranged from 1.3 to 8.2 dS m^{-1}, with BCM-3, BCM-5 and BSC-3 showing the highest values. This suggests a higher concentration of soluble salts in these biochars, which could affect their applicability in soils depending on soil salinity and the crops to be grown. In general, the yield percentage of the biochars decreased with increasing pyrolysis temperature, as expected, due to greater mass loss at higher temperatures (Muzyka et al., 2023). The inorganic constituents present in the ash of FSS-derived biochars act as flame retardants, thereby reducing mass loss during pyrolysis (Fan et al., 2020). The volatile matter (VM) concentration was higher in biochars pyrolyzed at 300 °C, as seen in BSC-3 with 72%, compared to those pyrolyzed at 550 °C, such as BSC-5 with 42%. This pattern indicates that higher pyrolysis temperatures promote greater volatilization of organic compounds, resulting in a biochar with lower volatile matter concentration and a higher proportion of fixed carbon (Ghorbani et al., 2022a).

Ash concentrations ranged from 32% to 78%, with biochars from FSS showing the highest ash concentrations, which reflects the large number of inorganic minerals present in sewage sludge, which do not volatilize during pyrolysis and remain in the biochar (Ghorbani et al., 2022b). The fixed carbon percentage increased with pyrolysis temperature, consistent with the thermal decomposition of volatile materials and the concentration of inert carbon. For example, BCM-5 had 11.1% fixed carbon, while BCM-3 had 9.3%. Biochars derived from FSC had a higher carbon concentration (41% for BSC-5) compared to those from sewage sludge (FSS) (12% for BSS-5). However, the carbon concentration in FCM biochar decreased with increasing pyrolysis temperature, which is consistent with findings reported by other studies (Rimena R. Domingues et al., 2017).

Nitrogen concentration was highest in biochars from BCS-3 (6.5%) compared to other types, as the nitrogen concentration and chemical species of N in the biochars are determined by the choice of feedstock and its initial N concentration (Schellekens et al., 2018). The C:N ratio, an important factor in biochar application in soil, varied significantly. Biochars from (BCM-3 and BCM-5) had higher C ratios (16.6 and 13.1, respectively), which could suggest potential benefits for carbon stability in the soil. In contrast, biochars from FSS had lower C:N ratios (10.3 for BSS-5), indicating a relatively higher potential for N mineralization (Clough et al., 2013). While the C and N in biochar are generally stable, especially at lower pyrolysis temperatures, these ratios provide insight into the comparative dynamics of these elements among different biochars.

In summary, the type of feedstock and pyrolysis temperature significantly affect the properties of biochar. Biochars from FCM and FSC showed higher alkalinity and C concentration, while those from FSS had higher ash concentration and lower C: N ratio. These characteristics should be considered when selecting biochar for specific soil applications to optimize agronomic and environmental benefits.

Table 8- Properties of the Biochar

Biochar	pH	EC	Yield	VM	Ash	FC	Elemental Composition		C: N Ratio
		(dS m^{-1})	--------------------------------(%)-------------------------------------						
							C	N	C: N
BCM-3	9.1	6.4	69	57	52	9.3	35	2.1	16.6
BCM-5	10.7	8.2	53	56	60	11.1	26	1.9	13.1
BSC-3	9.2	7.3	81	72	32	3.9	41	6.5	6.4
BSC-5	10.4	2.9	60	53	60	12.5	25	2.4	10.7
BSS-3	6.2	1.3	88	34	71	4.8	16	2.1	7.6
BSS-5	7.1	1.5	69	28	78	5.4	12	1.2	10.3

Values are mean ± standard deviation (n = 3), except yield (%) (n = 1); EC: electrical conductivity; VM: volatile matter; Ashes; FC: fixed carbon; C: Carbon; N: nitrogen; C/N: carbon/nitrogen ratio. BCM-3: chicken manure biochar at 300 °C; BCM-5: chicken manure biochar at 550 °C; BSC-3: shrimp shell biochar at 300 °C; BSC-5: shrimp shell biochar at 550 °C; BSS-3: sewage sludge biochar at 300 °C; BSS-5: sewage sludge biochar at 550 °C.

The composites derived from CCM/CS-5 and CCM/CO-5 exhibited substantial increases in pH, illustrating the impact of high-temperature treatment on carbonized matrix alkalinity (Table 4). Notably, CCM/CS-5 exhibited a considerable increase in pH from 5 at 300

°C to 10 at 550 °C, alongside a significant decrease in EC from 21 dS m^{-1} to 9 dS m^{-1}. Similarly, the pH of CCM/CO-5 increased to 10.6, while its EC decreased to 8.4 dS m^{-1}. These changes suggest that higher pyrolysis temperatures can enhance the composite's ability to correct soil acidity. The lower solubility of CuO results in fewer free ions in the solution, thereby reducing EC. Additionally, the basic nature of CuO contributes to a higher pH level in the biochar, making it more alkaline than the more acidic CuS (Zhao et al., 2023).

In contrast, lower pH values in CSS/CS-3 may indicate greater metal solubility, although solubility is conditioned by the degree of Cu complexation by organic compounds, reactivity and stability of Cu-organic complexes formed during pyrolysis (Zhao et al., 2023). Depending on the composite rate added to soil, the high EC observed for CSC/CS-3 could limit its application in saline soils or those susceptible to salt stress. The addition of CuO generally resulted in lower EC and higher pH compared to CuS across all feedstocks due to its basic nature, which neutralizes more acidic components present in the biochar (Zhao et al., 2023) and accelerates the production of hydroxyl and oxygen radicals in solution (C. Wang et al., 2023).

Increasing the temperature typically resulted in a decrease in biochar yield, but there was an increment in FC concentration, indicating a higher degree of carbonization. For instance, CCM/CO-3 had a higher yield (71%) and a lower FC of 10%, in contrast to CCM/CO-5, which yielded a 59% greater amount of biochar but increased FC to 37%. Elemental composition of Cu-enriched biochars revealed variations in C and N concentrations, significantly impacting the C: N ratio, crucial for nutrient release in soil applications. Remarkably, CSS/CS-3 displayed lower C:N ratios, such as CSC/CS-3 at 3.5, enhancing nutrient availability compared to those treated at 550 °C like CSC/CS-5 and CCM/CO-5, which exhibited C:N ratios of 5.5 and 10.8, respectively.

Table 9. Comparative Analysis of Composite Properties: Impact of Feedstock Type, Doping Agents, and Pyrolysis Temperatures on Chemical Parameters

Composite	pH	EC	Yield	VM	Ashes	FC	Elemental Composition	C:N Ratio
		(dS m^{-1})	--------------------------------			(%)---------------------------------		

							C	N	C:N
CCM/CS-3	4.8 ± 0.1	21 ± 0.1	65	25 ± 0.5	36 ± 0.1	36 ± 0.5	17 ± 0.1	3 ± 0.1	5 ± 0.1
CCM/CS-5	10 ± 0.1	9 ± 0.1	47	14 ± 0.1	19 ± 0.9	66 ± 0.9	19 ± 0.1	2.3 ± 0.1	8 ± 0.1
CCM/CO-3	8 ± 0.1	7 ± 0.1	71	44 ± 0.1	45 ± 1.4	10 ± 1.4	27 ± 0.1	4.6 ± 0.1	6 ± 0.1
CCM/CO-5	11 ± 0.1	8 ± 0.1	59	29 ± 0.5	33 ± 1.3	37 ± 1.8	22 ± 0.1	2 ± 0.1	11 ± 0.5
CSC/CS-3	5 ± 0. 1	23 ± 0.1	64	56 ± 0.1	33 ± 1.3	9 ± 1.1	13 ± 0.1	4 ± 0.1	3.5 ± 0.1
CSC/CS-5	10 ± 0.1	3.5 ± 0.1	44	20 ± 0.8	15 ± 0.9	64 ± 1.5	19.5 ± 0.1	4 ± 0.1	5.5 ± 0.1
CSC/CO-3	9 ± 0.1	5 ± 0.1	84	50 ± 0.4	46 ± 0.1	1.6 ± 0.5	26.5 ± 0.1	4.4 ± 0.4	6 ± 0.5
CSC/CO-5	10 ± 0.1	3 ± 0.1	54	22 ± 0.2	32 ± 1.2	46 ± 1.3	21 ± 0.1	3.3 ± 0.1	6.3 ± 0.2
CSS/CS-3	4 ± 0.1	25 ± 0.1	72	30 ± 0.2	29 ± 0.4	39 ± 0.6	6 ± 0.1	1.4 ± 0.2	4 ± 0.6
CSS/CS-5	7 ± 0.1	2 ± 0.1	48	8 ± 0.04	19 ± 0.1	73 ± 0.1	6 ± 0.1	1.2 ± 0.1	5.4 ± 0.1
CSS/CO-3	5 ± 0.1	3 ± 0.1	90	33 ± 0.1	27 ± 1.7	40 ± 1.6	13.5 ± 0.1	2.2 ± 0.1	6 ± 0.1
CSS/CO-5	8 ± 0.1	1 ± 0.1	72	28 ± 0.5	19 ± 1.4	46 ± 2.0	11 ± 0.1	1.4 ± 0.1	7.5 ± 0.1

Values are treatments mean (n = 3), except yield (%) (n = 1); pH, Electrical Conductivity (EC), Yield, and Proximate Composition (Volatile Matter (VM), Ash Concentration, Fixed Carbon (FC), Carbon (C), Nitrogen (N), and C:N, carbon/nitrogen ratio. Composites: CCM/CS-3: chicken manure + copper sulfate pyrolyzed at 300°C; CCM/CO-3: chicken manure + copper oxide at 300°C; CCM/CS-5: chicken manure + copper sulfate at 550°C; CCM/CO-5: chicken manure + copper oxide at 550°C; CSC/CS-3: shrimp waste + copper sulfate at 300°C; CSC/CO-3: shrimp residue + copper oxide at 300°C; CSC/CS-5: shrimp residue + copper sulfate at 550°C; CSC/CO-5: shrimp residue + copper oxide at 300°C; CSS/CS-3: sewage sludge + copper sulfate at 300°C; CSS/CO-3: sewage sludge + copper oxide at 300°C; CSS/CS-5: sewage sludge + copper sulfate at 550°C; CSS/CO-5: sewage sludge + copper oxide at 550°C.

These findings underscore that pyrolysis temperature is a pivotal factor in optimizing the properties of the composites. Higher temperatures increase pH and FC, which are advantageous for improving soil structure and soil acidity correction (Chaves Fernandes et al., 2020). However, these conditions can also decrease N availability due to volatilization (de Oliveira Paiva et al., 2024), associated with higher C: N ratios, suggesting carbon stabilization (Ghorbani et al., 2022a).

The increase in FC concentration and the decrease in yield at elevated temperatures indicate enhanced thermal stability of the composites (Tu et al., 2022). This stability is beneficial for applications requiring long-lasting C-rich materials, such as sustained soil amendment. Furthermore, the reduction in EC with increased temperature points to a decrease in soluble salts, which is favorable for preventing soil salinity. Nonetheless, this could also imply a reduction in readily available Cu levels in soil or adsorption in soil colloids, necessitating a balanced approach for the application of these composites, especially in micronutrient-deficient soils (Nepal et al., 2023).

The synthesized CSS/CS-5 composites exhibited the highest Cu retention, with a total Cu concentration reaching 338 g kg^{-1}. This high retention rate suggests an effective interaction between the raw material enriched with CuS, regardless of the pyrolysis temperature. Conversely, composites like CCM/CS-5 and CSC/CS-5, also produced with CuS, maintained high Cu levels regardless of the pyrolysis temperature, but did not surpass the FSS matrix in terms of Cu retention. In contrast, composites produced with CuO exhibited lower Cu retention, reflecting less effective Cu immobilization in the charred matrices, regardless of the pyrolysis temperature.

The FSS composites doped with CuS exhibited higher Cu concentration due to the presence of oxygen-containing functional groups, such as C-OH and COOH, which have a high capacity for Cu sorption (Dong et al., 2014). Additionally, FSS biochars generate a high nutrient concentration and possess a significant neutralization capacity, demonstrating their potential for use as fertilizers and soil conditioners (Das et al., 2021; Rimena R. Domingues et al., 2017). On the other hand, composites (CSC/CS-3) achieved higher Cu levels due to their greater aromaticity, which surpasses that of FCM, as shown in the study by (de Oliveira Paiva et al., 2024). The enhanced aromatic structure of FSC biochars contributes to a more efficient retention and stabilization of Cu, making them more effective in agricultural applications.

Additionally, the solubility of Cu varied among the composites, assessed via Cu-source water solubility index, NAC index, and CA% index. CSS/CS-3 had the highest solubility indices for different extracting solutions (W: 63%, NAC: 69%, CA%: 50%), indicating its capacity for controlled Cu release, which is beneficial for environmental applications and wheat nutrition in the long term (Table 10).

Table 10. Solubility and availability index of Cu-biochar composites

	Copper (Cu)						
Acronym	W	T	NAC	CA%	W Index	NAC Index	CA% Index
	------------------------($g\ kg^{-1}$) ----------------------				-----------------(%)----------------		
CCM/CS-3	78 ± 8.2	233 ± 3.3	147 ± 6.7	79 ± 6.2	33± 3.5	63 ± 2.6	34 ± 2.6
CCM/CS-5	0.1 ± 0. 1	282 ± 1.2	57 ± 0.7	30 ± 0.1	0.1 ± 0.1	20 ± 0.2	11 ± 0.1
CCM/CO-3	0.3 ± 0.1	111 ± 0.4	73 ± 3.9	8 ± 2.0	0.3 ± 0.1	65± 3.3	7 ± 1.8
CCM/CO-5	0.1 ± 0. 1	237 ± 1.0	141 ± 0.6	52 ± 1.3	0. 1 ± 0.1	60 ± 0.5	22 ± 0.6
CSC/CS-3	66 ± 0.1	302 ± 2.8	221 ± 0.7	135 ± 0.1	22 ± 0.2	72 ± 0.4	45 ± 0.4
CSC/CS-5	0.1 ± 0. 1	281 ± 0.8	29 ± 5.2	28 ± 2.3	0. 1 ± 0.1	10± 1.9	10 ± 0.8
CSC/CO-3	1.2 ± 0.2	241± 0.1	168 ± 2.1	16 ± 2.0	0.5 ± 0.1	70 ± 0.9	6.5 ± 0.8

CSC/CO-5	0.1 ± 0.1	233 ± 3.3	142 ± 0.1	42 ± 10.7	0.1 ± 0.1	61 ± 0.9	18 ± 4.5
CSS/CS-3	194 ± 7.2	309 ± 1.7	213 ± 1.5	155 ± 4.5	63 ± 2.1	69 ± 0.4	50 ± 1.6
CSS/CS-5	0.2 ± 0.1	338 ± 5.6	19 ± 1.1	31 ± 2.4	0.1 ± 0.1	6 ± 0.4	9 ± 0.6
CSS/CO-3	6 ± 0.1	204 ± 1.7	138 ± 4.2	55 ± 5.5	3 ± 0.3	68 ± 1.5	27 ± 2.9
CSS/CO-5	0.2 ± 0.1	215 ± 0.8	89 ± 2.4	30 ± 0.2	0.1 ± 0.1	42 ± 1.0	14 ± 0.1

Values are the treatment means (n = 3); copper in H_2O was determined ± 0.01 in water at a ratio of 1:10 (w/v); concentration of soluble copper in total (T) was determined by total digestion of the composites; copper in neutral ammonium citrate water (NAC); copper in concentration of copper soluble in citric acid at 2% (CA%); H_2O Index, NAC Index and CA% Index represent the copper concentration with the extractors and the total copper concentration. Composites: CCM/CS-3: chicken manure + copper sulfate pyrolyzed at 300°C; CCM/CO-3: chicken manure + copper oxide at 300°C; CCM/CS-5: chicken manure + copper sulfate at 550°C; CCM/CO-5: chicken manure + copper oxide at 550°C; CSC/CS-3: shrimp waste + copper sulfate at 300°C; CSC/CO-3: shrimp residue + copper oxide at 300°C; CSC/CS-5: shrimp residue + copper sulfate at 550°C; CSC/CO-5: shrimp residue + copper oxide at 300°C; CSS/CS-3: sewage sludge + copper sulfate at 300°C; CSS/CO-3: sewage sludge + copper oxide at 300°C; CSS/CS-5: sewage sludge + copper sulfate at 550°C; CSS/CO-5: sewage sludge + copper oxide at 550°C.

The influence of pyrolysis temperature and the type of organic matrix are critical factors affecting Cu solubility. The pyrolysis temperature of 550 ºC leads to decreased Cu solubility, as evidenced in CCM/CS-5, CSC/CS-5 and CSS/CS-5 where Cu was nearly insoluble in water, CA% and NAC solutions. This suggests that high pyrolysis temperatures of 550 ºC reduce the environmental mobility of Cu by reducing its solubility (Ghorbani et al., 2022a).

The CuS-biochar composites decrease the solubility of Cu in all tests as the temperature increases, while the CuO-biochar composites increase the solubility of Cu with rising temperature. An exception is the CSS/CO-5 composite, which shows a reduction in solubility in CA%. This is consistent with studies showing the conversion of Cu^{2+} to CuO and Cu monomers (Zhao et al., 2023), CuS-biochar decomposes $CuSO_4$ into CuO, releasing SO_3 and/or SO_2, resulting in a slight reduction in solubility.

The stability in solubility was notably identified in the CSS/CS-3 composite, which maintained solubility in all tests, indicating significant potential for use as a fertilizer (Brasil, 2016). At 550 °C, CuO-biochar increases solubility in CA%, an acidic chelating agent capable of solubilizing various forms of Cu, including oxides and carbonates (Di Palma and Mecozzi, 2007). This enhances thermal stability and maintains Cu availability after treatment, except in CuO-biochar composites, which remain more stable with the FSS matrix at 550 °C. In alkaline solutions, Cu atoms in CuO-biochar convert less readily to Cu^{2+}, which effectively activates superoxide radicals (O^{2-}) (Ling et al., 2022), promoting degradation and adsorption effects (Shuailong et al., 2020).

Organic matrices rich in humic substances, such as those found in composted FSS, tend to form more stable complexes, particularly when treated at high temperatures, as seen in CSS/CS-5, this not only enhances Cu retention but also alters its availability in the soil-plant system. Studies have shown that the total concentrations of Cu and other elements increased with the conversion of FSS into biochar and higher pyrolysis temperatures (Jin et al., 2016).

The choice of CuS versus CuO and its interaction with the contrasting feedstocks significantly determine the composites physical and chemical properties. Overall, CuS interact effectively with the feedstock during the pyrolysis process, likely due to its higher solubility over CuO, influencing the stability, reactivity and solubility and the release dynamics of Cu by the final composite. These findings highlight the importance of selecting appropriate Cu sources and the pyrolysis conditions to optimize the environmental and agricultural benefits of Cu-enriched composites (Nepal et al., 2023).

Radar chart analysis emphasized the variable efficacy of different biochars in adsorbing and retaining Cu, whose magnitude relies upon the feedstock and temperature applied during pyrolysis. Biochars derived from BCM-3, BCM-5, BSC-3, and BSC-5 displayed enhanced Cu chemical species and composite Cu solubility indices, contrasting with those from BSS-3 and BSS-5, which showed reduced agronomic effectiveness. Cluster analysis highlighted distinct chemical behaviors among the composites, particularly concerning Cu concentration and solubility indices. Significant variations were noted in the chemical properties of the composites, such as pH, EC, VM, ash concentration, FC, and C and N levels, influenced by both the temperature and the feedstock used in the composite production.

Radar data indicate that higher temperature treatments of 550 °C enhanced Cu stabilization, as demonstrated by nutrient availability indices in different chemical extractors

(I-NAC, I-CA%, I-W). These findings suggest that the interplay between pyrolysis conditions and feedstock directly influences Cu bioaccessibility (Figure 1). A direct correlation was observed between the pH of the composites and EC with Cu availability, suggesting that the alkalinity induced by pyrolysis could affect Cu mobility in the soil (Altıkat et al., 2024).

Composites utilizing CuS might contribute to increased Cu availability compared to those using CuO due to the sulfate component in CuS, which can enhance the solubility and availability of Cu. Conversely, composites with CuO exhibit more restrained Cu release, indicating a more stable incorporation of Cu into the matrix (Zhao et al., 2023). This observation is vital for the applications of these composites in nutrient supply or contaminant remediation (Rúa-Díaz et al., 2023). Moreover, composites made with CuO may have a lower impact on the pH and EC of the resulting biochar compared to those treated with CuS, as sulfate can potentially increase the acidity and conductivity of the composites. This aspect is crucial when considering biochar for soil amendment, as pH and EC significantly influence soil chemistry and plant growth (Ghorbani et al., 2022a).

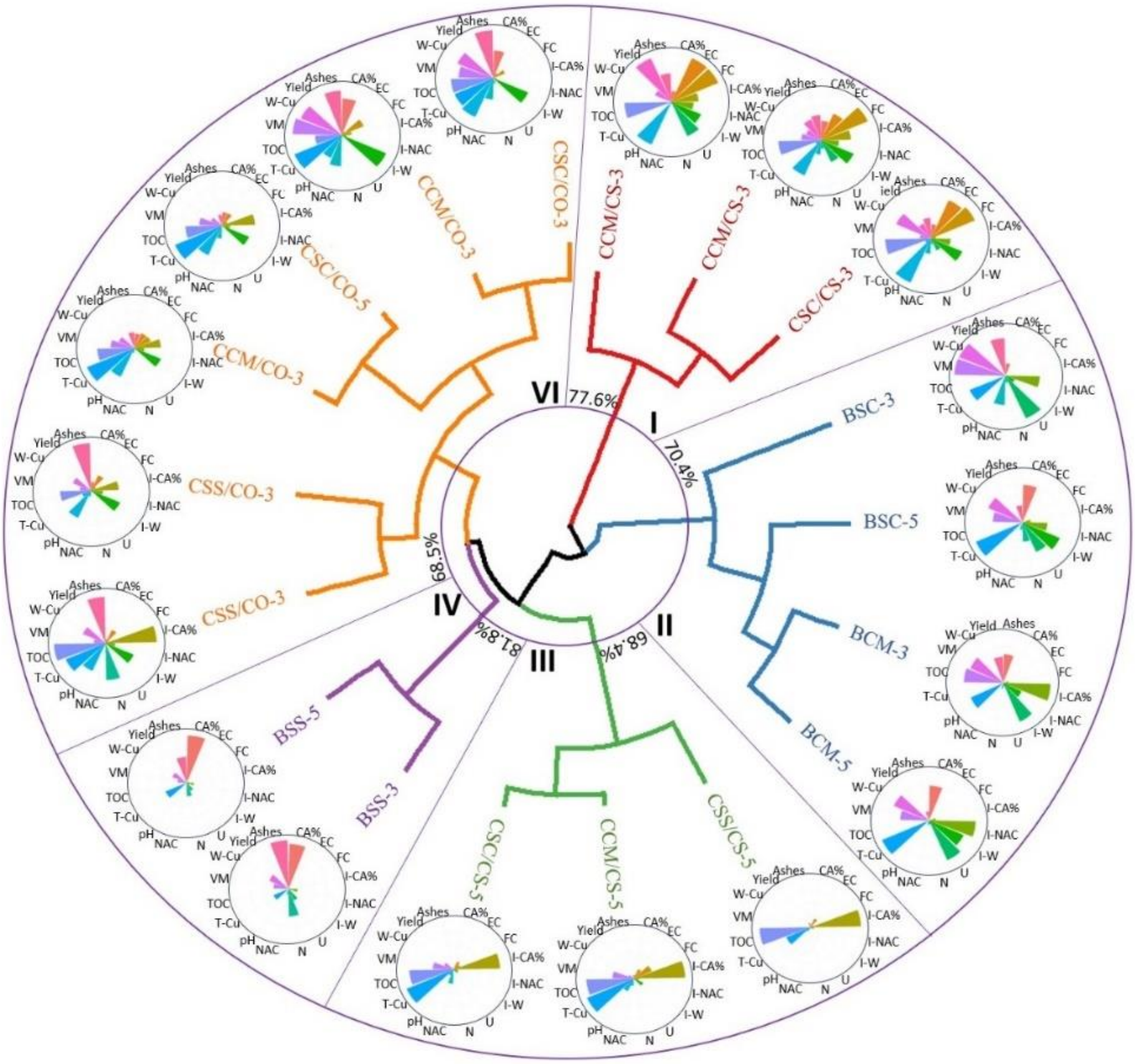

Figure 9. Normalized cluster analysis of biochar attributes (300 °C and 550 °C) shows the similarity percentage within each formed group (I, II, III, IV, and VI). Total Copper concentration (T-Cu); Copper concentration in neutral ammonium citrate (NAC); 2% Citric Acid Copper concentration (CA%); Water-available Copper concentration (W-Cu); Index representing the copper NAC concentration in relation to the extractors and the total (I-NAC); Index representing the copper AC% concentration (I-CA%); Index representing the water copper concentration (I-W); pH; electrical conductivity (EC); Yield concentration; volatile material concentration (MV); Ash concentration; fixed carbon concentration (FC); carbon concentration (C); nitrogen concentration (N). Radar charts at the ends of the terminal branches display the variable value ratio for each biochar or composite normalized by the maximum value of the analyzed variable. The range of normalized attributes varies from 0 to 1 (maximum in all samples).

The composites synthesized at higher temperatures tend to increase FC and reduce VM, which not only enhances the longevity of Cu in the soil but also minimizes nutrient leaching, making it a more sustainable option for enhancing soil fertility over the long-term. In addition to improving nutrient use efficiency, this strategy contributes to C sequestration in the soil, reducing carbon emissions associated with the decomposition of organic matter. These characteristics align with the findings of other studies, which have noted that higher pyrolysis temperatures generally improve biochar's chemical and physical stability, thereby reducing the environmental mobility of macro and micronutrients (Nan et al., 2021).

Incorporating CuO into the matrix provides a strategic advantage in the dynamics of Cu delivery. Unlike CuS, CuO is much less soluble, which controls the Cu release rate, preventing excessive initial bioavailability that could lead to plant toxicity. This slow-release mechanism ensures a steady supply of this micronutrient, which is crucial for plant health, particularly in supporting enzymatic processes and chlorophyll production. This controlled release also aligns with sustainable agricultural practices, minimizing the risk of Cu leaching into groundwater, thus protecting the environment and adhering to increasingly stringent regulations concerning soil and water quality (Hailegnaw et al., 2020). The application of CCM/CO-5 has the potential to significantly improve Cu retention capacity, offering a more controlled and sustained release of Cu in the soil. This is particularly advantageous in agricultural contexts, where Cu toxicity can be a concern (Joseph et al., 2013).

3.2 Infrared Spectroscopy

Fourier transform infrared spectroscopy with attenuated total reflection (ATR-FTIR) was employed to characterize the functional groups present in the composites produced from biochar doped with CuS and CuO at two different temperatures, 300 °C and 550 °C (Figure 3).

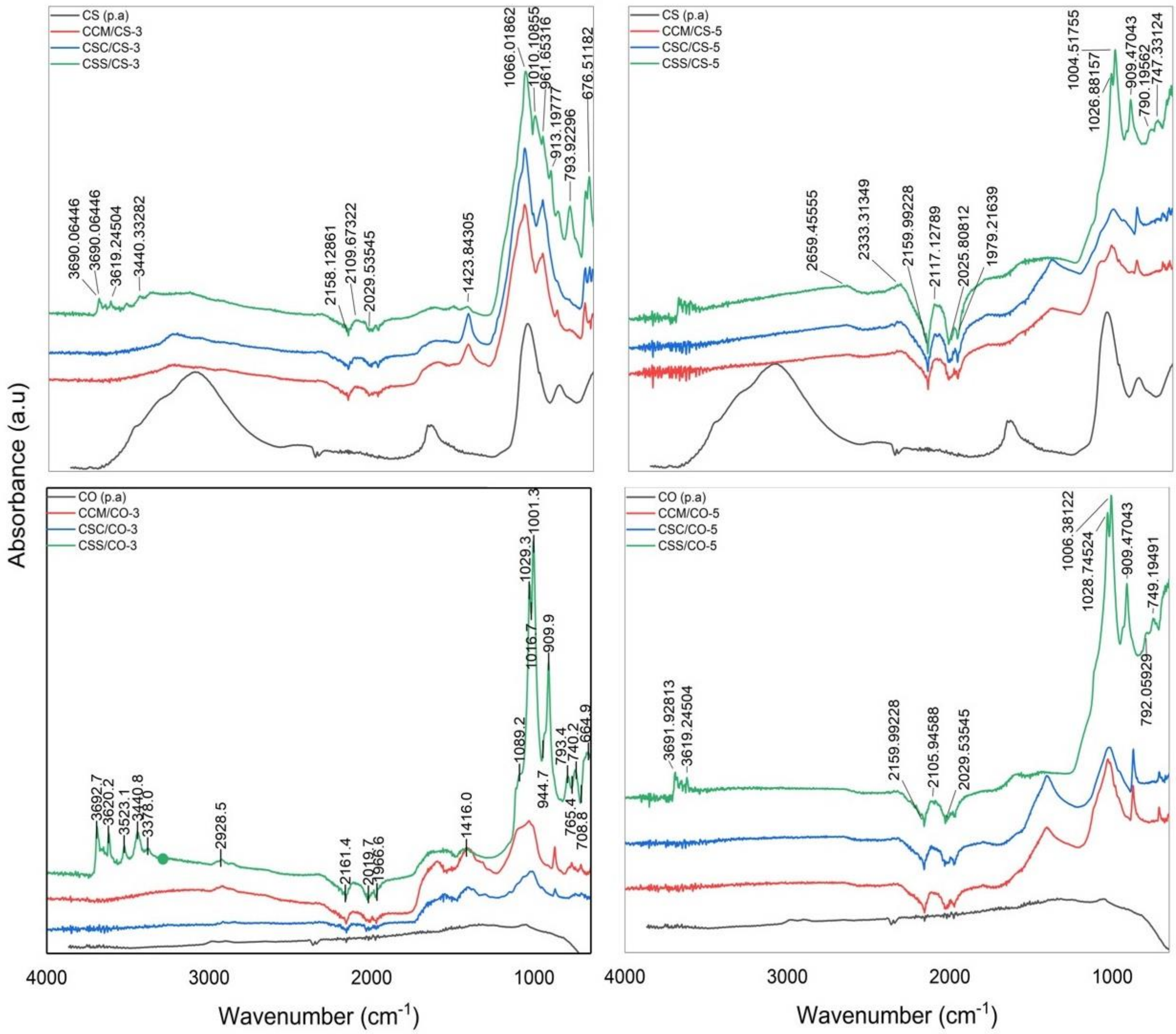

Figure 10. Fourier transform infrared spectroscopy with attenuated total reflection (ATR-FTIR) and the main peaks and characteristics of the chemical groups found in composites produced from biochar doped or not with copper sulfate or copper oxide. (a) composites doped with copper sulfate at 300 °C; (b) composites doped with copper sulfate at 550 °C; (c) composites doped with copper oxide at 300 °C and (d) composites doped with copper oxide at 550 °C.

The FCM e FSC, rich in nitrogenous compounds and organic matter, provides an excellent base for composite production. Upon doping, especially at higher temperatures, there is an enhancement in the functionalization of specific groups, such as amides and amines, as evidenced by the FTIR peaks. At the same time, the FSC, which is rich in chitin, showed an increase in chitin-related functional groups, such as amines and amides, evidenced by peaks at 1650 cm^{-1} and 1550 cm^{-1} (de Oliveira Paiva et al., 2024). The samples treated with CuS and CuO at 300 °C and 550 °C show significant differences in their FTIR spectra.

In the composites doped with CuS at 300 °C (Figure 3a), significant peaks are observed in the 3200-3600 cm^{-1} region, attributed to the stretching vibrations of hydroxyl (O-H) groups, suggesting the presence of alcohols or phenolic compounds. Peaks around 1650-1750 cm^{-1} indicate the presence of carbonyl-containing compounds, such as ketones, aldehydes, or carboxylic acids, while the C-O stretching vibrations (1000-1300 cm^{-1}) suggest the presence of alcohols, esters, and ethers. In the composites treated at 550 °C (Figure 3b), there is an increase in the intensity of peaks related to oxygenated functional groups, such as C=O and C-O, indicating more pronounced oxidation of the material. This suggests higher temperatures promote more intense thermal decomposition of volatile organic compounds, exposing more functional sites in the carbon structure (Xin Zhang et al., 2022b). Peaks at 1100 cm^{-1}, 650 cm^{-1}, and 1000-1200 cm^{-1} correspond to S=O stretching, O=S=O bending, and S-O stretching in sulfates, respectively.

For the composites doped with CuO at 300 °C (Figure 3c), the less pronounced peaks in the 3200-3600 cm^{-1} region indicate a reduction in OH-containing compounds. The presence of peaks around 1650-1750 cm^{-1} suggests the presence of carbonyl compounds. The C-O stretching between 1000-1300 cm^{-1} indicates the presence of esters, ethers, and alcohols. At 550 °C (Figure 3d), the composites doped with CuO show broadening or shifting of the C=O peaks around 1700 cm^{-1} and OH peaks around 3400 cm^{-1}, indicating possible interactions with organic compounds, potentially forming hydroxides or by adsorbing water. The presence of C≡C stretching in the 2100-2260 cm^{-1} region suggests the formation of triple carbon bonds. Materials doped with CuO exhibited ester stretching, primarily observed in the ranges of 1050-1150 cm^{-1} for simple C-O stretching and 1735-1750 cm^{-1} for C=O stretching, differentiating from carboxylic acids (Sadeek et al., 2020).

The different feedstocks resulted in varied FTIR profiles, reflecting differences in the functionalization of the composites after doping. Biochar derived from FCM showed a high presence of nitrogenous groups, with C≡N stretching standing out in the 2100-2260 cm^{-1} range, attributable to the high nitrogen concentration in the feedstock (Sadeek et al., 2020). Conversely, FSC, rich in chitin, showed increased chitin-related functional groups, such as amines and amides, evidenced by peaks at 1650 cm^{-1} and 1550 cm^{-1} (Younis et al., 2021).

The significant peaks observed in the samples doped with CuS at 550 °C, such as those in the 1000-1300 cm^{-1} (C-O) and 3200-3600 cm^{-1} (O-H) regions, suggest a greater incorporation of oxygen functional groups, which can be beneficial for pollutant adsorption applications, where such functionalities facilitate interaction with heavy metals and other organic compounds (C. Liu et al., 2021).

As shown in the graph, the CuS-doped composites exhibit notable peaks around 1120-1080 cm^{-1} (SO_4^{2-}) and enhanced absorption peaks around 1000-1100 cm^{-1}, indicative of sulfate-related complexes, and at 1423.8 cm^{-1} (C-O from carboxylic acids) (Atchaya and Meena Devi, 2024). The CuO-doped composites show peaks around 1083.2 cm^{-1} (Cu-O), 1029.3 cm^{-1} (Si-O-Cu), and 1441.6 cm^{-1}, with peaks around 600-700 cm^{-1} corresponding to Cu-O stretching, indicating the formation of pure Cu (Sukumar et al., 2020). Generally, the peaks related to carbonyl groups (C=O) around 1700 cm^{-1} may be more pronounced due to oxidation processes at higher temperatures (Kayani et al., 2015).

In general, composites CuS-doped exhibit more prominent peaks associated with hydroxyl groups, carbonyl groups, and sulfur-containing groups (sulfates). These peaks indicate a higher presence of alcohols, phenolic compounds, and sulfate groups. Conversely, composites doped with CuO display less pronounced hydroxyl group peaks, a broader or shifted carbonyl peak suggesting interactions with organic compounds or water adsorption, and distinctive peaks for triple carbon bonds and esters. These features suggest different chemical interactions compared to CuS-doped composites, highlighting the formation of esters and the possible formation of hydroxides.

3.3 Kinetics of Cu Release

The pyrolyzed composites at 300 °C exhibited a more gradual release of Cu than those processed at 550 °C. This indicates that lower temperatures may facilitate the formation of more stable Cu complexes within the matrix, which could benefit applications requiring controlled Cu release, such as in agricultural settings or crop fertilization (Fig. 4).

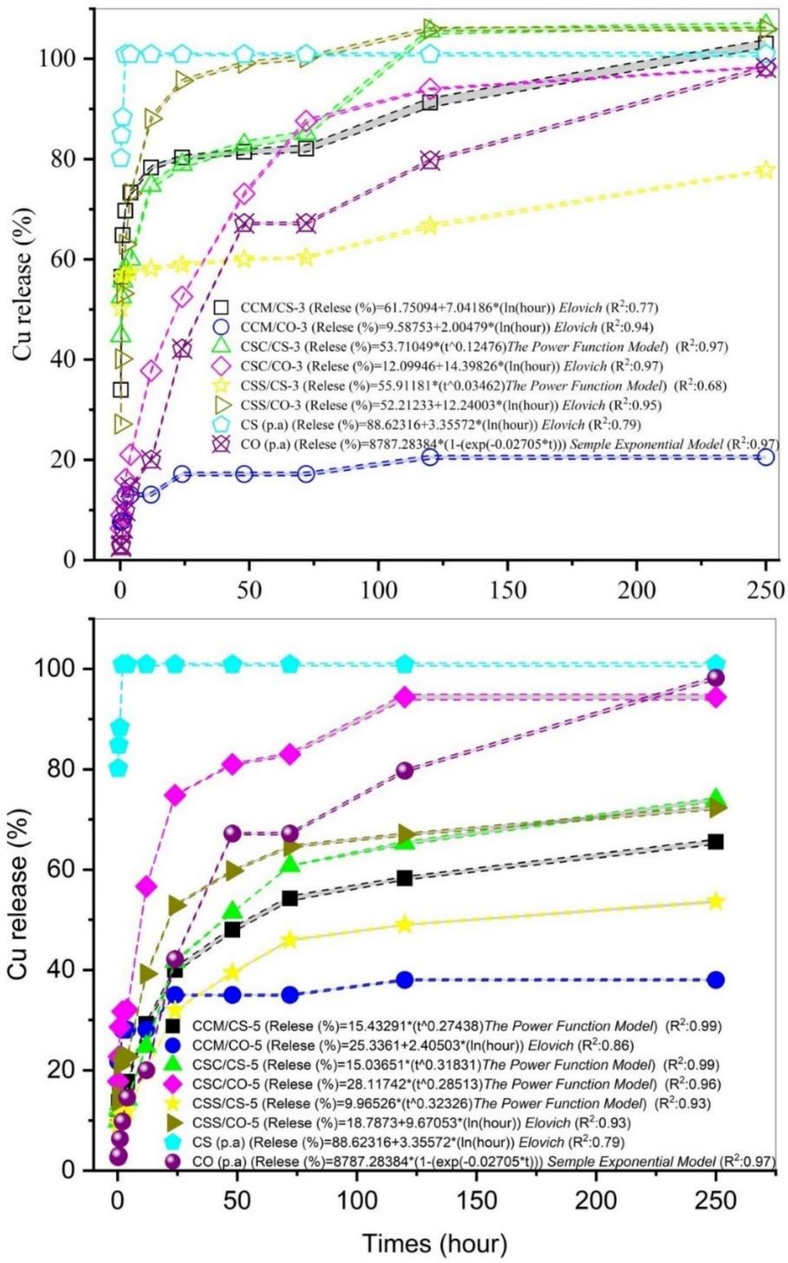

Figure 11. Kinetics of copper Release (Cu) as related to composites produced at 300°C (a) and 550°C (b) with the mixture of chicken manure, shrimp carcass and sewage sludge plus copper sulfate and copper oxide previously to pyrolysis.

Composites such as CCM/CS-3 and CSC/CS-3 showed a less gradual Cu release compared to those containing CuO as the Cu source. This suggests that CuS may form chemical bonds within the biochar matrix, resulting in a controlled and consistent release of Cu ions over time, as observed by (Li et al., 2023). The type of organic matrix and the Cu additive significantly impacted the release kinetics, as revealed by CSS/CS-3, which released more slowly than CuO. Composites with CuO exhibited a slower and more controlled release profile compared to those made with CuS, indicating that CuS interacts more effectively with organic components.

The release kinetics followed various models, including the Elovich model, the Power Function model, and the Simple Exponential model, with different degrees of fit (R^2 values). For instance, composites fitting the Elovich model, such as CCM/CO-3 ($R^2 = 0.94$), suggest a chemisorption process, whereas those following the Power Function model indicate a more complex, multi-phase release process. These differences emphasize the importance of selecting appropriate models to predict the behavior of biochar composites under different conditions.

At 550 °C, all composites demonstrated an increased rate of Cu release, with CSC/CO-5 showing the fastest release. This higher release rate can be attributed to the increased temperature destabilizing the Cu matrix interactions, leading to quicker dissolution and availability of Cu, as reported by (Nepal et al., 2023). Higher pyrolysis temperatures also raise pH levels, transforming Cu salts into CuO and causing, especially in ash-rich matrices, causing a reduction in the release rate of the composite in CA% solution. The type of biomass used for biochar production influences these outcomes, with high-ash concentration materials further increasing pH and promoting Cu precipitation. Therefore, understanding the interplay between pyrolysis temperature, biomass composition, and pH is essential for optimizing biochar for Cu fertilization in tropical soils.

The observed variations in kinetics are primarily due to physicochemical interactions between Cu compounds and organic substrates, influenced by the pyrolysis temperature. Lower temperatures seem to support the formation of more chemically stable complexes, likely due to less degradation of organic functional groups that interact with Cu (Abdullah et al., 2021). On the other hand, higher temperatures can lead to the fortification of these complexes, making faster Cu release impossible (Thapa et al., 2021). The CSS/CO-3 composite (52%) exhibited the highest Cu release when compared to CCM/CO-3 (10%) and CSC/CO-3 (12%). This may be due to the inherent properties of sewage sludge, which may increase the mobility of Cu through the ash-rich composite matrix. Chicken manure matrix composites showed intermediate release rates. In contrast, those derived from shrimp shells released the least amount of Cu, suggesting a potential for these compounds to stabilize Cu, correlating with Cu mobility in soil, as reported by (Lin et al., 2024).

Furthermore, the difference in Cu release rates between compounds synthesized with CuS and CuO suggests that CuS can form more extensively distributed complexes in the matrix, potentially due to its greater release power and reactivity than CuO. Variability in Cu release rates has significant implications for environmental safety and agricultural use. For environmental applications, slower release rates are preferable to minimize Cu leaching and potential toxicity to soil and water systems. On the other hand, in agricultural environments, a more controlled release can be beneficial to provide a sustained supply of nutrients to crops.

3.4 Scanning Electron Microscopy

Scanning Electron Microscopy (SEM), images revealed significant differences in the microstructure of composites processed at varying temperatures (Fig. 5). At 300 °C, the composites retained a more defined and structured morphology, indicating that this lower temperature is sufficient to preserve the composite matrix's integrity. In contrast, at 550 °C, the

SEM images showed clear signs of deformation and structural breakdown, suggesting that higher temperatures cause more intense thermal degradation of organic components.

FCM is rich in organic and inorganic nutrients, particularly N, P, and K (Manogaran et al., 2022). SEM analysis of composites containing FCM, such as CCM/CS-3 and CCM/CS-5, reveals a relatively porous and homogeneous structure. This porosity benefits applications requiring high specific surface areas, such as contaminant adsorption. However, thermal degradation of organic components at 550 °C results in a less defined and more fragmented structure, indicating the volatilization of organic materials (Akhil et al., 2021).

FSC is rich in chitin, a polysaccharide that contributes to the rigidity and structural integrity of the composites (Sieber et al., 2018). Thus, composites CSC/CS-3 and CSC/CS-5 exhibit a distinct morphology with robust structures and more uniform Cu distribution when doped with CuS. The presence of chitin provides greater thermal resistance up to 300 °C. However, at higher temperatures (550 °C), a more pronounced degradation occurs, resulting in increased porosity and potential structural collapse.

FSS is a complex feedstock comprising organic and inorganic substances (Penido et al., 2019). Composites CSS/CS-3 and CSS/CS-5 derived from FSS show a highly porous structure and heterogeneous distribution of elements. The chemical complexity of FSS can lead to varied interactions with Cu dopants (CuS or CuO), resulting in diverse morphologies. SEM analysis shows that at 300 °C, the composites maintain reasonable structural integrity, while at 550 °C, the structure becomes significantly more porous, indicating intense thermal decomposition.

The inclusion of Cu, either as CuS or CuO, significantly influenced the composites' physical texture and chemical properties, thereby affecting their suitability for environmental and agricultural applications. For example, the composites CSS/CS-3 and CSS/CO-3 exhibited more porous structures, which could enhance their effectiveness in applications requiring large surface areas, such as adsorption and desorption processes.

The type of Cu additive notably impacted the microstructure. Composites such as CCM/CS-3 and CSS/CS-3 showed a more homogeneous distribution of Cu compared to those with CuO. This can be attributed to the superior solubility and integration capability of CuS within the organic matrix. Temperature variations also played a crucial role. Increasing the temperature from 300 °C to 550 °C generally led to greater porosity and surface roughness, indicating more extensive thermal decomposition and structural changes. The choice of doping agent (CuS versus CuO) affected the samples' thermal stability and structural development. CuO-doped samples usually exhibited smoother surfaces at lower temperatures but developed significant porosity at higher temperatures.

Composites of Cu doped with CuS (CCM/CS-3 and CSS/CS-3) displayed a more uniform Cu distribution. This homogeneity can be attributed to the greater solubility and integration of CuS in the organic matrix. In contrast, CuO-doped composites (CCM/CO-3 and CSS/CO-3) exhibited less uniform Cu distribution, likely due to different chemical interactions between CuO and the organic matrix (Zhao et al., 2023) and stable training (Abbasi et al., 2024). These findings underscore the importance of optimizing thermal processing conditions and selecting appropriate Cu additives to enhance the structural and functional properties of the composites, tailoring them for specific environmental and agricultural applications.

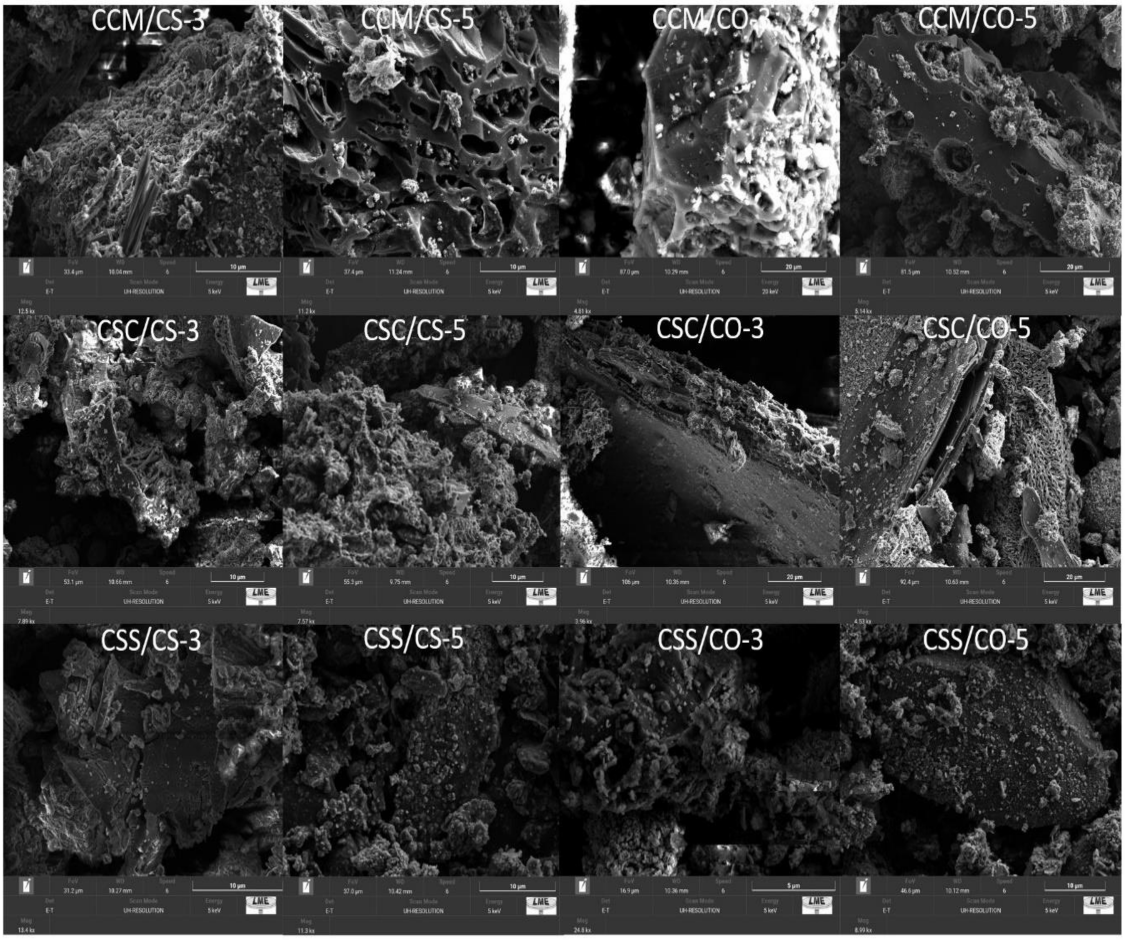

Figure 12. Scanning microscopy was obtained by FCM, FSC, and FSS, both under the influence of temperatures 300 and 550 °C and doped with CuS or CuO. Images magnified at 10 μm.

3.5 Agronomic Impact of Composites on wheat growth

The effect of composite fertilization on the growth characteristics of wheat and Cu nutrition in different types of Oxisols was evaluated by analyzing Shoot Dry Matter (SDM), Root Dry Matter (RDM), Grain Dry Matter, and Total Dry Matter (TDM) under various treatments (Figure 6). The study was conducted on two soil types: Yellow-Red Oxisol (RYL) and Dystrophic Red Oxisol (DRL).

In RYL, significant differences in TDM and SDM production were observed among the treatments. The highest production was observed in the CSS/CS-5, CSC/CS-3, and CSS/CO-3 treatments, which significantly outperformed both the control (NO) and copper sulfate (CS) treatments. Similar results have been reported in other studies, where Cu in organic form showed superior outcomes to control (Elsherpiny, 2023). RDM was notably higher in the

CSC/CS-3 treatment. The CSS/CS-5 and CSS/CO-3 treatments for grain production were particularly effective, indicating that combining FSS with a Cu source boosts productivity. This enhancement is attributed to the redox-active functional groups in the matrix, which play a significant role in facilitating electron transfer (Lou et al., 2024). The NO treatment consistently resulted in the lowest dry matter production, underscoring the importance of Cu supplementation in this soil type.

In contrast, the DRL soil demonstrated a unique pattern in dry matter production. The CSS/CS-5 treatment achieved the highest TDM, SDM, RDM, and grain production, followed closely by the CSC/CS-3 treatment. The differences between the top-performing treatments and the control (NO) were more pronounced in DRL, with the NO treatment showing significantly lower dry matter production across all parameters. In this context, FCS is rich in calcium, chitin, and protein, and as a carbon source, can produce biochar containing residual calcium and nitrogen (Bhatnagar and Sillanpää, 2009; Xiao et al., 2017), providing active functional groups that form strong complexes with metals according to the literature (Dai et al., 2018).

Interestingly, the CuS treatment performed better in DRL than in RYL, although it still lagged behind the composite treatments. The CSS/CO-3 treatment also showed a significant improvement in TDM compared to the control, similar to the results seen in RYL but with a relatively larger increase. However, CuO (CSS/CO-3) was less effective in enhancing wheat productivity than the other composites. This is due to the concentration of H^+ in the solution, as Cu atoms in CuO-biochar are not easily converted into free Cu^{2+}. This conversion affects the activation of superoxide radicals (O^{2-}) (Ling et al., 2022), which in turn modulates the intensification of the adsorption strength (Shuailong et al., 2020). These findings indicate that soil type significantly affects the efficacy of different fertilization treatments. The greater effectiveness of composite treatments in both soil types underscores their potential for boosting wheat productivity in the long term.

This study evaluated the impact of Cu accumulation on the dry matter production of wheat in contrasting Oxisols. Understanding how different fertilization treatments influence nutrient uptake in nutrient-poor soils is crucial for developing sustainable agricultural practices. In RYL, the treatments CSS/CS-5 and CSC/CS-3 resulted in the highest copper accumulation in the total dry matter of wheat, with average values around 2.5 mg per pot. These treatments did not show significant differences between each other. Still, they were significantly higher than the control (NO), which had the lowest Cu accumulation, less than 1.0 mg per pot (Tukey's test, $p < 0.05$). The CSS/CO-3 treatment also led to relatively high copper accumulation, although not as high as CSS/CS-5 and CSC/CS-3. Treatment with pure CuS (p.a) resulted in intermediate Cu accumulation, indicating that adding organic compounds to CuS can further increase Cu uptake and accumulation by plants (Karimi et al., 2021).

These results suggest that combining organic materials with Cu sulfate at high temperatures significantly improves Cu availability in RYL. The thermal treatment likely modifies the organic matrix, enhancing the mobilization and solubility of Cu, which aligns with previous studies that have shown improved nutrient uptake with organic amendments (Meenu et al., 2024).

In DRL, the effects of the treatments were more pronounced. The CSS/CS-5 treatment led to the highest Cu accumulation in total dry matter, averaging over 3.0 mg per pot, significantly higher than all other treatments. The CSC/CS-3, CSS/CO-3, and CS treatments had similar Cu accumulations, all significantly higher than the control (NO), which had the lowest accumulation, around 1.0 mg per plant. This indicates that while all Cu treatments improved Cu nutrition compared to the control, CSS/CS-5 was the most effective.

In conclusion, this study reveals substantial differences in the effectiveness of fertilization treatments depending on soil type, highlighting the need for tailored approaches to maximize wheat productivity. With its sandy texture and low organic matter concentration, the RYL showed significant improvements in dry matter production and total Cu accumulation when treated with CSC/CS-3 and CSS/CS-5 composites. These composites, enriched with ash due to high-temperature processing, ensured a controlled release of Cu, improving retention and reducing leaching in the sandy soil (Jalali et al., 2023; Lamichhane et al., 2018). Their low solubility makes them particularly suitable for acidic soils, providing Cu and basic cations in stable forms like carbonates, oxides, and hydroxides over time (Wu et al., 2023). Additionally, the CSS/CS-5 composite demonstrated higher stability due to its lower solubility, which is advantageous for prolonged nutrient availability.

By contrast, the CSC/CS-3 composite showed a more controlled initial release of Cu, followed by a complete release after 50 hours, making it ideal for soils needing an immediate yet sustained nutrient supply. Its higher solubility and abundance of functional groups, including sulfate complexes, carboxylic acids, and nitrogen-linked groups (Dai et al., 2018; Xiao et al., 2017), enhance its efficacy in nutrient-deficient soils.

On the other hand, the DRL, a clay-rich soil with higher organic matter concentration, responded best to the CSS/CS-5 composite. The high-temperature treatment at 550°C likely enhanced the biochar's porosity and surface area, improving its ability to retain and gradually release nutrients, including Cu, vital for efficient nutrient uptake and overall plant health. This enhanced nutrient retention and release, combined with better soil structure and water retention, supports robust root development and plant growth (H. Wang et al., 2023).

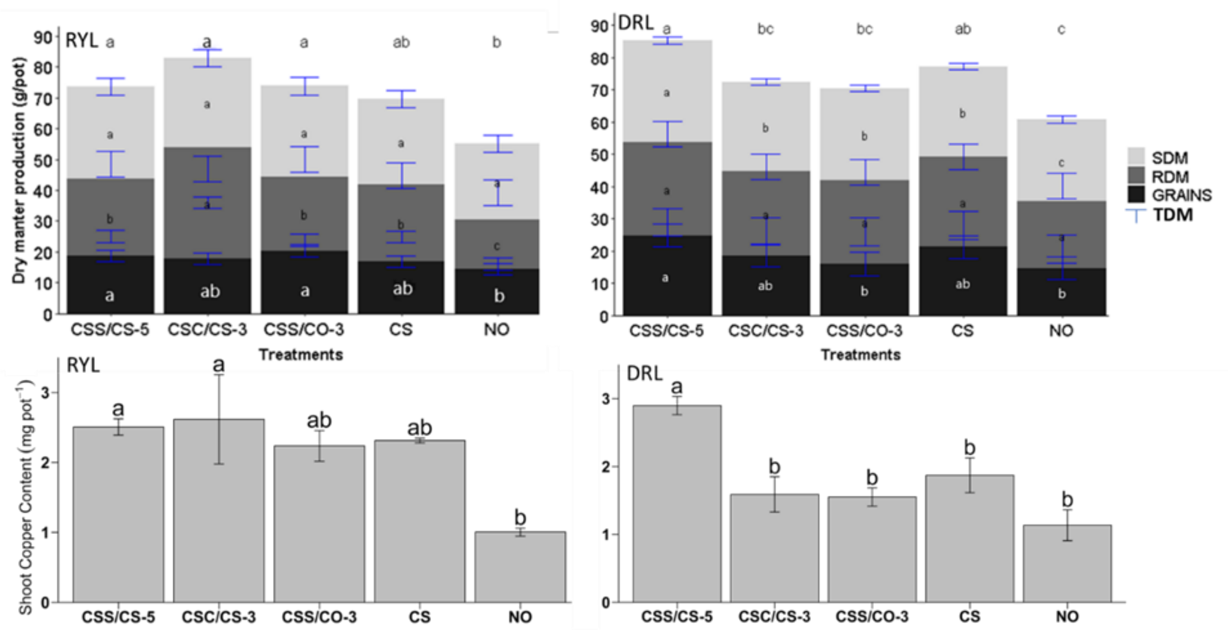

Figure 13. Impact of fertilization with composites on wheat growth characteristics and Cu accumulation evaluated in contrasting Oxisols: Shoot Dry Matter (SDM), Root Dry Matter (RDM), and Grain Dry Matter (Grains) and Total Dry Matter (TDM). Soils: RYL: yellow red Oxisol and DRL: dystrophic red oxisol. Lowercase letters were used to compare the means of each parameter evaluated between treatments using the Tukey test ($p < 0.05$). Composites: CSS/CS-5: sewage sludge + copper sulfate at 550°C; CSC/CS-3: shrimp waste + copper sulfate at 300°C; CSS/CO-3: sewage sludge + copper oxide at 300°C; CS: copper sulfate (p.a); NO: without copper application.

This study also assessed the availability of Cu in the soil solution and the residual Cu extracted by EDTA (Figure 7). The graph presents the results of Cu-based fertilization on soil solution, comparing different treatments over 1, 7, and 15 days. Analyzing these treatments in RYL and DRL provides insights into the dynamics of Cu availability in various soil types.

In RYL, characterized by its sandy texture and low organic matter concentration, the concentration of Cu in the soil solution varied significantly over time within each treatment. All composite treatments (CSS/CS-5, CSC/CS-3, CSS/CO-3) showed a notable increase in Cu concentration from day 1 to day 7, followed by a reduction on day 15. This initial spike and subsequent decrease can be attributed to the high initial solubility and subsequent precipitation or adsorption of Cu onto soil particles. The CSS/CS-5 and CSC/CS-3 treatments demonstrated effective initial Cu release due to their high ash concentration and thermal processing, likely increasing the bioavailability of Cu. The significant drop in Cu concentration by day 15 suggests that these treatments provide a controlled release, preventing excessive leaching and ensuring sustained availability of Cu.

Similarly, CSS/CO-3 peaked at day 7, followed by a decline at day 15, indicating its lower solubility and gradual release of Cu, which is beneficial for maintaining adequate nutrient levels over time. The pure CS treatment exhibited high solubility with no significant difference between days 1 and 7. Still, there was a drastic decrease by day 15, reflecting Cu's quick release and rapid leaching, making it less effective for long-term nutrient supply. The control (NO) treatment maintained consistently low Cu concentrations, indicating negligible background Cu levels in the soil solution. These observations suggest that the composite treatments, especially CSS/CS-5 and CSC/CS-3, are more effective in providing a sustained release of Cu in RYL, enhancing nutrient availability and reducing the risk of leaching in sandy soils.

In DRL, which is more clayey and has higher organic matter concentration, the concentration of Cu in the soil solution also varied over time within each treatment, but with different patterns compared to RYL. The CSS/CS-5 and CSC/CS-3 treatments showed a significant increase in Cu concentration from day 1, followed by a marked decrease on subsequent days. The high initial release could be due to the enhanced interaction between the clay particles and Cu, which is then followed by adsorption onto the soil colloids, reducing the Cu concentration in the solution by day 15. CSS/CO-3, unlike in RYL, exhibited a significant increase in Cu concentration from day 1 to day 7 and a significant decrease by day 15, with all means significantly different from each other, suggesting a more controlled release and efficient nutrient supply suitable for the higher organic matter concentration of DRL. Similar to RYL, the CS (p.a) treatment showed a quick initial release of Cu with a significant drop by day 15, indicating its less effective long-term nutrient availability due to rapid leaching. The control (NO) treatment maintained consistently low Cu concentrations, reflecting the minimal background levels of Cu in the soil solution. The higher organic matter and clay concentration in DRL facilitate stronger adsorption and complexation of Cu, leading to a more pronounced fluctuation in Cu availability. The CSS/CS-5 composite, with its high-temperature treatment enhancing porosity and nutrient retention, proved particularly effective in DRL, ensuring a more sustained and controlled release of Cu.

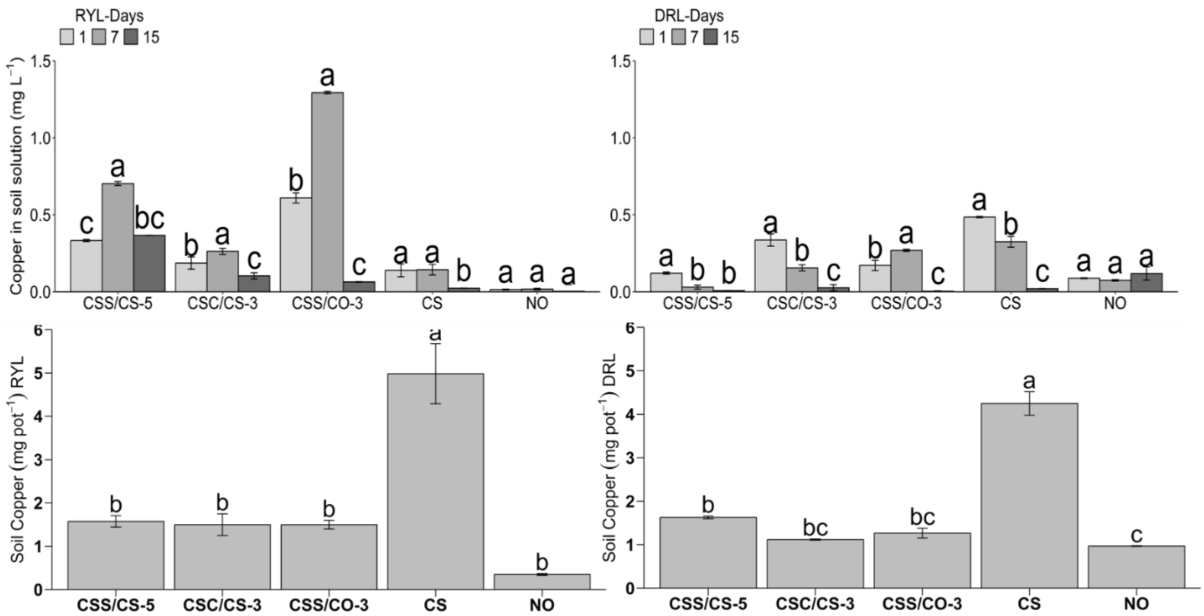

Figure 14. Impact of Cu-based composite fertilization on soil solution Cu availability and residual Cu extracted by EDTA in contrasting oxisols cultivated with wheat. Lowercase letters were utilized for comparing means of each evaluated parameter between treatments using the tukey test ($p < 0.05$). Composites: CSS/CS-5: sewage sludge + copper sulfate at 550°C; CSC/CS-3: shrimp waste + copper sulfate at 300°C; CSS/CO-3: sewage sludge + copper oxide at 300°C; CS: copper sulfate (p.a); NO: without copper application.

The graph shows the impact of Cu-based fertilization on Cu residue extracted by EDTA in contrasting Oxisols cultivated with wheat. In the RYL, characterized by its sandy texture and low organic matter concentration, the CS (p.a) treatment resulted in the highest residual Cu concentration in the soil, significantly exceeding all other treatments ($p < 0.05$). This outcome is consistent with the high solubility of CuS, which facilitates immediate availability but also leads to higher residual Cu accumulation in soil RYL, as reported by (Alva et al., 1995), which can increase phytotoxicity (Lamichhane et al., 2018).

The organic composite treatments (CSS/CS-5, CSC/CS-3, CSS/CO-3) exhibited similar residual Cu concentrations, significantly higher than the control (NO) but lower than the CS treatment. Due to their high ash concentration and thermal processing, these composites provide a more gradual Cu release, resulting in lower residual concentrations after initial plant uptake. Studies have found that Cu-biochar can reduce residual Cu levels in the soil, improving soil quality and plant health in the long term (Lamichhane et al., 2018) while also reducing the risk of leaching and environmental contamination (Karimi et al., 2021). This controlled release mechanism is particularly advantageous in sandy soils with low cation exchange capacity (CEC), as it reduces the risk of Cu leaching.

In the DRL, which has a clayey texture and higher organic matter concentration, the pattern was similar, with the CS treatment resulting in the highest residual Cu concentration, significantly higher than other treatments ($p < 0.05$). However, there was greater variability among the organic composites. The CSS/CS-5 treatment exhibited a significantly higher residual Cu concentration than CSC/CS-3 and CSS/CO-3 but still lower than the CS treatment. This can be attributed to differences in the composition and thermal processing of the organic composites, affecting Cu release rates and mobility. The higher CEC and organic matter concentration in DRL enhance Cu retention, resulting in more complex interactions between organic matter and soil components, which may explain the observed variability (Alva et al., 1995).

Comparative analysis between the two soils reveals that RYL retains less residual Cu from organic composite treatments than DRL. This is likely due to the distinct physicochemical properties of the soils, such as CEC, pH, and organic matter concentration, which influence Cu retention and mobility. RYL's sandy texture and lower CEC result in less effective Cu retention, leading to lower residual concentrations. DRL's higher clay concentration and organic matter enhance Cu adsorption and retention, resulting in higher residual levels.

The findings demonstrate that Cu-based fertilization significantly impacts Cu availability and residuals in the soil. The CS (p.a) treatment showed the highest residual Cu concentration, indicating rapid release and a higher propensity for soil accumulation. In contrast, the organic composites, especially those treated at high temperatures like CSS/CS-5, provided a more controlled Cu release, resulting in lower residual concentrations. These results have important implications for fertilization strategies, suggesting that organic composites are preferable for sustainable nutrient management, minimizing excessive Cu accumulation in the soil. The composites enhanced Cu availability in the soil solution and impacted residual Cu, which has implications for long-term soil fertility management and succession of crops cultivated without Cu fertilization (Xu et al., 2023). This innovative strategy fosters agricultural productivity and promotes environmental sustainability by preventing detrimental effects associated with high levels of Cu in polluted soils.

4. Conclusions

This study demonstrates the effectiveness of Cu-biochar composites in enhancing wheat growth in two contrasting Oxisols. In the RYL, characterized by sandy texture and low organic matter, the CSC/CS-3 treatment resulted in the highest shoot and root dry matter and grain production. The composite's optimized solubility and controlled Cu release enhanced nutrient uptake while effectively addressing soil retention challenges. With clayey texture and higher organic matter in the DRL, the CSS/CS-5 treatment showed superior results in shoot and root dry matter, grain production, and Cu uptake. High-temperature processing enhanced biochar stability and Cu retention, fitting DRL’s complex soil structure.

Residual Cu levels were highest with the CS (p.a) treatment in both soils, indicating rapid release and higher accumulation. In DRL, the CSS/CS-5 treatment also exhibited significant residual Cu, correlating with increased wheat growth and suggesting efficient Cu management. This study underscores the importance of selecting Cu-biochar composites based on specific soil characteristics to maximize agricultural benefits and minimize environmental risks. Future research should explore long-term environmental impacts, varying biochar application rates, different Cu sources, and their interactions in field trials to optimize fertilization strategies.

Funding

This research and scholarship were funded by the Coordination for the Improvement of Higher Education Personnel (CAPES), CAPES-PROEX/AUXPE 593/2018, the National Council for Scientific and Technological Development (CNPq, grants # 307447/2019-7 and 311212/2023-9)), and the Minas Gerais State Research Support Foundation (FAPEMIG) for financial support.

Acknowledgments

This work was financially supported by CAPES (CAPES-PROEX/AUXPE 593/2018), CNPq and FAPEMIG for the funding and research grants granted. The Federal University of Lavras (UFLA) is a provider of opportunities.

5. References

Abbasi, M., Rizvi, O.S., Hussain, S.Z., Jilani, A., Osra, F. a, Kajjumba, G.W., Bhatnagar, A., Khan, E., Abbas, T., 2024. Nano-zerovalent copper biochar composite for treating selenium oxyanions in water: synthesis, evaluation, removal mechanism, density functional theory, and molecular dynamics simulations. Chemical Engineering Journal 485, 149954. https://doi.org/https://doi.org/10.1016/j.cej.2024.149954

Abdullah, R., Ishak, C.F., Osman, N., Halim, N.S.A., Panhwar, Q.A., 2021. Determining the characteristics and potential of plantbased biochars to reduce copper uptake in maize. Bragantia.

Agricolae, 2022. Pacote Agricolae- CRAN - Embalagem Agrícola [WWW Document]. 2022. URL https://cran.r-project.org/web/packages/agricolae/index.html (accessed 8.14.23).

Akaike, H., 1979. A Bayesian extension of the minimum AIC procedure of autoregressive model fitting. Biometrika 66, 237–242. https://doi.org/10.1093/BIOMET/66.2.237

Akhil, D., Lakshmi, D., Kartik, A., Vo, D.-V.N., Arun, J., Gopinath, K.P., 2021. Production, characterization, activation and environmental applications of engineered biochar: a review. Environmental Chemistry Letters 19, 2261–2297. https://doi.org/10.1007/s10311-020-01167-7

Aleosfoor, A., Rahimpour, M.R., 2024. Highly dispersed copper on biochar carbon as a promising catalyst for reverse water gas shift reaction. Journal of the Energy Institute 115, 101680. https://doi.org/https://doi.org/10.1016/j.joei.2024.101680

Almutairi, A.A., Ahmad, M., Rafique, M.I., Al-Wabel, M.I., 2023. Variations in composition and stability of biochars derived from different feedstock types at varying pyrolysis temperature. Journal of the Saudi Society of Agricultural Sciences 22, 25–34. https://doi.org/10.1016/J.JSSAS.2022.05.005

Altıkat, Alperay, Alma, M.H., Altıkat, Aysun, Bilgili, M.E., Altıkat, S., 2024. A Comprehensive Study of Biochar Yield and Quality Concerning Pyrolysis Conditions: A Multifaceted Approach. Sustainability. https://doi.org/10.3390/su16020937

Alva, A.K., Graham, J.H., Anderson, C.A., 1995. Soil pH and copper effects on young ‘Hamlin’orange trees. Soil Science Society of America Journal 59, 481–487.

ASTM International, 1984. Standard Test Method for Chemical Analysis of Wood Charcoal - Designation: D 1762 – 84 (Reapproved 2001). Annual Book of ASTM Standards 84, 292–293. https://doi.org/10.1520/D1762-84R07.2

Atchaya, S., Meena Devi, J., 2024. Experimental Investigation on Structural, Optical, Electrical and Magnetic Properties of Copper Oxide Nanoparticles. Proceedings of the National Academy of Sciences, India Section A: Physical Sciences 94, 153–160. https://doi.org/10.1007/s40010-023-00855-7

Ateş, A., Aydemir, B., Emre, K., 2023a. Investigation of physicochemical and biological properties of boron - doped biochar. Biomass Conversion and Biorefinery. https://doi.org/10.1007/s13399-023-04567-1

Ateş, A., Aydemir, B., Öksüz, K.E., 2023b. Investigation of physicochemical and biological properties of boron-doped biochar. Biomass Conversion and Biorefinery. https://doi.org/10.1007/s13399-023-04567-1

Balwant Singh , Marta Camps Arbestain, J.L., 2017. Biochar: A Guide to Analytical Methods.

Barrow, N.J., Hartemink, A.E., 2023. The effects of pH on nutrient availability depend on both soils and plants. Plant and Soil 487, 21–37. https://doi.org/10.1007/s11104-023-05960-5

Baty, F., Charles, S., Flandrois, J., Delignette-Muller, M.-L., 2015a. The R package nlstools: a toolbox for nonlinear regression. Journal of Statistical Software 66, 1–21.

Baty, F., Ritz, C., Charles, S., Brutsche, M., Flandrois, J.P., Delignette-Muller, M.L., 2015b. A Toolbox for Nonlinear Regression in R: The Package nlstools. Journal of Statistical Software 66, 1–21. https://doi.org/10.18637/JSS.V066.I05

Bhatnagar, A., Sillanpää, M., 2009. Applications of chitin-and chitosan-derivatives for the detoxification of water and wastewater—a short review. Advances in colloid and Interface science 152, 26–38.

Bhupenchandra, I., Basumatary, A., Dutta, S., Das, A., Choudhary, A.K., Lal, R., Dhanachandra Sharma, A., Sen, A., Prabhabati, Y., Ranjan Sahoo, M., 2024. Repercussions of fertilization with boron and enriched organic manure on soil chemical characteristics, boron and phosphorus fractions, and French bean productivity in an acidic Inceptisol of eastern Himalaya. Scientia Horticulturae 324, 304–4238. https://doi.org/10.1016/j.scienta.2023.112589

Bhupenchandra, I., Basumatary, A., Dutta, S., Singh, L.K., Datta, N., 2020. Impact of boron fertilization on boron fractions at different crop growth stages in cauliflower_cowpea_okra sequence in an inceptisols of North East India. Journal of Plant Nutrition 43, 1175–1188. https://doi.org/10.1080/01904167.2020.1724300

Bo, X., Guo, L., 2013. Carbonos mesoporosos dopados com boro ordenados como eletrocatalisadores isentos de metal para a reação de redução de oxigênio em solução alcalina. Physical Chemistry Chemical Physics 15, 2459–2465. https://doi.org/10.1039/c2cp43541a

Brasil, 2016. Instrução Normativa MAPA Nº 46 DE 22/11/2016 - Federal - LegisWeb [WWW Document]. URL https://www.legisweb.com.br/legislacao/?id=332894 (accessed 6.27.24).

Brasil, M. da A.P. e A., 2014. Manual De Métodos Analíticos oficiais para fertilizantes e corretivos.

Capo, L., Battisti, M., Blandino, M., 2024. The role of zinc fertilization and its interaction with nitrogen and phosphorus starter fertilization on early maize development and grain yield. Field Crops Research 307, 109245. https://doi.org/https://doi.org/10.1016/j.fcr.2023.109245

Carmo, D.L. do, Silva, C.A., Lima, J.M. de, Pinheiro, G.L., 2016. Electrical conductivity and chemical composition of soil solution: comparison of solution samplers in tropical soils. Revista brasileira de Ciência do Solo 40.

Carneiro, J.S. da S., Leite, D.A. da C., Castro, G.M. de, Franca, J.R., Botelho, L., Soares, J.R., Oliveira, J.E. de, Melo, L.C.A., 2022. Biochar-graphene oxide composite is efficient to adsorb and deliver copper and zinc in tropical soil. Journal of Cleaner Production 360, 132170. https://doi.org/https://doi.org/10.1016/j.jclepro.2022.132170

Carneiro, J.S. da S., Ribeiro, I.C.A., Nardis, B.O., Barbosa, C.F., Lustosa Filho, J.F., Melo, L.C.A., 2021. Long-term effect of biochar-based fertilizers application in tropical soil:

Agronomic efficiency and phosphorus availability. Science of the Total Environment 760, 143955. https://doi.org/10.1016/j.scitotenv.2020.143955

Chaves Fernandes, B.C., Ferreira Mendes, K., Dias Júnior, A.F., da Silva Caldeira, V.P., da Silva Teófilo, T.M., Severo Silva, T., Mendonça, V., de Freitas Souza, M., Valadão Silva, D., 2020. Impact of Pyrolysis Temperature on the Properties of Eucalyptus Wood-Derived Biochar. Materials. https://doi.org/10.3390/ma13245841

Chen, C., Zhou, L.L., Huang, Y.N., Wang, W.K., Xu, J., 2022. Boron regulates catalytic sites of biochar to enhance the formation of surface-confined complex for improved peroxydisulfate activation. Chemosphere 301, 134690. https://doi.org/10.1016/J.CHEMOSPHERE.2022.134690

Chen, H., Gao, Y., El-Naggar, A., Niazi, N.K., Sun, C., Shaheen, S.M., Hou, D., Yang, X., Tang, Z., Liu, Z., Hou, H., Chen, W., Rinklebe, J., Pohořelý, M., Wang, H., 2022. Enhanced sorption of trivalent antimony by chitosan-loaded biochar in aqueous solutions: Characterization, performance and mechanisms. Journal of Hazardous Materials 425, 127971. https://doi.org/https://doi.org/10.1016/j.jhazmat.2021.127971

Chen, J., Zhu, J., Wang, N., Feng, J., Yan, W., 2019. Hydrophilic polythiophene/SiO2 composite for adsorption engineering: Green synthesis in aqueous medium and its synergistic and specific adsorption for heavy metals from wastewater. Chemical Engineering Journal 360, 1486–1497. https://doi.org/https://doi.org/10.1016/j.cej.2018.10.228

Chen, Z., Xu, Q., Yan, L., Wang, Y., Sun, A., Liu, Q., 2024. Fractionation of stable boron isotopes in alfisols: Application of a novel tool for tracing boron behavior in two soil profiles. Geoderma 441, 116766. https://doi.org/10.1016/J.GEODERMA.2023.116766

Cho, D.-W., Kim, S., Tsang, Y.F., Song, H., 2019. Preparation of nitrogen-doped Cu-biochar and its application into catalytic reduction of p-nitrophenol. Environmental

Geochemistry and Health 41, 1729–1737. https://doi.org/10.1007/s10653-017-9966-x

Clough, T.J., Condron, L.M., Kammann, C., Müller, C., 2013. A Review of Biochar and Soil Nitrogen Dynamics. Agronomy. https://doi.org/10.3390/agronomy3020275

Conte, P., Bertani, R., Sgarbossa, P., Bambina, P., Schmidt, H.-P., Raga, R., Lo Papa, G., Chillura Martino, D.F., Lo Meo, P., 2021. Recent Developments in Understanding Biochar's Physical–Chemistry. Agronomy. https://doi.org/10.3390/agronomy11040615

D1762-84, A., 2013. Standard test method for chemical analysis of wood charcoal.

Dai, L., Zhu, W., He, L., Tan, F., Zhu, N., Zhou, Q., He, M., Hu, G., 2018. Calcium-rich biochar from crab shell: an unexpected super adsorbent for dye removal. Bioresource technology 267, 510–516.

Damasceno, A.S. da S., Boechat, C.L., Souza, H.A. de, Capristo-Silva, G.F., Mendes, W. de S., Teodoro, P.E., Morais, P.G.C., Oliveira, R.I. de, Della-Silva, J.L., Souza, I.A.M. de, Silva Junior, C.A. da, 2023. Nutritional monitoring of boron in Eucalyptus spp. in the Brazilian cerrado by multispectral bands of the MSI sensor (Sentinel-2). Remote Sensing Applications: Society and Environment 29, 100913. https://doi.org/10.1016/J.RSASE.2022.100913

Das, S.K., Ghosh, G.K., Avasthe, R.K., Sinha, K., 2021. Compositional heterogeneity of different biochar: Effect of pyrolysis temperature and feedstocks. Journal of Environmental Management 278. https://doi.org/10.1016/j.jenvman.2020.111501

de Mello Prado, R., 2021. Boron BT - Mineral nutrition of tropical plants, in: de Mello Prado, R. (Ed.), . Springer International Publishing, Cham, pp. 175–190. https://doi.org/10.1007/978-3-030-71262-4_10

de Mendiburu, F., de Mendiburu, M.F., 2019. Package 'agricolae.' R Package, version 1, 1143–1149.

de Oliveira Paiva, I., de Morais, E.G., Jindo, K., Silva, C.A., 2024. Biochar N Content, Pools and Aromaticity as Affected by Feedstock and Pyrolysis Temperature. Waste and Biomass Valorization. https://doi.org/10.1007/s12649-023-02415-x

Deng, J., Liu, Y., Liu, S., Zeng, G., Tan, X., Huang, B., Tang, X., Wang, S., Hua, Q., Yan, Z., 2017. Competitive adsorption of Pb(II), Cd(II) and Cu(II) onto chitosan-pyromellitic dianhydride modified biochar. Journal of Colloid and Interface Science 506, 355–364. https://doi.org/https://doi.org/10.1016/j.jcis.2017.07.069

Di Palma, L., Mecozzi, R., 2007. Heavy metals mobilization from harbour sediments using EDTA and citric acid as chelating agents. Journal of Hazardous Materials 147, 768–775. https://doi.org/https://doi.org/10.1016/j.jhazmat.2007.01.072

Ding, Y., Liu, Y., Liu, S., Huang, X., Li, Z., Tan, X., Zeng, G., Zhou, L., 2017. Potential Benefits of Biochar in Agricultural Soils: A Review. Pedosphere 27, 645–661. https://doi.org/10.1016/S1002-0160(17)60375-8

do Amaral Leite, A., de Souza Cardoso, A.A., de Almeida Leite, R., Barrera, A.M.V., Queiroz, D.D.L., Viana, T.C., de Oliveira-Longatti, S.M., Silva, C.A., de Souza Moreira, F.M., Lehmann, J., Melo, L.C.A., 2024. Phosphate-solubilizing bacteria increase maize phosphorus uptake from magnesium-enriched poultry manure biochar. Biology and Fertility of Soils 60, 421–436. https://doi.org/10.1007/s00374-024-01808-x

do Carmo, D.L., Silva, C.A., de Lima, J.M., Pinheiro, G.L., 2016. Electrical Conductivity and Chemical Composition of Soil Solution: Comparison of Solution Samplers in Tropical Soils. Revista Brasileira de Ciência do Solo 40. https://doi.org/10.1590/18069657RBCS20140795

Domingues, Rimena R., Trugilho, P.F., Silva, C.A., De Melo, I.C.N.A., Melo, L.C.A., Magriotis, Z.M., Sánchez-Monedero, M.A., 2017. Properties of biochar derived from wood and high-nutrient biomasses with the aim of agronomic and environmental benefits. PLoS ONE 12, 1–19. https://doi.org/10.1371/journal.pone.0176884

Domingues, Rimena R, Trugilho, P.F., Silva, C.A., Melo, I.C.N.A. de, Melo, L.C.A., Magriotis, Z.M., Sánchez-Monedero, M.A., 2017. Properties of biochar derived from wood and high-nutrient biomasses with the aim of agronomic and environmental benefits. PLOS ONE 12, e0176884.

Dong, X., Wang, C., Li, H., Wu, M., Liao, S., Zhang, D., Pan, B., 2014. The sorption of heavy metals on thermally treated sediments with high organic matter content. Bioresource technology 160, 123–128.

Du, Y., Dai, M., Naz, I., Hao, X., Wei, X., Rong, R., Peng, C., Ali, I., 2021. Carbothermal reduction synthesis of zero-valent iron and its application as a persulfate activator for ciprofloxacin degradation. Separation and Purification Technology 275, 119201. https://doi.org/10.1016/j.seppur.2021.119201

Elsherpiny, mohamed atef, 2023. Effect of Organic Amendments and Synthetic Substances on Copper Availability, Absorption, and Wheat Productivity. Egyptian Journal of Soil Science 63, 429–442. https://doi.org/10.21608/ejss.2023.220516.1614

Erenstein, O., Jaleta, M., Sonder, K., Mottaleb, K., Prasanna, B.M., 2022. Global maize production, consumption and trade: trends and R&D implications. Food Security 14, 1295–1319. https://doi.org/10.1007/s12571-022-01288-7

Extract, 2020. Extract and Visualize the Results of Multivariate Data Analyses [R package factoextra version 1.0.7].

Factoextra, 2022. R: The R Project for Statistical Computing [WWW Document]. URL https://www.r-project.org/ (accessed 8.14.23).

Fan, J., Li, Yan, Yu, H., Li, Yuxuan, Yuan, Q., Xiao, H., Li, F., Pan, B., 2020. Using sewage sludge with high ash content for biochar production and Cu(II) sorption. Science of The Total Environment 713, 136663. https://doi.org/https://doi.org/10.1016/j.scitotenv.2020.136663

Faria, W.M., Figueiredo, C.C. de, Coser, T.R., Vale, A.T., Schneider, B.G., 2018. Is sewage sludge biochar capable of replacing inorganic fertilizers for corn production? Evidence from a two-year field experiment. Archives of Agronomy and Soil Science 64, 505–519. https://doi.org/10.1080/03650340.2017.1360488

Ferreira, G.A., Hippler, F.W.R., Prado, L.A. do. S., Rima, J.A.H., Boaretto, R.M., Quaggio, J.A., Façanha, A.R., Mattos-Jr, D., 2021. Boron modulates the plasma membrane H+-ATPase activity affecting nutrient uptake of Citrus trees. Annals of Applied Biology 178, 293–303. https://doi.org/10.1111/AAB.12630

Friedrich, N., Brandimarte, P., Li, J., Saito, S., Yamaguchi, S., Pozo, I., Peña, D., Frederiksen, T., Garcia-Lekue, A., Sánchez-Portal, D., Pascual, J.I., 2020. Magnetism of Topological Boundary States Induced by Boron Substitution in Graphene Nanoribbons. PHYSICAL REVIEW LETTERS 125, 146801. https://doi.org/10.1103/PhysRevLett.125.146801

Fuentez-Torres, M.O., Ortiz-Chi, F., Espinosa-González, C.G., Aleman, M., Cervantes-Uribe, A., Torres-Torres, J.G., Kesarla, M.K., Collins-Martínez, V., Godavarthi, S., Martínez-Gómez, L., 2021. Facile Synthesis of Zn Doped g-C3N4 for Enhanced Visible Light Driven Photocatalytic Hydrogen Production. Topics in Catalysis 64, 65–72. https://doi.org/10.1007/s11244-020-01298-9

Gao, Y., Wang, Q., Ji, G., Li, A., Niu, J., 2021. Doping strategy, properties and application of heteroatom-doped ordered mesoporous carbon. RSC Advances 11, 5361–5383. https://doi.org/10.1039/D0RA08993A

Ghorbani, M., Amirahmadi, E., Neugschwandtner, R.W., Konvalina, P., Kopecký, M., Moudrý, J., Perná, K., Murindangabo, Y.T., 2022a. The Impact of Pyrolysis Temperature on Biochar Properties and Its Effects on Soil Hydrological Properties. Sustainability. https://doi.org/10.3390/su142214722

Ghorbani, M., Konvalina, P., Walkiewicz, A., Neugschwandtner, R.W., Kopecký, M., Zamanian, K., Chen, W.-H., Bucur, D., 2022b. Feasibility of Biochar Derived from Sewage Sludge to Promote Sustainable Agriculture and Mitigate GHG Emissions—A Review. International Journal of Environmental Research and Public Health. https://doi.org/10.3390/ijerph191912983

GRANULOMÉTRICA, B.A., 2014. Manual de métodos analíticos oficiais para fertilizantes minerais, orgânicos, organominerais e corretivos.

Hailegnaw, N.S., Mercl, F., Pračke, K., Praus, L., Száková, J., Tlustoš, P., 2020. The Role of Biochar and Soil Properties in Determining the Available Content of Al, Cu, Zn, Mn, and Cd in Soil. Agronomy. https://doi.org/10.3390/agronomy10060885

Hansson, K., Laclau, J.P., Saint-André, L., Mareschal, L., van der Heijden, G., Nys, C., Nicolas, M., Ranger, J., Legout, A., 2020. Fertilidade química dos ecossistemas florestais. Parte 1: Análises químicas comuns do solo foram preditores fracos da produtividade do povoamento em uma ampla gama de solos florestais ácidos. Ecologia e manejo florestal 461, 117843. https://doi.org/10.1016/j.foreco.2019.117843

Hao, W., Luo, P., Wu, Z., Mi, Y., Gao, Z., 2021. The effect of biomass pyrolysis temperature on the performance of biochar-fed molten hydroxide direct carbon fuel cells. Biomass and Bioenergy 150, 106122. https://doi.org/10.1016/j.biombioe.2021.106122

Haque, A., Al-Balushi, R.A., Raithby, P.R., Khan, M.S., 2020. Recent Advances in π-Conjugated N^C-Chelate Organoboron Materials. Molecules. https://doi.org/10.3390/molecules25112645

Heckler, G.S., da Costa, R.C., Fransozo, A., Rosso, S., Munehisa Shimizu, R., 2014. Long-term Patterns of Spatial and Temporal Distribution in the Seabob Shrimp Xiphopenaeus kroyeri (Decapoda: Penaeidae) Population in Southeastern Brazil. Journal of Crustacean Biology 34, 326–333. https://doi.org/10.1163/1937240X-00002231

Hodecker, B.E.R., De Barros, N.F., Da Silva, I.R., Diola, V., Sarkis, J.E.S., Loureiro, M.E.,

2014. Boron delays dehydration and stimulates root growth in Eucalyptus urophylla (Blake, S.T.) under osmotic stress. Plant and Soil 384, 185–199. https://doi.org/10.1007/S11104-014-2196-4/FIGURES/7

Hortin, J.M., Anderson, A.J., Britt, D.W., Jacobson, A.R., McLean, J.E., 2020. Copper oxide nanoparticle dissolution at alkaline pH is controlled by dissolved organic matter: influence of soil-derived organic matter, wheat, bacteria, and nanoparticle coating. Environmental Science: Nano 7, 2618–2631.

Houben, D., Evrard, L., Sonnet, P., 2013. Mobility, bioavailability and pH-dependent leaching of cadmium, zinc and lead in a contaminated soil amended with biochar. Chemosphere 92, 1450–1457. https://doi.org/https://doi.org/10.1016/j.chemosphere.2013.03.055

Hu, Z., Wei, L., 2023. Review on Characterization of Biochar Derived from Biomass Pyrolysis via Reactive Molecular Dynamics Simulations. Journal of Composites Science. https://doi.org/10.3390/jcs7090354

Huang, J., Zhu, Y., Bian, H., Song, L., Liu, Y., Lv, Y., Ye, X., Lin, C., Li, X., 2023. Insights into Enhanced Peroxydisulfate Activation with B and Fe Co-Doped Biochar from Bark for the Rapid Degradation of Guaiacol. Molecules. https://doi.org/10.3390/molecules28227591

Huang, Q., Song, S., Chen, Z., Hu, B., Chen, J., Wang, X., 2019. Biochar-based materials and their applications in removal of organic contaminants from wastewater: state-of-the-art review. Biochar 2019 1:1 1, 45–73. https://doi.org/10.1007/S42773-019-00006-5

Husson, F., Josse, J., Le, S., Mazet, J., Husson, M.F., 2016. Package ‘factominer.’ An R package 96, 698.

Ippolito, J.A., Liqiang Cui, ·, Kammann, C., Wrage-Mönnig, N., Estavillo, J.M., Fuertes-Mendizabal, T., Cayuela, M.L., Gilbert Sigua, ·, Novak, J., Spokas, K., Borchard, N.,

2020. Feedstock choice, pyrolysis temperature and type influence biochar characteristics: a comprehensive meta-data analysis review 1, 421–438. https://doi.org/10.1007/s42773-020-00067-x

Jalali, Mohsen, Imanifard, A., Jalali, Mahdi, 2023. Heavy metals accumulation in wheat (Triticum aestivum L.) roots and shoots grown in calcareous soils treated with non-spiked and spiked sewage sludge. Environmental Science and Pollution Research 30, 20862–20873.

Jez, E., Pellegrini, E., Contin, M., 2023. Copper bioavailability and leaching in conventional and organic viticulture under environmental stress. Applied Sciences 13, 2595.

Jha, S.K., Mishra, V.K., Damodaran, T., Singh, A.K., Singh, Y.P., Sharma, D.K., 2022. Does conservation tillage on partially reclaimed sodic soil restore land degradation by influencing boron dynamics, bioavailability for plant's uptake and nutritional security? Land Degradation & Development 33, 1260–1268. https://doi.org/10.1002/LDR.4206

Jia, M., Wang, F., Bian, Y., Jin, X., Song, Y., Kengara, F.O., Xu, R., Jiang, X., 2013. Effects of pH and metal ions on oxytetracycline sorption to maize-straw-derived biochar. Bioresource Technology 136, 87–93. https://doi.org/10.1016/j.biortech.2013.02.098

Jin, H., Zhang, D., Yan, Y., Yang, C., Fang, B., Li, X., Shao, Y., Wang, H., Yue, J., Wang, Y., Cheng, H., Shi, Y., Qin, F., 2022. Short-term application of chicken manure under different nitrogen rates alters structure and co-occurrence pattern but not diversity of soil microbial community in wheat field. Frontiers in Microbiology 13.

Jin, J., Li, Y., Zhang, Jianyun, Wu, S., Cao, Y., Liang, P., Zhang, Jin, Wong, M.H., Wang, M., Shan, S., 2016. Influence of pyrolysis temperature on properties and environmental safety of heavy metals in biochars derived from municipal sewage sludge. Journal of hazardous materials 320, 417–426.

Johnston, C.T., 2017. Biochar analysis by Fourier-transform infra-red spectroscopy, in: Singh, B., Camps-Arbestain, M., Lehmann, J. (Eds.), Biochar: A Guide to Analytical Methods. CRC Press/Taylor and Francis Group, LLC, Boca Raton, pp. 199–213.

Jones, J.B., 2001. Laboratory guide for conducting soil tests and plant analysis. CRC press.

Joseph, S., Cowie, A.L., Van Zwieten, L., Bolan, N., Budai, A., Buss, W., Cayuela, M.L., Graber, E.R., Ippolito, J.A., Kuzyakov, Y., Luo, Y., Ok, Y.S., Palansooriya, K.N., Shepherd, J., Stephens, S., Weng, Z., Lehmann, J., 2021. How biochar works, and when it doesn't: A review of mechanisms controlling soil and plant responses to biochar. GCB Bioenergy 13, 1731–1764. https://doi.org/10.1111/gcbb.12885

Joseph, S., Graber, E.R., Chia, C., Munroe, P., Donne, S., Thomas, T., Nielsen, S., Marjo, C., Rutlidge, H., Pan, G.X., Li, L., Taylor, P., Rawal, A., Hook, J., 2013. Shifting paradigms: development of high-efficiency biochar fertilizers based on nano-structures and soluble components. Carbon Management 4, 323–343. https://doi.org/10.4155/cmt.13.23

Kabiri, P., Motaghian, H., Hosseinpur, A., 2021. Impact of Biochar on Release Kinetics of Pb (II) and Zn (II) in a Calcareous Soil Polluted with Mining Activities. Journal of Soil Science and Plant Nutrition 21, 22–34. https://doi.org/10.1007/s42729-020-00336-5

Kalbarczyk, M., Szcześ, A., Belcarz, A., Kazimierczak, P., May, Z., 2023. Zn-doped Mono- and Biphasic Calcium Phosphate Materials Derived from Agriculture Waste and Their Potential Biomedical Applications: Part I. Materials. https://doi.org/10.3390/ma16051971

Karimi, B., Masson, V., Guilland, C., Leroy, E., Pellegrinelli, S., Giboulot, E., Maron, P.-A., Ranjard, L., 2021. Ecotoxicity of copper input and accumulation for soil biodiversity in vineyards. Environmental Chemistry Letters 19, 2013–2030. https://doi.org/10.1007/s10311-020-01155-x

Kassambara, A., Mundt, F., 2017. Package 'factoextra.' Extract and visualize the results of multivariate data analyses 76.

Kayani, Z.N., Umer, M., Riaz, S., Naseem, S., 2015. Characterization of copper oxide nanoparticles fabricated by the sol–gel method. Journal of Electronic Materials 44, 3704–3709.

Khan, A., Harfield, D., Hillen, B., Stenzel, F., Homung, A., 2017. Long-termaging of biochar. https://doi.org/10.13140/RG.2.2.21385.75366

Khan, S., Irshad, S., Mehmood, K., Hasnain, Z., Nawaz, M., Rais, A., Gul, S., Wahid, M.A., Hashem, A., Abd_Allah, E.F., Ibrar, D., 2024. Biochar Production and Characteristics, Its Impacts on Soil Health, Crop Production, and Yield Enhancement: A Review. Plants. https://doi.org/10.3390/plants13020166

Khaokaew, S., Landrot, G., Chaney, R.L., Pandya, K., Sparks, D.L., 2012. Speciation and Release Kinetics of Zinc in Contaminated Paddy Soils. Environmental Science & Technology 46, 3957–3963. https://doi.org/10.1021/es204007t

Kim, S., Kim, U. gi, Ryu, J., Kim, D., Kim, M., Joo, Y.C., Lee, S.Y., 2023. Boron-doped amorphous carbon deposited by DC sputtering for a hardmask: Microstructure and dry etching properties. Applied Surface Science 637, 157895. https://doi.org/10.1016/J.APSUSC.2023.157895

Kiralj, R., Ferreira, M.M.C., 2009. Basic validation procedures for regression models in QSAR and QSPR studies: theory and application. Journal of the Brazilian Chemical Society 20, 770–787. https://doi.org/10.1590/S0103-50532009000400021

Kleber, M., Bourg, I.C., Coward, E.K., Hansel, C.M., Myneni, S.C.B., Nunan, N., 2021. Dynamic interactions at the mineral–organic matter interface. Nature Reviews Earth & Environment 2, 402–421.

Labanya, R., Srivastava, P.C., Pachauri, S.P., Shukla, A.K., Shrivastava, M., Mukherjee, P., Srivastava, P., 2022. Sorption–desorption of some transition metals, boron and sulphur in a multi-ionic system onto phyto-biochars prepared at two pyrolysis temperatures. Environmental Science: Processes & Impacts 24, 2378–2397. https://doi.org/10.1039/D2EM00212D

Lamichhane, J.R., Osdaghi, E., Behlau, F., Köhl, J., Jones, J.B., Aubertot, J.-N., 2018. Thirteen decades of antimicrobial copper compounds applied in agriculture. A review. Agronomy for Sustainable Development 38, 28. https://doi.org/10.1007/s13593-018-0503-9

Lê, S., Josse, J., Husson, F., 2008a. FactoMineR: An R Package for Multivariate Analysis. Journal of Statistical Software 25, 1–18. https://doi.org/10.18637/JSS.V025.I01

Lê, S., Josse, J., Husson, F., 2008b. FactoMineR: an R package for multivariate analysis. Journal of statistical software 25, 1–18.

Lehmann, J., Joseph, S., 2024. Biochar for environmental management: science, technology and implementation. Taylor & Francis.

Leitner, J., Sedmidubský, D., Jankovský, O., 2018. Effect of ZnO nanosizing on its solubility in aqueous media. Micro & Nano Letters 13, 1585–1589.

Leng, L., Xu, S., Liu, R., Yu, T., Zhuo, X., Leng, S., Xiong, Q., Huang, H., 2020. Nitrogen containing functional groups of biochar: An overview. Bioresource Technology 298, 122286. https://doi.org/https://doi.org/10.1016/j.biortech.2019.122286

Li, L., Niu, W., Cong, H., Meng, H., Niu, Z., Shen, X., Cao, L., Kong, X., 2023. Effects of Pyrolysis Temperature on the Release Characteristics of Polycyclic Aromatic Hydrocarbons during Pyrolysis of Corn Stover Pellet. BioResources 18, 2112–2136. https://doi.org/10.15376/biores.18.1.2112-2136

Liang, H., Zhao, Y., Liu, T., Li, Ruijuan, Li, Rumei, Zhu, Y., Fang, F., 2024. Zn-Doped MnCO3/CS Composite Photocatalyst for Visible-Light-Driven Decomposition of Organic Pollutants. Molecules. https://doi.org/10.3390/molecules29051094

Liberda, D., Pięta, E., Pogoda, K., Piergies, N., Roman, M., Koziol, P., Wrobel, T.P., Paluszkiewicz, C., Kwiatek, W.M., 2021. The impact of preprocessing methods for a successful prostate cell lines discrimination using partial least squares regression and discriminant analysis based on Fourier transform infrared imaging. Cells 10, 953.

Lin, C.-W., Chen, F.-Y., Liu, S.-H., Ma, C.-Y., 2024. Optimized combination of zero-valent iron and oxygen-releasing biochar as cathodes of microbial fuel cells to enhance copper migration in sediment. Bioelectrochemistry 158, 108699. https://doi.org/https://doi.org/10.1016/j.bioelechem.2024.108699

Ling, C., Wu, S., Han, J., Dong, T., Zhu, C., Li, X., Xu, L., Zhang, Y., Zhou, M., Pan, Y., 2022. Sulfide-modified zero-valent iron activated periodate for sulfadiazine removal: Performance and dominant routine of reactive species production. Water Research 220, 118676.

Liu, B., Guo, W., Wang, H., Si, Q., Zhao, Q., Luo, H., Ren, N., 2020. B-doped graphitic porous biochar with enhanced surface affinity and electron transfer for efficient peroxydisulfate activation. Chemical Engineering Journal 396, 125119. https://doi.org/10.1016/J.CEJ.2020.125119

Liu, C., Lin, J., Chen, H., Wang, W., Yang, Y., 2021. Comparative Study of Biochar Modified with Different Functional Groups for Efficient Removal of Pb(II) and Ni(II). https://doi.org/10.21203/rs.3.rs-487894/v1

Liu, J., Wang, F., Xu, W., 2023. Characteristics of zinc adsorption onto biochars derived from different feedstocks. Water 15, 3789.

Liu, Q., Zang, G.-L., Zhao, Q., 2021. Removal of copper ions by functionalized biochar based on a multicomponent Ugi reaction. RSC Advances 11, 25880–25891. https://doi.org/10.1039/D1RA04156H

Lou, T., Yin, Y., Wang, J., 2024. Mechanisms of biochar promoting medium chain fatty acids production from sewage sludge: Effect of biochar type. Journal of Cleaner Production 451, 141995. https://doi.org/https://doi.org/10.1016/j.jclepro.2024.141995

Luo, M., Zhu, C., Chen, Q., Song, F., Hao, W., Shen, Z., Konhauser, K.O., Alessi, D.S., Zhong, C., 2023. In-situ growth of ZIF-8 nanocrystals on biochar for boron adsorption. Colloids and Surfaces A: Physicochemical and Engineering Aspects 657, 130504. https://doi.org/https://doi.org/10.1016/j.colsurfa.2022.130504

Lustosa Filho, J.F., Penido, E.S., Castro, P.P., Silva, C.A., Melo, L.C.A., 2017. Co-Pyrolysis of Poultry Litter and Phosphate and Magnesium Generates Alternative Slow-Release Fertilizer Suitable for Tropical Soils. ACS Sustainable Chemistry and Engineering 5, 9043–9052. https://doi.org/10.1021/ACSSUSCHEMENG.7B01935/ASSET/IMAGES/LARGE/SC-2017-01935U_0005.JPEG

Manogaran, M.D., Shamsuddin, R., Mohd Yusoff, M.H., Lay, M., Siyal, A.A., 2022. A review on treatment processes of chicken manure. Cleaner and Circular Bioeconomy 2, 100013. https://doi.org/https://doi.org/10.1016/j.clcb.2022.100013

Maqbool, M.A., Beshir, A., 2019. Zinc biofortification of maize (Zea mays L.): Status and challenges. Plant breeding 138, 1–28.

Masek, O., Buss, W., Sohi, S., 2018. Standard biochar materials. Environmental science & technology 52, 9543–9544.

Mašek, O., Buss, W., Sohi, S., 2018. Standard Biochar Materials. Environmental Science and Technology 52, 9543–9544. https://doi.org/10.1021/acs.est.8b04053

McAfee, L., 2000. Infrared and Raman spectra of inorganic and coordination compounds. Part A: theory and applications in inorganic chemistry; Part B: application in coordination, organometallic, and bioinorganic chemistry, (Nakamoto, Kazuo).

Meenu, Rani, M., Shanker, U., 2024. Efficient photodegradation of hexabromocyclododecane leached from polystyrene by biochar and sulfur doped CuO nanocomposite: Optimization factors, kinetics, and photoactivity. Environmental Pollution 340, 122818. https://doi.org/https://doi.org/10.1016/j.envpol.2023.122818

Morais, E.G., Jindo, K., Silva, C.A., 2023. Biochar-Based Phosphate Fertilizers: Synthesis, Properties, Kinetics of P Release and Recommendation for Crops Grown in Oxisols. Agronomy. https://doi.org/10.3390/agronomy13020326

Morais, E.G., Silva, C.A., Jindo, K., 2021. Humic Acid Improves Zn Fertilization in Oxisols Successively Cultivated with Maize–Brachiaria. Molecules. https://doi.org/10.3390/molecules26154588

Morais, E.G., Silva, C.A., Maluf, H.J.G.M., Guilherme, L.R.G., 2022. Slow-Release Humic Acid-Based Zinc Fertilizers Improve Growth and Nutrition of Maize and Brachiaria Grass Successively Grown in Oxisols. ACS Agricultural Science & Technology 3, 17–32.

Mortvedt, J.J., Gilkes, R.J., 1993. Zinc fertilizers, in: Zinc in Soils and Plants: Proceedings of the International Symposium on 'Zinc in Soils and Plants' Held at The University of Western Australia, 27–28 September, 1993. Springer, pp. 33–44.

Muzyka, R., Misztal, E., Hrabak, J., Banks, S.W., Sajdak, M., 2023. Various biomass pyrolysis conditions influence the porosity and pore size distribution of biochar. Energy 263, 126128. https://doi.org/https://doi.org/10.1016/j.energy.2022.126128

Nakamoto, K., 2009. Infrared and Raman spectra of inorganic and coordination compounds, part B: applications in coordination, organometallic, and bioinorganic chemistry. John Wiley & Sons.

Nan, H., Yin, J., Yang, F., Luo, Y., Zhao, L., Cao, X., 2021. Pyrolysis temperature-dependent carbon retention and stability of biochar with participation of calcium: Implications to carbon sequestration. Environmental Pollution 287, 117566.

https://doi.org/https://doi.org/10.1016/j.envpol.2021.117566

Nepal, J., Ahmad, W., Munsif, F., Khan, A., Zou, Z., 2023. Advances and prospects of biochar in improving soil fertility, biochemical quality, and environmental applications . Frontiers in Environmental Science .

Nguyen, N.-T., Lee, S.-Y., Chen, S.-S., Nguyen, N.-C., Chang, C.-T., Hsiao, S.-S., Trang, L.T., Kao, C.-Y., Lin, M.-F., Wang, L., 2018. Preparation of Zn-Doped Biochar from Sewage Sludge for Chromium Ion Removal. Journal of nanoscience and nanotechnology 18, 5520–5527. https://doi.org/10.1166/jnn.2018.15392

NIST-SRM-1573a, 2018. Standard Reference Material 1573 - Tomato Leaves.

Novais, R.F. de, Neves, J.C.L., Barros, N.F. de, 1991. Ensaio em ambiente controlado. Métodos de pesquisa em fertilidade do solo. Brasília: Embrapa-SEA 392.

Omiri, J., Snoussi, Y., Bhakta, A.K., Truong, S., Ammar, S., Khalil, A.M., Jouini, M., Chehimi, M.M., 2022. Citric-Acid-Assisted Preparation of Biochar Loaded with Copper/Nickel Bimetallic Nanoparticles for Dye Degradation. Colloids and Interfaces. https://doi.org/10.3390/colloids6020018

ON THE OCCURRENCE OF COPPER IN TROPICAL SOILS Author (s): J . G . VERMAAT and G . J . VAN DER BIE Published by : Springer Stable URL : https://www.jstor.org/stable/42931553, 1950. 2, 257–282.

Otoni, J.P., Matoso, S.C.G., Pérez, X.L.O., da Silva, V.B., 2024. Potential for agronomic and environmental use of biochars derived from different organic waste. Journal of Cleaner Production 449, 141826. https://doi.org/https://doi.org/10.1016/j.jclepro.2024.141826

Pan, G., Wei, J., Xu, M., Li, Jiamei, Wang, L., Li, Y., Cui, N., Li, Jun, Wang, Z., 2023a. Insight into boron-doped biochar as efficient metal-free catalyst for peroxymonosulfate activation: Important role of -O-B-O- moieties. Journal of Hazardous Materials 445, 130479. https://doi.org/https://doi.org/10.1016/j.jhazmat.2022.130479

Pan, G., Wei, J., Xu, M., Li, Jiamei, Wang, L., Li, Y., Cui, N., Li, Jun, Wang, Z., 2023b. Insight into boron-doped biochar as efficient metal-free catalyst for peroxymonosulfate activation: Important role of -O-B-O- moieties. Journal of Hazardous Materials 445, 130479. https://doi.org/10.1016/j.jhazmat.2022.130479

Penido, E.S., Martins, G.C., Mendes, T.B.M., Melo, L.C.A., do Rosário Guimarães, I., Guilherme, L.R.G., 2019. Combining biochar and sewage sludge for immobilization of heavy metals in mining soils. Ecotoxicology and Environmental Safety 172, 326–333. https://doi.org/https://doi.org/10.1016/j.ecoenv.2019.01.110

Piash, M.I., Iwabuchi, K., Itoh, T., 2022. Synthesizing biochar-based fertilizer with sustained phosphorus and potassium release: Co-pyrolysis of nutrient-rich chicken manure and Ca-bentonite. Science of The Total Environment 822, 153509. https://doi.org/10.1016/J.SCITOTENV.2022.153509

Quílez-Bermejo, J., Morallón, E., Cazorla-Amorós, D., 2020. Metal-free heteroatom-doped carbon-based catalysts for ORR: A critical assessment about the role of heteroatoms. Carbon 165, 434–454. https://doi.org/10.1016/J.CARBON.2020.04.068

R-Core-Team, 2020. R: A language and environment for statistical computing.

Rafique, M.I., Usman, A.R.A., Ahmad, M., Sallam, A., Al-Wabel, M.I., 2020. In situ immobilization of Cr and its availability to maize plants in tannery waste–contaminated soil: effects of biochar feedstock and pyrolysis temperature. Journal of Soils and Sediments 20, 330–339. https://doi.org/10.1007/S11368-019-02399-Z/TABLES/5

Rødde, R.H., Einbu, A., Vårum, K.M., 2008. A seasonal study of the chemical composition and chitin quality of shrimp shells obtained from northern shrimp (Pandalus borealis). Carbohydrate Polymers 71, 388–393. https://doi.org/https://doi.org/10.1016/j.carbpol.2007.06.006

Roy, P.P., Paul, S., Mitra, I., Roy, K., 2009. On Two Novel Parameters for Validation of

Predictive QSAR Models. Molecules 2009, Vol. 14, Pages 1660-1701 14, 1660–1701. https://doi.org/10.3390/MOLECULES14051660

Rúa-Díaz, S., Forjan, R., Lago-Vila, M., Cerqueira, B., Arco-Lázaro, E., Marcet, P., Baragaño, D., Gallego, J.L.R., Covelo, E.F., 2023. Pyrolysis temperature influences the capacity of biochar to immobilize copper and arsenic in mining soil remediation. Environmental Science and Pollution Research 30, 32882–32893. https://doi.org/10.1007/s11356-022-24492-6

Ruangratanakorn, J., Suwonsichon, T., Kasemsumran, S., Thanapase, W., 2020. Installation design of on-line near infrared spectroscopy for the production of compound fertilizer. Vibrational Spectroscopy 106, 103008. https://doi.org/10.1016/J.VIBSPEC.2019.103008

Ryota Suzuki, A., 2022. Package “pvclust” Title Hierarchical Clustering with P-Values via Multiscale Bootstrap Resampling.

Sadeek, S.A., Mohammed, E.A., Shaban, M., Abou Kana, M.T.H., Negm, N.A., 2020. Synthesis, characterization and catalytic performances of activated carbon-doped transition metals during biofuel production from waste cooking oils. Journal of Molecular Liquids 306, 112749. https://doi.org/https://doi.org/10.1016/j.molliq.2020.112749

Saha, S., Islam, M.T., Calhoun, J., Reza, T., 2023. Effect of Hydrothermal Carbonization on Fuel and Combustion Properties of Shrimp Shell Waste. Energies. https://doi.org/10.3390/en16145534

Salawu, O.A., Han, Z., Adeleye, A.S., 2022. Shrimp waste-derived porous carbon adsorbent: Performance, mechanism, and application of machine learning. Journal of Hazardous Materials 437, 129266. https://doi.org/10.1016/J.JHAZMAT.2022.129266

Sánchez-Rodríguez, A.R., Rey, M.-D., Nechate-Drif, H., Castillejo, M.Á., Jorrín-Novo, J. V, Torrent, J., del Campillo, M.C., Sacristán, D., 2021. Combining P and Zn fertilization to enhance yield and grain quality in maize grown on Mediterranean soils. Scientific Reports 11, 7427. https://doi.org/10.1038/s41598-021-86766-2

Schellekens, J., Silva, C.A., Buurman, P., Rittl, T.F., Domingues, R.R., Justi, M., Vidal-Torrado, P., Trugilho, P.F., 2018. Molecular characterization of biochar from five Brazilian agricultural residues obtained at different charring temperatures. Journal of Analytical and Applied Pyrolysis 130, 106–117.

Schmidt, M.P., Siciliano, S.D., Peak, D., 2021. The role of monodentate tetrahedral borate complexes in boric acid binding to a soil organic matter analogue. Chemosphere 276, 130150. https://doi.org/10.1016/j.chemosphere.2021.130150

Shaban, M., Zayed, M., Hamdy, H., 2017. Nanostructured ZnO thin films for self-cleaning applications. RSC Advances 7, 617–631. https://doi.org/10.1039/C6RA24788A

Shabbir, Z., Sardar, A., Shabbir, A., Abbas, G., Shamshad, S., Khalid, S., Natasha, Murtaza, G., Dumat, C., Shahid, M., 2020. Copper uptake, essentiality, toxicity, detoxification and risk assessment in soil-plant environment. Chemosphere 259, 127436. https://doi.org/https://doi.org/10.1016/j.chemosphere.2020.127436

Shireen, F., Nawaz, M.A., Chen, C., Zhang, Q., Zheng, Z., Sohail, H., Sun, J., Cao, H., Huang, Y., Bie, Z., 2018. Boron: Functions and Approaches to Enhance Its Availability in Plants for Sustainable Agriculture. International Journal of Molecular Sciences. https://doi.org/10.3390/ijms19071856

Shuailong, C., Qintie, L.I.N., Rongbo, X., Haoyu, L.U.O., Hengyi, F.U., 2020. Removal of EDTA-Cu in wastewater by copper-based biochar activated sodium persulfate. Chinese Journal of Environmental Engineering 14, 3298–3307.

Sieber, V., Hofer, M., Brück, W.M., Garbe, D., Brück, T., Lynch, C.A., 2018. ChiBio: An Integrated Bio-refinery for Processing Chitin-Rich Bio-waste to Specialty Chemicals BT - Grand Challenges in Marine Biotechnology, in: Rampelotto, P.H., Trincone, A. (Eds.),

. Springer International Publishing, Cham, pp. 555–578. https://doi.org/10.1007/978-3-319-69075-9_14

Silva, F.C. da, 2009. Manual de análises químicas de solos, plantas e fertilizantes, Empresa Brasileira de Pesquisa Agropecuária Embrapa Solos Embrapa Informática Agropecuária Ministério da Agricultura, Pecuária e Abastecimento.

Silverstein, R.M., Bassler, G.C., 1962. Spectrometric identification of organic compounds. Journal of Chemical Education 39, 546.

Singh, A., Yadav, K., Thakur, P., Wan, F., Ravelo, B., Thakur, A., 2024. Review on the amelioration of ZnO and its composites: synthesis and applications. Indian Journal of Physics. https://doi.org/10.1007/s12648-024-03181-9

Singh, B., Dolk, M.M., Shen, Q., Camps-Arbestain, M., 2017. Biochar: A Guide to Analytical Methods, in: Singh, B., Camps-Arbestain, M., Lehmann, J. (Eds.), Biochar: A Guide to Analytical Methods. CRC Press/Taylor and Francis Group, LLC, Boca Raton, pp. 23–38.

Socrates, G., 2004. Infrared and Raman characteristic group frequencies: tables and charts. John Wiley & Sons.

Stuart, B.H., 2004. Infrared Spectroscopy: Fundamentals and Applications, Analytical Techniques in the Sciences. John Wiley & Sons, Ltd, Chichester, UK. https://doi.org/10.1002/0470011149

Sui, L., Tang, C., Du, Q., Zhao, Y., Cheng, K., Yang, F., 2021. Preparation and characterization of boron-doped corn straw biochar: Fe (II) removal equilibrium and kinetics. Journal of Environmental Sciences 106, 116–123. https://doi.org/https://doi.org/10.1016/j.jes.2021.01.001

Sukumar, S., Rudrasenan, A., Padmanabhan Nambiar, D., 2020. Green-synthesized rice-shaped copper oxide nanoparticles using Caesalpinia bonducella seed extract and their applications. ACS omega 5, 1040–1051.

Sun, F., Bin Wu, H., Liu, X., Liu, F., Han, R., Qu, Z., Pi, X., Wang, L., Gao, J., Lu, Y., 2018a. A high-rate and ultrastable anode enabled by boron-doped nanoporous carbon spheres for high-power and long life lithium ion capacitors. https://doi.org/10.1016/j.mtener.2018.07.009

Sun, F., Qu, Z., Gao, J., Wu, H. Bin, Liu, F., Han, R., Wang, L., Pei, T., Zhao, G., Lu, Y., 2018b. In Situ Doping Boron Atoms into Porous Carbon Nanoparticles with Increased Oxygen Graft Enhances both Affinity and Durability toward Electrolyte for Greatly Improved Supercapacitive Performance. Advanced Functional Materials 28. https://doi.org/10.1002/ADFM.201804190

Suzuki, R., Terada, Y., Shimodaira, H., Suzuki, M.R., 2019. Package 'pvclust.' R Package. Hierarchical Clustering with P-Values via Multiscale Bootstrap Resampling. Version 2.

Taiyun Wei, M., Taiyun Wei cre, A., Simko aut, V., Levy ctb, M., Xie ctb, Y., Jin ctb, Y., Zemla ctb, J., Freidank ctb, M., Cai ctb, J., Protivinsky ctb, T., 2022. Package "corrplot" Title Visualization of a Correlation Matrix NeedsCompilation no.

Teixeira, P.C., Donagemma, G.K., Fontana, A., Teixeira, W.G., 2017a. Manual de Métodos de Análise de Solo 3ª edição revista e ampliada. Manual de métodos de análise de solo - Capítulo 8 - Densidade de partículas 574.

Teixeira, P.C., Donagemma, G.K., Fontana, A., Teixeira, W.G., 2017b. Manual de métodos de análise de solo.

Thapa, S., Bhandari, A., Ghimire, R., Xue, Q., Kidwaro, F., Ghatrehsamani, S., Maharjan, B., Goodwin, M., 2021. Managing Micronutrients for Improving Soil Fertility, Health, and Soybean Yield. Sustainability. https://doi.org/10.3390/su132111766

Thirumal, V., Pandurangan, A., Jayavel, R., Ilangovan, R., 2016. Synthesis and characterization of boron doped graphene nanosheets for supercapacitor applications. https://doi.org/10.1016/j.synthmet.2016.07.011

Tu, P., Zhang, G., Wei, G., Li, J., Li, Y., Deng, L., Yuan, H., 2022. Influence of pyrolysis temperature on the physicochemical properties of biochars obtained from herbaceous and woody plants. Bioresources and Bioprocessing 9, 131. https://doi.org/10.1186/s40643-022-00618-z

Vale, F., Alcarde, J.C., 2002. Extratores para avaliar a disponibilidade do zinco em fertilizantes. Revista Brasileira de Ciência do Solo.

Vinodkumar, R., Navas, I., Porsezian, K., Ganesan, V., Unnikrishnan, N. V, Pillai, V.P.M., 2014. Structural, spectroscopic and electrical studies of nanostructured porous ZnO thin films prepared by pulsed laser deposition. Spectrochimica Acta Part A: Molecular and Biomolecular Spectroscopy 118, 724–732.

Waclawska, I., 1995. Thermal decomposition of borax. Journal of thermal analysis 43, 261–269. https://doi.org/10.1007/BF02635993

Wang, C., Dai, H., Liang, L., Li, N., Cui, X., Yan, B., Chen, G., 2023. Enhanced mechanism of copper doping in magnetic biochar for peroxymonosulfate activation and sulfamethoxazole degradation. Journal of Hazardous Materials 458, 132002. https://doi.org/https://doi.org/10.1016/j.jhazmat.2023.132002

Wang, C., Huang, C., Qian, J., Xiao, J., Li, H., Wen, Y., He, X., Ran, W., Shen, Q., Yu, G., 2014. Rapid and Accurate Evaluation of the Quality of Commercial Organic Fertilizers Using Near Infrared Spectroscopy. PLOS ONE 9, e88279. https://doi.org/10.1371/JOURNAL.PONE.0088279

Wang, H., Chen, D., Wen, Y., Cui, T., Liu, Y., Zhang, Y., Xu, R., 2023. Insights into influence of aging processes on zero-valent iron modified biochar in copper(II) immobilization: from batch solution to pilot-scale investigation. Frontiers of Chemical Science and Engineering 17, 880–892. https://doi.org/10.1007/s11705-022-2282-8

Wang, H., Dong, Y., Yang, Y., Toor, G.S., Zhang, X., 2013. Changes in heavy metal contents in animal feeds and manures in an intensive animal production region of China. Journal of Environmental Sciences 25, 2435–2442. https://doi.org/10.1016/S1001-0742(13)60473-8

Wang, P., Tang, L., Wei, X., Zeng, G., Zhou, Y., Deng, Y., Wang, J., Xie, Z., Fang, W., 2017. Synthesis and application of iron and zinc doped biochar for removal of p-nitrophenol in wastewater and assessment of the influence of co-existed Pb(II). Applied Surface Science 392, 391–401. https://doi.org/10.1016/j.apsusc.2016.09.052

Wang, Z., Xu, X., Ma, S., Wang, H., Zhao, H., Wang, Y., Tong, S., Su, Z., Wang, W., Bai, J., 2021. The superior adsorption capacity of boron-nitrogen co-doping walnut shell biochar powder for Au(III), Pt(IV), and Pd(II). Journal of Environmental Chemical Engineering 9, 106288. https://doi.org/https://doi.org/10.1016/j.jece.2021.106288

Wei, T., Simko, V., Levy, M., Xie, Y., Jin, Y., Zemla, J., 2017. Package ‘corrplot.’ Statistician 56, e24.

Werheit, H., Au, T., Schmechel, R., Shalamberidze, S.O., Kalandadze, G.I., Eristavi, A.M., 2000. IR-Active Phonons and Structure Elements of Isotope-Enriched Boron Carbide. Journal of Solid State Chemistry 154, 79–86. https://doi.org/10.1006/JSSC.2000.8815

Wickham, H., Averick, M., Bryan, J., Chang, W., D’, L., Mcgowan, A., François, R., Grolemund, G., Hayes, A., Henry, L., Hester, J., Kuhn, M., Lin Pedersen, T., Miller, E., Bache, S.M., Müller, K., Ooms, J., Robinson, D., Seidel, D.P., Spinu, V., Takahashi, K., Vaughan, D., Wilke, C., Woo, K., Yutani, H., 2019. Welcome to the Tidyverse. Journal of Open Source Software 4, 1686. https://doi.org/10.21105/JOSS.01686

Wickham, H., Wickham, M.H., 2019. Package ‘tidyverse.’ See http://tidyverse. tidyverse. org 1–5.

Wijitkosum, S., Jiwnok, P., 2019. Elemental Composition of Biochar Obtained from Agricultural Waste for Soil Amendment and Carbon Sequestration. Applied Sciences.

https://doi.org/10.3390/app9193980

Wu, D., Sun, F., Qu, Z., Wang, H., Lou, Z., Wu, B., Zhao, G., 2022. Multi-scale structure optimization of boron-doped hard carbon nanospheres boosting the plateau capacity for high performance sodium ion batteries. Journal of Materials Chemistry A 10, 17225–17236. https://doi.org/10.1039/D2TA04194D

Wu, P., Cui, P., Fang, G., Gao, J., Zhou, D., Wang, Y., 2018. Sorption mechanism of zinc on reed, lignin, and reed- and lignin-derived biochars: kinetics, equilibrium, and spectroscopic studies. Journal of Soils and Sediments 18, 2535–2543. https://doi.org/10.1007/s11368-018-1928-0

Wu, P., Guo, Z., Hua, K., Wang, D., 2023. Long-term application of organic amendments changes heavy metals accumulation in wheat grains by affecting soil chemical properties and wheat yields. Journal of Soils and Sediments 23, 2136–2147. https://doi.org/10.1007/s11368-023-03473-3

Wydro, U., Jankowska, M., Wołejko, E., Kondzior, P., Łozowicka, B., Kaczyński, P., Rodziewicz, J., Janczukowicz, W., Pietryczuk, A., Cudowski, A., Jabłońska-Trypuć, A., 2022. Changes in Soil Biological Properties after Sewage Sludge and Pesticide Application in Wheat Cultivation. Applied Sciences. https://doi.org/10.3390/app122211452

Xiao, Y., Xue, Y., Gao, F., Mosa, A., 2017. Sorption of heavy metal ions onto crayfish shell biochar: effect of pyrolysis temperature, pH and ionic strength. Journal of the Taiwan Institute of Chemical Engineers 80, 114–121.

Xinxin, M.O., Siebecker, M.G., Wenxian, G.O.U., Ling, L.I., Wei, L.I., 2021. A review of cadmium sorption mechanisms on soil mineral surfaces revealed from synchrotron-based X-ray absorption fine structure spectroscopy: Implications for soil remediation. Pedosphere 31, 11–27.

Xu, L., Qi, Y., He, S., Wang, C., Jin, X., Wang, Q., Wang, K., Jin, P., 2025. Facile synthesis of boron-doped porous biochar as a metal-free adsorbent for efficient removal of aqueous tetracycline antibiotics. Journal of Environmental Sciences 152, 235–247. https://doi.org/https://doi.org/10.1016/j.jes.2024.04.044

Xu, L., Xing, X., Peng, J., Ji, M., 2022. Effects of In Situ Remediation on Copper Distribution and Soil Aggregate Adsorption–Desorption Characteristics in Smelter-Impacted Soil . Frontiers in Environmental Science .

Xu, P., Gao, Y., Cui, Z., Wu, B., Yan, B., Wang, Yifan, Zaitongguli, K., Wen, M., Wang, H., Jing, N., Wang, Yingze, Chao, C., Xue, W., 2023. Research Progress on Effects of Biochar on Soil Environment and Crop Nutrient Absorption and Utilization. Sustainability. https://doi.org/10.3390/su15064861

Yang, F., Wang, C., Sun, H., 2021. A comprehensive review of biochar-derived dissolved matters in biochar application: Production, characteristics, and potential environmental effects and mechanisms. Journal of Environmental Chemical Engineering 9, 105258. https://doi.org/10.1016/J.JECE.2021.105258

Yang, H., Sheng, K., 2012. Characterization of Biochar Properties Affected by Different Pyrolysis Temperatures Using Visible-Near-Infrared Spectroscopy. International Scholarly Research Network ISRN Spectroscopy 2012. https://doi.org/10.5402/2012/712837

Yang, Z., Yao, Z., Li, G., Fang, G., Nie, H., Liu, Z., Zhou, X., Chen, an, Huang, S., 2011. Sulfur-Doped Graphene as an Efficient Metal-free Cathode Catalyst for Oxygen Reduction. https://doi.org/10.1021/nn203393d

Younis, U., Rahi, A.A., Danish, S., Ali, M.A., Ahmed, N., Datta, R., Fahad, S., Holatko, J., Hammerschmiedt, T., Brtnicky, M., Zarei, T., Baazeem, A., Sabagh, A. El, Glick, B.R., 2021. Fourier Transform Infrared Spectroscopy vibrational bands study of Spinacia oleracea and Trigonella corniculata under biochar amendment in naturally contaminated soil. PloS one 16, e0253390. https://doi.org/10.1371/journal.pone.0253390

Yue, X., Fei-Yue, L., Xing-Jun, F., Shui-Jin, H., Xin, X., Jian-Fei, W., 2018. Cite this article as: Chinese. CHINESE JOURNAL OF ANALYTICAL CHEMISTRY 46, 609–615. https://doi.org/10.1016/S1872-2040(17)61081-8

Zhang, D., Sun, J., Li, Q., Song, H., Xia, D., 2022. Cu-Doped magnetic loofah biochar for tetracycline degradation via peroxymonosulfate activation. New Journal of Chemistry 46, 17223–17234. https://doi.org/10.1039/D2NJ02885A

Zhang, H., Cao, Q., Zhang, K., Xie, L., Xu, K., Qin, Y., Zhang, L., Chai, X., 2023. Boron-doped biochar-nano loaded zero-valent iron to activate persulfate for the degradation of oxytetracycline. Journal of Environmental Chemical Engineering 11, 111502. https://doi.org/10.1016/J.JECE.2023.111502

Zhang, J., Koubaa, A., Xing, D., Liu, W., Wang, Q., Wang, X., Wang, H., 2020a. Improving lignocellulose thermal stability by chemical modification with boric acid for incorporating into polyamide. Materials & Design 191, 108589. https://doi.org/https://doi.org/10.1016/j.matdes.2020.108589

Zhang, J., Koubaa, A., Xing, D., Liu, W., Wang, Q., Wang, X.M., Wang, H., 2020b. Improving lignocellulose thermal stability by chemical modification with boric acid for incorporating into polyamide. Materials & Design 191, 108589. https://doi.org/10.1016/J.MATDES.2020.108589

Zhang, Xu, Gang, D.D., Zhang, J., Lei, X., Lian, Q., Holmes, W.E., Zappi, M.E., Yao, H., 2022. Insight into the activation mechanisms of biochar by boric acid and its application for the removal of sulfamethoxazole. Journal of Hazardous Materials 424, 127333. https://doi.org/https://doi.org/10.1016/j.jhazmat.2021.127333

Zhang, Xin, Zhao, B., Liu, H., Zhao, Y., Li, L., 2022a. Effects of pyrolysis temperature on biochar's characteristics and speciation and environmental risks of heavy metals in sewage sludge biochars. Environmental Technology & Innovation 26, 102288. https://doi.org/10.1016/j.eti.2022.102288

Zhang, Xin, Zhao, B., Liu, H., Zhao, Y., Li, L., 2022b. Effects of pyrolysis temperature on biochar's characteristics and speciation and environmental risks of heavy metals in sewage sludge biochars. Environmental Technology & Innovation 26, 102288. https://doi.org/https://doi.org/10.1016/j.eti.2022.102288

Zhang, Y., Zhang, W., Zhang, H., He, D., 2023. Nano-Zero-Valent Zinc-Modified Municipal Sludge Biochar for Phosphorus Removal. Molecules 28, 3231.

Zhao, J., Li, H., Wang, Y., Yu, J., Li, N., Wang, S., 2023. Cu/CuO-Decorated Peanut-Shell-Derived Biochar for the Efficient Degradation of Tetracycline via Peroxymonosulfate Activation. Catalysts. https://doi.org/10.3390/catal13091246

Zhou, Y., Yan, W., Yu, X., Chen, T., Wang, S., Zhao, W., 2020. Boron and nitrogen co-doped porous carbon for supercapacitors: A comparison between a microwave-assisted and a conventional hydrothermal process. Journal of Energy Storage 32, 101706. https://doi.org/10.1016/j.est.2020.101706

Zhu, X., Chen, B., Zhu, L., Xing, B., 2017. Effects and mechanisms of biochar-microbe interactions in soil improvement and pollution remediation: A review. Environmental Pollution 227, 98–115. https://doi.org/https://doi.org/10.1016/j.envpol.2017.04.032

Supplementary Material

Table S 1. Chemical characterization of the raw material, biochar and composites produced.

ID	Al	B	Ca	Cu	Fe	Mg	Mn	Na	P	Zn
	(mg kg^{-1})									
FCM	2669	299	102606	178	2533	6466	462	2929	21060	551
FSC	1844	222	96764	98	1137	8433	92	1774	18473	109
FSS	6867	47	9471	348	11106	2489	200	922	3843	623
BCM-3	2780	243	108732	166	2170	9516	597		30035	787
BSC-3	2268	162	86603	147	3437	8513	114	IN	23074	1683
BSS-3	7399	94	10293	423	5565	2347	230	IN	4745	812
BCM-5	4719	196	105307	169	3657	13158	882	IN	46275	968
BSC-5	3648	164	125101	188	4749	17627	156	IN	44359	2238
BSS-5	10537	95	12647	481	11439	2738	301	IN	6129	922
CCM/CS-3	6334	129.5	101517	232979	3271	<LQ	1857	7527	27145	567
CCM/CO-3	4879	10.0	108679	111412	2712	<LQ	1843	84240	29341	233
CCM/CS-5	7342	459.0	157750	282412	4312	<LQ	2143	11461	32208	412
CCM/CO-5	7169	18.4	142800	237358	4366	<LQ	2185	77565	33387	338
CSC/CS-3	2275	189.3	112591	302437	1601	12482	52	20552	44250	4105
CSC/CO-3	2567	434.8	83212	241562	1547	9455	62	145502	36883	1238
CSC/CS-5	3356	958.9	237362	281037	1839	19350	127	24298	68037	3865
CSC/CO-5	3446	491.4	292200	233291	1629	22464	154	129040	66508	1640
CSS/CS-3	77711	134.3	2465	309250	41466	3622	126	10527	11182	1366
CSS/CO-3	260387	475.6	2411	203825	135316	4983	210	96636	12786	1151
CSS/CS-5	35608	78.2	<LQ	337858	28450	<LQ	1240	677	<LQ	111
CSS/CS-5	35104	147.8	<LQ	214850	10251	<LQ	1137	77757	<LQ	163

Figure S 1. Location of the study's raw material collection area. Map of Brazil highlighting the states of Minas Gerais and Espírito Santo, with emphasis on the cities of Lavras, Nepomuceno, and Linhares.

CHAPTER III

IMPACT OF ZINC-BIOCHAR COMPOSITES ON ENHANCING Zn AVAILABILITY, UPTAKE, AND MAIZE YIELD IN CONTRASTING OXISOLS

Loren Chisté[1], Leônidas Carrijo Azevedo Melo[1*], Carlos Alberto Silva[1]; Flávio Henrique Silveira Rabêlo[2]; Keiji Jindo[3]

1Department of Soil Science, School of Agricultural Sciences, Federal University of Lavras, Lavras, Minas Gerais 37203-202, Brazil;

2Department of Soil Science, Luiz de Queiroz College of Agriculture, University of São Paulo, Piracicaba, São Paulo 13418-900, Brazil;

3Agrosystems Research, Wageningen University & Research, PO Box 16, 6700 AA Wageningen, Holanda.

*Corresponding author: leonidas.melo@ufla.br

Abstract

Maize (*Zea mays L.*) is a versatile crop that thrives under diverse environmental conditions to meet its zinc (Zn) nutritional requirement. Therefore, maize yield and productivity is significantly affected by soil Zn availability, often limited in tropical soils by strong adsorption on Al and Fe colloids, ionic competition, and climatic factors. Thus, Zn fertilization in a protected form such as in biochar composites might be an option to enhance Zn use efficiency in tropical soils. This study investigated the effects of Zn-doped biochar composites (Zn-biochar) on maize growth in two RYL- Red Yellow Oxisols (medium texture); DRL- Dystroferric Red Oxisols. The Zn-biochar blends were prepared using shrimp shells (SC), chicken manure (CM), and sewage sludge (SS) combined with zinc sulfate (ZnS) or zinc oxide (ZnO), and pyrolyzed at 300 °C and 550 °C. Results showed that CSS/ZnS-3 and pure ZnS treatments achieved the highest Zn concentration in maize shoot and soil residual available Zn. Zinc release kinetics indicated higher Zn release for ZnO-doped biochars. CSC/ZnS-5 optimized grain yield in the Red Yellow Oxisol (RYL), while CSC/ZnS-3 excelled in delivering Zn to plans in the Red Oxisol (DRL). The Zn-biochar composites optimized Zn availability in soils, crop yield and dry matter. CSS/ZnS-3 and ZnS treatments are particularly promising for improving Zn availability in highly weathered soils. Future research should address long-term impacts, cost-effectiveness, and environmental sustainability of Zn-biochar composites in field trials.

Keywords: Zn-doped biochar, tropical soils, Zn availability, Organo-Zn complexes, soil residual Zn.

1. Introduction

Maize (*Zea mays L.*) is highly sensitive to low levels of zinc (Zn) in soil, which can significantly affect its growth and productivity (Sánchez-Rodríguez et al., 2021). Zinc is crucial for plant metabolism, acting as a cofactor for several enzymes involved in various metabolic processes, including protein synthesis and energy production. It also plays a role in carbohydrate metabolism and indoleacetic acid synthesis, while maintaining the integrity of plant cell membranes (Maqbool and Beshir, 2019; Rengel et al., 2022). In Brazil, where maize is widely cultivated, Zn deficiency is a common challenge to overcome in crop fields (Erenstein et al., 2022). Proper Zn fertilization is essential to improve agricultural production in highly weathered soils, which are often Zn-deficient due to low soil pH, and intense weathering process, presence of low-activity colloids (kaolinite, Fe and Al oxides) prone to adsorb and cause Zn fixation (Capo et al., 2024; Sánchez-Rodríguez et al., 2021).

Despite the importance of Zn fertilization, conventional Zn fertilizers can have low efficiency due to leaching, Zn precipitation, adsorption and, sometimes, fixation and runoff, especially in acidic cultivated soils (Conte et al., 2021; Morais et al., 2021). The availability of Zn in soil is influenced by the magnitude of the adsorption and precipitation processes, with Zn sorption increasing as soil pH rises due to the increase density of negative charges in Oxisol colloids and conversion of Zn to less soluble forms (Xinxin et al., 2021; Morais et al., 2021). Organic compounds present in soils also affect the magnitude of Zn sorption, as the charge density of soil colloids and stability of organometallic complexes increase with pH (Kleber et al., 2021).

Zinc (Zn)-doped biochar is emerging as a promising alternative to enhance Zn fertilizer efficiency (Conte et al., 2021; Morais et al., 2021). Produced by pyrolysis of organic waste, biochar improves soil fertility and overall ecosystem health (Joseph et al., 2021). It mitigates adverse Zn-soil interactions, increasing Zn availability in organometallic forms (Kleber et al., 2021; Y. Zhang et al., 2023). The functional groups in biochar, such as carboxyl and hydroxyl, efficiently adsorb Zn ions, and this process is influenced by soil pH, Zn sources, and biochar properties, which are shaped by pyrolysis conditions. Biochar produced at temperatures above 500 °C gains alkaline properties that form stable Zn-organic complexes, enhancing Zn mobility and plant uptake (Liu et al., 2023). Chelation further improves Zn solubility and transport, which is influenced by the biochar's origin, pyrolysis temperature, and the interaction of organic compounds (Wang et al., 2017).

In order to develop an innovative approach for supplying Zn-biochar to soil without causing secondary pollution, we selected three raw organic materials for the biochar-composite production: chicken manure (CM), shrimp shell (SC), and sewage sludge (SS). These organic wastes are globally discarded wastes or underutilized resources with unique humified or high N concentration features, making them excellent candidates for producing Zn-biochar composites. Importantly, these wastes do not contain significant levels of toxic metals, ensuring environmental safety (Liang et al., 2024). They offer a sustainable carbon source free from leachable metals, potentially replacing fossil fuels. Moreover, their surface functional groups play a crucial role in determining the relationship between processing parameters and the structural properties of the resulting biochar, thus enhancing its agronomic efficiency as a fertilizer.

The use of Zn during the *in situ* doping process in biochar production results in unique and highly functional properties within its carbon matrix (Fuentez-Torres et al., 2021). This process can also regulate the electronic characteristics of the biochar C chemical species by altering electron transfer dynamics (Fuentez-Torres et al., 2021). Doping biochar with Zn enhances its catalytic properties (Liang et al., 2024), improves soil nutrition, and supports plant growth (Kalbarczyk et al., 2023). This method achieves the desired effects at extremely low dosages due to a controlled/slow-release characteristic, making it a candidate for an efficient and sustainable agricultural practice.

Our hypothesis is that doping biochar with zinc sulfate ($ZnSO_4$) and zinc oxide (ZnO), two of the most common Zn fertilizers used in agriculture (Mortvedt and Gilkes, 1993), will result in structural modifications to the biochar, leading to greater efficiency in Zn fertilization for maize, depending on the soil types. The effectiveness of these modifications is influenced by the pyrolysis temperature, varying among the contrasting biomasses in terms of N concentration, organic matter stability, and the presence of humified material, particularly in sewage sludge. The specific hypotheses include: i) $ZnSO_4$ will lead to greater Zn release at lower pyrolysis temperatures (300 °C), while ZnO will promote a more controlled and long-term release at higher temperatures (550 °C); ii) sewage sludge, due to its high concentration of humified compounds, will facilitate the formation of more stable Zn-biochar complexes, increasing Zn availability to plants; and iii) shrimp shell, due to its calcium carbonate concentration, will have a unique interaction with Zn, altering the adsorption and release behavior. The objectives of this study are to characterize the formation of Zn-biochar complexes through FTIR analyse, evaluate the impact of Zn-doped biochar composites on zinc availability and release kinetics in Red-Yellow and Dystroferric Red Latosol soils, and assess their agronomic efficiency in enhancing maize growth, zinc uptake, and yield under greenhouse conditions. Additionally, the study aims to investigate the long-term residual effects of these composites on soil zinc concentration and fertility, providing insights into their sustainability as a Zn fertilization strategy in tropical soils.

2. Materials and Methods

2.1. *Preparation and Characterization of biochar*

Three types of feedstocks were selected for the synthesis of biochars and composites: chicken manure (FCM), shrimp shell (FSC), and sewage sludge (FSS). The FCM was sourced from a farm in Nepomuceno, Minas Gerais, Brazil (Latitude: -21.236110° S; Longitude: -45.234970° W). The FSS was collected from the sewage treatment plant at the Federal University of Lavras (UFLA) in Lavras, Minas Gerais, Brazil (Latitude: -21.23008° S; Longitude: -44.98981° W). The FSC were obtained from a seafood processing company in Linhares, Espírito Santo, Brazil (Latitude: -19.373030° S; Longitude: -40.054680° W).

The raw materials were initially air-dried at room temperature to eliminate surface moisture. They were then dried in a forced-air oven at 65 °C until they reached a constant weight. After drying, the materials were ground and sieved to achieve a uniform particle size of less than 0.25 mm. The prepared samples were stored in desiccators and sealed plastic bags to prevent reabsorption of moisture (Table 1).

Table 11- Identification of the samples, biochar, and acronyms of composites produced with pyrolysis (300 °C and 550 °C) and mixtures of feedstocks and Zn sources

Acronym	Feedstock	Temperature (°C)	Zn Source
FCM	Chicken Manure	60	no
FSC	Shrimp Carcass		
FSS	Sewage Sludge		
BCM-3	Chicken Manure	300	no
BSC-3	Shrimp Carcass		
BSS-3	Sewage Sludge		
CCM/ZnS-3	Chicken Manure	300	Zinc Sulfate
CCM/ZnO-3	Chicken Manure		Zinc Oxide
CSC/ZnS-3	Shrimp Carcass		Zinc Sulfate
CSC/ZnO-3	Shrimp Carcass		Zinc Oxide
CSS/ZnS-3	Sewage Sludge		Zinc Sulfate
CSS/ZnO-3	Sewage Sludge		Zinc Oxide
BCM-5	Chicken Manure	550	no

BSC-5	Shrimp Carcass		
BSS-5	Sewage Sludge		
CCM/ZnS-5	Chicken Manure	550	Zinc Sulfate
CCM/ZnO-5	Chicken Manure		Zinc Oxide
CSC/ZnS-5	Shrimp Carcass		Zinc Sulfate
CSC/ZnO-5	Shrimp Carcass		Zinc Oxide
CSS/ZnS-5	Sewage Sludge		Zinc Sulfate
CSS/ZnO-5	Sewage Sludge		Zinc Oxide

2.2. *Synthesis of Biochar and Zn-Doped Biochar*

Six biochars were produced by pyrolyzing each feedstock at either 300 °C and 550 °C in a JUNG muffle furnace. The pyrolysis process had a heating rate of 10 °C per minute and a dwell time of 60 minutes. Twelve Zn-doped composites were created by mixing the feedstocks with zinc sulfate ($ZnSO_4 \cdot 7H_2O$) or zinc oxide (ZnO) from Química Moderna and VETEC Química, achieving a target Zn concentration of 20% in the final composite. Preliminary studies indicated that a 20% Zn concentration optimizes the catalytic properties of biochar, enhancing both catalytic activity and structural stability while preventing excessive agglomeration of Zn particles and ensuring uniform metal distribution (Nguyen et al., 2018). This concentration was chosen to ensure efficient synthesis without compromising the biochar's properties and integrity.

The pre-treated mixtures, each weighing 100 g, were subjected to the same pyrolysis conditions as the undoped biochars. After synthesis, all samples were ground and sieved through a 60-mesh screen to ensure consistency and uniformity. The processed samples were stored in desiccators until further analysis, (Table S 1). The details of the nomenclature used for feedstocks, biochars and composites are shown in Table 1.

2.3. *Biochar and composite characterization*

The concentrations of volatile matter (VM), moisture (M), and ash were determined according to ASTM D1762-84, with modifications for biochar (Eqs. 1-3) (Singh et al., 2017).

Biochar yield was calculated using Eq. 5. After determining the volatile matter, the ash concentration was measured by incinerating the sample at 750 °C for six hours. Fixed carbon concentration was calculated using Eq. 4.

$$VM(\%) = \frac{DW\ at\ 105°C - DW\ at\ 950°C}{DW\ at\ 105°C}\ x100 \quad \text{(Eq. 1)}$$

$$M(\%) = \frac{RW - DW\ at\ 105°C}{RW}\ x\ 100 \quad \text{(Eq. 2)}$$

$$\text{As}(\%) = \frac{\text{RW} - \text{DW at 750ºC}}{\text{DW AT 105ºC}}\ \text{x}\ 100 \quad \text{(Eq. 3)}$$

$$\text{FC}(\%) = \frac{\text{DW at 105ºC} - \text{DW at 950ºC} - \text{DW at 750ºC}}{\text{DW at 105ºC}}\ \text{x}\ 100 \quad \text{(Eq. 4)}$$

$$\text{Y}(\%) = 100\ \text{x}\ \frac{\text{biochar mass}}{\text{105 ºC dried feedstock}} \quad \text{(Eq. 5)}$$

The pH and electrical conductivity (EC) of the samples were measured using a 1:10 biochar-to-water ratio and a digital pH and EC meter (Toledo CE, Mettler-Toledo AG) (Singh et al., 2017). Carbon concentration was analyzed through dry combustion using a TOC Vario cube analyzer (Elementar, Germany). Total nitrogen concentration was measured following sulfuric acid digestion using the Kjeldahl method (Singh et al., 2017). Post-digestion, nutrient concentrations were quantified using inductively coupled plasma optical emission spectroscopy (ICP-OES), ensuring quality control with certified reference materials. Certified tomato leaf samples from the National Institute of Standards and Technology (NIST) SRM 1573a, and biochar samples derived from sewage sludge and wheat straw from the UK (supplied by the Biochar Research Centre, University of Edinburgh) were used (Masek et al., 2018).

Water-soluble (W), 2% citric acid-soluble (CA%), and neutral ammonium citrate-soluble (NAC) Zn levels were assessed in filtrate using standard methods (GRANULOMÉTRICA, 2014). The Zn concentration in the sources was analyzed via ICP-OES. To compare Zn solubility, a Zn index was calculated based on the ratio of soluble fractions of Zn (Zn-W, Zn-CA%, Zn-NAC) to the total Zn concentration of each matrix, according to Eq. 6.

$$\text{Zn (\%)} = \frac{\text{Soluble Zn (g kg}^{-1})}{\text{Total Zn (g kg}^{-1})} \times 100 \qquad \text{(Eq. 6)}$$

2.4. *Infrared Spectroscopy*

Spectral signature characterization was performed using Fourier-transform infrared spectroscopy (FTIR) with attenuated total reflectance (ATR) on an Agilent® Cary 630 FTIR spectrometer equipped with a ZnSe-ATR crystal (Agilent Technologies, U.S.). The analysis was conducted with a scan resolution of 4 cm^{-1} over a wavelength range of 4000 to 650 cm^{-1}. Each FTIR spectrum underwent normalization (Liberda et al., 2021). Interpretation and identification of specific spectral bands for Zn-treated biochars were carried out using reference libraries and the assignment of bands and organic groups as described by (Singh et al., 2017).

2.5. *Zinc Release Kinetics*

To assess the kinetics of Zn release from various matrices through sequential extractions over time, the dynamics of Zn release were quantified. The experimental procedure involved weighing 1.0 g of each sample and transferring it to a 50 mL falcon tube, followed by the addition of 20 mL of a 2% citric acid solution. The mixture was horizontally shaken at 90 rotations per minute (rpm). Extracts were collected at predetermined intervals: 15 minutes, 30 minutes, 1 hour, 2 hours, 4 hours, 12 hours, 24 hours, 48 hours, 72 hours, 120 hours, and 250 hours. After each extraction phase, the tubes were centrifuged for 5 minutes at 3500 rpm. The resultant supernatant was carefully collected and transferred to another falcon tube reserved for further analysis. Zn determination in the leachate extracts was conducted using ICP-OES.

2.6. *Maize cultivation conditions*

The agronomic study was carried out in a greenhouse, where Maize (*Zea mays L.*) was grown in surface soil samples (0-20 cm) from typical Dystrophic Red-Yellow Oxisol (RYL, Oxisol according to the Soil Taxonomy) and Dystroferric Red Oxisol (DRL, Oxisol according to the Soil Taxonomy). The primary characteristics of these soils are detailed in Table 2.

Table 12. The main chemical, physicochemical, and texture of the Oxisols used for maize cultivation.

Oxisol	pH	C	Clay	Silt	Sand	N	P	K^+	Ca^{2+}	Mg^{2+}	Fe^{2+}	Mn^{2+}	B	Cu^{2+}	Zn^{2+}
		----------------- g kg^{-1} -----------------					- mg dm^{-3} -		$cmol_c$ dm^{-3}		--------------- mg dm^{-3} ---------------				
RYL	4.7	4.5	460	85	455	329	6.1	217.5	0.8	0.4	35.7	3.0	0.1	0.0	0.2
DRL	4.5	19.8	770	100	130	2580	8.3	30.1	0.3	0.2	50.6	3.4	0.06	1.1	0.3

RYL- Red Yellow Oxisol (medium texture); DRL-Dystroferric Red Oxisol; pH in a soil-water-Ratio of 1:2.5; C: carbon determined (dry combustion) in an automatic TOC analyzer; clay, silt and sand analyzed by the Boyoucos method. All methods are described in detail (Teixeira et al., 2017b); N: total nitrogen – Kjeldahl; P: available phosphorus determined by the resin soil test; K, Fe^{2+}, Mn^{2+}, Cu^{2+} and Zn^{2+}: available determined by the Mehlich^{-1} soil test; B: EDTA extractor; exchangeable calcium (Ca^{2+}), exchangeable magnesium ($Mg^{2+)}$ extracted by a 1 mol L^{-1} KCl solution soil test.

Soil samples were air-dried, ground, and sieved (2 mm) to obtain fine dry earth (TFSA). Soil acidity was adjusted using calcium carbonate ($CaCO_3$) and magnesium carbonate ($MgCO_3$) in a 4:1 molar ratio to achieve a target pH of 5.5 ± 0.2. This pH was selected to maximize the availability of essential macro and micronutrients and optimize maize growth conditions, while avoiding aluminum toxicity common in Oxisols. This approach ensures optimal soil conditions for plentiful maize growht, promoting a balanced environment for healthy plant development (Barrow and Hartemink, 2023). The lime application aimed to provide optimal growth conditions and ensure the availability of calcium (Ca) and magnesium (Mg) in the soil (Teixeira et al., 2017b).

A randomized complete block design with a 2x5x3 factorial arrangement was used, involving two soil types and five tested Zn-biochar composites: CSC/ZnS-3, CSC/ZnS-5, CSS/ZnS-3, a no-zinc control (No Zn addition), and a positive control using analytical-grade $ZnSO_4 \cdot 7H_2O$. Zinc was added to the Oxisols at a concentration of 20.0 mg kg^{-1} (Erenstein et al., 2022). The composites CSC/ZnS-3, CSC/ZnS-5 and CSS/ZnS-3 were chosen for their specific properties, kinetics of Zn release and potential agronomic efficiency, including physical and chemical characteristics that enhance Zn availability, uniform Zn distribution, Zn in soluble forms and stable Zn organic complexes.

After liming, each pot containing 3 kg of soil was fertilized, and maize was sown with two seeds per pot. The maize fertilization included the supply of 300 mg kg^{-1} N, 600 mg kg^{-1}

P for DRL (300 mg kg^{-1} for RYL), 300 mg kg^{-1} K, 40 mg kg^{-1} S, 1.80 mg kg^{-1} B, 5 mg kg^{-1} Mn, 20 mg kg^{-1} Zn, 0.15 mg kg^{-1} Fe, and 0.05 mg kg^{-1} Mo. Nutrient sources included $NH_4H_2PO_4$, K_2SO_4, H_3BO_3, $MnCl_2 \cdot 4H_2O$, and $(NH_4)_6Mo_7O_2 \cdot 4H_2O$, with N and K added to soil in three topdressing fertilization at 7, 15, and 30 days after maize seed germination (Novais et al., 1991). Throughout the entire experiment, water was supplied to the maize plants to maintain soil moisture at approximately 70% of the soil's maximum water-holding capacity. The maize plants were cultivated for 190 days, with daily adjustments to the soil water levels.

At the beginning of the experiment, a Suolo Acqua® sampler (Carmo et al., 2016) was installed in the lower third of the pots to avoid air entry in the soil-water-sampler system. The first soil solution aliquot (20 mL) was collected 12 hours after maize sowing, and subsequently at 1, 7, and 15 days. The collected solution was filtered through a 0.45 µm membrane, and soil Zn concentration was determined by ICP-OES. Three days after sowing, 50 g of soil was collected from each experimental unit, dried, and sieved (2 mm). The Zn concentration in the soil was measured at the end of the experiment to evaluate residual availability post-cultivation (Teixeira et al., 2017b).

Upon harvest, maize plants were separated into shoot, root, and grain. The dry matter weight for each part was determined after drying samples at 60 °C. Samples were weighed to determine shoot dry matter (SDM), root dry matter (SDR), and grain yield, then ground in a Wiley mill, sieved (1 mm), and digested in a nitro-perchloric mixture (Jones, 2001). The Zn concentration in plant tissue was determined using ICP-OES. Zinc accumulation in the shoot dry matter (SDM) was calculated by multiplying the dry matter by the Zn concentration in the shoot (Eq. 7).

$$Shoot\ Zn\ content\ =\ shoot\ dry\ matter\ (g)\ \times\ Zn\ concentration\ in\ the\ shoot\ tissue\ (mg\ g^{-1}) \qquad \text{(Eq. 7)}$$

2.7. *Statistical analysis*

Data were processed to obtain mean values, which were then analyzed using a Two-Way ANOVA to identify statistically significant differences ($p<0.05$). When significant differences were found, treatment means were compared using Tukey's test to account for multiple comparisons. All assumptions for ANOVA were verified, and significance was determined at $p<0.05$ using R software (Lê et al., 2008b). Multivariate analyses were also performed in R to explore the relationships between the properties and Zn pools within the composites. The R packages used for these analyses included agricolae, factoextra, FactoMineR, pvclust, corrplot, tidyverse, and nlstools (Baty et al., 2015a; de Mendiburu and de Mendiburu, 2019; Husson et al., 2016; Kassambara and Mundt, 2017; Suzuki et al., 2019; Wei et al., 2017; Wickham and Wickham, 2019).

The dataset for Zn release kinetics in 2% citric acid (CA%) was fitted to various non-linear mathematical models to describe the relationship between incubation time and the amount of Zn released from each source. The models fitted to the Zn kinetics data included the Elovich model (Eq. 12), simple exponential model (Eq. 13), power function (Eq. 14), and hyperbolic model (Eq. 15). In the models: Nt represents the fraction of Zn released at time t, a denotes the initial Zn release rate, b is the constant rate of Zn release, and N0 is the maximum amount of Zn released during the kinetics study.

$$Nt = a + blnt \quad \text{(Eq. 16)}$$

$$Nt = N0(1 - e^{-kt}) \quad \text{(Eq. 17)}$$

$$Nt = a \, x \, b^{t} \quad \text{(Eq. 18)}$$

$$Nt = \frac{N0 \, x \, t}{(N0 \, x \, b + t)} \quad \text{(Eq. 19)}$$

3. Results and Discussion

The chemical and physical properties of zinc-doped biochar composites (ZnS and ZnO) produced at different pyrolysis temperatures (300 °C and 550 °C) are shown in Table 3. The pH of the composites ranged from 5.0 to 9.0. In general, composites produced at 300 °C exhibited lower pH values than those produced at 550 °C. This trend can be explained by the increased carbonization and reduction in volatile matter at higher pyrolysis temperatures, which leads to the formation of more stable, alkaline functional groups (such as carbonates and ash) in the biochar matrix. These alkaline groups buffer the pH, increasing it as the pyrolysis temperature rises, regardless of the feedstock or Zn source used. Therefore, the pyrolysis temperature plays a critical role in determining the final pH of the composites. ZnO-doped composites tended to have higher pH levels compared to the pH of composites doped with ZnS. The lowest pH (5.0) was determined for CSS/ZnS-5, while the highest pH (9.0) was verified for CSC/ZnO-3. These findings are in line with the results reported by (Conte et al., 2021), that a higher pyrolysis temperature tend to increase the pH of biochar due to the greater thermal degradation of acidic functional groups.

Electrical conductivity values varied from 1.4 to 23 dS m^{-1}, with the highest values observed for CCM-based composites. In general, composites produced at 550 °C showed higher EC values, suggesting a greater concentration of soluble mineral salts in the composite ash. ZnS-doped biochars tended to have higher EC compared to ZnO-doped biochars, with CCM/ZnS-3 having the highest EC (21.5 dS m^{-1}), which signalizes for a higher solubility of Zn sulfate over pyrolyzed ZnO. This increase in EC at highest pyrolysis temperature (550 ^{o}C) is consistent with previous studies indicating a greater potential mineralization rate and the release of inorganic ions (Morais et al., 2021).

The yield of the composites varied from 55% to 80%, with the highest yields associated with CCM-based composites. Higher pyrolysis temperatures (550 °C) resulted in lower yields due to greater thermal degradation of organic matter during the carbonization process (Wang et al., 2017). In general, ZnO-doped composites exhibited slightly higher composite yield. These observations align with findings reported by (Erenstein et al., 2022), who noted that higher pyrolysis temperatures lead to increased thermal degradation of organic compounds, thereby reducing biochar yield.

Volatile matter ranged from 23 to 44%, with higher values for biochars produced at 300 °C, indicating lower thermal decomposition. ZnS-doping resulted in a more significant reduction in VM compared to ZnO. CSS/ZnO-5 had the lowest VM concentration (23%). This reduction in VM with increased pyrolysis temperature is due to the breakdown of volatile compounds as shown by (Sánchez-Rodríguez et al., 2021).

Ash concentration ranged from 17 to 74%, increasing with higher pyrolysis temperatures, which is an indication of high ash concentration of biochar generated at high pyrolysis temperature, thus, a higher presence of soluble Zn salts in the composites. Therefore, composites produced at 550 °C showed significantly higher ash concentration, reflecting a potential greater mineralization rate and Zn release with CSC/ZnS-5 having the highest ash concentration (74%). The correlation between pyrolysis temperature and ash concentration is well-documented, indicating greater retention of inorganic constituents at biochar matrices produced at elevated temperatures, (> 500 ^{o}C) (Y. Zhang et al., 2023).

Fixed carbon ranged from 26 to 73%, with the highest values observed in FSS-based composites pyrolyzed at 550 °C. Higher pyrolysis temperatures led to increased FC, reflecting greater conversion of organic C to FC. ZnO-doped composites had higher FC concentration compared to the ZnS-doped ones. Carbon concentration ranged from 14% to 68%, while N concentration varied from 0.03% to 2.03%, with CSC/ZnO-3 having the highest C concentration (68%). ZnS-doping did not significantly affect N retention in the composites. These findings are in agreement with (Kleber et al., 2021), who reported that increased pyrolysis temperatures enhance C stability and retention in biochar.

Pyrolysis temperature had a significant impact on all analyzed composite attributes. At 550 °C, there was an increase in pH, EC, ash concentration, and FC, along with a decrease in yield and VM. These results are consistent with the literature, which reports greater carbonization and potential mineralization rate of biochars produced at higher temperatures (Maqbool and Beshir, 2019). Doping with ZnS and ZnO influenced various properties of the biochars. ZnO-doped composites showed slightly higher yields and greater FC retention, while ZnS-doped composites exhibited higher EC and ash concentration. These differences are likely due to the distinct chemical interactions between the dopants and feedstocks during pyrolysis.

Table 13. The main chemical and physical properties of Zn-biochar composites

Composite	**pH**	**EC**	**Yield**	**MV**	**Ashes**	**FC**	**Elemental Composition**		**C:N Ratio**
		(dS m^{-1})	-- (%)------------------------------------						
							C	N	C:N
CCM/ZnS-3	6 ± 0.01	21.5 ± 0.01	80	28 ± 0.15	43 ± 0.49	28 ± 0.28	19.5 ± 0.08	3 ± 0.21	6 ± 0.4
CCM/ZnS-5	8.5 ± 0.01	11 ± 0.01	54	17 ± 0.68	16 ± 0.36	66 ± 0.21	16 ± 0.08	2 ± 0.03	9 ± 0.13
CCM/ZnO-3	8.4 ± 0.01	6.5 ± 0.01	75	31 ± 0.11	42 ± 0.4	26.5 ± 0.52	24 ± 0.08	4 ± 0.12	7 ± 0.23
CCM/ZnO-5	11 ± 0.03	8 ± 0.03	61	24 ± 0.13	36 ± 2.23	40 ± 2.48	19 ± 0.08	2 ± 0.09	10 ± 0.5
CSC/ZnS-3	7 ± 0.01	23 ± 0.03	87	45 ± 0.22	49 ± 0.46	5 ± 0.7	18 ± 0.08	5 ± 0.21	4 ± 0.17
CSC/ZnS-5	8 ± 0.01	6 ± 0.01	50	35 ± 0.24	16.5 ± 0.88	47 ± 1.15	16 ± 0.08	3 ± 0.01	6 ± 0.03
CSC-ZnO-5	10.6 ± 0.04	3 ± 0.01	55	18 ± 0.05	31.5 ± 0.46	49 ± 0.7	18.5 ± 0.08	3 ± 0.03	6.5 ± 0.08
CSC/ZnO-3	9 ± 0.01	6 ± 0.01	85	47 ± 0.96	48 ± 0.06	4 ± 1.01	27 ± 0.08	5 ± 0.21	6 ± 0.26
CSS/ZnS-3	5± 0.01	21.5 ± 0.05	94	35 ± 0.09	25 ± 0.78	39 ± 0.83	8 ± 0.08	1.5 ± 0.03	5 ± 0.14
CSS/ZnS-5	6.6 ± 0.01	3.5 ± 0.01	63	23 ± 0.47	11 ± 2.1	66 ± 1.64	7 ± 0.08	1.4 ± 0.03	5 ± 0.09
CSS/ZnO-3	6.5 ± 0.01	1.4 ± 0.01	92	44 ± 0.09	27 ± 0.72	28 ± 0.73	13 ± 0.08	2 ± 0.15	7.5 ± 0.64
CSS/ZnO-5	7 ± 0.05	1 ± 0.01	74	16 ± 0.08	12 ± 0.24	72.5 ± 0.17	10 ± 0.08	1.4 ± 0.03	7 ± 0.19

Values are mean (n = 3), except yield (%) (n = 1); pH, Electrical Conductivity (EC), Yield, and Proximate Composition (Volatile Matter (VM), Ash Concentration, Fixed Carbon (FC), Carbon (C), Nitrogen (N), and C:N carbon/nitrogen ratio. Composites: CCM/ZnS-3: chicken manure + zinc sulfate at 300 °C; CCM/ZnO-3: chicken manure + zinc oxide at 300 °C; CCM/ZnS-5: chicken manure + Zinc sulfate at 550 °C; CCM/ZnO-5: chicken manure + zinc oxide at 550 °C; CSC/ZnS-3: shrimp waste + zinc sulfate at 300 °C; CSC/ZnO-3: shrimp residue + zinc oxide at 300 °C; CSC/ZnS-5: shrimp residue + zinc sulfate at 550°C; CSC/ZnO-5: shrimp residue + zinc oxide at 300 °C; CSS/ZnS-3: sewage sludge + zinc sulfate at 300 °C; CSS/ZnO-3: sewage sludge + zinc oxide at 300 °C; CSS/ZnS-5: sewage sludge + zinc sulfate at 550 °C; CSS/ZnO-5: sewage sludge + zinc oxide at 550 °C.

The data presented in Table 4 highlight significant variations in the solubility of Zn in biochar composites depending on the type of dopant ($ZnSO_4$ or ZnO) and the pyrolysis temperature. For instance, the CSS/ZnS-3 composite, derived from sewage sludge and doped with $ZnSO_4$, showed the highest Zn concentration in water (201 ± 0.18 g.kg^{-1}) compared to other composites, indicating a higher Zn release at lower pyrolysis temperatures (300 °C). In contrast, ZnO-doped composites generally exhibited lower Zn solubility in water, which may be attributed to the lower solubility of ZnO under aqueous conditions (Leitner et al., 2018; Singh et al., 2024).

This difference in solubility between $ZnSO_4$ and ZnO can be compared to the properties of biochar composites modified with graphene oxide, as reported by (Carneiro et al., 2022). Graphene oxide, when incorporated into biochar, has demonstrated an efficient capacity to adsorb metals such as copper (Cu) and Zn, while maintaining relatively low solubility in water. This characteristic arises from the strong interactions between graphene and the metals, forming stable complexes that reduce solubility in aqueous solutions. Similarly, ZnO-doped biochar composites also form less soluble complexes, suggesting that the carbonized matrix at higher temperatures (>500 °C) promotes the formation of more stable and less soluble Zn species, as observed in the CSS/ZnO-5 composite. Furthermore, studies on Zn extractors, such as the work by (Vale and Alcarde, 2002), emphasize the importance of selecting appropriate extractors to evaluate Zn availability in fertilizers. The use of water, neutral ammonium citrate, and citric acid (2%) as extractors in this study allows for a comprehensive understanding of Zn availability in different soil conditions, reinforcing the necessity to tailor fertilizer strategies according to specific soil requirements.

Comparing biochar composites doped with Zn to those modified with graphene oxide underscores the significance of chemical interactions in controlling solubility and nutrient availability in the soil. Both types of composites offer advantages in terms of adsorption and controlled release of micronutrients, which can be leveraged to develop more efficient fertilization strategies, particularly in tropical soils that pose challenges related to nutrient leaching and fixation.

The total Zn concentration, determined after the full digestion of the composites, showed significant variations. CSS-derived biochars displayed high Zn concentration, with CSS/ZnO-5 (158 ± 2.35 $g.kg^{-1}$) and CSS/ZnS-3 (155 ± 1.43 $g.kg^{-1}$) having the highest values. FCM and FSC-derived biochars showed lower total Zn concentration, especially at the higher pyrolysis temperature (550 °C), suggesting a greater extent of Zn losses or transformation into stable and low-soluble chemical species when pyrolysis took place at elevated temperatures (H. Chen et al., 2022; Deng et al., 2017).

Zinc solubility in NAC also varied widely, thus, the highest NAC-soluble Zn was found in CSS/ZnO-5 (212 ± 10.0 $g.kg^{-1}$), while the lowest was in CCM/ZnO-5 (19 ± 0.01 $g.kg^{-1}$). This indicates that NAC is an effective extractor for Zn from FSS-derived biochars. Biochars doped with ZnO generally showed lower NAC-soluble Zn compared to those doped with ZnS. These results align with findings indicating that NAC is particularly effective in extracting Zn from sewage sludge biochars (Chen et al., 2019).

The solubility of Zn in citric acid ranged from 0.01 to 46.5%. The highest CA% Zn was observed in CCM/ZnO-3 (46.5 ± 0.67%), while the lowest was in CSC/ZnO-5 (0.21 ± 0.51%). This suggests that citric acid is particularly effective in extracting Zn from FCM-derived biochars doped with ZnO. The variability in CA% values indicates that citric acid solubility depends significantly on both the feedstock, pyrolysis temperature and the type of Zn dopant used.

The Zn solubility in W, NAC, and CA (Zn solubility index) represent the proportion of Zn extracted relative to the total Zn concentration in the respective composite. Higher index indicates a greater proportion of Zn being extracted by the respective solution. For example, the W index was highest for CSS/ZnS-3 (129.4 ± 1.07%), indicating a significant portion of Zn is W-soluble in this composite. Similarly, the NAC index was highest for CSS/ZnO-5 (134 ± 4.98%), showing that NAC extracts a substantial amount of Zn from this biochar.

The feedstock, type of Zn dopant, and pyrolysis temperature significantly influence the solubility and availability of Zn in the biochar composites. FSS-derived biochars generally exhibited higher Zn concentration and solubility, making them potentially more effective for increasing soil Zn availability. ZnS-doped biochars showed higher Zn solubility in water and NAC, while ZnO-doped biochars had higher Zn solubility in CA%. Higher pyrolysis temperatures generally reduced Zn solubility, likely due to increased Zn volatilization (since Zn metal volatilizes at around 907 °C, with precautions typically needed at temperatures starting from 500 °C to 600 °C to mitigate the risk of Zn losses in volatile forms, especially in high-temperature processes like metal smelting or the production of Zn-containing materials such as biochar composites). Additionally, Zn may transform into less soluble forms during pyrolysis at elevated temperatures, further reducing its availability (Conte et al., 2021; Kleber et al., 2021).

Understanding the solubility of Zn in biochar composites using different extractors is crucial for predicting their agronomic effectiveness as soil Zn source for fertilization. Composites with higher W and NAC-soluble Zn, such as those derived from FSS and doped with ZnS, may provide more readily available Zn for plant uptake. In contrast, composites with higher CA%-soluble Zn may release Zn more slowly, potentially providing longer-term Zn availability. These findings highlight the importance of selecting appropriate feedstocks, biochar types and Zn dopants to meet specific plant nutrient requirements.

Table 14. Solubility of zinc (Zn) in composites using different extractors

	Zinc (Zn)						
Composite	**W**	**T**	**NAC**	**CA%**	**W Index**	**NAC Index**	**CA% Index**
	------------------------(g kg^{-1}) -----------------------				-----------------(%)----------------		
CCM/ZnS-3	155 ± 0.09	137 ± 0.16	174 ± 0.83	22.5 ± 16.83	113 ± 0.2	127 ± 0.46	16.5 ± 12.34
CCM/ZnS-5	0.2 ± 0.01	165 ± 2.4	14 ± 0.19	2 ± 0.02	0.1 ± 0.01	9 ± 0.14	1 ± 0.01
CCM/ZnO-3	1 ± 0.0	167 ± 1.31	173 ± 1.79	46.5 ± 0.67	0.6 ± 0.01	104 ± 1.09	28 ± 0.47
CCM/ZnO-5	0.01 ± 0.0	185 ± 1.74	206 ± 2.11	21 ± 0.51	0.01 ± 0.0	112 ± 2.16	11 ± 0.25
CSC/ZnS-3	147 ± 1.21	156 ± 2.16	195 ± 0.25	3.5 ± 0.17	94.5 ± 1.0	125 ± 1.64	2.± 0.13
CSC/ZnS-5	0.2 ± 0.0	191 ± 0.46	54 ± 1.76	2.2 ± 0.05	0.1 ± 0.01	28 ± 0.89	1.± 0.02
CSC-ZnO-5	0.01 ± 0.0	184 ± 0.64	193 ± 1.85	20 ± 0.25	0.01 ± 0.01	105 ± 1.16	11 ± 0.1
CSC/ZnO-3	0.3 ± 0.01	195 ± 1.47	236 ± 1.69	29 ± 0.21	0.2 ± 0.01	121 ± 1.16	15 ± 0.2
CSS/ZnS-3	201 ± 0.18	155 ± 1.43	216 ± 2.57	2 ± 0.02	129.4 ± 1.07	140 ± 2.74	1.5 ± 0.02
CSS/ZnS-5	22.5 ± 0.17	184 ± 1.07	24 ± 0.08	2 ± 0.02	12 ± 0.08	13 ± 0.12	1 ± 0.01
CSS/ZnO-3	2 ± 0.01	163 ± 1.19	221 ± 0.25	42.5 ± 0.53	1 ± 0.01	136 ± 0.84	26 ± 0.43
CSS/ZnO-5	0.2 ± 0.01	158 ± 2.35	212 ± 10.0	12 ± 0.56	0.1 ± 0.01	134 ± 4.98	8 ± 0.45

Values are mean (n = 3); zinc in H_2O was determined ± 0.01 in solution in H_2O at a ratio of 1:10 (w/v); concentration of soluble zinc in total (T) was determined by total digestion of the composites; zinc in neutral ammonium citrate water (NAC); zinc in concentration of zinc soluble in citric acid at 2% (CA%); H_2O Index, NAC Index and CA% Index represent the zinc concentration in relation to the extractors and the total zinc concentration. Composites: CCM/ZnS-3: chicken manure + zinc sulfate at 300 °C; CCM/ZnO-3: chicken manure + zinc oxide at 300 °C; CCM/ZnS-5: chicken manure + Zinc sulfate at 550 °C; CCM/ZnO-5: chicken manure +

zinc oxide at 550 °C; CSC/ZnS-3: shrimp waste + zinc sulfate at 300 °C; CSC/ZnO-3: shrimp residue + zinc oxide at 300 °C; CSC/ZnS-5: shrimp residue + zinc sulfate at 550 °C; CSC/ZnO-5: shrimp residue + zinc oxide at 300 °C; CSS/ZnS-3: sewage sludge + zinc sulfate at 300 °C; CSS/ZnO-3: sewage sludge + zinc oxide at 300 °C; CSS/ZnS-5: sewage sludge + zinc sulfate at 550 °C; CSS/ZnO-5: sewage sludge + zinc oxide at 550 °C.

Data shown in Figure 1 illustrate the kinetics of Zn release from composites over time. The left graph represents the release kinetics for composites produced at 300 °C, while the right graph shows the release kinetics for composites produced at 550 °C.

For composites produced at 300 °C, CCM/ZnS-3 demonstrated an initial rapid release, stabilizing at approximately 55% after about 50 hours, following the adjust of dataset to the Elovich model with an R^2 of 0.64. CCM/ZnO-3 showed a high initial release, reaching 81% within 10 hours and maintaining this level throughout the kinetics study period, following a mathematical adjust to the exponential model with a R^2 of 0.98. CSC/ZnS-3 released Zn steadily, stabilizing at around 73% after 50 hours, modeled exponentially with an R^2 of 0.99. Similarly, CSC/ZnO-3 displayed a release pattern that stabilized at 77%, which was explained by an exponential mathematical model with a R^2 of 0.95. CSS/ZnS-3 released Zn slowly, stabilizing at around 15%, whose dataset were fitted to an exponential model with a R^2 of 0.89.

These results suggest that in general ZnO-doped composites exhibited higher Zn release rate, compared to the ZnS-doped ones. Specifically, CCM composites showed significant differences in Zn release kinetics, which relied on the Zn dopant, with ZnO leading to higher Zn release over time. FSC composites exhibited similar Zn release patterns for both dopants (ZnS and ZnO), while FSS composites had the lowest Zn release over time.

For composites produced at 550 °C, CCM/ZnS-5 showed a slow release, stabilizing at around 15%, following a power model with an R^2 of 0.80. CCM/ZnO-5 exhibited a high initial release, reaching 84% quickly and maintaining this level, modeled exponentially with an R^2 of 0.96. CSC/ZnS-5 displayed a gradual release, stabilizing at around 19%, following a power model with an R^2 of 0.70. CSC/ZnO-5 released Zn steadily, reaching 80%, with an exponential model and an R^2 of 0.89. CSS/ZnS-5 had a very slow release, stabilizing around 12%, following a power model with an R^2 of 0.99.

These results indicate that higher pyrolysis temperatures generally lead to lower Zn release percentages, except for ZnO-doped composites, which maintained high release rates. Notably, CCM/ZnO-5 showed the highest Zn release, similar to its lower temperature counterpart. CSC-based composites displayed intermediate Zn release, while CSS-based composites had the lowest release rates. Comparing the two pyrolysis temperatures, composites produced at 300 °C released Zn more rapidly and to a higher extent compared to those produced at 550 °C (Kabiri et al., 2021).

Regarding the impact of dopants, ZnO-doped composites consistently exhibited higher Zn release rates, compared to ZnS-doped composites, regardless of the pyrolysis temperature. Feedstock also influenced Zn release, with CCM-based composites releasing Zn more efficiently than CSC and CSS-based composites, particularly when doped with ZnO.

The Zn release kinetics indicate that biochar composites produced at lower pyrolysis temperatures may be more suitable for applications requiring rapid and higher Zn availability. Conversely, those produced at higher temperatures could be more appropriate for long-term, slow Zn release. The choice of dopant also plays a crucial role, with ZnO proving more effective for higher Zn release compared to ZnS. These findings are essential for optimizing the use of Zn-biochar composites in tropical cropland areas, particularly for tailored nutrient management strategies in Cerrado soils.

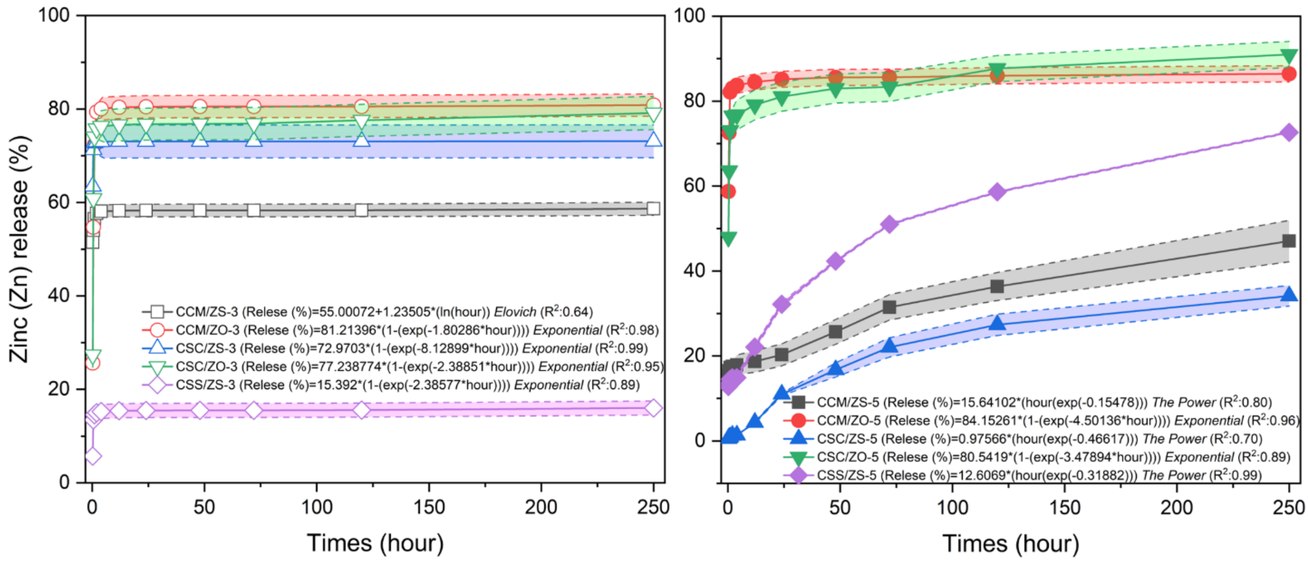

Figure 15. Zinc release as a percentage of total Zn used in the kinetics study for the Zn-biochar composites produced at 300 °C (left) and 550 °C (right).

The FTIR spectra of biochar composites doped with ZnS and ZnO, produced from FCM, FSC and FSS at pyrolysis temperatures of 300 °C and 550 °C, are shown in Figure 2. For ZnS-doped composites at 300 °C (CCM/ZnS-3, CSC/ZnS-3, CSS/ZnS-3) and 550 °C (CCM/ZnS-5, CSC/ZnS-5, CSS/ZnS-5), broad bands around 3600-3000 cm^{-1} indicate O-H stretching vibrations, showing the presence of hydroxyl groups and adsorbed water (Silverstein and Bassler, 1962). Small bands between 2000-1800 cm^{-1} are related to C=O stretching vibrations from carbonyl or carboxyl groups (Socrates, 2004). The region from 1500-1000 cm^{-1} shows bands for C-H stretching and C-O deformation, while characteristic ZnS bands appear around 600 cm^{-1} (Stuart, 2004).

At 550°C, similar bands are observed with changes in intensity and width, indicating structural changes due to increased pyrolysis temperature. The ZnS bands around 600 cm^{-1} are more defined at higher temperatures (McAfee, 2000).

For ZnO-doped composites at 300°C (CCM/ZnO-3, CSC/ZnO-3, CSS/ZnO-3) and 550 °C (CCM/ZnO-5, CSC/ZnO-5, CSS/ZnO-5), broad bands in the 3600-3000 cm^{-1} region indicate hydroxyl groups' presence. Bands between 2100-1800 cm^{-1} are related to C=O stretching, and the region from 1500-1000 cm^{-1} shows C-H stretching and C-O deformation bands. The ZnO characteristic bands are more defined in the 500-400 cm^{-1} region (Shaban et al., 2017). At 550 °C, the spectra reveal intensified and better-defined ZnO bands, particularly in the 1400-1000 cm^{-1} region, suggesting more significant organic compound decomposition and oxide formation (Vinodkumar et al., 2014).

Overall, ZnS-doping in composites led to a reduction in the intensity of O-H bands with increasing temperature, indicating the loss of hydroxyl groups or adsorbed water. The C=O bands (2000-1800 cm^{-1}) became more defined after thermal treatment, suggesting the formation of stable carbonyl compounds. The intensity of C-H and C-O bands (1500-1000 cm^{-1}) decreased due to the decomposition of volatile organic compounds. The ZnS bands (~600 cm^{-1}) became more defined with higher temperatures, indicating better incorporation of ZnS. In the FSC and FSS matrix, there was improved definition of ZnS bands and changes in organic bands, indicating decomposition and formation of new structures.

For ZnO-doped composites at 550 °C, the intensity of O-H bands decreased similarly to ZnS-doped composites. The C=O bands became more defined after thermal treatment, while the C-H and C-O bands (1500-1000 cm^{-1}) decreased in intensity due to the decomposition of volatile organic compounds. Particularly in the FSC and FSS matrices, there was improved definition of ZnO bands and changes in organic bands, indicating decomposition and formation of new structures. Therefore, thermal treatment at 550°C in the FSC and FSS matrices generally enhances the quality of Zn-doped composites by increasing the definition of ZnS and ZnO bands, potentially improving the fertilizing properties of the composites.

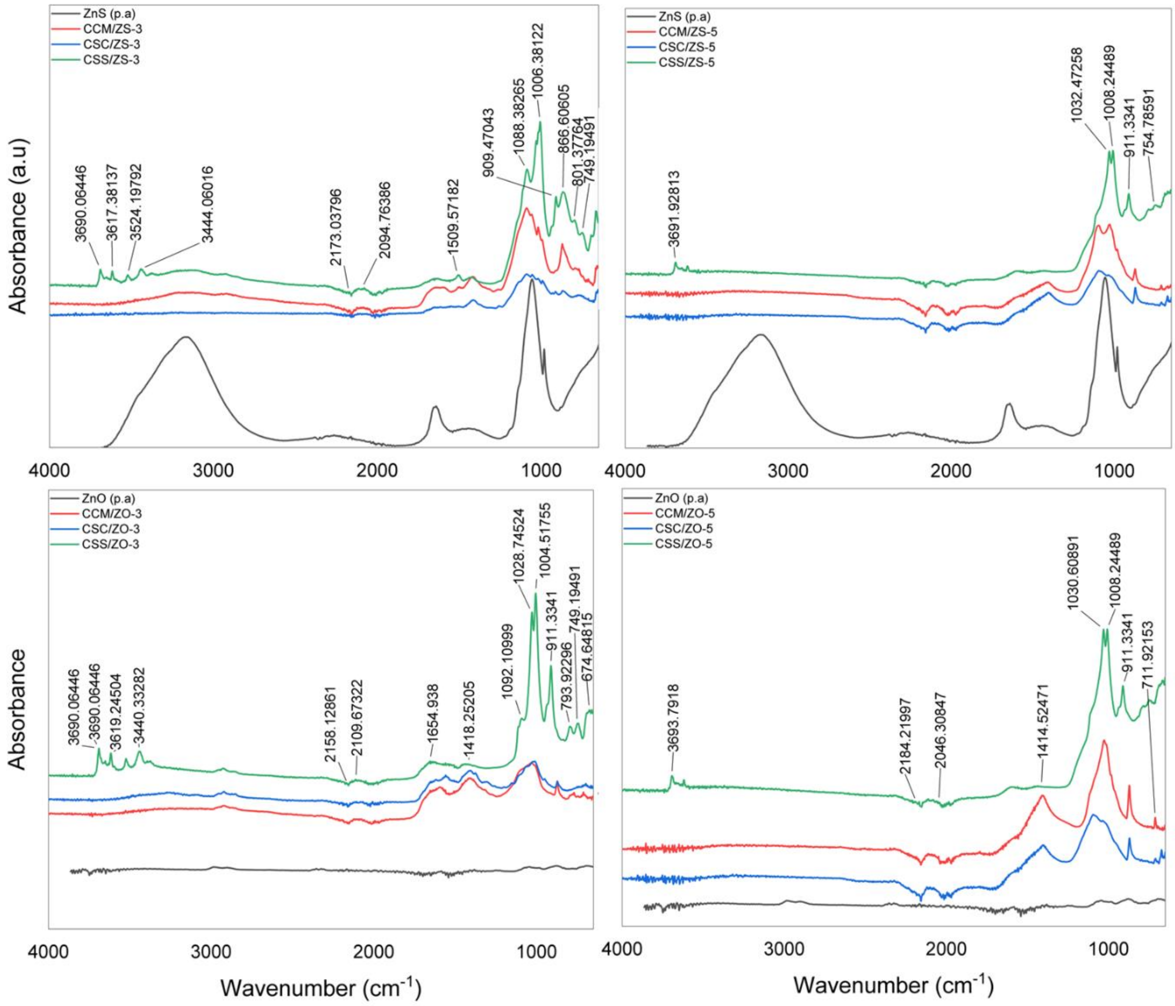

Figure 16. FTIR Analysis of Zinc-Doped Biochar Composites

Figure 17 illustrates the impact of different treatments on the production of grains, root dry matter (RDM), and shoot dry matter (SDM) in corn. The letters above the bars indicate statistical groupings based on the total dry matter production (grains + RDM + SDM) for each treatment.

In RYL soil, the CSC/ZS-5 treatment produced the highest grain yield (indicated by 'a'), with a moderate shoot and root biomass ('b' for both SDM and RDM). The CSC/ZS-3 treatment, contrary to earlier misinterpretation, showed higher root production (RDM marked by 'a') compared to the other treatments but lower grain yield ('b') and shoot biomass ('c'). The CSS/ZS-3 treatment resulted in the lowest grain production ('d') but exhibited moderate RDM and SDM levels ('b' and 'c' respectively). The ZnS treatment produced a moderate grain yield ('b') and a balanced RDM ('a') and SDM ('b'). Finally, the NO (control) treatment resulted in the lowest grain yield ('d') but showed relatively high RDM ('a') and moderate SDM ('b').

These results suggest that, in RYL soil, the CSC/ZS-5 treatment is the most effective for grain production, while CSC/ZS-3 promotes better root development. Treatments with Zn sulfate (ZnS) showed balanced performance in all parameters. As mentioned in other studies, Zn bioavailability can improve crop yield, especially when using biochar-based fertilizers (Sánchez-Rodríguez et al., 2021; Kleber et al., 2021).

In DRL soil, similar trends were observed, although the performance of treatments varied. The CSC/ZS-3 treatment showed a high grain yield ('a') along with significant RDM and SDM ('a' and 'b', respectively). The CSC/ZS-5 treatment also produced high grain yields ('a'), with slightly lower RDM ('b') and SDM ('c') than CSC/ZS-3. The CSS/ZS-3 treatment exhibited lower grain yield ('b') and moderate RDM and SDM ('c' and 'e', respectively). The ZnS treatment produced a moderate grain yield ('b') and maintained balanced RDM and SDM ('a' and 'b'). As with RYL soil, the NO treatment showed the lowest grain yield ('c') but relatively high RDM ('b') and moderate SDM ('d').

These results indicate that in DRL soil, both CSC/ZS-3 and CSC/ZS-5 are the most effective treatments for increasing grain yield, with CSC/ZS-3 contributing more to root and shoot biomass. These observations align with the findings of studies on biochar's role in nutrient retention and crop yield improvement in soils with varying textures and organic matter content (Carneiro et al., 2022).

Comparing the two soil types, it is evident that RYL soil benefits more from treatments doped with Zn oxide (ZnO), which resulted in higher grain and SDM production. In contrast, DRL soil, with its higher clay and organic matter content, favors Zn sulfate (ZnS)-doped treatments, such as CSC/ZS-3 and CSC/ZS-5, which offer a more balanced nutrient supply.

These findings are consistent with the hypothesis that Zn bioavailability and uptake can vary depending on the soil type and the form of Zn applied (Capo et al., 2024; Morais et al., 2021).

Mechanistically, the higher efficiency of ZnO-doped treatments in RYL soil may be attributed to better Zn availability and faster nutrient uptake by plants, as observed in other studies (Wu et al., 2018). The sandy texture of RYL soil facilitates quicker nutrient leaching, making treatments that offer sustained nutrient release, such as CSC/ZS-5, more effective. Conversely, the higher organic matter and clay content in DRL soil likely retains nutrients better, which explains the effectiveness of CSC/ZS-3 and CSC/ZS-5 due to their balanced Zn supply.

These results highlight the importance of tailoring biochar treatments to specific soil types to optimize maize yield and biomass production. This is further supported by other studies that emphasize the role of biochar in enhancing soil fertility and nutrient availability, especially in tropical soils (Kalbarczyk et al., 2023).

In conclusion, for RYL soil, the CSC/ZS-5 treatment is optimal for grain production due to its significantly higher grain yield. For DRL soil, the CSC/ZS-3 treatment is optimal for both grain yield and overall biomass. These results underscore the importance of selecting the appropriate Zn-doped biochar treatment based on soil type to maximize agricultural productivity and sustainability. Future studies should explore the long-term impacts of these treatments on soil health, crop yield, and environmental sustainability, as recommended by other researchers (Carneiro et al., 2022).

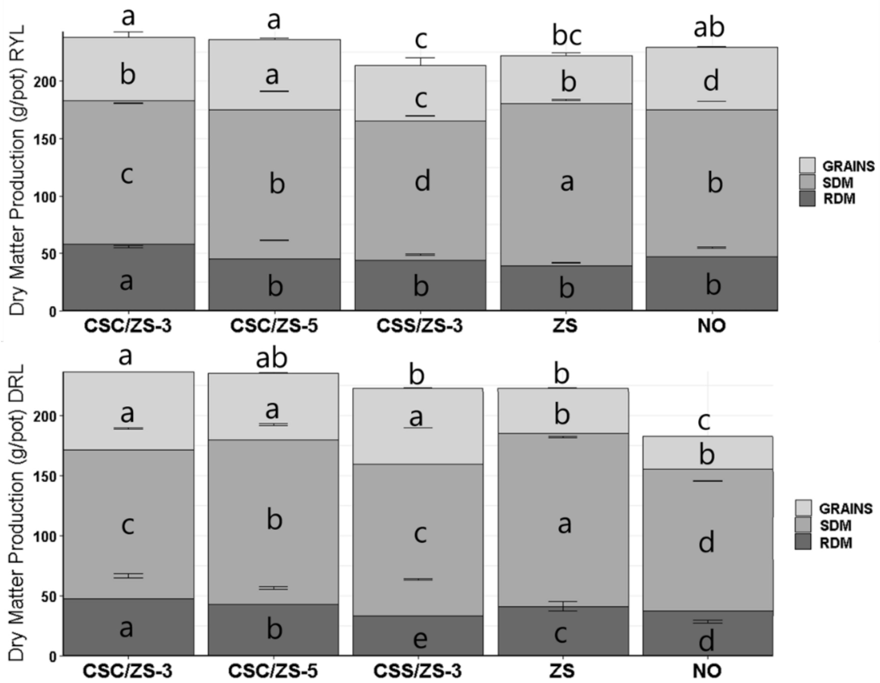

Figure 17. Impact of treatments on the production of grains, root dry matter (RDM), and shoot dry matter (SDM) in maize.

In RYL soil, the Zn concentration in the soil solution varied significantly across treatments and time points. On day 1, the CSS/ZS-3 treatment exhibited the highest Zn concentration, peaking at 1.4 mg L^{-1} ('a'), but this value decreased significantly by day 7 and day 15 to less than 0.5 mg L^{-1} ('b'). The CSC/ZS-3 treatment showed a moderate Zn concentration on day 1 (0.5 mg L^{-1}, 'ab') and remained steady across the period, reaching 0.7 mg L^{-1} by day 15. The CSC/ZS-5 treatment maintained a stable Zn concentration, ranging between 0.4 mg L^{-1} and 0.5 mg L^{-1}, indicating a more consistent release of Zn over time ('ab'). The ZnS treatment also showed a steady increase in Zn concentration, starting at 0.5 mg L^{-1} on day 1 and reaching 0.8 mg L^{-1} by day 15 ('a'). The control (NZ) consistently exhibited the lowest Zn concentrations at all time points ('b').

In DRL soil, the Zn concentration followed a similar pattern but with different magnitudes. On day 1, the CSS/ZS-3 treatment resulted in a lower Zn concentration (0.4 mg

L^{-1}, 'b'), but it increased significantly by day 15 to 1.2 mg L^{-1} ('a'). The CSC/ZS-3 treatment showed moderate Zn concentrations across all time points, starting at 0.4 mg L^{-1} on day 1 and increasing slightly by day 15. The CSC/ZS-5 treatment remained stable throughout the experiment, with Zn concentrations similar to CSC/ZS-3. The ZnS treatment displayed the highest Zn concentration by day 15 (1.5 mg L^{-1}, 'a'), indicating its strong slow-release properties in the soil. The control (NZ) consistently exhibited the lowest Zn concentrations ('c').

These results suggest that in RYL soil, the CSS/ZS-3 treatment provided the highest Zn release initially, but its effect diminished quickly over time. The ZnS treatment, with its steady release pattern, demonstrated the best overall performance in maintaining Zn availability in sandy soils with low organic matter. In DRL soil, CSS/ZS-3 and ZnS treatments were the most effective by day 15, indicating strong Zn retention and availability in soils with higher clay content. This confirms the potential of Zn-doped biochar to enhance nutrient management, improving Zn availability over time and under different soil conditions (Lehmann and Joseph, 2024; Morais et al., 2021).

Zinc Concentration in Plant Tissue

The Zn concentration in plant shoots reflected the availability of Zn in the soil solution. In RYL soil, the CSS/ZS-3 treatment led to the highest Zn concentration in plant tissue, particularly on day 7, coinciding with the high Zn levels observed in the soil solution on day 1. The CSC/ZS-3 and ZnS treatments also resulted in elevated Zn concentrations in the shoots, particularly by day 15, reflecting their consistent Zn release into the soil. The control (NZ) exhibited the lowest Zn concentration in plant tissues, confirming the limited Zn availability without treatment.

In DRL soil, the Zn concentration in plant shoots was highest in the CSS/ZS-3 and ZnS treatments by day 15, corresponding with the increased Zn availability in the soil solution at this time point. The CSC/ZS-3 treatment also showed moderate Zn accumulation in plant tissues, while the control (NZ) consistently had the lowest Zn concentration. This demonstrates the efficacy of biochar treatments in enhancing Zn uptake in plants, aligning with findings from other studies that highlight the benefits of biochar in increasing Zn bioavailability and plant nutrition (Morais et al., 2022; Sánchez-Rodríguez et al., 2021).

Biomass Production and Grain Yield

When evaluating biomass production and grain yield, the treatments showed results consistent with the Zn availability patterns in the soil solution and plant tissues. In RYL soil, the CSC/ZS-5 treatment resulted in the highest grain yield and shoot biomass, indicating that the steady Zn release provided by this treatment supported sustained plant growth. The CSS/ZS-3 treatment, despite its high initial Zn release, resulted in lower biomass and grain production, likely due to the rapid depletion of available Zn. The ZnS treatment showed a moderate performance in terms of biomass production and grain yield, reflecting its balanced Zn release. In DRL soil, the CSC/ZS-3 treatment resulted in the highest biomass production and grain yield, consistent with its effectiveness in providing steady Zn availability and promoting overall plant growth. The CSS/ZS-3 and ZnS treatments also performed well, particularly in terms of biomass production, as Zn availability peaked on day 15. The control (NZ) consistently showed the lowest biomass and grain yield, confirming the importance of Zn supplementation for optimal crop performance.

In conclusion, the results underscore the necessity of tailoring biochar treatments to specific soil types to optimize Zn availability and improve crop productivity. In RYL soil, the CSC/ZS-5 treatment was most effective in promoting grain production, while in DRL soil, the CSC/ZS-3 treatment yielded the best results for both biomass and grain yield. These findings align with other studies that emphasize the role of biochar and Zn-based fertilizers in improving soil properties, nutrient availability, and crop yields (Houben et al., 2013; Khaokaew et al., 2012; Morais et al., 2022). The integration of biochar with Zn-based fertilizers offers a promising strategy for enhancing sustainable agricultural practices and soil health (Wu et al., 2018).

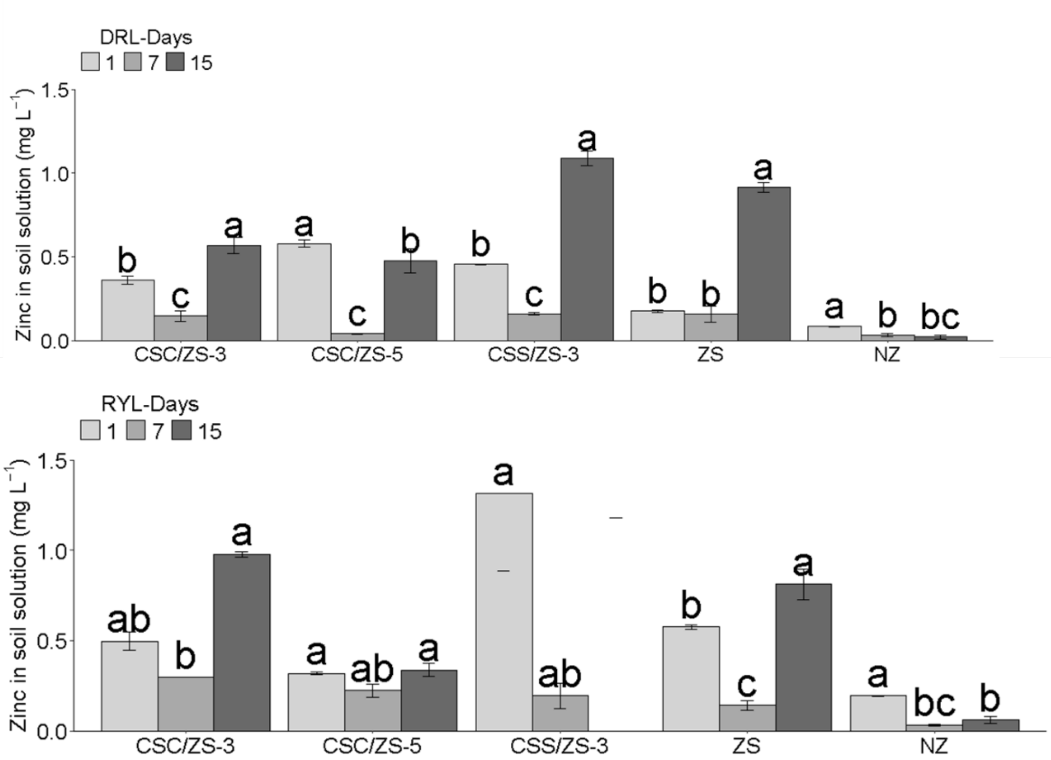

Figure 18. Zinc in soil solution across treatments and time points (days 1, 7, and 15) in RYL and DRL soils. CSC/ZS-3: Shrimp shell biochar with Zn sulfate at 300°C; CSC/ZS-5: Shrimp shell biochar with Zn sulfate at 550°C; CSS/ZS-3: Sewage sludge biochar with Zn sulfate at 300°C and ZS: Zinc sulfate treatment.

Figure 19 shows the Zn concentration in the shoot of maize plants and the residual Zn content in the soil after harvest, across different treatments for both DRL and RYL soils.

In DRL soil, the treatments did not show significant statistical differences ($p > 0.05$) in Zn concentration in the shoot dry matter. The CSC/ZS-3 treatment resulted in moderate Zn content, and the CSC/ZS-5 treatment showed a similar Zn concentration, contrary to what was previously described. The CSS/ZS-3 and ZnS treatments resulted in the highest Zn concentrations, although not statistically different from CSC/ZS-3. The control (NZ) treatment, as expected, showed the lowest Zn concentration in the plant shoot, indicating minimal Zn uptake from the untreated soil, in line with what was observed in other studies on untreated soils (Sánchez-Rodríguez et al., 2021; Wu et al., 2018).

In RYL soil, the results followed a similar trend. The CSS/ZS-3 and ZnS treatments resulted in the highest Zn content in the maize shoot, but again, there were no statistically significant differences between these treatments ($p > 0.05$). The CSC/ZS-3 and CSC/ZS-5 treatments also had similar Zn concentrations, which were lower than CSS/ZS-3 and ZnS but still higher than the control (NZ), which displayed the lowest Zn content. The similarities between the treatments show that Zn availability was sufficient across most treatments, but the higher Zn concentration in CSS/ZS-3 reflects its higher release capacity, consistent with previous research on Zn-doped biochar (Houben et al., 2013; Morais et al., 2021).

The second set of graphs in Figure 19 illustrates the residual Zn content in the soil after maize cultivation. In DRL soil, the CSS/ZS-3 treatment left the highest residual Zn levels in the soil, followed by the ZnS treatment, though there was no significant statistical difference between them ($p > 0.05$). The CSC/ZS-5 and CSC/ZS-3 treatments also left moderate levels of residual Zn, with the control (NZ) showing the lowest residual Zn content.

In RYL soil, a similar pattern was observed. The CSS/ZS-3 and ZnS treatments resulted in the highest residual Zn content, but again, no significant statistical differences were detected between these treatments and the other biochar treatments. The CSC/ZS-5 treatment left higher residual Zn than CSC/ZS-3, but these levels were not significantly different. The control (NZ) had the lowest residual Zn content in both soils, indicating minimal retention of Zn in untreated soils, as has been reported in studies with low-input soil systems (Lehmann and Joseph, 2024; Morais et al., 2022).

The results presented in Figure 19 indicate that there were no significant differences between most of the treatments in terms of Zn concentration in plant tissues and residual Zn in the soil ($p > 0.05$). While CSS/ZS-3 and ZnS treatments showed the highest Zn content in both maize shoots and residual soil Zn, they were statistically comparable to the other treatments, suggesting that all Zn-doped biochar treatments effectively supplied Zn to the plants and contributed to residual Zn in the soil. The control (NZ) treatment consistently resulted in the lowest Zn levels, confirming the limited availability and uptake of Zn in untreated soils. These findings align with other research demonstrating the potential of Zn-doped biochar to enhance Zn availability in agricultural systems, but also highlight the need for further studies on long-term Zn retention and availability (Houben et al., 2013; Morais et al., 2021; Sánchez-Rodríguez et al., 2021).

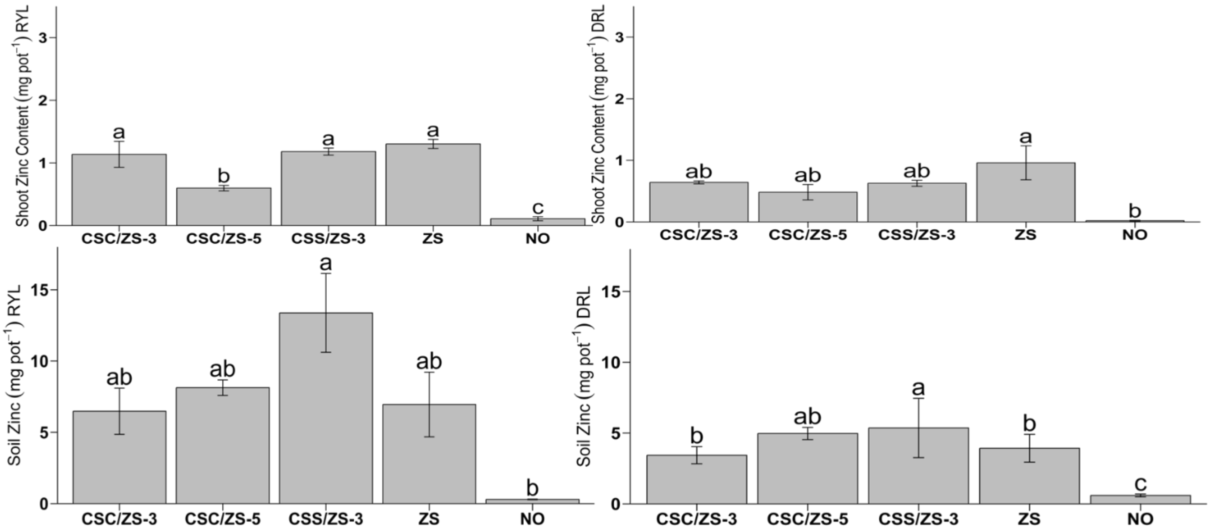

Figure 19. Zinc concentration in maize shoot dry matter (mg pot^{-1}) and the residual zinc levels in the soil (mg pot^{-1}) after harvest, across different treatments.

The control (NO) consistently showed the lowest Zn content in dry matter and residual Zn, indicating low natural Zn availability without treatment. The CSS/ZS-3 and ZS treatments were the most effective for enhancing Zn content in corn and maintaining soil Zn levels across both soil types. This is aligned with studies on the efficacy of Zn-based organomineral fertilizers in improving Zn availability and crop yield (Morais et al., 2022, 2021) and biochar-based micronutrient fertilizers, which demonstrated increased efficiency in highly weathered soils (Carneiro et al., 2022).

4. Conclusion

This study underscores the critical role of pyrolysis in the production of Zn-biochar composites, significantly enhancing zinc (Zn) availability and uptake in maize, particularly in highly weathered soils. The agronomic tests revealed that CSS/ZnS-3 and ZnS treatments were most effective in increasing Zn concentration in maize dry matter and maintaining high residual Zn levels in both RYL and DRL soils. Notably, the CSC/ZnS-5 composite demonstrated superior performance in maximizing maize grain yield in RYL soil, while CSC/ZnS-3 was most effective in DRL soil. These results suggest that the choice of Zn source and pyrolysis temperature should be tailored to the specific soil type to optimize grain production. The Zn release kinetics, particularly from ZnO-doped composites, further highlight the importance of selecting the appropriate Zn source for sustained Zn availability.

The findings of this study strongly advocate for the strategic use of biochar composites doped with Zn, customized to the soil type and production goals, to enhance crop yield and ensure sustainable agricultural practices. Future research should prioritize identifying the specific attributes of Zn-biochar that most effectively contribute to grain production and explore the broader agronomic implications across various crops, soil types, and environmental conditions. Additionally, long-term studies are essential to assess the sustainability, cost-effectiveness, and environmental impact of these treatments, ensuring that Zn-biochar composites not only improve Zn use efficiency but also contribute to maintaining soil health and achieving higher crop yields in the long run.

Funding

This research was funded by the Coordination for the Improvement of Higher Education Personnel (CAPES), CAPES-PROEX/AUXPE 593/2018 Scholarship, the National Council for Scientific and Technological Development (CNPq) 311212/2023-9 e 307447/2019-7, and the Minas Gerais State Research Support Foundation (FAPEMIG).

Acknowledgments

This work was financially supported by the CAPES agencies (CAPES-PROEX/AUXPE 593/2018), CNPq and FAPEMIG, for the funding and research grants granted. The Federal University of Lavras (UFLA) is a provider of opportunities.

5. References

Abbasi, M., Rizvi, O.S., Hussain, S.Z., Jilani, A., Osra, F. a, Kajjumba, G.W., Bhatnagar, A., Khan, E., Abbas, T., 2024. Nano-zerovalent copper biochar composite for treating selenium oxyanions in water: synthesis, evaluation, removal mechanism, density functional theory, and molecular dynamics simulations. Chemical Engineering Journal 485, 149954. https://doi.org/https://doi.org/10.1016/j.cej.2024.149954

Abdullah, R., Ishak, C.F., Osman, N., Halim, N.S.A., Panhwar, Q.A., 2021. Determining the characteristics and potential of plantbased biochars to reduce copper uptake in maize. Bragantia.

Agricolae, 2022. Pacote Agricolae- CRAN - Embalagem Agrícola [WWW Document]. 2022. URL https://cran.r-project.org/web/packages/agricolae/index.html (accessed 8.14.23).

Akaike, H., 1979. A Bayesian extension of the minimum AIC procedure of autoregressive model fitting. Biometrika 66, 237–242. https://doi.org/10.1093/BIOMET/66.2.237

Akhil, D., Lakshmi, D., Kartik, A., Vo, D.-V.N., Arun, J., Gopinath, K.P., 2021. Production, characterization, activation and environmental applications of engineered biochar: a review. Environmental Chemistry Letters 19, 2261–2297. https://doi.org/10.1007/s10311-020-01167-7

Aleosfoor, A., Rahimpour, M.R., 2024. Highly dispersed copper on biochar carbon as a promising catalyst for reverse water gas shift reaction. Journal of the Energy Institute 115, 101680. https://doi.org/https://doi.org/10.1016/j.joei.2024.101680

Almutairi, A.A., Ahmad, M., Rafique, M.I., Al-Wabel, M.I., 2023. Variations in composition and stability of biochars derived from different feedstock types at varying pyrolysis temperature. Journal of the Saudi Society of Agricultural Sciences 22, 25–34. https://doi.org/10.1016/J.JSSAS.2022.05.005

Altıkat, Alperay, Alma, M.H., Altıkat, Aysun, Bilgili, M.E., Altıkat, S., 2024. A Comprehensive Study of Biochar Yield and Quality Concerning Pyrolysis Conditions: A Multifaceted Approach. Sustainability. https://doi.org/10.3390/su16020937

Alva, A.K., Graham, J.H., Anderson, C.A., 1995. Soil pH and copper effects on young 'Hamlin'orange trees. Soil Science Society of America Journal 59, 481–487.

ASTM International, 1984. Standard Test Method for Chemical Analysis of Wood Charcoal - Designation: D 1762 – 84 (Reapproved 2001). Annual Book of ASTM Standards 84, 292–293. https://doi.org/10.1520/D1762-84R07.2

Atchaya, S., Meena Devi, J., 2024. Experimental Investigation on Structural, Optical, Electrical and Magnetic Properties of Copper Oxide Nanoparticles. Proceedings of the National Academy of Sciences, India Section A: Physical Sciences 94, 153–160. https://doi.org/10.1007/s40010-023-00855-7

Ateş, A., Aydemir, B., Emre, K., 2023a. Investigation of physicochemical and biological properties of boron - doped biochar. Biomass Conversion and Biorefinery. https://doi.org/10.1007/s13399-023-04567-1

Ateş, A., Aydemir, B., Öksüz, K.E., 2023b. Investigation of physicochemical and biological properties of boron-doped biochar. Biomass Conversion and Biorefinery. https://doi.org/10.1007/s13399-023-04567-1

Balwant Singh , Marta Camps Arbestain, J.L., 2017. Biochar: A Guide to Analytical Methods.

Barrow, N.J., Hartemink, A.E., 2023. The effects of pH on nutrient availability depend on both soils and plants. Plant and Soil 487, 21–37. https://doi.org/10.1007/s11104-023-05960-5

Baty, F., Charles, S., Flandrois, J., Delignette-Muller, M.-L., 2015a. The R package nlstools: a toolbox for nonlinear regression. Journal of Statistical Software 66, 1–21.

Baty, F., Ritz, C., Charles, S., Brutsche, M., Flandrois, J.P., Delignette-Muller, M.L., 2015b. A Toolbox for Nonlinear Regression in R: The Package nlstools. Journal of Statistical Software 66, 1–21. https://doi.org/10.18637/JSS.V066.I05

Bhatnagar, A., Sillanpää, M., 2009. Applications of chitin-and chitosan-derivatives for the detoxification of water and wastewater—a short review. Advances in colloid and Interface science 152, 26–38.

Bhupenchandra, I., Basumatary, A., Dutta, S., Das, A., Choudhary, A.K., Lal, R., Dhanachandra Sharma, A., Sen, A., Prabhabati, Y., Ranjan Sahoo, M., 2024. Repercussions of fertilization with boron and enriched organic manure on soil chemical characteristics, boron and phosphorus fractions, and French bean productivity in an acidic Inceptisol of eastern Himalaya. Scientia Horticulturae 324, 304–4238. https://doi.org/10.1016/j.scienta.2023.112589

Bhupenchandra, I., Basumatary, A., Dutta, S., Singh, L.K., Datta, N., 2020. Impact of boron fertilization on boron fractions at different crop growth stages in cauliflower_cowpea_okra sequence in an inceptisols of North East India. Journal of Plant Nutrition 43, 1175–1188. https://doi.org/10.1080/01904167.2020.1724300

Bo, X., Guo, L., 2013. Carbonos mesoporosos dopados com boro ordenados como eletrocatalisadores isentos de metal para a reação de redução de oxigênio em solução alcalina. Physical Chemistry Chemical Physics 15, 2459–2465. https://doi.org/10.1039/c2cp43541a

Brasil, 2016. Instrução Normativa MAPA Nº 46 DE 22/11/2016 - Federal - LegisWeb [WWW Document]. URL https://www.legisweb.com.br/legislacao/?id=332894 (accessed 6.27.24).

Brasil, M. da A.P. e A., 2014. Manual De Métodos Analíticos oficiais para fertilizantes e corretivos.

Capo, L., Battisti, M., Blandino, M., 2024. The role of zinc fertilization and its interaction with nitrogen and phosphorus starter fertilization on early maize development and grain yield. Field Crops Research 307, 109245. https://doi.org/https://doi.org/10.1016/j.fcr.2023.109245

Carmo, D.L. do, Silva, C.A., Lima, J.M. de, Pinheiro, G.L., 2016. Electrical conductivity and chemical composition of soil solution: comparison of solution samplers in tropical soils. Revista brasileira de Ciência do Solo 40.

Carneiro, J.S. da S., Leite, D.A. da C., Castro, G.M. de, Franca, J.R., Botelho, L., Soares, J.R., Oliveira, J.E. de, Melo, L.C.A., 2022. Biochar-graphene oxide composite is efficient to adsorb and deliver copper and zinc in tropical soil. Journal of Cleaner Production 360, 132170. https://doi.org/https://doi.org/10.1016/j.jclepro.2022.132170

Carneiro, J.S. da S., Ribeiro, I.C.A., Nardis, B.O., Barbosa, C.F., Lustosa Filho, J.F., Melo, L.C.A., 2021. Long-term effect of biochar-based fertilizers application in tropical soil: Agronomic efficiency and phosphorus availability. Science of the Total Environment 760, 143955. https://doi.org/10.1016/j.scitotenv.2020.143955

Chaves Fernandes, B.C., Ferreira Mendes, K., Dias Júnior, A.F., da Silva Caldeira, V.P., da Silva Teófilo, T.M., Severo Silva, T., Mendonça, V., de Freitas Souza, M., Valadão Silva, D., 2020. Impact of Pyrolysis Temperature on the Properties of Eucalyptus Wood-Derived Biochar. Materials. https://doi.org/10.3390/ma13245841

Chen, C., Zhou, L.L., Huang, Y.N., Wang, W.K., Xu, J., 2022. Boron regulates catalytic sites of biochar to enhance the formation of surface-confined complex for improved peroxydisulfate activation. Chemosphere 301, 134690. https://doi.org/10.1016/J.CHEMOSPHERE.2022.134690

Chen, H., Gao, Y., El-Naggar, A., Niazi, N.K., Sun, C., Shaheen, S.M., Hou, D., Yang, X., Tang, Z., Liu, Z., Hou, H., Chen, W., Rinklebe, J., Pohořelý, M., Wang, H., 2022. Enhanced sorption of trivalent antimony by chitosan-loaded biochar in aqueous solutions: Characterization, performance and mechanisms. Journal of Hazardous Materials 425, 127971. https://doi.org/https://doi.org/10.1016/j.jhazmat.2021.127971

Chen, J., Zhu, J., Wang, N., Feng, J., Yan, W., 2019. Hydrophilic polythiophene/SiO2 composite for adsorption engineering: Green synthesis in aqueous medium and its synergistic and specific adsorption for heavy metals from wastewater. Chemical Engineering Journal 360, 1486–1497. https://doi.org/https://doi.org/10.1016/j.cej.2018.10.228

Chen, Z., Xu, Q., Yan, L., Wang, Y., Sun, A., Liu, Q., 2024. Fractionation of stable boron isotopes in alfisols: Application of a novel tool for tracing boron behavior in two soil profiles. Geoderma 441, 116766. https://doi.org/10.1016/J.GEODERMA.2023.116766

Cho, D.-W., Kim, S., Tsang, Y.F., Song, H., 2019. Preparation of nitrogen-doped Cu-biochar and its application into catalytic reduction of p-nitrophenol. Environmental Geochemistry and Health 41, 1729–1737. https://doi.org/10.1007/s10653-017-9966-x

Clough, T.J., Condron, L.M., Kammann, C., Müller, C., 2013. A Review of Biochar and Soil Nitrogen Dynamics. Agronomy. https://doi.org/10.3390/agronomy3020275

Conte, P., Bertani, R., Sgarbossa, P., Bambina, P., Schmidt, H.-P., Raga, R., Lo Papa, G., Chillura Martino, D.F., Lo Meo, P., 2021. Recent Developments in Understanding Biochar's Physical–Chemistry. Agronomy. https://doi.org/10.3390/agronomy11040615

D1762-84, A., 2013. Standard test method for chemical analysis of wood charcoal.

Dai, L., Zhu, W., He, L., Tan, F., Zhu, N., Zhou, Q., He, M., Hu, G., 2018. Calcium-rich biochar from crab shell: an unexpected super adsorbent for dye removal. Bioresource technology 267, 510–516.

Damasceno, A.S. da S., Boechat, C.L., Souza, H.A. de, Capristo-Silva, G.F., Mendes, W. de S., Teodoro, P.E., Morais, P.G.C., Oliveira, R.I. de, Della-Silva, J.L., Souza, I.A.M. de, Silva Junior, C.A. da, 2023. Nutritional monitoring of boron in Eucalyptus spp. in the Brazilian cerrado by multispectral bands of the MSI sensor (Sentinel-2). Remote Sensing Applications: Society and Environment 29, 100913. https://doi.org/10.1016/J.RSASE.2022.100913

Das, S.K., Ghosh, G.K., Avasthe, R.K., Sinha, K., 2021. Compositional heterogeneity of different biochar: Effect of pyrolysis temperature and feedstocks. Journal of

Environmental Management 278. https://doi.org/10.1016/j.jenvman.2020.111501

de Mello Prado, R., 2021. Boron BT - Mineral nutrition of tropical plants, in: de Mello Prado, R. (Ed.), . Springer International Publishing, Cham, pp. 175–190. https://doi.org/10.1007/978-3-030-71262-4_10

de Mendiburu, F., de Mendiburu, M.F., 2019. Package 'agricolae.' R Package, version 1, 1143–1149.

de Oliveira Paiva, I., de Morais, E.G., Jindo, K., Silva, C.A., 2024. Biochar N Content, Pools and Aromaticity as Affected by Feedstock and Pyrolysis Temperature. Waste and Biomass Valorization. https://doi.org/10.1007/s12649-023-02415-x

Deng, J., Liu, Y., Liu, S., Zeng, G., Tan, X., Huang, B., Tang, X., Wang, S., Hua, Q., Yan, Z., 2017. Competitive adsorption of Pb(II), Cd(II) and Cu(II) onto chitosan-pyromellitic dianhydride modified biochar. Journal of Colloid and Interface Science 506, 355–364. https://doi.org/https://doi.org/10.1016/j.jcis.2017.07.069

Di Palma, L., Mecozzi, R., 2007. Heavy metals mobilization from harbour sediments using EDTA and citric acid as chelating agents. Journal of Hazardous Materials 147, 768–775. https://doi.org/https://doi.org/10.1016/j.jhazmat.2007.01.072

Ding, Y., Liu, Y., Liu, S., Huang, X., Li, Z., Tan, X., Zeng, G., Zhou, L., 2017. Potential Benefits of Biochar in Agricultural Soils: A Review. Pedosphere 27, 645–661. https://doi.org/10.1016/S1002-0160(17)60375-8

do Amaral Leite, A., de Souza Cardoso, A.A., de Almeida Leite, R., Barrera, A.M.V., Queiroz, D.D.L., Viana, T.C., de Oliveira-Longatti, S.M., Silva, C.A., de Souza Moreira, F.M., Lehmann, J., Melo, L.C.A., 2024. Phosphate-solubilizing bacteria increase maize phosphorus uptake from magnesium-enriched poultry manure biochar. Biology and Fertility of Soils 60, 421–436. https://doi.org/10.1007/s00374-024-01808-x

do Carmo, D.L., Silva, C.A., de Lima, J.M., Pinheiro, G.L., 2016. Electrical Conductivity and Chemical Composition of Soil Solution: Comparison of Solution Samplers in Tropical Soils. Revista Brasileira de Ciência do Solo 40. https://doi.org/10.1590/18069657RBCS20140795

Domingues, Rimena R., Trugilho, P.F., Silva, C.A., De Melo, I.C.N.A., Melo, L.C.A., Magriotis, Z.M., Sánchez-Monedero, M.A., 2017. Properties of biochar derived from wood and high-nutrient biomasses with the aim of agronomic and environmental benefits. PLoS ONE 12, 1–19. https://doi.org/10.1371/journal.pone.0176884

Domingues, Rimena R, Trugilho, P.F., Silva, C.A., Melo, I.C.N.A. de, Melo, L.C.A., Magriotis, Z.M., Sánchez-Monedero, M.A., 2017. Properties of biochar derived from wood and high-nutrient biomasses with the aim of agronomic and environmental benefits. PLOS ONE 12, e0176884.

Dong, X., Wang, C., Li, H., Wu, M., Liao, S., Zhang, D., Pan, B., 2014. The sorption of heavy metals on thermally treated sediments with high organic matter content. Bioresource technology 160, 123–128.

Du, Y., Dai, M., Naz, I., Hao, X., Wei, X., Rong, R., Peng, C., Ali, I., 2021. Carbothermal reduction synthesis of zero-valent iron and its application as a persulfate activator for ciprofloxacin degradation. Separation and Purification Technology 275, 119201. https://doi.org/10.1016/j.seppur.2021.119201

Elsherpiny, mohamed atef, 2023. Effect of Organic Amendments and Synthetic Substances on Copper Availability, Absorption, and Wheat Productivity. Egyptian Journal of Soil

Science 63, 429–442. https://doi.org/10.21608/ejss.2023.220516.1614

Erenstein, O., Jaleta, M., Sonder, K., Mottaleb, K., Prasanna, B.M., 2022. Global maize production, consumption and trade: trends and R&D implications. Food Security 14, 1295–1319. https://doi.org/10.1007/s12571-022-01288-7

Extract, 2020. Extract and Visualize the Results of Multivariate Data Analyses [R package factoextra version 1.0.7].

Factoextra, 2022. R: The R Project for Statistical Computing [WWW Document]. URL https://www.r-project.org/ (accessed 8.14.23).

Fan, J., Li, Yan, Yu, H., Li, Yuxuan, Yuan, Q., Xiao, H., Li, F., Pan, B., 2020. Using sewage sludge with high ash content for biochar production and Cu(II) sorption. Science of The Total Environment 713, 136663. https://doi.org/https://doi.org/10.1016/j.scitotenv.2020.136663

Faria, W.M., Figueiredo, C.C. de, Coser, T.R., Vale, A.T., Schneider, B.G., 2018. Is sewage sludge biochar capable of replacing inorganic fertilizers for corn production? Evidence from a two-year field experiment. Archives of Agronomy and Soil Science 64, 505–519. https://doi.org/10.1080/03650340.2017.1360488

Ferreira, G.A., Hippler, F.W.R., Prado, L.A. do. S., Rima, J.A.H., Boaretto, R.M., Quaggio, J.A., Façanha, A.R., Mattos-Jr, D., 2021. Boron modulates the plasma membrane H+-ATPase activity affecting nutrient uptake of Citrus trees. Annals of Applied Biology 178, 293–303. https://doi.org/10.1111/AAB.12630

Friedrich, N., Brandimarte, P., Li, J., Saito, S., Yamaguchi, S., Pozo, I., Peña, D., Frederiksen, T., Garcia-Lekue, A., Sánchez-Portal, D., Pascual, J.I., 2020. Magnetism of Topological

Boundary States Induced by Boron Substitution in Graphene Nanoribbons. PHYSICAL REVIEW LETTERS 125, 146801. https://doi.org/10.1103/PhysRevLett.125.146801

Fuentez-Torres, M.O., Ortiz-Chi, F., Espinosa-González, C.G., Aleman, M., Cervantes-Uribe, A., Torres-Torres, J.G., Kesarla, M.K., Collins-Martínez, V., Godavarthi, S., Martínez-Gómez, L., 2021. Facile Synthesis of Zn Doped g-C3N4 for Enhanced Visible Light Driven Photocatalytic Hydrogen Production. Topics in Catalysis 64, 65–72. https://doi.org/10.1007/s11244-020-01298-9

Gao, Y., Wang, Q., Ji, G., Li, A., Niu, J., 2021. Doping strategy, properties and application of heteroatom-doped ordered mesoporous carbon. RSC Advances 11, 5361–5383. https://doi.org/10.1039/D0RA08993A

Ghorbani, M., Amirahmadi, E., Neugschwandtner, R.W., Konvalina, P., Kopecký, M., Moudrý, J., Perná, K., Murindangabo, Y.T., 2022a. The Impact of Pyrolysis Temperature on Biochar Properties and Its Effects on Soil Hydrological Properties. Sustainability. https://doi.org/10.3390/su142214722

Ghorbani, M., Konvalina, P., Walkiewicz, A., Neugschwandtner, R.W., Kopecký, M., Zamanian, K., Chen, W.-H., Bucur, D., 2022b. Feasibility of Biochar Derived from Sewage Sludge to Promote Sustainable Agriculture and Mitigate GHG Emissions—A Review. International Journal of Environmental Research and Public Health. https://doi.org/10.3390/ijerph191912983

GRANULOMÉTRICA, B.A., 2014. Manual de métodos analíticos oficiais para fertilizantes minerais, orgânicos, organominerais e corretivos.

Hailegnaw, N.S., Mercl, F., Pračke, K., Praus, L., Száková, J., Tlustoš, P., 2020. The Role of Biochar and Soil Properties in Determining the Available Content of Al, Cu, Zn, Mn, and Cd in Soil. Agronomy. https://doi.org/10.3390/agronomy10060885

Hansson, K., Laclau, J.P., Saint-André, L., Mareschal, L., van der Heijden, G., Nys, C., Nicolas, M., Ranger, J., Legout, A., 2020. Fertilidade química dos ecossistemas florestais. Parte 1: Análises químicas comuns do solo foram preditores fracos da produtividade do povoamento em uma ampla gama de solos florestais ácidos. Ecologia e manejo florestal 461, 117843. https://doi.org/10.1016/j.foreco.2019.117843

Hao, W., Luo, P., Wu, Z., Mi, Y., Gao, Z., 2021. The effect of biomass pyrolysis temperature on the performance of biochar-fed molten hydroxide direct carbon fuel cells. Biomass and Bioenergy 150, 106122. https://doi.org/10.1016/j.biombioe.2021.106122

Haque, A., Al-Balushi, R.A., Raithby, P.R., Khan, M.S., 2020. Recent Advances in π-Conjugated N^C-Chelate Organoboron Materials. Molecules. https://doi.org/10.3390/molecules25112645

Heckler, G.S., da Costa, R.C., Fransozo, A., Rosso, S., Munehisa Shimizu, R., 2014. Long-term Patterns of Spatial and Temporal Distribution in the Seabob Shrimp Xiphopenaeus kroyeri (Decapoda: Penaeidae) Population in Southeastern Brazil. Journal of Crustacean Biology 34, 326–333. https://doi.org/10.1163/1937240X-00002231

Hodecker, B.E.R., De Barros, N.F., Da Silva, I.R., Diola, V., Sarkis, J.E.S., Loureiro, M.E., 2014. Boron delays dehydration and stimulates root growth in Eucalyptus urophylla (Blake, S.T.) under osmotic stress. Plant and Soil 384, 185–199. https://doi.org/10.1007/S11104-014-2196-4/FIGURES/7

Hortin, J.M., Anderson, A.J., Britt, D.W., Jacobson, A.R., McLean, J.E., 2020. Copper oxide nanoparticle dissolution at alkaline pH is controlled by dissolved organic matter: influence of soil-derived organic matter, wheat, bacteria, and nanoparticle coating.

Environmental Science: Nano 7, 2618–2631.

Houben, D., Evrard, L., Sonnet, P., 2013. Mobility, bioavailability and pH-dependent leaching of cadmium, zinc and lead in a contaminated soil amended with biochar. Chemosphere 92, 1450–1457. https://doi.org/https://doi.org/10.1016/j.chemosphere.2013.03.055

Hu, Z., Wei, L., 2023. Review on Characterization of Biochar Derived from Biomass Pyrolysis via Reactive Molecular Dynamics Simulations. Journal of Composites Science. https://doi.org/10.3390/jcs7090354

Huang, J., Zhu, Y., Bian, H., Song, L., Liu, Y., Lv, Y., Ye, X., Lin, C., Li, X., 2023. Insights into Enhanced Peroxydisulfate Activation with B and Fe Co-Doped Biochar from Bark for the Rapid Degradation of Guaiacol. Molecules. https://doi.org/10.3390/molecules28227591

Huang, Q., Song, S., Chen, Z., Hu, B., Chen, J., Wang, X., 2019. Biochar-based materials and their applications in removal of organic contaminants from wastewater: state-of-the-art review. Biochar 2019 1:1 1, 45–73. https://doi.org/10.1007/S42773-019-00006-5

Husson, F., Josse, J., Le, S., Mazet, J., Husson, M.F., 2016. Package ‘factominer.’ An R package 96, 698.

Ippolito, J.A., Liqiang Cui, ·, Kammann, C., Wrage-Mönnig, N., Estavillo, J.M., Fuertes-Mendizabal, T., Cayuela, M.L., Gilbert Sigua, ·, Novak, J., Spokas, K., Borchard, N., 2020. Feedstock choice, pyrolysis temperature and type influence biochar characteristics: a comprehensive meta-data analysis review 1, 421–438. https://doi.org/10.1007/s42773-020-00067-x

Jalali, Mohsen, Imanifard, A., Jalali, Mahdi, 2023. Heavy metals accumulation in wheat (Triticum aestivum L.) roots and shoots grown in calcareous soils treated with non-spiked and spiked sewage sludge. Environmental Science and Pollution Research 30, 20862–20873.

Jez, E., Pellegrini, E., Contin, M., 2023. Copper bioavailability and leaching in conventional and organic viticulture under environmental stress. Applied Sciences 13, 2595.

Jha, S.K., Mishra, V.K., Damodaran, T., Singh, A.K., Singh, Y.P., Sharma, D.K., 2022. Does conservation tillage on partially reclaimed sodic soil restore land degradation by influencing boron dynamics, bioavailability for plant's uptake and nutritional security? Land Degradation & Development 33, 1260–1268. https://doi.org/10.1002/LDR.4206

Jia, M., Wang, F., Bian, Y., Jin, X., Song, Y., Kengara, F.O., Xu, R., Jiang, X., 2013. Effects of pH and metal ions on oxytetracycline sorption to maize-straw-derived biochar. Bioresource Technology 136, 87–93. https://doi.org/10.1016/j.biortech.2013.02.098

Jin, H., Zhang, D., Yan, Y., Yang, C., Fang, B., Li, X., Shao, Y., Wang, H., Yue, J., Wang, Y., Cheng, H., Shi, Y., Qin, F., 2022. Short-term application of chicken manure under different nitrogen rates alters structure and co-occurrence pattern but not diversity of soil microbial community in wheat field. Frontiers in Microbiology 13.

Jin, J., Li, Y., Zhang, Jianyun, Wu, S., Cao, Y., Liang, P., Zhang, Jin, Wong, M.H., Wang, M., Shan, S., 2016. Influence of pyrolysis temperature on properties and environmental safety of heavy metals in biochars derived from municipal sewage sludge. Journal of hazardous materials 320, 417–426.

Johnston, C.T., 2017. Biochar analysis by Fourier-transform infra-red spectroscopy, in: Singh, B., Camps-Arbestain, M., Lehmann, J. (Eds.), Biochar: A Guide to Analytical Methods.

CRC Press/Taylor and Francis Group, LLC, Boca Raton, pp. 199–213.

Jones, J.B., 2001. Laboratory guide for conducting soil tests and plant analysis. CRC press.

Joseph, S., Cowie, A.L., Van Zwieten, L., Bolan, N., Budai, A., Buss, W., Cayuela, M.L., Graber, E.R., Ippolito, J.A., Kuzyakov, Y., Luo, Y., Ok, Y.S., Palansooriya, K.N., Shepherd, J., Stephens, S., Weng, Z., Lehmann, J., 2021. How biochar works, and when it doesn't: A review of mechanisms controlling soil and plant responses to biochar. GCB Bioenergy 13, 1731–1764. https://doi.org/10.1111/gcbb.12885

Joseph, S., Graber, E.R., Chia, C., Munroe, P., Donne, S., Thomas, T., Nielsen, S., Marjo, C., Rutlidge, H., Pan, G.X., Li, L., Taylor, P., Rawal, A., Hook, J., 2013. Shifting paradigms: development of high-efficiency biochar fertilizers based on nano-structures and soluble components. Carbon Management 4, 323–343. https://doi.org/10.4155/cmt.13.23

Kabiri, P., Motaghian, H., Hosseinpur, A., 2021. Impact of Biochar on Release Kinetics of Pb (II) and Zn (II) in a Calcareous Soil Polluted with Mining Activities. Journal of Soil Science and Plant Nutrition 21, 22–34. https://doi.org/10.1007/s42729-020-00336-5

Kalbarczyk, M., Szcześ, A., Belcarz, A., Kazimierczak, P., May, Z., 2023. Zn-doped Mono- and Biphasic Calcium Phosphate Materials Derived from Agriculture Waste and Their Potential Biomedical Applications: Part I. Materials. https://doi.org/10.3390/ma16051971

Karimi, B., Masson, V., Guilland, C., Leroy, E., Pellegrinelli, S., Giboulot, E., Maron, P.-A., Ranjard, L., 2021. Ecotoxicity of copper input and accumulation for soil biodiversity in vineyards. Environmental Chemistry Letters 19, 2013–2030. https://doi.org/10.1007/s10311-020-01155-x

Kassambara, A., Mundt, F., 2017. Package ‘factoextra.’ Extract and visualize the results of multivariate data analyses 76.

Kayani, Z.N., Umer, M., Riaz, S., Naseem, S., 2015. Characterization of copper oxide nanoparticles fabricated by the sol–gel method. Journal of Electronic Materials 44, 3704–3709.

Khan, A., Harfield, D., Hillen, B., Stenzel, F., Homung, A., 2017. Long-termaging of biochar. https://doi.org/10.13140/RG.2.2.21385.75366

Khan, S., Irshad, S., Mehmood, K., Hasnain, Z., Nawaz, M., Rais, A., Gul, S., Wahid, M.A., Hashem, A., Abd_Allah, E.F., Ibrar, D., 2024. Biochar Production and Characteristics, Its Impacts on Soil Health, Crop Production, and Yield Enhancement: A Review. Plants. https://doi.org/10.3390/plants13020166

Khaokaew, S., Landrot, G., Chaney, R.L., Pandya, K., Sparks, D.L., 2012. Speciation and Release Kinetics of Zinc in Contaminated Paddy Soils. Environmental Science & Technology 46, 3957–3963. https://doi.org/10.1021/es204007t

Kim, S., Kim, U. gi, Ryu, J., Kim, D., Kim, M., Joo, Y.C., Lee, S.Y., 2023. Boron-doped amorphous carbon deposited by DC sputtering for a hardmask: Microstructure and dry etching properties. Applied Surface Science 637, 157895. https://doi.org/10.1016/J.APSUSC.2023.157895

Kiralj, R., Ferreira, M.M.C., 2009. Basic validation procedures for regression models in QSAR and QSPR studies: theory and application. Journal of the Brazilian Chemical Society 20, 770–787. https://doi.org/10.1590/S0103-50532009000400021

Kleber, M., Bourg, I.C., Coward, E.K., Hansel, C.M., Myneni, S.C.B., Nunan, N., 2021.

Dynamic interactions at the mineral–organic matter interface. Nature Reviews Earth & Environment 2, 402–421.

Labanya, R., Srivastava, P.C., Pachauri, S.P., Shukla, A.K., Shrivastava, M., Mukherjee, P., Srivastava, P., 2022. Sorption–desorption of some transition metals, boron and sulphur in a multi-ionic system onto phyto-biochars prepared at two pyrolysis temperatures. Environmental Science: Processes & Impacts 24, 2378–2397. https://doi.org/10.1039/D2EM00212D

Lamichhane, J.R., Osdaghi, E., Behlau, F., Köhl, J., Jones, J.B., Aubertot, J.-N., 2018. Thirteen decades of antimicrobial copper compounds applied in agriculture. A review. Agronomy for Sustainable Development 38, 28. https://doi.org/10.1007/s13593-018-0503-9

Lê, S., Josse, J., Husson, F., 2008a. FactoMineR: An R Package for Multivariate Analysis. Journal of Statistical Software 25, 1–18. https://doi.org/10.18637/JSS.V025.I01

Lê, S., Josse, J., Husson, F., 2008b. FactoMineR: an R package for multivariate analysis. Journal of statistical software 25, 1–18.

Lehmann, J., Joseph, S., 2024. Biochar for environmental management: science, technology and implementation. Taylor & Francis.

Leitner, J., Sedmidubský, D., Jankovský, O., 2018. Effect of ZnO nanosizing on its solubility in aqueous media. Micro & Nano Letters 13, 1585–1589.

Leng, L., Xu, S., Liu, R., Yu, T., Zhuo, X., Leng, S., Xiong, Q., Huang, H., 2020. Nitrogen containing functional groups of biochar: An overview. Bioresource Technology 298, 122286. https://doi.org/https://doi.org/10.1016/j.biortech.2019.122286

Li, L., Niu, W., Cong, H., Meng, H., Niu, Z., Shen, X., Cao, L., Kong, X., 2023. Effects of Pyrolysis Temperature on the Release Characteristics of Polycyclic Aromatic Hydrocarbons during Pyrolysis of Corn Stover Pellet. BioResources 18, 2112–2136. https://doi.org/10.15376/biores.18.1.2112-2136

Liang, H., Zhao, Y., Liu, T., Li, Ruijuan, Li, Rumei, Zhu, Y., Fang, F., 2024. Zn-Doped MnCO3/CS Composite Photocatalyst for Visible-Light-Driven Decomposition of Organic Pollutants. Molecules. https://doi.org/10.3390/molecules29051094

Liberda, D., Pięta, E., Pogoda, K., Piergies, N., Roman, M., Koziol, P., Wrobel, T.P., Paluszkiewicz, C., Kwiatek, W.M., 2021. The impact of preprocessing methods for a successful prostate cell lines discrimination using partial least squares regression and discriminant analysis based on Fourier transform infrared imaging. Cells 10, 953.

Lin, C.-W., Chen, F.-Y., Liu, S.-H., Ma, C.-Y., 2024. Optimized combination of zero-valent iron and oxygen-releasing biochar as cathodes of microbial fuel cells to enhance copper migration in sediment. Bioelectrochemistry 158, 108699. https://doi.org/https://doi.org/10.1016/j.bioelechem.2024.108699

Ling, C., Wu, S., Han, J., Dong, T., Zhu, C., Li, X., Xu, L., Zhang, Y., Zhou, M., Pan, Y., 2022. Sulfide-modified zero-valent iron activated periodate for sulfadiazine removal: Performance and dominant routine of reactive species production. Water Research 220, 118676.

Liu, B., Guo, W., Wang, H., Si, Q., Zhao, Q., Luo, H., Ren, N., 2020. B-doped graphitic porous biochar with enhanced surface affinity and electron transfer for efficient peroxydisulfate activation. Chemical Engineering Journal 396, 125119. https://doi.org/10.1016/J.CEJ.2020.125119

Liu, C., Lin, J., Chen, H., Wang, W., Yang, Y., 2021. Comparative Study of Biochar Modified with Different Functional Groups for Efficient Removal of Pb(II) and Ni(II). https://doi.org/10.21203/rs.3.rs-487894/v1

Liu, J., Wang, F., Xu, W., 2023. Characteristics of zinc adsorption onto biochars derived from different feedstocks. Water 15, 3789.

Liu, Q., Zang, G.-L., Zhao, Q., 2021. Removal of copper ions by functionalized biochar based on a multicomponent Ugi reaction. RSC Advances 11, 25880–25891. https://doi.org/10.1039/D1RA04156H

Lou, T., Yin, Y., Wang, J., 2024. Mechanisms of biochar promoting medium chain fatty acids production from sewage sludge: Effect of biochar type. Journal of Cleaner Production 451, 141995. https://doi.org/https://doi.org/10.1016/j.jclepro.2024.141995

Luo, M., Zhu, C., Chen, Q., Song, F., Hao, W., Shen, Z., Konhauser, K.O., Alessi, D.S., Zhong, C., 2023. In-situ growth of ZIF-8 nanocrystals on biochar for boron adsorption. Colloids and Surfaces A: Physicochemical and Engineering Aspects 657, 130504. https://doi.org/https://doi.org/10.1016/j.colsurfa.2022.130504

Lustosa Filho, J.F., Penido, E.S., Castro, P.P., Silva, C.A., Melo, L.C.A., 2017. Co-Pyrolysis of Poultry Litter and Phosphate and Magnesium Generates Alternative Slow-Release Fertilizer Suitable for Tropical Soils. ACS Sustainable Chemistry and Engineering 5, 9043–9052. https://doi.org/10.1021/ACSSUSCHEMENG.7B01935/ASSET/IMAGES/LARGE/SC-2017-01935U_0005.JPEG

Manogaran, M.D., Shamsuddin, R., Mohd Yusoff, M.H., Lay, M., Siyal, A.A., 2022. A review on treatment processes of chicken manure. Cleaner and Circular Bioeconomy 2, 100013. https://doi.org/https://doi.org/10.1016/j.clcb.2022.100013

Maqbool, M.A., Beshir, A., 2019. Zinc biofortification of maize (Zea mays L.): Status and challenges. Plant breeding 138, 1–28.

Masek, O., Buss, W., Sohi, S., 2018. Standard biochar materials. Environmental science & technology 52, 9543–9544.

Mašek, O., Buss, W., Sohi, S., 2018. Standard Biochar Materials. Environmental Science and Technology 52, 9543–9544. https://doi.org/10.1021/acs.est.8b04053

McAfee, L., 2000. Infrared and Raman spectra of inorganic and coordination compounds. Part A: theory and applications in inorganic chemistry; Part B: application in coordination, organometallic, and bioinorganic chemistry, (Nakamoto, Kazuo).

Meenu, Rani, M., Shanker, U., 2024. Efficient photodegradation of hexabromocyclododecane leached from polystyrene by biochar and sulfur doped CuO nanocomposite: Optimization factors, kinetics, and photoactivity. Environmental Pollution 340, 122818. https://doi.org/https://doi.org/10.1016/j.envpol.2023.122818

Morais, E.G., Jindo, K., Silva, C.A., 2023. Biochar-Based Phosphate Fertilizers: Synthesis, Properties, Kinetics of P Release and Recommendation for Crops Grown in Oxisols. Agronomy. https://doi.org/10.3390/agronomy13020326

Morais, E.G., Silva, C.A., Jindo, K., 2021. Humic Acid Improves Zn Fertilization in Oxisols Successively Cultivated with Maize–Brachiaria. Molecules. https://doi.org/10.3390/molecules26154588

Morais, E.G., Silva, C.A., Maluf, H.J.G.M., Guilherme, L.R.G., 2022. Slow-Release Humic Acid-Based Zinc Fertilizers Improve Growth and Nutrition of Maize and Brachiaria

Grass Successively Grown in Oxisols. ACS Agricultural Science & Technology 3, 17–32.

Mortvedt, J.J., Gilkes, R.J., 1993. Zinc fertilizers, in: Zinc in Soils and Plants: Proceedings of the International Symposium on 'Zinc in Soils and Plants' Held at The University of Western Australia, 27–28 September, 1993. Springer, pp. 33–44.

Muzyka, R., Misztal, E., Hrabak, J., Banks, S.W., Sajdak, M., 2023. Various biomass pyrolysis conditions influence the porosity and pore size distribution of biochar. Energy 263, 126128. https://doi.org/https://doi.org/10.1016/j.energy.2022.126128

Nakamoto, K., 2009. Infrared and Raman spectra of inorganic and coordination compounds, part B: applications in coordination, organometallic, and bioinorganic chemistry. John Wiley & Sons.

Nan, H., Yin, J., Yang, F., Luo, Y., Zhao, L., Cao, X., 2021. Pyrolysis temperature-dependent carbon retention and stability of biochar with participation of calcium: Implications to carbon sequestration. Environmental Pollution 287, 117566. https://doi.org/https://doi.org/10.1016/j.envpol.2021.117566

Nepal, J., Ahmad, W., Munsif, F., Khan, A., Zou, Z., 2023. Advances and prospects of biochar in improving soil fertility, biochemical quality, and environmental applications . Frontiers in Environmental Science .

Nguyen, N.-T., Lee, S.-Y., Chen, S.-S., Nguyen, N.-C., Chang, C.-T., Hsiao, S.-S., Trang, L.T., Kao, C.-Y., Lin, M.-F., Wang, L., 2018. Preparation of Zn-Doped Biochar from Sewage Sludge for Chromium Ion Removal. Journal of nanoscience and nanotechnology 18, 5520–5527. https://doi.org/10.1166/jnn.2018.15392

NIST-SRM-1573a, 2018. Standard Reference Material 1573 - Tomato Leaves.

Novais, R.F. de, Neves, J.C.L., Barros, N.F. de, 1991. Ensaio em ambiente controlado. Métodos de pesquisa em fertilidade do solo. Brasília: Embrapa-SEA 392.

Omiri, J., Snoussi, Y., Bhakta, A.K., Truong, S., Ammar, S., Khalil, A.M., Jouini, M., Chehimi, M.M., 2022. Citric-Acid-Assisted Preparation of Biochar Loaded with Copper/Nickel Bimetallic Nanoparticles for Dye Degradation. Colloids and Interfaces. https://doi.org/10.3390/colloids6020018

ON THE OCCURRENCE OF COPPER IN TROPICAL SOILS Author (s): J . G . VERMAAT and G . J . VAN DER BIE Published by : Springer Stable URL : https://www.jstor.org/stable/42931553, 1950. 2, 257–282.

Otoni, J.P., Matoso, S.C.G., Pérez, X.L.O., da Silva, V.B., 2024. Potential for agronomic and environmental use of biochars derived from different organic waste. Journal of Cleaner Production 449, 141826. https://doi.org/https://doi.org/10.1016/j.jclepro.2024.141826

Pan, G., Wei, J., Xu, M., Li, Jiamei, Wang, L., Li, Y., Cui, N., Li, Jun, Wang, Z., 2023a. Insight into boron-doped biochar as efficient metal-free catalyst for peroxymonosulfate activation: Important role of -O-B-O- moieties. Journal of Hazardous Materials 445, 130479. https://doi.org/https://doi.org/10.1016/j.jhazmat.2022.130479

Pan, G., Wei, J., Xu, M., Li, Jiamei, Wang, L., Li, Y., Cui, N., Li, Jun, Wang, Z., 2023b. Insight into boron-doped biochar as efficient metal-free catalyst for peroxymonosulfate activation: Important role of -O-B-O- moieties. Journal of Hazardous Materials 445, 130479. https://doi.org/10.1016/j.jhazmat.2022.130479

Penido, E.S., Martins, G.C., Mendes, T.B.M., Melo, L.C.A., do Rosário Guimarães, I., Guilherme, L.R.G., 2019. Combining biochar and sewage sludge for immobilization of heavy metals in mining soils. Ecotoxicology and Environmental Safety 172, 326–333. https://doi.org/https://doi.org/10.1016/j.ecoenv.2019.01.110

Piash, M.I., Iwabuchi, K., Itoh, T., 2022. Synthesizing biochar-based fertilizer with sustained phosphorus and potassium release: Co-pyrolysis of nutrient-rich chicken manure and Ca-bentonite. Science of The Total Environment 822, 153509. https://doi.org/10.1016/J.SCITOTENV.2022.153509

Quílez-Bermejo, J., Morallón, E., Cazorla-Amorós, D., 2020. Metal-free heteroatom-doped carbon-based catalysts for ORR: A critical assessment about the role of heteroatoms. Carbon 165, 434–454. https://doi.org/10.1016/J.CARBON.2020.04.068

R-Core-Team, 2020. R: A language and environment for statistical computing.

Rafique, M.I., Usman, A.R.A., Ahmad, M., Sallam, A., Al-Wabel, M.I., 2020. In situ immobilization of Cr and its availability to maize plants in tannery waste–contaminated soil: effects of biochar feedstock and pyrolysis temperature. Journal of Soils and Sediments 20, 330–339. https://doi.org/10.1007/S11368-019-02399-Z/TABLES/5

Rødde, R.H., Einbu, A., Vårum, K.M., 2008. A seasonal study of the chemical composition and chitin quality of shrimp shells obtained from northern shrimp (Pandalus borealis). Carbohydrate Polymers 71, 388–393. https://doi.org/https://doi.org/10.1016/j.carbpol.2007.06.006

Roy, P.P., Paul, S., Mitra, I., Roy, K., 2009. On Two Novel Parameters for Validation of Predictive QSAR Models. Molecules 2009, Vol. 14, Pages 1660-1701 14, 1660–1701. https://doi.org/10.3390/MOLECULES14051660

Rúa-Díaz, S., Forjan, R., Lago-Vila, M., Cerqueira, B., Arco-Lázaro, E., Marcet, P., Baragaño, D., Gallego, J.L.R., Covelo, E.F., 2023. Pyrolysis temperature influences the capacity of biochar to immobilize copper and arsenic in mining soil remediation. Environmental Science and Pollution Research 30, 32882–32893. https://doi.org/10.1007/s11356-022-24492-6

Ruangratanakorn, J., Suwonsichon, T., Kasemsumran, S., Thanapase, W., 2020. Installation design of on-line near infrared spectroscopy for the production of compound fertilizer. Vibrational Spectroscopy 106, 103008. https://doi.org/10.1016/J.VIBSPEC.2019.103008

Ryota Suzuki, A., 2022. Package “pvclust” Title Hierarchical Clustering with P-Values via Multiscale Bootstrap Resampling.

Sadeek, S.A., Mohammed, E.A., Shaban, M., Abou Kana, M.T.H., Negm, N.A., 2020. Synthesis, characterization and catalytic performances of activated carbon-doped transition metals during biofuel production from waste cooking oils. Journal of Molecular Liquids 306, 112749. https://doi.org/https://doi.org/10.1016/j.molliq.2020.112749

Saha, S., Islam, M.T., Calhoun, J., Reza, T., 2023. Effect of Hydrothermal Carbonization on Fuel and Combustion Properties of Shrimp Shell Waste. Energies. https://doi.org/10.3390/en16145534

Salawu, O.A., Han, Z., Adeleye, A.S., 2022. Shrimp waste-derived porous carbon adsorbent: Performance, mechanism, and application of machine learning. Journal of Hazardous Materials 437, 129266. https://doi.org/10.1016/J.JHAZMAT.2022.129266

Sánchez-Rodríguez, A.R., Rey, M.-D., Nechate-Drif, H., Castillejo, M.Á., Jorrín-Novo, J. V, Torrent, J., del Campillo, M.C., Sacristán, D., 2021. Combining P and Zn fertilization to enhance yield and grain quality in maize grown on Mediterranean soils. Scientific Reports 11, 7427. https://doi.org/10.1038/s41598-021-86766-2

Schellekens, J., Silva, C.A., Buurman, P., Rittl, T.F., Domingues, R.R., Justi, M., Vidal-Torrado, P., Trugilho, P.F., 2018. Molecular characterization of biochar from five Brazilian agricultural residues obtained at different charring temperatures. Journal of Analytical and Applied Pyrolysis 130, 106–117.

Schmidt, M.P., Siciliano, S.D., Peak, D., 2021. The role of monodentate tetrahedral borate complexes in boric acid binding to a soil organic matter analogue. Chemosphere 276, 130150. https://doi.org/10.1016/j.chemosphere.2021.130150

Shaban, M., Zayed, M., Hamdy, H., 2017. Nanostructured ZnO thin films for self-cleaning applications. RSC Advances 7, 617–631. https://doi.org/10.1039/C6RA24788A

Shabbir, Z., Sardar, A., Shabbir, A., Abbas, G., Shamshad, S., Khalid, S., Natasha, Murtaza, G., Dumat, C., Shahid, M., 2020. Copper uptake, essentiality, toxicity, detoxification and risk assessment in soil-plant environment. Chemosphere 259, 127436. https://doi.org/https://doi.org/10.1016/j.chemosphere.2020.127436

Shireen, F., Nawaz, M.A., Chen, C., Zhang, Q., Zheng, Z., Sohail, H., Sun, J., Cao, H., Huang, Y., Bie, Z., 2018. Boron: Functions and Approaches to Enhance Its Availability in Plants for Sustainable Agriculture. International Journal of Molecular Sciences. https://doi.org/10.3390/ijms19071856

Shuailong, C., Qintie, L.I.N., Rongbo, X., Haoyu, L.U.O., Hengyi, F.U., 2020. Removal of EDTA-Cu in wastewater by copper-based biochar activated sodium persulfate. Chinese Journal of Environmental Engineering 14, 3298–3307.

Sieber, V., Hofer, M., Brück, W.M., Garbe, D., Brück, T., Lynch, C.A., 2018. ChiBio: An Integrated Bio-refinery for Processing Chitin-Rich Bio-waste to Specialty Chemicals BT - Grand Challenges in Marine Biotechnology, in: Rampelotto, P.H., Trincone, A. (Eds.), . Springer International Publishing, Cham, pp. 555–578. https://doi.org/10.1007/978-3-319-69075-9_14

Silva, F.C. da, 2009. Manual de análises químicas de solos, plantas e fertilizantes, Empresa Brasileira de Pesquisa Agropecuária Embrapa Solos Embrapa Informática Agropecuária Ministério da Agricultura, Pecuária e Abastecimento.

Silverstein, R.M., Bassler, G.C., 1962. Spectrometric identification of organic compounds. Journal of Chemical Education 39, 546.

Singh, A., Yadav, K., Thakur, P., Wan, F., Ravelo, B., Thakur, A., 2024. Review on the amelioration of ZnO and its composites: synthesis and applications. Indian Journal of Physics. https://doi.org/10.1007/s12648-024-03181-9

Singh, B., Dolk, M.M., Shen, Q., Camps-Arbestain, M., 2017. Biochar: A Guide to Analytical Methods, in: Singh, B., Camps-Arbestain, M., Lehmann, J. (Eds.), Biochar: A Guide to Analytical Methods. CRC Press/Taylor and Francis Group, LLC, Boca Raton, pp. 23–38.

Socrates, G., 2004. Infrared and Raman characteristic group frequencies: tables and charts. John Wiley & Sons.

Stuart, B.H., 2004. Infrared Spectroscopy: Fundamentals and Applications, Analytical Techniques in the Sciences. John Wiley & Sons, Ltd, Chichester, UK. https://doi.org/10.1002/0470011149

Sui, L., Tang, C., Du, Q., Zhao, Y., Cheng, K., Yang, F., 2021. Preparation and characterization of boron-doped corn straw biochar: Fe (II) removal equilibrium and kinetics. Journal of Environmental Sciences 106, 116–123. https://doi.org/https://doi.org/10.1016/j.jes.2021.01.001

Sukumar, S., Rudrasenan, A., Padmanabhan Nambiar, D., 2020. Green-synthesized rice-shaped copper oxide nanoparticles using Caesalpinia bonducella seed extract and their applications. ACS omega 5, 1040–1051.

Sun, F., Bin Wu, H., Liu, X., Liu, F., Han, R., Qu, Z., Pi, X., Wang, L., Gao, J., Lu, Y., 2018a. A high-rate and ultrastable anode enabled by boron-doped nanoporous carbon spheres for high-power and long life lithium ion capacitors. https://doi.org/10.1016/j.mtener.2018.07.009

Sun, F., Qu, Z., Gao, J., Wu, H. Bin, Liu, F., Han, R., Wang, L., Pei, T., Zhao, G., Lu, Y., 2018b. In Situ Doping Boron Atoms into Porous Carbon Nanoparticles with Increased Oxygen Graft Enhances both Affinity and Durability toward Electrolyte for Greatly Improved Supercapacitive Performance. Advanced Functional Materials 28. https://doi.org/10.1002/ADFM.201804190

Suzuki, R., Terada, Y., Shimodaira, H., Suzuki, M.R., 2019. Package 'pvclust.' R Package. Hierarchical Clustering with P-Values via Multiscale Bootstrap Resampling. Version 2.

Taiyun Wei, M., Taiyun Wei cre, A., Simko aut, V., Levy ctb, M., Xie ctb, Y., Jin ctb, Y., Zemla ctb, J., Freidank ctb, M., Cai ctb, J., Protivinsky ctb, T., 2022. Package "corrplot" Title Visualization of a Correlation Matrix NeedsCompilation no.

Teixeira, P.C., Donagemma, G.K., Fontana, A., Teixeira, W.G., 2017a. Manual de Métodos de Análise de Solo 3ª edição revista e ampliada. Manual de métodos de análise de solo - Capítulo 8 - Densidade de partículas 574.

Teixeira, P.C., Donagemma, G.K., Fontana, A., Teixeira, W.G., 2017b. Manual de métodos de análise de solo.

Thapa, S., Bhandari, A., Ghimire, R., Xue, Q., Kidwaro, F., Ghatrehsamani, S., Maharjan, B., Goodwin, M., 2021. Managing Micronutrients for Improving Soil Fertility, Health, and Soybean Yield. Sustainability. https://doi.org/10.3390/su132111766

Thirumal, V., Pandurangan, A., Jayavel, R., Ilangovan, R., 2016. Synthesis and characterization of boron doped graphene nanosheets for supercapacitor applications. https://doi.org/10.1016/j.synthmet.2016.07.011

Tu, P., Zhang, G., Wei, G., Li, J., Li, Y., Deng, L., Yuan, H., 2022. Influence of pyrolysis temperature on the physicochemical properties of biochars obtained from herbaceous and woody plants. Bioresources and Bioprocessing 9, 131. https://doi.org/10.1186/s40643-022-00618-z

Vale, F., Alcarde, J.C., 2002. Extratores para avaliar a disponibilidade do zinco em fertilizantes. Revista Brasileira de Ciência do Solo.

Vinodkumar, R., Navas, I., Porsezian, K., Ganesan, V., Unnikrishnan, N. V, Pillai, V.P.M., 2014. Structural, spectroscopic and electrical studies of nanostructured porous ZnO thin films prepared by pulsed laser deposition. Spectrochimica Acta Part A: Molecular and Biomolecular Spectroscopy 118, 724–732.

Waclawska, I., 1995. Thermal decomposition of borax. Journal of thermal analysis 43, 261–269. https://doi.org/10.1007/BF02635993

Wang, C., Dai, H., Liang, L., Li, N., Cui, X., Yan, B., Chen, G., 2023. Enhanced mechanism of copper doping in magnetic biochar for peroxymonosulfate activation and sulfamethoxazole degradation. Journal of Hazardous Materials 458, 132002. https://doi.org/https://doi.org/10.1016/j.jhazmat.2023.132002

Wang, C., Huang, C., Qian, J., Xiao, J., Li, H., Wen, Y., He, X., Ran, W., Shen, Q., Yu, G., 2014. Rapid and Accurate Evaluation of the Quality of Commercial Organic Fertilizers Using Near Infrared Spectroscopy. PLOS ONE 9, e88279. https://doi.org/10.1371/JOURNAL.PONE.0088279

Wang, H., Chen, D., Wen, Y., Cui, T., Liu, Y., Zhang, Y., Xu, R., 2023. Insights into influence of aging processes on zero-valent iron modified biochar in copper(II) immobilization: from batch solution to pilot-scale investigation. Frontiers of Chemical Science and Engineering 17, 880–892. https://doi.org/10.1007/s11705-022-2282-8

Wang, H., Dong, Y., Yang, Y., Toor, G.S., Zhang, X., 2013. Changes in heavy metal contents in animal feeds and manures in an intensive animal production region of China. Journal of Environmental Sciences 25, 2435–2442. https://doi.org/10.1016/S1001-0742(13)60473-8

Wang, P., Tang, L., Wei, X., Zeng, G., Zhou, Y., Deng, Y., Wang, J., Xie, Z., Fang, W., 2017. Synthesis and application of iron and zinc doped biochar for removal of p-nitrophenol in wastewater and assessment of the influence of co-existed Pb(II). Applied Surface Science 392, 391–401. https://doi.org/10.1016/j.apsusc.2016.09.052

Wang, Z., Xu, X., Ma, S., Wang, H., Zhao, H., Wang, Y., Tong, S., Su, Z., Wang, W., Bai, J., 2021. The superior adsorption capacity of boron-nitrogen co-doping walnut shell biochar powder for Au(III), Pt(IV), and Pd(II). Journal of Environmental Chemical Engineering 9, 106288. https://doi.org/https://doi.org/10.1016/j.jece.2021.106288

Wei, T., Simko, V., Levy, M., Xie, Y., Jin, Y., Zemla, J., 2017. Package ‘corrplot.’

Statistician 56, e24.

Werheit, H., Au, T., Schmechel, R., Shalamberidze, S.O., Kalandadze, G.I., Eristavi, A.M., 2000. IR-Active Phonons and Structure Elements of Isotope-Enriched Boron Carbide. Journal of Solid State Chemistry 154, 79–86. https://doi.org/10.1006/JSSC.2000.8815

Wickham, H., Averick, M., Bryan, J., Chang, W., D', L., Mcgowan, A., François, R., Grolemund, G., Hayes, A., Henry, L., Hester, J., Kuhn, M., Lin Pedersen, T., Miller, E., Bache, S.M., Müller, K., Ooms, J., Robinson, D., Seidel, D.P., Spinu, V., Takahashi, K., Vaughan, D., Wilke, C., Woo, K., Yutani, H., 2019. Welcome to the Tidyverse. Journal of Open Source Software 4, 1686. https://doi.org/10.21105/JOSS.01686

Wickham, H., Wickham, M.H., 2019. Package 'tidyverse.' See http://tidyverse. tidyverse. org 1–5.

Wijitkosum, S., Jiwnok, P., 2019. Elemental Composition of Biochar Obtained from Agricultural Waste for Soil Amendment and Carbon Sequestration. Applied Sciences. https://doi.org/10.3390/app9193980

Wu, D., Sun, F., Qu, Z., Wang, H., Lou, Z., Wu, B., Zhao, G., 2022. Multi-scale structure optimization of boron-doped hard carbon nanospheres boosting the plateau capacity for high performance sodium ion batteries. Journal of Materials Chemistry A 10, 17225–17236. https://doi.org/10.1039/D2TA04194D

Wu, P., Cui, P., Fang, G., Gao, J., Zhou, D., Wang, Y., 2018. Sorption mechanism of zinc on reed, lignin, and reed- and lignin-derived biochars: kinetics, equilibrium, and spectroscopic studies. Journal of Soils and Sediments 18, 2535–2543. https://doi.org/10.1007/s11368-018-1928-0

Wu, P., Guo, Z., Hua, K., Wang, D., 2023. Long-term application of organic amendments changes heavy metals accumulation in wheat grains by affecting soil chemical properties and wheat yields. Journal of Soils and Sediments 23, 2136–2147. https://doi.org/10.1007/s11368-023-03473-3

Wydro, U., Jankowska, M., Wołejko, E., Kondzior, P., Łozowicka, B., Kaczyński, P., Rodziewicz, J., Janczukowicz, W., Pietryczuk, A., Cudowski, A., Jabłońska-Trypuć, A., 2022. Changes in Soil Biological Properties after Sewage Sludge and Pesticide Application in Wheat Cultivation. Applied Sciences. https://doi.org/10.3390/app122211452

Xiao, Y., Xue, Y., Gao, F., Mosa, A., 2017. Sorption of heavy metal ions onto crayfish shell biochar: effect of pyrolysis temperature, pH and ionic strength. Journal of the Taiwan Institute of Chemical Engineers 80, 114–121.

Xinxin, M.O., Siebecker, M.G., Wenxian, G.O.U., Ling, L.I., Wei, L.I., 2021. A review of cadmium sorption mechanisms on soil mineral surfaces revealed from synchrotron-based X-ray absorption fine structure spectroscopy: Implications for soil remediation. Pedosphere 31, 11–27.

Xu, L., Qi, Y., He, S., Wang, C., Jin, X., Wang, Q., Wang, K., Jin, P., 2025. Facile synthesis of boron-doped porous biochar as a metal-free adsorbent for efficient removal of aqueous tetracycline antibiotics. Journal of Environmental Sciences 152, 235–247. https://doi.org/https://doi.org/10.1016/j.jes.2024.04.044

Xu, L., Xing, X., Peng, J., Ji, M., 2022. Effects of In Situ Remediation on Copper Distribution and Soil Aggregate Adsorption–Desorption Characteristics in Smelter-Impacted Soil . Frontiers in Environmental Science .

Xu, P., Gao, Y., Cui, Z., Wu, B., Yan, B., Wang, Yifan, Zaitongguli, K., Wen, M., Wang, H., Jing, N., Wang, Yingze, Chao, C., Xue, W., 2023. Research Progress on Effects of Biochar on Soil Environment and Crop Nutrient Absorption and Utilization. Sustainability. https://doi.org/10.3390/su15064861

Yang, F., Wang, C., Sun, H., 2021. A comprehensive review of biochar-derived dissolved matters in biochar application: Production, characteristics, and potential environmental effects and mechanisms. Journal of Environmental Chemical Engineering 9, 105258. https://doi.org/10.1016/J.JECE.2021.105258

Yang, H., Sheng, K., 2012. Characterization of Biochar Properties Affected by Different Pyrolysis Temperatures Using Visible-Near-Infrared Spectroscopy. International Scholarly Research Network ISRN Spectroscopy 2012. https://doi.org/10.5402/2012/712837

Yang, Z., Yao, Z., Li, G., Fang, G., Nie, H., Liu, Z., Zhou, X., Chen, an, Huang, S., 2011. Sulfur-Doped Graphene as an Efficient Metal-free Cathode Catalyst for Oxygen Reduction. https://doi.org/10.1021/nn203393d

Younis, U., Rahi, A.A., Danish, S., Ali, M.A., Ahmed, N., Datta, R., Fahad, S., Holatko, J., Hammerschmiedt, T., Brtnicky, M., Zarei, T., Baazeem, A., Sabagh, A. El, Glick, B.R., 2021. Fourier Transform Infrared Spectroscopy vibrational bands study of Spinacia oleracea and Trigonella corniculata under biochar amendment in naturally contaminated soil. PloS one 16, e0253390. https://doi.org/10.1371/journal.pone.0253390

Yue, X., Fei-Yue, L., Xing-Jun, F., Shui-Jin, H., Xin, X., Jian-Fei, W., 2018. Cite this article as: Chinese. CHINESE JOURNAL OF ANALYTICAL CHEMISTRY 46, 609–615. https://doi.org/10.1016/S1872-2040(17)61081-8

Zhang, D., Sun, J., Li, Q., Song, H., Xia, D., 2022. Cu-Doped magnetic loofah biochar for tetracycline degradation via peroxymonosulfate activation. New Journal of Chemistry 46, 17223–17234. https://doi.org/10.1039/D2NJ02885A

Zhang, H., Cao, Q., Zhang, K., Xie, L., Xu, K., Qin, Y., Zhang, L., Chai, X., 2023. Boron-doped biochar-nano loaded zero-valent iron to activate persulfate for the degradation of oxytetracycline. Journal of Environmental Chemical Engineering 11, 111502. https://doi.org/10.1016/J.JECE.2023.111502

Zhang, J., Koubaa, A., Xing, D., Liu, W., Wang, Q., Wang, X., Wang, H., 2020a. Improving lignocellulose thermal stability by chemical modification with boric acid for incorporating into polyamide. Materials & Design 191, 108589. https://doi.org/https://doi.org/10.1016/j.matdes.2020.108589

Zhang, J., Koubaa, A., Xing, D., Liu, W., Wang, Q., Wang, X.M., Wang, H., 2020b. Improving lignocellulose thermal stability by chemical modification with boric acid for incorporating into polyamide. Materials & Design 191, 108589. https://doi.org/10.1016/J.MATDES.2020.108589

Zhang, Xu, Gang, D.D., Zhang, J., Lei, X., Lian, Q., Holmes, W.E., Zappi, M.E., Yao, H., 2022. Insight into the activation mechanisms of biochar by boric acid and its application for the removal of sulfamethoxazole. Journal of Hazardous Materials 424, 127333. https://doi.org/https://doi.org/10.1016/j.jhazmat.2021.127333

Zhang, Xin, Zhao, B., Liu, H., Zhao, Y., Li, L., 2022a. Effects of pyrolysis temperature on biochar's characteristics and speciation and environmental risks of heavy metals in sewage sludge biochars. Environmental Technology & Innovation 26, 102288. https://doi.org/10.1016/j.eti.2022.102288

Zhang, Xin, Zhao, B., Liu, H., Zhao, Y., Li, L., 2022b. Effects of pyrolysis temperature on biochar's characteristics and speciation and environmental risks of heavy metals in sewage sludge biochars. Environmental Technology & Innovation 26, 102288. https://doi.org/https://doi.org/10.1016/j.eti.2022.102288

Zhang, Y., Zhang, W., Zhang, H., He, D., 2023. Nano-Zero-Valent Zinc-Modified Municipal Sludge Biochar for Phosphorus Removal. Molecules 28, 3231.

Zhao, J., Li, H., Wang, Y., Yu, J., Li, N., Wang, S., 2023. Cu/CuO-Decorated Peanut-Shell-Derived Biochar for the Efficient Degradation of Tetracycline via Peroxymonosulfate Activation. Catalysts. https://doi.org/10.3390/catal13091246

Zhou, Y., Yan, W., Yu, X., Chen, T., Wang, S., Zhao, W., 2020. Boron and nitrogen co-doped porous carbon for supercapacitors: A comparison between a microwave-assisted and a conventional hydrothermal process. Journal of Energy Storage 32, 101706. https://doi.org/10.1016/j.est.2020.101706

Zhu, X., Chen, B., Zhu, L., Xing, B., 2017. Effects and mechanisms of biochar-microbe interactions in soil improvement and pollution remediation: A review. Environmental Pollution 227, 98–115. https://doi.org/https://doi.org/10.1016/j.envpol.2017.04.032

Supplementary Material

Table S 1. Chemical characterization of the raw material, biochar and composites produced.

ID	Al	B	Ca	Cu	Fe	Mg	Mn	Na	P	Zn
	---- (mg kg^{-1}) ----									
FCM	2669	299	102606	178	2533	6466	462	2929	21060	551
FSC	1844	222	96764	98	1137	8433	92	1774	18473	109
FSS	6867	47	9471	348	11106	2489	200	922	3843	623
BCM-3	2780	243	108732	166	2170	9516	597		30035	787
BSC-3	2268	162	86603	147	3437	8513	114	IN	23074	1683
BSS-3	7399	94	10293	423	5565	2347	230	IN	4745	812
BCM-5	4719	196	105307	169	3657	13158	882	IN	46275	968
BSC-5	3648	164	125101	188	4749	17627	156	IN	44359	2238
BSS-5	10537	95	12647	481	11439	2738	301	IN	6129	922
CCM/ZnS-3	6334	129.5	101517	14657	3271	<LQ	1857	7527	27145	140108.3
CCM/ZnO-3	4879	10.0	108679	<LQ	2712	<LQ	1843	84240	29341	166675.0
CCM/ZnS-5	7342	459.0	157750	<LQ	4312	<LQ	2143	11461	32208	161925.0
CCM/ZnO-5	7169	18.4	142800	<LQ	4366	<LQ	2185	77565	33387	181612.5
CSC/ZnS-3	2275	189.3	112591	1396	1601	12482	52	20552	44250	159300.0
CSC/ZnO-3	2567	434.8	83212	2364	1547	9455	62	145502	36883	194700.0
CSC/ZnS-5	3356	958.9	237362	326	1839	19350	127	24298	68037	188087.5
CSC/ZnO-5	3446	491.4	292200	256	1629	22464	154	129040	66508	180262.5
CSS/ZnS-3	77711	134.3	2465	1788	41466	3622	126	10527	11182	155075.0
CSS/ZnO-3	260387	475.6	2411	546	135316	4983	210	96636	12786	162812.5
CSS/ZnS-5	35608	78.2	<LQ	719	28450	<LQ	1240	677	<LQ	187700.0
CSS/ZnS-5	35104	147.8	<LQ	<LQ	10251	<LQ	1137	77757	<LQ	158404.2

Concluding Remarks

The integration of Boron (B), Copper (Cu), and Zinc (Zn) into biochar composites as a fertilizer demonstrates a promising advancement in sustainable agriculture, particularly in optimizing nutrient availability and crop productivity in highly weathered tropical soils. Each element plays a distinct but complementary role in enhancing plant growth and soil health, with their effectiveness being heavily influenced by factors such as feedstock type, pyrolysis conditions, and the specific element's chemical form.

The B-biochar composites have shown remarkable potential in stabilizing and efficiently releasing B into the soil, particularly when boric acid is used as a precursor. This approach not only reduces volatilization losses during pyrolysis but also enhances the agronomic performance by improving B availability in oxisols, which is crucial for crops like eucalyptus. The strategic use of nitrogen-rich feedstocks, such as chicken manure, further amplifies the benefits, ensuring sustained B availability even in soils with low organic matter concentration.

Cu-biochar composites have been instrumental in addressing the nutrient uptake challenges posed by the contrasting textures of oxisols. The tailored Cu release profiles from these composites, especially those processed at higher temperatures, align well with the specific needs of different soil types, thereby optimizing wheat growth. The careful selection of feedstocks and pyrolysis conditions has allowed for enhanced Cu retention in soils, which is critical for long-term soil fertility and crop productivity.

Zn-biochar composites stand out for their ability to significantly increase Zn availability in crops like maize, particularly in soils prone to nutrient fixation and leaching. The findings underscore the importance of choosing the appropriate Zn source and pyrolysis temperature to match specific soil types. ZnO-doped biochar composites have demonstrated superior performance in providing a sustained release of Zn, crucial for maximizing grain yield in both sandy and clayey oxisols. These results highlight the strategic advantage of using biochar as a carrier for micronutrients, offering a controlled release mechanism that supports prolonged crop nutrition and soil health.

Collectively, the studies on B, Cu, and Zn biochar composites emphasize the critical role of tailored biochar formulations in enhancing the availability and uptake of essential micronutrients in crops. The integration of these composites into soil management practices not only improves crop yield and nutrient use efficiency but also contributes to the long-term sustainability of agricultural systems by maintaining soil health. Future research should focus on scaling these findings to field applications, exploring the long-term environmental impacts, and optimizing the cost-effectiveness of these biochar composites across various crops and soil types. This holistic approach will be crucial in meeting the demands of sustainable agriculture and ensuring food security in the face of global environmental challenges.